RECONSTRUCTION OF PAST CHANGES IN THE OXYGEN MINIMUM ZONE OF THE ARABIAN SEA FROM SEDIMENTARY RECORDS

Thesis submitted for the degree of
DOCTORATE IN PHILOSOPHY
in
MARINE SCIENCES
to the
GOA UNIVERSITY

By

ALEXANDRINA WITTY D'SOUZA
National Institute of Oceanography
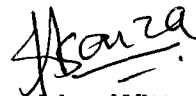Dona Paula, Goa 403 004

July 2007

To

My Mother

STATEMENT

As required under the University ordinance 0.19.8. (vi), I state that the present thesis entitled **"RECONSTRUCTION OF PAST CHANGES IN THE OXYGEN MINIMUM ZONE OF THE ARABIAN SEA FROM SEDIMENTARY RECORDS"**, is my original contribution and the same has not been submitted on any previous occasion. To the best of my knowledge, the present study is the first comprehensive work of its kind from the area mentioned.

The literature related to the problem investigated has been cited. Due acknowledgement have been made wherever facilities and suggestions have been availed of.

Alexandrina Witty D'Souza

राष्ट्रीय समुद्र विज्ञान संस्थान
national institute of oceanography

CERTIFICATE

This is to certify that the thesis entitled **"RECONSTRUCTION OF PAST CHANGES IN THE OXYGEN MINIMUM ZONE OF THE ARABIAN SEA FROM SEDIMENTARY RECORDS"**, submitted by Ms **Alexandrina Witty D'Souza** for the award of the degree of Doctor or Philosophy in Marine Science is based on her original studies carried out by her under my supervision. The thesis or any part thereof has not been previously submitted for any other degree or diploma in any university or institution.

Dr. M. Dileep Kumar
Research Guide
Scientist, Deputy Director
Chemical Oceanography Division
National Institute of Oceanography
Dona Paula – 403 004
Goa, India

All the suggestions made by the examiners have been incorporated in the thesis.

01/7/08

(P. C. Narayana)

CONTENTS

REFERENCES

LIST OF TABLES

LIST OF FIGURES

Figure 2.5   Schematic diagram of an Inductively Coupled Plasma Atomic Emmission Spectrometer (ICP-AES) for elemental analysis.

CHAPTER 3

Figure 3.1   Modern sea surface temperature (°C) and general wind pattern during SW and NE monsoon period. The thick arrow represents axis of Findlater Jet. The dashed line over Asia indicates elevations >3,000 meters. Dashed arrow indicates direction of relatively weak winds during NE monsoon period (modified from Prell, 1984a).

Figure 3.2   Surface circulations in the Indian Ocean during the SW and NE monsoon period (after Wyrtki, 1973). MC – Monsoon Current, SC – Somali Current, SEC – South Equatorial Current, NEC – North Equatorial Current, ECC – Equatorial Counter Current.

Figure 3.3   Map of Arabian Sea demarcating the OMZ region in terms of secondary nitrite (NO_2^-) maxima and oxygen (O_2) concentrations (μM). Hatched areas represent zones of upwelling off Arabia (A), Somalia (B) and Southwest India (C). Figure modified from Naqvi (1991).

Figure 3.4   (a)Cruise track (+) of U.S. JGOFS cruise TN050 (August-September) (b)Distribution of NO_3^- (nitrate data from U.S. JGOFS cruise TN050) indicating long distance (>1000Km) transport of upwelled waters reaching well within the OMZ region. (Figure adapted and modified from Naqvi et al., 2006b).

Figure 3.5   Distribution of (a)temperature (b)salinity (c)O_2 and (d)NO_2^- in the upper 1 Km off Goa (see inset in (b) for station locations) during December 1998. Modified from Navqi et al. (2006b).

while station 3202 was sampled down to 3 km [data points marked with filled circles (•)].

Figure 3.12b Vertical profiles of oxygen, nitrate and nitrite at the two stations 3201 and 3202 sampled during the FORV Sagar Sampada cruise SS119 in April 1994. Station 3201 was sampled down to ~1.5 km [data points marked with plus (+)], while station 3202 was sampled down to 3 km [data points marked with filled circles (•)].

Figure 3.13 Vertical profiles of oxygen (O_2), nitrate (NO_3^-), nitrite (NO_2^-) and nitrous oxide (N_2O) at 19°N, 67°E (data from TN039 cruise of U.S. JGOFS – station 18; during October 1994). **(a)** O_2 (circles) and NO_3^- (triangles); **(b)** N_2O (circles) and NO_2^- (triangles); **(c)** NO_3^- deficit according to Codispoti et al. (2001) are shown with dots connected by solid line, "excess nitrogen (N_2)" calculated from the N_2/Ar ratio (larger unconnected symbols – crosses for the data collected on two different cruises from this station and triangles for those from other stations also located within the denitrification zone) and N* according to Gruber and Sarmiento (2002) (small filled triangles connected by dashed line). N/Ar data are from Devol et al., (2006a).

CHAPTER 4

Figure 4.1 Core locations of three shallow cores raised from the inner and mid shelf region off Goa.

Figure 4.2 Age curves for cores SaSu-1 and SaSu-3B based on measurements of ^{210}Pb dates. Data points with blue filled circles (•) are experimental ^{210}Pb dates. The calculated Sedimentation (Sed.) rates are indicated. The age curves shown in above plots are for full length of the cores sampled.

Latitude Isostack Plot from Bassinot et al. (1994). Oxygen
Isotope Stages (OIS) and AMS ^{14}C dates are indicated.

Figure 5.3 Age-depth model based on AMS ^{14}C dates along with tie points
from low latitude isostack of Bassinot et al. (1994) used to
develop chronology. The tie points marked with red asterisks,
are reservoir corrected radiocarbon dates in sequential order as
given at the side of each plot. Average Sedimentation (Av. Sed.)
rates are indicated.

Figure 5.4 Downcore variation of δ^{18}O with planktonic species
Globigerinoide ruber in cores (a)AAS-42/15 and (b)AAS-42/12A.
Oxygen Isotope Stages (OIS) are indicated in numbers (1-9).
Shaded areas represent glacial periods.

Figure 5.5 Downcore variation of δ^{18}O with benthic species *Cibicidoides
wuellerstorfi* in cores (a)AAS-42/15 and (b)AAS-42/12A. Oxygen
Isotope Stages (OIS) are indicated in numbers (1-9). Shaded
areas represent glacial periods.

Figure 5.6 Downcore variation of δ^{13}C with planktonic species
Globigerinoide ruber in cores (a)AAS-42/15 and (b)AAS-42/12A.
Oxygen Isotope Stages (OIS) are indicated in numbers (1-9).
Shaded areas represent glacial periods.

Figure 5.7 Downcore variation of δ^{13}C with benthic species of *Cibicidoes
wuellerstorfi* in cores (a)AAS-42/15 and (b)AAS-42/12A. Oxygen
Isotope Stages (OIS) are indicated in numbers (1-9). Shaded
areas represent glacial periods.

Figure 5.8 Downcore variations of (a)δ^{13}C (b)C_{org} in core AAS-42/15 and
(c)δ^{13}C (d)C_{org} in core AAS-42/12A. The δ^{13}C variation of benthic

species *Cibicidoides wuellerstorfi* is compared with C_{org} in both the cores. Oxygen Isotope Stages (OIS) are indicated in numbers (1-9). Shaded areas represent glacial periods.

Figure 5.9 Downcore variation of (a)C_{org} (b)N_{org} (c)$\delta^{18}O$ (d)C/N (e)$CaCO_3$ in core AAS-42/15. Oxygen Isotope Stages (OIS) are indicated in numbers (1-6). Shaded areas represent glacial periods.

Figure 5.10 Downcore variation of (a)C_{org} (b)N_{org} (c)$\delta^{18}O$ (d)C/N (e)$CaCO_3$ in core AAS-42/12A. Oxygen Isotope Stages (OIS) are indicated in numbers (1-9). Shaded areas represent glacial periods.

Figure 5.11 Downcore variation of (a)$\delta^{13}C_{org}$ (b)$\delta^{15}N$ in core AAS-42/15 and (c)$\delta^{13}C_{org}$ (d)$\delta^{15}N$ in core AAS-42/12A. Oxygen Isotope Stages (OIS) are indicated in numbers (1-9). Shaded areas represent glacial periods.

Figure 5.12 Downcore variation of (a)C_{org} (b)C_{org} flux (c)$CaCO_3$ (d)$\delta^{13}C_{G.ruber}$ (e)C/N and (f)$\delta^{13}C_{org}$ in core AAS-42/15. Oxygen Isotope Stages (OIS) are in bold numbers (1-6) and shaded areas represent glacial periods.

Figure 5.13 Downcore variation of (a)C_{org} (b)C_{org} flux (c)$CaCO_3$ (d)$\delta^{13}C_{G.ruber}$ (e)$\delta^{13}C_{org}$ and (f)C/N in core AAS-42/12A. Oxygen Isotope Stages (OIS) are indicated in numbers (1-9). Shaded areas represent glacial periods.

Figure 5.14 Downcore variation of (a)$\delta^{15}N$ (b)C_{org} (c)$\delta^{13}C_{G.ruber}$ for core AAS-42/15. Low productivity with corresponding decrease in denitrification is seen during the glacial periods. Proxies indicate influence of weakened summer monsoon during the glacial periods at the core site. Oxygen Isotope Stages (OIS) are

indicated in numbers (1-6). Shaded areas represent glacial periods.

Figure 5.15 Downcore variation of (a)$\delta^{15}N$ (b)C_{org} (c)$\delta^{13}C_{G.ruber}$ for AAS-42/12A. High and low variations in denitrification ($\delta^{15}N$) clearly indicate the corresponding levels of phytoplankton (C_{org}) and planktic foraminifers ($\delta^{13}C_{G.ruber}$) productivity. All the proxy variations are influenced by summer monsoon intensity during the various stages of glacial-interglacial perioids. Oxygen Isotope Stages (OIS) are indiacated in numbers (1-9) and shaded areas represent glacial periods.

Figure 5.16 Correlation plots of (a)$\delta^{13}C_{org}$ (b)C_{org} (c)N_{org} (d)C/N with $\delta^{15}N$ in core AAS-42/15. The scatter in C_{org} and N_{org} vs $\delta^{15}N$ plots with a positive correlation rule out the diagenetic effects on $\delta^{15}N$ depth profile. Poor correlations in $\delta^{15}N$ vs $\delta^{13}C_{org}$ and C/N show that downcore $\delta^{15}N$ signals are free from dilution effect due to terrestrial organic matter inputs.

Figure 5.17 Correlation plots of (a)$\delta^{13}C_{org}$ (b)C_{org} (c)N_{org} (d)C/N with $\delta^{15}N$ in core AAS-42/12A. The scatter in C_{org} and N_{org} vs $\delta^{15}N$ plots with a positive correlation rule out diagenetic effects on $\delta^{15}N$ depth profile. Poor correlations in $\delta^{15}N$ vs $\delta^{13}C_{org}$ and C/N show that downcore $\delta^{15}N$ signals are free from dilution effects due to terrestrial organic matter inputs.

Figure 5.18 Variations of major elements (Ti, Al, Fe, Mg and Sr) in comparison with C_{org} and $CaCO_3$ (indicator of overhead productivity), during various glacial-interglacial stages, in core AAS-42/15. Profiles of Ti, Al, Fe, Mg are presented with their total concentration while Sr is normalized to Al. Glacial stages

are indicated by shading. Oxygen Isotope Stages (OIS, 1-6) are indicated.

Figure 5.19 Variations of major elements (Ti, Al, Fe, Mg and Sr) in comparison with C_{org} and $CaCO_3$ (indicator of overhead productivity), during various glacial-interglacial stages, in core AAS-42/12A. Profiles of Ti, Al, Fe, Mg are presented with their total concentration while Sr is normalized to Al. Glacial stages are indicated by shading. Oxygen Isotope Stages (OIS, 1-9) are indicated.

Figure 5.20 Down core variations of redox sensitive elements (Fe, Mn, V, Co, Mo) in comparison with $\delta^{13}C$ of benthics (indicator of bottom water oxygen) and $\delta^{15}N$ (denitrification proxy), during various glacial-interglacial stages in core AAS-42/15. Glacial stages are indicated with shaded portions. Oxygen Isotope Stages (OIS, 1-6) are indicated.

Figure 5.21 Down core variations of redox sensitive elements (Fe, Mn, V, Mo) in comparison with $\delta^{13}C$ of benthics (indicator of bottom water oxygen) and $\delta^{15}N$ (denitrification proxy) during various glacial-interglacial stages in core AAS-42/12A. Glacial stages are indicated with shaded portions. Oxygen Isotope Stages (OIS, 1-9) are indicated.

Figure 5.22 Temporal variability of productivity proxies and micro-nutrient type elements in comparison with $\delta^{13}C$ of benthics, $\delta^{15}N$ and C_{org} during various glacial-interglacial stages in core AAS-42/15. Glacial stages are indicated by shading. Oxygen Isotope Stages (OIS, 1-6) are indicated.

Figure 5.23 Temporal variability of productivity proxies and micronutrient type elements, in comparison with $\delta^{13}C$ of benthics, $\delta^{15}N$ and C_{org} during various glacial-interglacial stages in core AAS-42/12A. Glacial stages are indicated by shaded portions. Oxygen Isotope Stages (OIS, 1-9) are indicated.

PREFACE

Nitrogen being a polyvalent element; its speciation, transformation and fluxes in aquatic environments are controlled by ambient oxygen (O_2) concentrations. As seawater is generally oxygenated, nitrogen in the ocean occurs largely in the most oxidized (5+) state, viz. nitrate ions (NO_3^-) except only in a few regions where a part of the water column gets nearly stripped of O_2. In these suboxic regions, microbes convert NO_3^- to molecular nitrogen (N_2), a process known as denitrification, which is the most important pathway for fixed nitrogen loss and a key player in the nitrogen budget. The most intense mid-water column oxygen deficient zones (ODZs) are found to occur in the Pacific and Indian Oceans. In the Pacific Ocean zones, ODZ occurs below the productive tropical eastern boundary upwelling zones whereas in the Indian Ocean it is located in the northern region, especially in the northeastern Arabian Sea. This anomaly results from its unusual Indian Ocean geography, i.e. mainly the presence of Asian landmass that restricts its northern expanse to the tropics and, to a smaller extent, a porous eastern boundary (openings between the Indonesian islands), which allows the exchange of water with the Pacific Ocean. The resultant circulation is not conducive for strong upwelling off the coasts of Myanmar and Australia, in comparison to that found off the west coasts of America. Instead, the most intense upwelling and consequently very high rates of primary production (PP) occur along the northwestern boundary of the Indian Ocean (the Somali and Arabian coasts). Despite the lateral supply of high salinity intermediate waters

from the Persian Gulf and the Red Sea, subsurface water renewal in the Indian Ocean occurs largely because of advection from the south. The waters derived from the Southern Hemisphere gradually lose O_2 but accumulate metabolic products (CO_2, nutrients) during their northward movement. Thus, a lower supply of O_2 together with its enhanced demand produces intense O_2 deficiency (Winkler $O_2 < 0.1$ mL L^{-1}; ~4 μM) over a wider depth range (~100/150 to 1,000 m) in the north, particularly in the North Eastern Arabian Sea.

Due to the semi-enclosed nature of the North Indian Ocean, the OMZ (oxygen minimum zone) impinges upon a very large area of the continental margin. Bottom waters with $O_2 < 0.5$ mL L^{-1} (22 μM) and < 0.2 mL L^{-1} (9 μM), are estimated to cover about 1.15×10^6 and 0.76×10^6 km^2 of the marginal seafloor in the region. However, the zone of perennial mid-water column denitrification is confined to the open ocean. Suboxic conditions develop over the inner and mid-shelf off the west coast of India only seasonally (during late summer and autumn). As compared to the open ocean system, the coastal suboxic system covers two orders-of-magnitude less volume, but experiences more extreme conditions (i.e. greater nitrate consumption leading to complete anoxia). Coastal hypoxia also appears to have intensified in the past few decades presumably due to enhanced nutrient loading from land.

Although a number of studies have been carried out both, in the open ocean and coastal regions of the Arabian Sea with respect to nitrogen cycling, very little information is available on the behaviour of redox sensitive trace metals (such as Fe, Mn, Mo, V and Co). Like nitrogen, these elements also undergo speciation changes depending upon the O_2 levels, and either get

deposited in or mobilized from sediments. However, several concerns are known in regard to the interpretation of metal trends with respect to past environmental variability. The most important of these is the diagenetic effect because of which metal concentrations in the sediments may not necessarily reflect redox conditions in overlying waters at the time of sediment deposition. Due to these constraints, a multi-proxy approach has to be adopted to reconstruct, from the sedimentary records, past variability of processes in the water column.

Over the past ten years, a number of sedimentary records of $\delta^{15}N$ have been published from different sites in the Arabian Sea representing a range of oceanographic settings and sedimentation rates. These records show higher enrichment of $\delta^{15}N$ (>8‰) in surface sediments not only throughout the Holocene but also during all interglacial periods over the past 1 Ma. In contrast lighter isotopic enrichment (~5-6‰), comparable to that found in non-reducing environments today, characterizes sediments accumulated during the glacial stages indicating the weakened denitrification or its absence during such periods. However, only a few of the cores studied so far, have been sampled from the core of the denitrification zone, and none of the previous work dealt with the seasonal coastal system.

In view of the limited proxies used previously to reconstruct past changes in Arabian Sea denitrification, and poor geographical coverage, the present study has been aimed to adopt a multi-proxy approach covering shallow as well as deep Arabian Sea. The results will help us to decipher the variations in the water column by providing insights into the response of

subsurface reducing environment to global and regional changes in climate and oceanographic processes (productivity and circulation). The present study is the first to use stable nitrogen isotopes and redox sensitive metals proxies, to construct paleo-redox conditions, in well-dated sediments of both the open ocean and coastal suboxic regions. The present study is dealt within six chapters.

Chapter 1 provides the introduction to the topic of research and study area - the Arabian Sea. It gives the background information covering the relevant works previously carried out in the region and other regions of the world oceans with pronounced OMZs. The need for undertaking the present work following a multi-proxy approach is emphasized, and the scope and objectives of the study are defined.

Chapter 2 contains descriptions of the material and methods used in the study, i.e. the details about the field work, techniques used for collection, handling and processing of samples. It also describes various analytical instruments used for chemical and isotopic analyses. Briefly, an Inductively Coupled Plasma Atomic Emission Spectrometer (ICP-AES) was used for trace metal measurements. The stable oxygen and carbon analyse/is were carried out using an Isotopic Ratio Mass Spectrometer (IRMS). Isotopic ratios of $^{15}N/^{14}N$ in sedimentary organic matter were measured using an elemental analyzer coupled with IRMS (EA-MS).

Chapter 3 gives a general account of the hydrography and circulation in the Arabian Sea, both in the offshore and coastal regions. Details about the open ocean system have long been available, and being the subject of several previous works, these are briefly dealt with here. Instead, greater

emphasis is laid on the coastal system. Seasonal changes that affect the biogeochemical cycling over the western continental margin of India are highlighted. These details of biogeochemical cycling over the Indian shelf and its changes, including evidence for recent intensification of the coastal oxygen-deficient environment, are provided.

Chapter 4 presents the results for the three short and shallow cores – CR-2, SaSu-1 and SaSu-3B, collected from the inner- and mid-shelf regions (water depths 45, 35 and 50 m, respectively) off Goa. Dating techniques employed for these cores indicate the temporal resolutions in all the three cores to be comparably high. Decreasing trends in $\delta^{15}N$ and $\delta^{13}C$ in both cores suggest increase in terrestrial inputs in the last few decades, consistent with the trace metal data (especially Al in SaSu-1). $\delta^{15}N$ does not appear to be a good proxy of denitrification in these cores. Enhancement of biological productivity in the region over the past few decades, suggested by the historical water column data, is supported by records of a number of proxies (especially N, P, $CaCO_3$ and Ba contents). In conformity with the increased productivity, the redox sensitive metals are indicative of intensified denitrification.

Chapter 5 presents the results for two deep-sea gravity cores, AAS – 42/15 (length 440 cm; taken from Raman Seamount; water depth 2525) and AAS – 42/12A (length 530 cm; taken from Wadia Seamount; water depth 2250 m). Both cores came from beneath the most intense water-column denitrification, but the sediments at the coring sites are currently not exposed to the OMZ (bottom water dissolved oxygen concentration close to the coring

sites is presently 2-2.5 mL/L). Oxygen isotope records were generated for planktonic foraminifer, *Globigerinoide ruber* in both the cores. The $\delta^{18}O$ record was similar in structure to the well-established oxygen isotope curves of the deep sea cores in that the first 6 Oxygen Isotope Stages (OIS) could be clearly identified for AAS-42/15, while in core AAS-42/12A the first 8 complete OIS with a part of OIS 9 could be identified. The upper portion of this core was subjected to AMS ^{14}C dating. Based on combined ^{14}C and ^{18}O data, this core has a very good chronology, covering a period of ~165 Ky and ~320 Ky respectively.

Since the OMZ does not reach the seafloor at the coring sites, the records generated enable evaluation of changes in the intermediate as well as bottom waters through comparison of different proxies of conditions in the two domains. For example, while the sedimentary $\delta^{15}N$ record can be taken to represent denitrification, those of benthic $\delta^{13}C$ and trace metals are expected to reflect conditions prevailing in near-bottom waters. The most important and unexpected result obtained in the present study is that the environmental changes in the intermediate and bottom waters, very often occurred in opposite directions, probably caused by reorganization of the subsurface circulation, over the past climatic cycles. A relaxation/cessation of denitrification during the glacial periods and intensification during interglacial times, as suggested by earlier works, is confirmed by results of this study as well. Moreover, such periods also appear to be characterized by low and high values of Ba/Al, respectively, indicating that productivity changes contributed to changes in denitrification. Records of other redox-sensitive metals

exhibiting changes, are in agreement with the δ^{13}C record rather than with the δ^{15}N record, which is consistent with the assumption that oxygenation in the mesopelagic and benthic environments is not occurring in the same way.

Chapter 6 summarizes the major findings of the present study and makes recommendations for future research.

ACKNOWLEDGEMENTS

constant encouragement and positive attitude, which made me sustain cheerful moments at times of total darkness. I greatly appreciate the goodwill and support of my colleagues **Dr. Rahul, Sushant, Prashant, Ashish, Archana, Anand, Kalindi, Lalit, Anayat** and many more at NCAOR, Goa.

My very special thanks to **Dr. Thamban Meloth** for extending his support and providing me every freedom to work in the laboratory.

A special note of thanks is due to my uncle, **Mr. Thomas D'Souza** who has been the active motivator for all my scholastic career achievements.

I would like to apologize to all those not mentioned by name. I am sure without their timely help my work would not have been a success. I thank them one and all.

Once again I would like to take the opportunity to thank my **dear brother** for extending his full support and helping me especially in arranging all the references, and being focal in getting the thesis to a completion with lot of patience during the last few days before submission.

Last but not least I would like to thank my family members for their unending love, support, guidance and extreme patience at all times.

CHAPTER 1

Chapter 1

INTRODUCTION

1.1 General Introduction

The oceans, which cover 71% of the Earth, are inextricably involved and play a major role in the physical, chemical and biological processes that regulate the total Earth system. Climate is a major component of the Earth system that involves coupled interactions between the atmosphere, oceans, ice sheets, land surface and biota. Global changes in climate can occur due to astronomical or man-made factors. There is a great deal of concern about the human beings affecting the climate through the ongoing increase in the concentrations of greenhouse gases, mostly carbon dioxide (CO_2) (IPCC, 2007). How the oceans respond to these human-induced changes in the atmospheric CO_2 will, to a large extent, determine the Earth's surface environment in the times to come. The impending global warming underscores the urgent need to develop a coherent and rational approach to understand the climate system.

The Earth's climate undergoes natural variations on inter-annual and longer timescales. The human-induced climate changes are thus expected to be superimposed on a background of the natural variations and hence it is absolutely essential for us to understand the natural variability and the causative processes to be able to make reliable predictions for future climatic alterations. This, of course, includes the role played by the oceans.

The seafloor is the main site of deposition for most materials produced in the ocean or transported from land by air and water. The sediments thus preserve records of past changes in the climate and in other physical and biogeochemical processes. It is for this reason that sediment cores have long been utilized to reconstruct paleo-climatic variations. Over the past few decades, a number of proxies have been developed that provide a wealth of information concerning changes in various climatic and environmental variables. Biological, biogeochemical, geochemical and sedimentological proxies are the most commonly used ones for this purpose. Apart from the reliability of these proxies, the nature of site selected is very important for the interpretation of paleo-data. The preservation of the paleo-signal is strongly dependent on environmental conditions in sediments and overlying water column and on the rate at which sediments accumulate which also determines the temporal resolution. Sedimentary records from the continental margins generally provide a better understanding of past variations because of higher sedimentation rates relative to deep ocean basins and also due to the fact that the continental margins directly receiving materials from land, are sites of greater burial of organic and inorganic carbon, and are affected by coastal processes such as upwelling, generally higher biological production and hypoxia.

1.2 Peculiarities/unique features of the Indian Ocean

The Indian Ocean extends from the Tropic of Cancer to the shores of Antarctica. Although accounting for only 20% of the world's ocean surface, the

2

Indian Ocean possesses several unique features that make it a very important region for both global climate and biogeochemical cycling. This is largely due to its unusual geographical setting. A brief overview of the factors that distinguish the Indian Ocean from other oceans is given below.

1.2.1 Geographic settings – impact on climate and oceanographic processes

Unlike the Atlantic and Pacific, the Indian Ocean is blocked by land at low latitudes (~25°N) (Figure 1.1) because of which, the region north of the equator does not contain temperate or polar areas (i.e. it is essentially tropical). This unusual geographical setting drastically influences the climate of the region and results in a number of unusual, even unique features. For example, it is the only region of the world where the atmospheric and surface circulations reverse every six months. This phenomenon, known as the monsoons, is caused by the differential heating of land and sea. The monsoonal reversals introduce enormous seasonality in physical and biogeochemical processes. In the tropical ocean that is generally stratified, fertilization of surface layer with essential nutrients usually occurs through upwelling along the ocean's eastern boundary (e.g. off California and Peru in the Pacific, and Mauritania and Namibia in the Atlantic). In the Indian Ocean, by contrast, there are no equivalent upwelling zones along its eastern boundary (e.g. off Myanmar and Australia). Instead, the most intense upwelling here occurs seasonally [during the summer or southwest monsoon (SWM)] along the western boundary (off Somalia, Yemen and Oman) in the

3
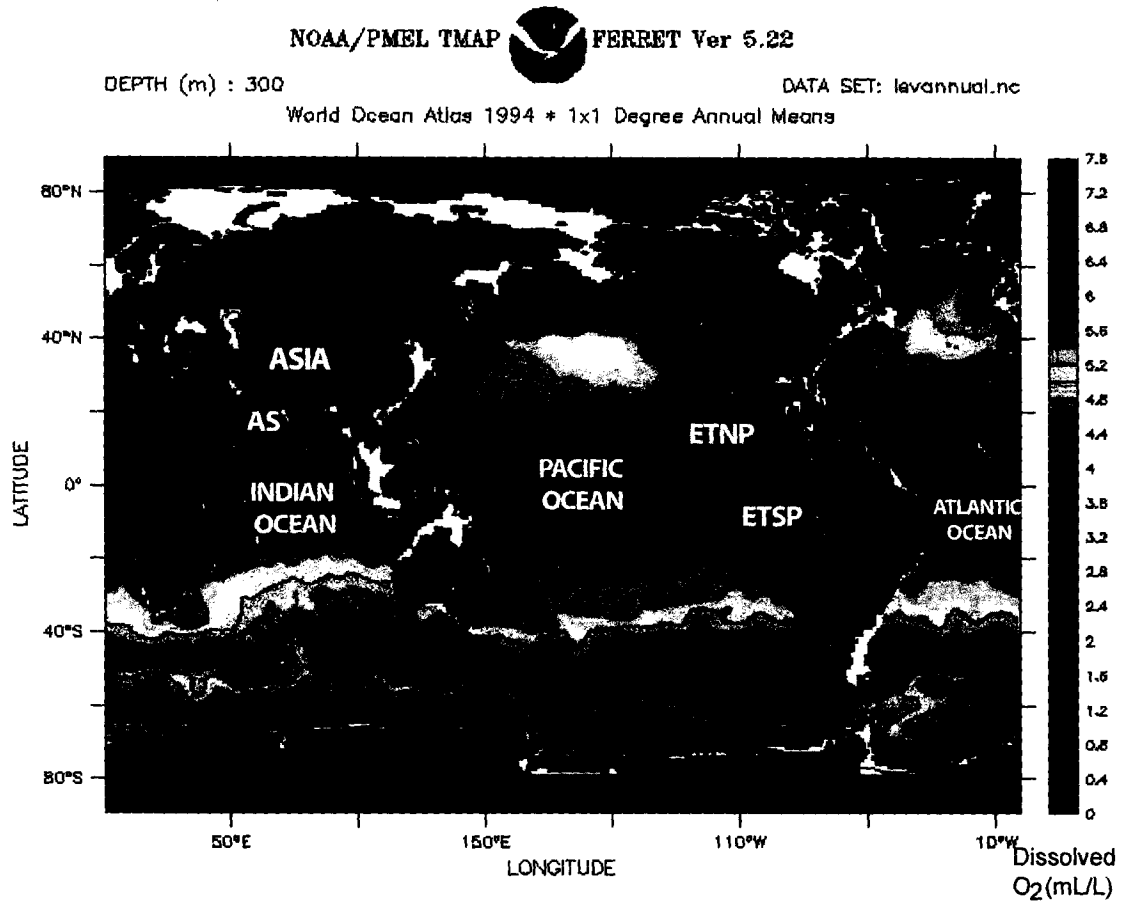
Figure 1.1: Figure showing the land locked Indian Ocean at low latitudes (~25°N), unlike the Atlantic and Pacific Oceans. Also shown are the major oxygen minimum zones of Eastern Tropical North Pacific (ETNP), Eastern Tropical South Pacific (ETSP) and Arabian Sea (AS).

northwestern part (the Arabian Sea) (Schott and McCreary, 2001 and references therein). This is because of different atmospheric and surface oceanic circulations. During the SWM strong winds blowing from the SW, forces the surface waters to move away from the coast replacing it with cold, nutrient-rich subsurface water. The upwelled water advects hundreds of kilometers from the shelf (please refer Figure 3.10 of Chapter 3). The resultant large-scale nutrient enrichment of the euphotic zones leads to extensive phytoplankton blooms (Naqvi et al., 2003). Fertilization of surface waters also occurs, albeit on a smaller scale, over a large area in the northern Arabian Sea during winter [the northeast monsoon (NEM)]. During this season, cold and dry winds of continental margin blow from the NE causing convection. Although this process is confined only to 100-125 m (Banse, 1984, 1987), it is sufficient to erode the upper portion of the thermocline, and since the nutrient concentrations are quite high at the depths to which convective mixing occurs, the resultant entrainment of nutrients in the surface layer is substantial (Madhupratap et al., 1996; Morrison et al., 1998; Naqvi, 2001). This again supports fairly extensive phytoplankton blooms (Banse and McClain, 1986; Wiggert et al., 2002; Naqvi et al., 2003). As a result of the diverse mechanisms that maintain large reflux of nutrients from the subsurface to surface waters, the annually averaged productivity in the Arabian Sea is comparable with that in the North Atlantic during the spring blooms (Barber et al., 2001). Thus the most productive part of the Indian Ocean is its northwestern portion rather than its eastern boundary.

Intermediate and deep waters of the oceans are formed through

cooling at mid and high latitudes. The lack of expanse of the Indian Ocean beyond the tropics in the northern hemisphere means that this process does not occur in the northern Indian Ocean. There are two sources of intermediate waters in the marginal seas, though – in the Red Sea and the Persian Gulf - where waters dense enough to penetrate the open ocean at depths of few hundred meters do get formed in winter but water densification in these areas is also aided by large rates of evaporation as these marginal seas are located in arid zones. Moreover, even though the outflows from these sources leave strong imprint on the salinity structure of the Arabian Sea, with the core layers identified by marked salinity maxima occurring at ~250 m for the Persian Gulf Water (PGW) and ~500 m for the Red Sea Water (RSW) (Wyrtki, 1971), their contribution to the water balance is not very large (Swallow, 1984). Furthermore, because of high salinity and relatively high temperatures, these water masses do not carry large amounts of dissolved oxygen (DO); Naqvi et al., (2007) estimate that, only ~10% of the oxygen used for subsurface respiration in the Arabian Sea is supplied by the PGW and RSW, with the remaining coming along with waters originating at south of the subtropical convergence. Because of the tortuous trajectories of their flow these waters lose most of the DO before reaching the Arabian Sea contributing to the formation of the thick, intense mesopelagic oxygen deficient zone (ODZ).

1.2.2 Oxygen deficiency in the oceans – its consequences

Surface seawater is generally well oxygenated everywhere in the oceans with DO concentrations normally close to the saturation values being

5

maintained by ocean-atmosphere interactions, photosynthetic activity and turbulence caused by winds, tides and waves. The DO concentrations in subsurface waters are determined by the balance between the physical supply (through advection and mixing) and removal for oxidation of organic matter (Wyrtki, 1962). In most parts of the ocean, the physical supply of oxygen is sufficient such that the water does not lose all of its DO content, even though a minimum in DO occurs in its vertical profiles representing the depth where the balance between the consumption and supply is more toward the former than at other horizons (Wyrtki, 1962). However, there are some areas where DO at the minimum reaches levels very close to zero (Deuser, 1975). Due to the difficulty in making precise DO measurements below about $0.1mL$ L^{-1}, the zones containing Winkler DO less than this nominal value are often called "oxygen-deficient". There are three major sites in the ocean where such an acute oxygen deficiency is observed in the water column; two of them lie in the eastern tropical Pacific Ocean whereas the third is located in the northern Indian Ocean (Figure 1.1). Smaller scale deficiency of similar magnitude also occurs off Namibia in the Benguela Current, but this is largely confined to the shelf (Calvert and Price, 1971).

The anomalous location of the zone of most intense oxygen deficiency (in the north rather than the east) is related to the combination of two above-mentioned peculiarities of the Indian Ocean: biological productivity is the highest in the north (especially in the Arabian Sea) and the subsurface layers in the northern Indian Ocean are largely ventilated from the Southern Hemisphere such that the age of the water at any horizon generally increases

northward. The combination of high oxygen demand and modest supply results in northward decrease in DO concentrations, especially across the Hydrochemical Front at about 10°S latitude (Wyrtki, 1973). The Front is formed due to the zonal flow in the upper kilometer such that cross equatorial water exchange is limited only to the western boundary of the Indian Ocean (i.e., off Africa; Swallow, 1984). Swallow (1984) called the complex equatorial current system to be a holding tank where intermediate waters of the southern origin lose their oxygen content before they enter the Arabian Sea. In the Arabian Sea, the DO content continues to decrease and north of about 12°N latitude, the approximate position of zero wind stress curl (Warren, 1994), within a layer below 100-150 m depth, the thickness of which generally increases northward, the DO concentrations are close to the detection limit (<1 µM, ~0.02 mL L^{-1}; Naqvi and Jayakumar, 2000; Codispoti et al., 2001). This makes the Arabian Sea the region with the thickest and the most intense oxygen minimum observed anywhere in the open ocean.

Due to the semi-enclosed nature of the North Indian Ocean, the ODZ impinges upon a very large area of the continental margin: bottom waters with O_2 < 0.5 mL L^{-1} (22 µM) and < 0.2 mL L^{-1} (9 µM), are estimated to cover about 1.15 x 10^6 and 0.76 x 10^6 km^2, respectively, of the marginal seafloor in the region, which amount to as much as 59 and 63%, of the corresponding global areas (Helly and Levin, 2004). Moreover, littoral countries of the North Indian Ocean approximately account for a quarter of the world's human population, which in conjunction with the ongoing rapid economic growth makes the region's coastal environments experiencing oxygen deficiency highly

vulnerable to human impact.

1.2.2.1 Geochemical impact

Water-column denitrification

As a consequence of the near absence of DO within the ODZ, the facultative bacteria switch over to nitrate (NO_3^-) as an oxidant for the degradation of organic matter, reducing NO_3^- to nitrite (NO_2^-) then to nitric oxide (NO), nitrous oxide (N_2O) and finally to molecular nitrogen (N_2). This reduction sequence, called denitrification, is a crucial biogeochemical process that compensates for the inputs of bio-utilizable combined or fixed nitrogen to the oceans through atmospheric deposition, N_2 fixation and river runoff; but for this process the atmospheric N_2 would be depleted in a few tens of million years (Deuser et al., 1978; Codispoti and Christensen, 1985; Codispoti et al., 2001). The rate of water column denitrification in the Arabian Sea is currently estimated to be around 35 Tg N y^{-1} (1 Tg = 10^{12} g), which is at least 1/3 of the global water column denitrification (Naqvi, 1987; Codispoti et al., 2001; Bange et al., 2005; Devol et al., 2006).

Denitrification invariably involves the accumulation of NO_2^-, the first intermediate formed through the reduction of NO_3^-. This feature often used as a diagnostic tool for locating denitrifying zones is called the secondary nitrite maximum (SNM). It is distinguished from the primary nitrite maximum by way of the associated DO levels (nearly zero). The primary nitrite maximum is found in the oxygenated part of the water column (close to the top of the thermocline/nitracline) where it is produced by two mechanisms - the

assimilatory reduction of NO_3^- by phytoplankton and the oxidation of NH_4^+ (nitrification) (Vaccaro, 1965; Wada and Hattori, 1971).

The geographical limits of the Arabian Sea denitrification zone have been delineated by Naqvi (1991) based on SNM. Operationally bounded by the 0.2 µM NO_2^- contour (Please refer Figure 3.3 of Chapter 3), the denitrifying zone is several hundred meters thick (maximum depth range 100-700 m), occupying the upper 1/2 to 1/3 of the ODZ, and spreading over an area measuring around 1.4 x 10^6 km^2 (Naqvi, 1994). Interestingly the denitrification zone lies outside the continental margins, and does not match with the most productive upwelling zones of the western Arabian Sea. Moreover, it has been pretty well defined and is fairly stable. Besides the Arabian Sea, the other areas with comparable SNM are the eastern-boundary upwelling zones in the eastern tropical South Pacific (ETSP) off Peru and Chile (Codispoti and Packard, 1980; Farias et al., 2007) and in the eastern tropical North Pacific (ETNP) off Mexico (Cline and Richards, 1972; Codispoti and Richards, 1976). Similar features with smaller volume but of greater intensity also occur off Namibia (Kuypers et al., 2005).

The SNM in the Arabian Sea, as in the ETNP (Cline and Richards, 1972), is associated with DO < 1 µM (Naqvi and Jayakumar, 2000; Codispoti et al., 2001; Naqvi et al., 2003). This threshold controls the reduction of NO_3^- to NO_2^-. The northern Indian Ocean contains a huge volume of water containing DO just below the threshold, and so a slight decrease in the DO concentration can potentially result in large increases in the rate of water

9

column denitrification. For example, the minimum DO concentration in the Bay of Bengal is no more than 2-3 μM lower than in the Arabian Sea. The Bay of Bengal is presently not denitrifying (i.e. it does not contain a SNM; Rao et al., 1994; Howell et al., 1997), but slight changes in circulation or productivity can turn this region denitrifying. The reason for the maintenance of DO concentrations just above the denitrification threshold in the Bay of Bengal is not clear. Naqvi et al. (1996) provided evidence for lower respiration rates in subsurface waters in this region compared with the Arabian Sea and suggested that, these were related to enormous inputs of lithogenic material by rivers that provides ballast to particulate matter such that it sinks rapidly through the water column with consequently smaller remineralization.

In addition to the perennial open-ocean denitrifying zone referred to above, oxygen deficient conditions also develop seasonally over the western Indian shelf. This process, first reported by Banse (1959) and Carruther et al. (1959), begins with the onset of upwelling in May following the reversal of coastal circulation. That is during the SWM the West India Coastal Current (WICC) is directed southward and the local winds are also upwelling favourable (Shetye et al., 1990). This makes the thermocline shoal up. But one unique feature of hydrography of this region is the presence of a warm, low salinity lens that is formed due to intense SWM rainfall in the coastal zone. The low density lens prevents the upwelled water from coming to the surface, resulting in very strong near-surface stratification. Respiration of locally-produced organic matter quickly removes all DO from the sub-pycnocline depth triggering vigorous denitrification that consumes all NO_3^- in

just about a month making the system sulphate reducing. This shallow suboxic zone is not contiguous to the larger open ocean system. However, despite the high specific rates the overall denitrification rate over the Indian shelf is only about 10% of the rate in the open ocean suboxic zone (Naqvi et al., 2006a,b). It is believed that the shallow water oxygen deficiency has undergone intensification in recent years presumably due to increased loading of fertilizers from land (Naqvi et al., 2000, 2006a,b).

Recently, Devol et al. (2006) have made direct measurements of denitrification rates in both the open ocean and coastal suboxic zones through incubations of water samples spiked with $^{15}NO_3^-$. Their data show higher rates $(21.6 \pm 46.8$ nM d^{-1}) for coastal suboxic zone than for open ocean $(8.8 \pm 3.8$ nM d^{-1}), reflecting greater amount of organic carbon availability and higher temperatures over the shelf. The overall rates for the open ocean are consistent with the rates estimated previously from NO_3^- deficits (the deficiency in NO_3^- with reference to the concentration expected from the Redfield stoichiometry) (Naqvi, 1987) or from the activity of the respiratory electron transport system (ETS) (Naqvi and Shailaja, 1993). In the coastal region, however, the rates are lower than those suggested by the observed $^{15}NO_3^-$ loss (Naqvi et al., 2006a,b). Devol et al. (2006) also measured the N_2/Ar ratio in the open ocean and observed large increases in the ratio within the SNM. Unexpectedly, the N_2 "excess" computed from the N_2/Ar data are much higher (up to twice) than the corresponding NO_3^- deficits. Although it is possible that sedimentary denitrification contributes to some extent to the observed N_2 excess, the two potentially more important processes causing

the discrepancy are anammox (anaerobic ammonium oxidation: $NO_2^- + NH_4^+$ → $N_2 + 2H_2O$) and mineralization within the ODZ of organic matter produced by nitrogen fixers that has non-Redfieldian elemental composition (N:P >> 16) (Codispoti et al., 2001; Devol et al., 2006). It may be pointed out that anammox is a recently discovered process that in some areas has been found to be the dominant pathway of NO_3^- loss in suboxic environments (Kuypers et al., 2005; Thamdrup et al., 2006). The importance of this process in the Arabian Sea is still uncertain inspite of a recent report (Nicholls et al., 2007).

Nitrous oxide cycling

N_2O is a by-product of nitrification and an intermediate of denitrification (i.e. it is both, produced as well as consumed during the reduction of NO_3^- to N_2). Denitrification is, of course, an anaerobic process, and so it's associated cycling is dependent on the ambient DO levels. Low DO concentrations affect the yield of N_2O via nitrification as well; that is, the N_2O/NO_3^- ratio increases as the DO approaches suboxia (Goreau et al., 1980). In well-oxygenated water columns, the surface waters are slightly super saturated with respect to atmospheric N_2O, with a small flux to the atmosphere (Weiss, 1978; Butler et al., 1989). Yoshinari (1976) demonstrated that the depth profile of N_2O is a mirror image of the DO profile, and interpreted this observation to indicate nitrification as the dominant production mechanism. In the Indian Ocean, surface waters of the Arabian Sea have been found to exhibit unusually high degree of supersaturation, especially during the periods and within the zones of upwelling. The reported values are: 330% off Somalia (De Wilde and Helder, 1997), 230% off Oman (Bange et al., 1996) and 8,250% off India

(Naqvi et al., 2005). The unusually high supersaturation observed by Naqvi et al. (1998, 2000, 2006a,b) in coastal waters off western India during the period of suboxia have been proposed to arise from denitrification. By contrast, in the open ocean suboxic zone N_2O profiles invariably exhibit a minimum within the SNM sandwiched between two maxima at the peripheries of this feature (Naqvi and Noronha, 1991; Naqvi et al., 1998). In areas where the SNM is not present (e.g. in the western and southern Arabian Sea and the Bay of Bengal), a single broad maximum in N_2O is observed (Naqvi and Noronha, 1991; Naqvi et al., 1994; Bange et al., 2001). Thus the concentrations and even distribution pattern of N_2O in oxygen depleted waters are quite variable, and changes in the DO field can greatly alter the water column inventory of N_2O and its flux to the atmosphere. Overall, since the ODZ like those found in the northern Indian Ocean, are conducive for vigorous production as well as consumption of N_2O, but overall serve as strong net sources of this important greenhouse gas (Cohen and Gordon, 1978; Elkins et al., 1978; Codispoti and Christensen, 1985; Nevison et al., 2003; Naqvi et al., 2005), an expansion of these zones is expected to lead to an increase in its emission to the atmosphere.

Sedimentary Respiration

The areas having pronounced ODZs are distinguished by the accumulation of organic matter (OM) in the underlying sediments, and this applies to the northern Indian Ocean as well (Paropkari et al. 1993a,b). The reason for this has been a subject of considerable debate in the literature, though. This is because the ODZs are generally regions of high productivity,

and so the rate of deposition of organic matter at the seafloor is higher. On the other hand, low DO in bottom waters overlying the continental margin sediments is expected to favour greater preservation of organic matter. While Pedersen et al. (1992, 1993), favoured the production hypothesis, Paropkari et al. (1993a,b) emphasized the role of preservation of organic matter in the Arabian Sea sediments. The two hypotheses, however, are most likely not mutually exclusive. The availability of large amounts of organic matter in continental margin sediments is believed to fuel high benthic respiration rates, both aerobic and anaerobic (denitrification and sulphate reduction). Since the organic-rich shelf and slope sediments are generally reducing, they are expected to support high anaerobic respiration rates. The few data on denitrification (Naik and Naqvi, 2002) and sulphate reduction (Schmaljohann et al., 2001) rates, that are available from the Arabian Sea, however, indicate that the sedimentary respiration rates are well within the ranges reported from other areas.

Redox Sensitive Elements

In addition to nitrogen, reducing conditions in the ODZs also affect cycling of several other polyvalent elements. Such redox-sensitive elements include manganese (Mn), iron (Fe), molybdenum (Mo), cadmium (Cd), cobalt (Co), copper (Cu), vanadium (V) and iodine (I). For example, dissolved Mn (II) concentrations rise abruptly due to the reductive solubilization of particulate Mn hydroxides (Lewis and Luther, 2000), when DO concentration levels fall below the suboxic threshold. Diffusion of Mn (II) into the water column also occurs from the reducing continental margin sediments (Saager et al., 1989;

Lewis and Luther, 2000). When reduced Mn enters the oxic zone from the suboxic/anoxic environment, it quickly gets oxidized to insoluble Mn (IV). Fe (II) also follows a similar pattern (Saager et al., 1989). In contrast, Cd, Co and Mo get precipitated in suboxic environments and are solubilized in oxic environments. These elements have been found to accumulate in sediments under suboxic conditions irrespective of whether the water column is oxic or suboxic (Klinkhammer and Palmer, 1991; Rosenthal et al., 1995a; van Geen et al., 1995; Crusius et al., 1996; Nameroff et al., 2002) and under anoxic conditions (Anderson et al., 1989a,b; Emerson and Huested, 1991; Colodner et al., 1993, 1995). As a consequence of the low DO levels in the Arabian Sea, the cycling of redox sensitive elements is expected to be different from the more common oxic environments.

1.2.2.2 Biological effects

Oxygen depletion in the water column affects the behaviour of marine organisms below DO levels of ~60 μM (Howell and Simpson 1994). The intense oxygen deficiency occurring within the ODZs exerts a strong influence on the abundance and composition of marine organisms in the mesopelagic realm. For example, in the ETNP as well as in the Arabian Sea, most zooplanktons are excluded from the ODZ, due to their inability to cope up with suboxic conditions (Wishner et al., 1998; Morrison et al., 1999). The majority of marine organisms migrate to other oxic environments. In the open Arabian Sea, the fraction of total biomass (0–1000 m) that migrates into the upper layer (0–100 m) at night has been found to be the lowest at locations having

the most pronounced oxygen minimum (Wishner et al., 1998). In a diurnal study carried out by Madhupratap et al. (1990) close to the shallow time-series site monitored in this study, zooplankton counts and biomass within the oxic mixed layer were found to be much higher than in the oxygen depleted subsurface waters.

When the ODZ shoals up to within the euphotic zone, as happens over the Indian shelf, a very interesting phenomenon occurs. The oxygen-depleted waters contain nutrients in high concentrations; yet, the photosynthetic production rate, measured with the radiocarbon technique, is very low even when these waters are well within the euphotic zone (e.g. Naqvi et al., 2003, 2006a). This has been ascribed to the inability of "normal" phytoplankton (e.g. diatoms) to function in waters with very low ambient DO because they require oxygen for their metabolism (Naqvi et al., 2006a). This is despite the fact that phytoplankton produce oxygen during photosynthesis. However, some cyanobacteria can probably survive in low oxygen waters (Goericke et al., 2000), and when the system turns anoxic, some primary production can still be carried out by anoxygenic photosynthetic organisms (Repetta et al., 1989). Unfortunately, nothing is known from the Arabian Sea about such autotrophs.

When the system turns completely anoxic, NH_4^+ becomes the dominant form of combined nitrogen fuelling new primary production (Naqvi et al., 2000, 2006a). This is an unusual situation because new production in the ocean is almost always supported by NO_3^-. It is believed that diatoms require NO_3^- for their healthy growth and the presence of NH_4^+ in high concentrations has an inhibitory effect on NO_3^- uptake (Dugdale et al., 2002). However, although the

composition of phytoplankton was somewhat different, diatoms were found to be by far the dominant micro phytoplankton group at stations experiencing complete anoxia over the Indian shelf (Naqvi et al., 2006a).

Chemical and biological processes within the sediments and at the sediment-water interface contribute significantly to oceanic biogeochemical cycles, especially in the Arabian Sea due to its uncommon geographical setting. When the entire continental shelf off India gets enveloped by subsurface/bottom waters with $O_2 < 0.5$ mL L^{-1}, as observed by Naqvi et al., (2000), the benthic fauna gets profoundly impacted. Among the first to notice this effect were Carruthers et al. (1959) who reported an absence of benthic animals off Bombay at depths where DO content of the bottom water was < 0.5 mL L^{-1}.

The most important impact of the oxygen deficiency in coastal waters is on fisheries, which is an important source of protein and one of the key commercial activities for the coastal population. This aspect has, not surprisingly, received a great deal of attention (e.g., Banse, 1959, 1968; Carruthers et al., 1959; Hida and Pereira, 1966). Analyzing the fish landing data for Goa during the period 1995-2001, Naqvi et al. (2006a) reported a substantial decrease in the demersal fish catch over the past few years. However, a similar significant decline was not observed in case of pelagic fishes and hence Naqvi et al. (2006a) concluded that the onset of anoxic conditions (appearance of hydrogen sulphide) could be the main cause of the declining demersal fish catch. Besides the adverse impact on fisheries, the oxygen deficiency is also known to result in fish mortality when the fishes are

unable to escape from the anoxic upwelled waters. For example, Naqvi et al. (1998) and Ramaiah et al. (2005) recorded instances of fish mortality off Kerala during the upwelling season apparently caused by asphyxiation.

1.3 Role of nitrogen in climate control

Nitrogen is a major component of atmosphere and an essential nutrient for all forms of life. It is a polyvalent element that occurs in oxidation states ranging from 3– to 5+ (Table 1.1). Among all species of nitrogen, NO_3^- is the most oxidized form, while NH_4^+ is the most reduced one. N_2 is by far the most abundant chemical species and the major constituent of the Earth's atmosphere. N_2O is the next most abundant species of nitrogen in the atmosphere. It is an important trace gas that plays a significant role in global warming and stratosphere ozone depletion. Aside from its reaction with ozone in the stratosphere, N_2O is quite inert in the atmosphere and also in the surface layer of the ocean. However, since it is an intermediate of the redox chemistry of the nitrogen system, it gets involved in chemical transformations where rapid changes in oxidation state of nitrogen take place (e.g. in soils and subsurface waters). However, in spite of its large abundance in the atmosphere (as N_2), biological productivity both on land and in the ocean is often nitrogen-limited. This is because, few plant species of autotrophs (cyanobacteria) are capable of using (fixing) it. The species that can be readily utilized by plants are combined inorganic forms such as NO_3^- and NH_4^+, the former being the most abundant form of fixed nitrogen in nature, and organic forms such as urea $((NH_2)_2CO)$.

Table 1.1

Common species of marine nitrogen and its oxidation states.

Species	Molecular formula	Oxidation number of nitrogen
Nitrate ion	NO_3^-	5+
Nitrite ion	NO_2^-	4+
Nitrous oxide gas	N_2O	1+
Nitric oxide gas	NO	2+
Nitrogen gas	N_2	0
Ammonia gas	NH_3	3-
Ammonium ion	NH_4^+	3-
Organic amine	RNH_2	3-

An important component of the oceanic nitrogen cycle (Figure 1.2), is the uptake of combined nitrogen by phytoplankton in the euphotic zone, mostly as NO_3^-. But since, N in the biological materials is present in the most reduced (3-) form (as amino nitrogen), NO_3^- must first be reduced, and most plants are enzymatically equipped to carry out this (assimilatory) reduction. The organic matter produced by plants is eventually remineralized by the heterotrophs, and N is first released as NH_4^+ that is oxidized by nitrifiers to NO_3^-, with NO_2^- as one of the intermediates and N_2O as a byproduct (Figure 1.2; Codispoti and Christensen, 1985). If there were no other process, the entire N in nature would eventually be converted to NO_3^- because the Earth's surface environment is mostly oxidizing. This is not the case as reducing conditions also develop on account of bacterial oxygen consumption in soils, oceanic sediments, and in waters, both on land and in some parts of the ocean, as stated above. Within these reducing environments, NO_3^- is utilized as an oxidant for the degradation of organic matter by heterotrophic microbes. This process known as denitrification completes the N cycle as it leads to the production of gaseous N, mostly N_2 and to a lesser extent N_2O (Figure 1.2). More recently, another pathway of N_2 production (anammox) has been discovered (Strous et al., 1999). It involves the reaction of NO_2^- with NH_4^+ ($NO_2^- + NH_4^+ \rightarrow N_2 + 2H_2O$). Unlike denitrification, anammox is an autotrophic process. Its significance in N_2 production is being increasingly realized (Dalsgard et al., 2003; Kuypers et al., 2003, 2005; Thamdrup et al., 2006).

Irrespective of the production pathway, N_2 produced in the anaerobic
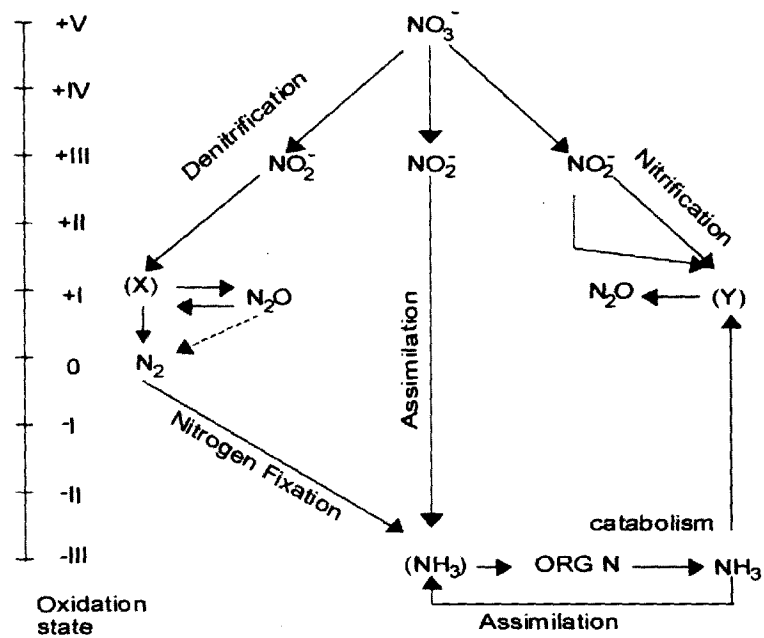
Figure 1.2: A view of the oceanic nitrogen cycle (adapted from Codispoti et al., 2001). The intra-cellular intermediates that do not appear to accumulate in seawater are represented with (X) and (Y) denotations. Modifications have been done in the diagram to suggest the production of N_2O as well as its consumption during denitrification.

environments on land and ocean keeps its inventory constant on the geological time scales. In the oceans too, the inventory of fixed nitrogen should attain some kind of a steady state over long-enough time scales. That is, net inputs of fixed N to the ocean through N_2 fixation (the major fixed N source in spite of the inability of prokaryotes to carry out this process), atmospheric deposition and river runoff should balance the net loss, most of which occurs through sedimentary and water column denitrification, with some permanent burial in sediments and even smaller emission of N_2O to the atmosphere. Whether or not such a steady state exists in today's ocean is a matter of intense ongoing debate. While Gruber and Sarmiento (1997) and Gruber (2004) believe that the marine fixed nitrogen budget is close to balance, the current best estimates of the various input and sink terms suggest a grossly off-balance budget with the losses exceeding the inputs by >200 Tg N y^{-1} (Table 1.2; Codispoti et al., 2001). Obviously, such a large imbalance cannot be sustained over long periods of times because it would result in a substantial change in the oceanic combined N inventory and its isotopic composition (see below), for which there is no evidence in the recent (past few thousand years) sedimentary record (Altabet, 2006). However, as pointed out by Codispoti (2007), the data used to generate the current fixed N budget have been collected only in the last few decades, and it is possible that these represent an anthropogenically altered N budget which would not have created a sedimentary imprint yet.

The major loss terms in the fixed nitrogen budget are dependent on the oxygen distribution in the ocean (for water column denitrification) as well as

Table 1.2

Marine combined nitrogen budget (from Codispoti et al., 2001).

Process	Gruber and Sarmiento (1997) 10^{12}g N yr^{-1}	Codispoti et al. (2001) 10^{12}g N yr^{-1}
Sources		
Pelagic N_2 fixation	110 ± 40	110
Benthic N_2 fixation	15 ± 10	15
River input (DN)	34 ± 10	34
River input (PON)	42 ± 10	42
Atmospheric deposition (Net)	30 ± 10	30
Atmospheric deposition (DON)		56
Total Sources	231 ± 44	287
Sinks		
Organic N export		1
Benthic denitrification	95 ± 20	300
Water column denitrification	80 ± 20	150
Sedimentation	25 ± 10	25
N_2O loss	4 ± 2	6
Total Sinks	204 ± 30	482

the sea level (which determines the area of the continental margins where most of the sedimentary denitrification occurs). Both of these undergo changes associated with climatic cycles. It is therefore almost certain that, the loss term is variable on geological time scales. Evidence for this can be found in the sedimentary record, as summarized below and also to be provided in Chapters 4 and 5 based on the results of the present study. The crucial question is whether or not the input terms (largely N_2 fixation) also keep pace with these changes in the oceanic denitrification rate? There is growing realization that denitrification and N_2 fixation may, in fact, be tightly coupled. This is because denitrification produces a pool of excess phosphate (relative to the Redfield N:P ratio of 16:1; Redfield et al., 1963) that should stimulate N_2 fixation (Deutsch et al., 2007; Naqvi, 2007), such that increases in oceanic denitrification rate would be accompanied by enhanced N_2 fixation in the oceans. Whether or not this occurred in the past is not clear at this point of time. If the changes in the denitrification rate were not compensated quickly enough by N_2 fixation, a change in oceanic fixed N inventory would occur (Altabet, 2007). This would affect the rate of primary production.

The possible link between changes in the oceanic fixed N inventory and climatic cycles was first postulated by McElroy (1983) in order to explain the cyclic changes in atmospheric CO_2 as revealed by the analysis of air trapped in polar ice caps (the atmospheric CO_2 has been lowered by ~100 ppm during peak glacial periods as compared to the interglacial times during past few hundred years of Earth's history for which the ice-core data are available; see, for example, Petit et al., 1999). The hypothesis is essentially

based on the observation that, in large areas of oceans where the upper water column is stratified (generally in the tropics) fixed nitrogen is nearly depleted in the euphotic zone, thereby limiting primary production (Codispoti, 1989). The production of particulate organic matter and its export to the deep sea (the biological pump) is a key process that is responsible for the sequestration of CO_2 from the atmosphere. Changes in the fixed N inventory would thus affect the strength of the biological pump thereby changing the atmospheric CO_2 content and global climate. Specifically, sequestration of CO_2 from the atmosphere may decrease when losses of combined nitrogen through denitrification exceed inputs from N_2 fixation, plus supply from land and atmosphere; while during the period of weak pelagic and sedimentary denitrification, fixed nitrogen would accumulate in the ocean, stimulating photosynthesis in turn lowering the atmospheric CO_2. While the former situation is suggested to have prevailed during the interglacials, the latter would apply to glacial times (McElroy, 1983; Altabet et al., 1995, 2002; Ganeshram et al., 1995, 2000).

1.4 Previous Studies

1.4.1 Water column denitrification in the Arabian Sea

The severe oxygen depletion in subsurface waters of the Arabian Sea was first observed during the John Murray Expedition (1933-34) and Gilson was the first to investigate nitrogen cycling in the region (Gilson, 1937). Surprisingly, this work was not followed up by more detailed studies for several decades, probably because of the outbreak of the Second World War

and the subsequent political changes, but despite few observations, the Arabian Sea has long been recognized as a site of water column denitrification [as mentioned by Richards (1965) in his classical treatment of anoxic basins and fjords]. The International Indian Ocean Expedition (IIOE; 1962-65) resulted in the generation of a large amount of data, including on dissolved inorganic nitrogen, mostly NO_3^- and in some cases NO_2^-, but these data were largely used to prepare maps showing the distributions of oxygen and NO_3^- along various horizontal and vertical planes (Wyrtki, 1971). Some of these data, along with new observations, were used by Sen Gupta and his coworkers, who made the first concerted effort to specifically address the Arabian Sea denitrification problem (Sen Gupta et al., 1976a,b). Shortly afterwards Deuser et al. (1978) provided the first estimate of the rate of water column denitrification in the region (0.1-1 Tg N y^{-1}). The two groups quantified NO_3^- deficits resulting from denitrification following different approaches: a Redfield stoichiometry-based approach by Sen Gupta et al. (1976a,b) and coworkers and NO_3^--salinity relationship by Deuser et al. (1978). Naqvi et al. (1982) evaluated the two approaches and found that the method of Deuser et al. (1978) underestimated NO_3^- deficits. Subsequent studies by Naqvi and others focused on refinement of methods for estimating NO_3^- deficits (Naqvi and Sen Gupta, 1985; Naqvi et al., 1990; Codispoti et al., 2001), demarcation of the Arabian Sea denitrification zone (Naqvi, 1991; Naqvi et al., 2000), quantification of denitrification rates from box models (Naqvi, 1987), activity of the respiratory electron transport system (ETS) (Naqvi and Shailaja, 1993) and on deck incubations (Devol et al., 2006) and N_2O cycling (Naqvi and

Noronha, 1991; Patra et al., 1999). The salient results of these studies are as follows:

1. The perennial, open ocean denitrification zone of the Arabian Sea is a fairly well-defined and stable system that does not seem to have undergone any discernible change over the past three to four decades for which reliable data are available. This zone is anomalously located in that; it is geographically separated from centres of the most intense upwelling regions (i.e. off Somalia and Oman).

2. Contrary to earlier belief, the oxygen-deficient waters are renewed quickly (τ < 10 y), accounting for the short term temporal changes even within the core of the SNM.

3. Rate of water column denitrification in the open suboxic zone has been found to range from 10 to 44 Tg N y^{-1}, with most recent estimates closer to the upper end of this range. Thus water column denitrification in the Arabian Sea is globally highly significant.

4. The N_2/Ar ratio confirm the presence of large excess of N_2 with the N_2 anomalies far exceeding NO_3^- deficits.

5. The severe oxygen deficiency leads to rapid turnover of N_2O with the Arabian Sea serving as a strong net source of this gas to the atmosphere.

6. In addition to the perennial open ocean suboxic zone, severe depletion of oxygen also occurs in bottom waters over the Indian shelf during late summer and autumn. Although the rate of denitrification in this shallower system is modest, the rate of production of N_2O – mostly through denitrification is disproportionately very large.

Due to the above mentioned rapid renewal of waters within the Arabian Sea ODZ, substantial inter-annual and even intra-annual changes in the extent of denitrification have been recorded (Naqvi, 1987; Naqvi et al., 1990). For example, Naqvi et al. (1990) found substantial oscillations on a seasonal scale in denitrification along the Indian continental margin. This was attributed to the presence of an undercurrent that supplies oxygen to intermediate layers in this region; and as this supply is associated with the SW Monsoon circulation; lower deficits were found during this season. However, direct observations of these changes have been limited to the last 3-4 decades. In order to investigate variability of the process on geological time scale, one has to inevitably turn to the geological record. The present study is largely concerned with such changes.

1.4.2 Paleo-Climatic studies in the Arabian Sea

A comprehensive paleoclimatic/ paleoceanographic data set and information are available from the western and northwestern Arabian Sea (Prell et al., 1980; Prell, 1984a,b; Prell and Van Campo, 1986; Clemens and Prell, 1990; Anderson and Prell, 1993; Sirocko et al. 1993, 1996, 2000; Reichart, 1997, Naidu and Niitsuma, 2003; Naidu, 2004; Higginson et al. 2004). For the first time century scale variations in SW monsoon intensity were observed by Sirocko et al. (1993) during the past 24 Ky in a sediment core - 74 KL, from western Arabian Sea. Later using various biogenic and geochemical proxies, history of the SW monsoon has been deciphered by several workers (Emeis et al. 1995; Rostek et al. 1997; Reichart, 1997; Naidu,

1998). Moreover in the western Arabian Sea, using sedimentary $\delta^{15}N$, Altabet et al. (1995) observed synchroneity between past variations in denitrifcation and other hydrographic and oceanographic features such as sea surface salinity, temperature and surface productivity during glacial-interglacial transitions. All these studies indicated the surface productivity in the western and northwestern Arabian Sea during the late Quaternary period to be primarily controlled by changes in wind intensity associated with the summer (SW) monsoon. Biogenic proxy records of upwelling and surface productivity also inferred that, monsoon intensity varied in phase at periodicities near the earth's precessional cycle (23 Ky) for the last 140 Ky (Prell and Van Campo, 1986). Adding to all these studies, Clemens and Prell, (2003) created two very similar multiproxy records viz - Summer-Monsoon Stack (SMS) and Summer-Monsoon Factor (SMF), of summer-monsoon variability for 350 Ky time period; by combining five individual summer-monsoon proxies (biological, isotopic, geochemical and physical) from the Northern Arabian Sea using stacking and principal component analysis (PCA). These multi-proxies, SMS and SMF were found to be spectrally very similar, dominated by variance in the 41-Ky (obliquity) and 23-Ky (precession) bands with very little variance at the 100-Ky (eccentricity) band associated with large-scale changes in global ice-volume. Denitrification intensity in Arabian Sea has also been reported by Reichart et al. (1998); Ganeshram et al. (2000); Suthhof et al. (2001); Banakar et al. (2005). Sirocko et al. (1993) and Reichart, (1997), reported records of continental aridity employing elemental proxies such as Ti/Al and Mg/Al from the western and northwestern regions of Arabian Sea. Studies

from these regions later also revealed the teleconnections between sub-tropical monsoon and high latitude climate (Sirocko et al. 1996; Naidu and Malmgren, 1995; Schulz et al. 1998). Among monsoon oriented studies in the northern Arabian Sea, some detailed studies have focused on the variation of Oxygen Minimum Zone of the northern Arabian Sea (Murray Ridge, Off Oman and Pakistan Margins; Reichart et al., 1997, 1998, 2002 respectively). Apart from the variability and intensity of summer monsoon, surface productivity and sub-surface denitrification; the bottom water redox conditions also gets influenced by the export flux of organic matter. To understand these effects, Somayajulu et al. (1994), Tribovillard et al. (1996), Morford and Emerson (1999); employed several trace elements (such as Mn, Cr, V, Ni, Zn, Mo, U, Re and Cu) to track past changes in the bottom water redox conditions under which they had been precipitated/ migrated.

Similar to the availability of paleoclimatic record from the western and northwestern Arabian Sea, the eastern Arabian Sea is also expected to provide and have indeed furnished clues to past monsoon changes in terms of surface productivity, sub-surface denitrification and bottom water redox conditions. Moreover, recently, the eastern Arabian Sea has received increased attention after the realization that it is a potential source of atmospheric N_2O (a green house gas), a future threat to global climate (Patra et al. 1999; Naqvi et al. 2000 and references therein).

The first detailed paleoclimatic/ paleoceanographic study in the eastern Arabian Sea was by Duplessy (1982). Using $\delta^{18}O$ of planktonic foraminifera, he showed that the SW monsoon was much weaker during the last glacial

maximum (LGM, ~18 Ka BP) than present; whereas, the NE monsoon was much stronger. Later, Sarkar et al. (1990) corroborated these findings using $\delta^{18}O$ of surface dwelling foraminifera and other geochemical proxies. Sonzogni et al. (1998) used the alkenone method to estimate sea surface temperatures from as many as twenty deep-sea sediment cores raised from the tropical Indian Ocean, (of which five cores were from the eastern Arabian Sea) and concluded that the tropics were about 1.5-2.5 °C colder during the last glacial period. In conjunction with the oxygen isotope stratigraphy, Prabhu et al. (2004) has also discussed about the longest pollen record (200 Ky) from the eastern Arabian Sea. They concluded a reduction in SST by ~2 °C during the glacial periods together with a rise in salinity of 1 psu due to lessened fresh water input to the Arabian Sea as a result of weakened southwest monsoon and strong northeast monsoons. Besides the above mentioned records, there are a number of studies pertaining to $\delta^{18}O$ carried out on different species of planktic and benthic foraminifers, which delivers detail inferences about the Holocene monsoon record from the eastern Arabian Sea (Sarkar et al. 2000, Thamban et al. 2001; Agnihotri et al. 2003a; Tiwari et al. 2005a; Tiwari et al. 2006). Simultaneously, studies have also been carried out by various researchers on the eastern Arabian Sea using proxies such as C_{org}, $CaCO_3$, SiO_2, $\delta^{15}N$ and trace metals.

C_{org}, a traditional proxy for surface productivity has shown inconsistent behaviour from region to region during glacial-interglacial transition (Sirocko et al. 2000, Thamban et al. 2001; Agnihotri et al. 2003b) and hence its application to construct the paleo-productivity has remained a controversial

topic in case of sediments from the Arabian Sea. Sarkar et al. (1993) observed a significant C_{org}, enhancement during the LGM (known to be a period of low productivity) from a southeastern Arabian Sea sediment core and attributed this to better preservation due to prevailing anoxic conditions in bottom waters based on uranium enrichment. However, using organic indicators of bottom water redox conditions, Schutle et al. (1999) did not find any appreciable signatures of anoxicity in bottom waters for sediment cores collected from the northeastern (off Pakistan) and southeastern (close to Maldives) Arabian Sea in the last ~330 Ky, and assigned the accumulation of organic carbon to be controlled mainly by primary productivity. Emeis et al. (1995), however found it difficult to interpret C_{org} accumulation rate in terms of surface productivity changes in the northwestern Arabian Sea, where the depth profiles of C_{org} accumulation was found to be significantly affected by variations in sedimentation rates. Due to this problem, Emeis et al. (1995) and Schulz et al. (1998) emphasized that C_{org} concentration is a better indicator of surface productivity rather than its accumulation rate. Based on a multiproxy approach (C_{org}, organic nitrogen, $CaCO_3$, Sr and Ba) for three cores from eastern and southeastern Arabian Sea, Agnihotri et al. (2003b) deciphered decreased surface productivity during LGM in agreement with records of Pattan et al. (2003). Recently Banakar et al. (2005), however has reported increased productivity during the LGM period as observed from high concentrations of marine C_{org}, Σalkenones and C_{org} flux for a core collected from the eastern Arabian Sea (off Goa). Examining the response of denitrification with productivity variation, they observed a decoupling between

the two for the LGM period, while they covaried during other climatic periods. The reduced LGM denitrification inspite of increased productivity was attributed to effective ventilation of the EAS- thermocline by the intensified formation of Arabian Sea High Salinity Waters (ASHSW) in the northern Arabian Sea, resulting in well sustained oxygenation throughout the LGM. Recently, a study on the variability of primary productivity and OMZ intensity at millennial scale was reported by Singh et al. (2006), from a core collected along the western continental margin of India (water depth 200m).

Inspite of all the investigations from eastern Arabian Sea, there still exist a scarcity of data for inferring the presence and variations of OMZ during the past. Though few studies have furnished the same with a single proxy (for e.g. enrichment of Uranium by Sarkar et al., 1993), a multiproxy approach is lacking.

Also, not many studies on the variation of oxygen concentrations in the past have been taken up along the Western Continental Margin of India and the coastal areas. The deposition of sediments along the continental shelf and slope regions is controlled by paleo-topography of the late Pleistocene, sea-level fluctuations, monsoon intensity and sediment input from rivers (Narayana et al. 2005). As these areas focuses on the shallow region suboxic environments developed due to the ongoing anthropogenic activities, the sedimentary records from continental margins with shallow water depth would help as an ideal archive to study various sedimentary processes for deciphering the past fluctuations in the climate and environmental systems on a decadal to centennial timescales.

Initial studies along the West Coast of India started with Murthy et al. (1969), reporting the distribution of organic matter in the marine sediments. Further investigations on organic carbon and inorganic geochemistry from the western continental margin of India, led Marchig, (1972) towards two main observations of (1) Fe and Ti to be concentrated in the lithogenic, quartz-rich and coarse-grained sediments of the shelf and upper slope, and (2) while Mn, Ni, Cu, and Zn mostly associated with the clay mineral-rich, fine-grained sediments of the lower slope and deep ocean. These studies were then followed by Paropkari et al. (1978, 1987, 1993a), focusing on environmental controls on the distribution and enrichment of organic carbon along the continental marginal sediments, attributing the preservation of organic carbon mainly to bottom water anoxia. However, all Paropkari et al., studies were based on surficial sediment samples. Later, Narayana and Singh (1997) reported 4 - 5 episodes of intense upwelling at different time intervals, in a core collected from the inner shelf off Mangalore, based on $CaCO_3$, organic matter and percentage of planktic foraminifers (Globigerina bulloides and Globigerinata glutinata) proxies. Pandarinath and Narayana (1998) studied inner shelf surficial sediments off Coondapur, West coast of India with respect to the distribution of 12 elements (Al, Ca, Fe, Mn, Ti, Cu, Ni, Cr, Pb, Zn, Co and V), and concluded the inner shelf environment to be unpolluted.

Recently Agnihotri et al. (2007, a study based on a core collected from the inner shelf region off Goa, from a water depth of ~45 m) found the marine productivity to be in tandem with external solar forcing throughout the core. Intensity of subsurface denitrification was also found to be dominantly

controlled by surface productivity prior to anthropogenic period (~700 to 150 years BP). However a decrease in denitrification was observed after ~150 yrs BP in contrast to the increased productivity. The change in denitrification trend could be an artifact of dilution of sedimentary signal by isotopically lighter nitrogen supply from land or higher current rate of denitrification, that it didn't leave its heavy isotope imprint on sedimentary nitrogen. They also recorded decrease in sedimentary $\delta^{15}N$ during the Little Ice Age (LIA) due to lower productivity most likely induced by a weakened summer monsoon.

In general, the geochemistry of surface Arabian Sea sediments is reasonably well understood. However no study has yet been made with a multiproxy approach simultaneously using the sediment cores collected from wide ranging bottom environments of (i) oxygen deficient marginal waters and (ii) deep sea. Thus, this study has been planned to investigate the two environmental sediments with a multiporxy approach. In the following section, a brief on the usefulness of proxies - $\delta^{15}N$ and trace metals in particular is given. The other proxies - C_{org}, C/N, $CaCO_3$, SiO_2, $\delta^{13}C_{org}$, $\delta^{18}O$, $\delta^{13}C_{forams}$, have been described in chapter 4 and 5.

1.4.3 Sedimentary nitrogen isotope composition as a denitrification proxy

The most commonly used proxy of past denitrification is the ratio of $^{15}N/^{14}N$ in sedimentary organic matter (conventionally expressed in delta notation: $\delta^{15}N = 1000 \times [(^{15}N/^{14}N)_{sam}/(^{15}N/^{14}N)_{std}) -1]$, where the subscript 'sam' and 'std' denote isotope ratios in the sample and atmospheric N_2,

respectively). This theoretical framework and scientific rationale behind this application are as follows:

Nitrogen has two stable isotopes with mass numbers of 15 and 14 (^{15}N and ^{14}N) of which the lighter isotope is far more abundant (99.63%). Like all biogeochemical processes, denitrification also involves mass dependent fractionation of isotopes whereby $^{14}NO_3^-$ is preferentially reduced leaving the residual NO_3^- enriched with ^{15}N (Cline and Kaplan, 1975; Liu and Kaplan, 1989; Brandes et al., 1998; Voss et al., 2001). In the Arabian Sea, $\delta^{15}N$ of NO_3^- increases from ~6‰ in deep waters (2500-3000 m), comparable with values from other areas (Sigman et al., 1997), to 15-18‰ within the core of the denitrifying layer; the $\delta^{15}N$ of N_2 concurrently decreases from ~0.6‰ to ~0.2‰ (Brandes et al., 1998; Altabet et al., 1999b). Brandes et al. (1998) combined the isotopic data with NO_3^- deficits derived from the NO-temperature relationship, and used an advection-reaction model (Rayleigh fractionation) and a diffusion-reaction model to compute the fractionation factor (ε) of 22‰ and 25‰, respectively. Altabet et al. (1999b) obtained a somewhat higher value (~30‰) taking $-N^*$ as the NO_3^- deficit and assuming Rayleigh fractionation. These estimates of ε for the Arabian Sea are similar to those for the eastern tropical North Pacific (Brandes et al., 1998; Cline and Kaplan, 1975), implying relative constancy of isotopic fractionation associated with open-ocean denitrification.

If and when the isotopically heavy NO_3^- from the ODZ is brought up to the euphotic zone through upwelling and vertical mixing and locally consumed on an annual basis, the signature of elevated $\delta^{15}N$ would then be transferred

to the sinking particulate organic matter (POM) and ultimately preserved in sediments (Schäfer and Ittekkot, 1993; Altabet et al., 1995). Thus, the sedimentary $^{15}N/^{14}N$ would reflect the degree of subsurface denitrification and the ODZ's intensity at the time of sediment deposition. This premise, however, needs to be qualified with several caveats (Naqvi, 2007): (1)The $^{15}N/^{14}N$ of the particulate organic matter (POM) is determined by the balance between denitrification and N_2-fixation, and how this balance changed with time in the past is not known. (2)Early diagenesis causes an enrichment of ^{15}N in surface sediments relative to sinking POM by 2-3‰, although this effect is not seen at locations receiving high flux of POM (Gaye-Haake et al., 2005). (3) Sites of the most intense upwelling in the Arabian Sea are found along its western boundary (off Oman and Somalia), which are located outside the denitrification zone (Naqvi, 1991). The water that upwells here is derived from the south and its NO_3^- is not expected to be isotopically heavy. However, as it is advected ~1000 km from the coast before its NO_3^- is fully consumed (refer Figure 3.4 for nitrate profile, of chapter 3), substantial enrichment of ^{15}N must occur due to fractionation during phytoplankton uptake. Thus, even though on the basin scale, the NO_3^- upwelled is fully consumed annually, one may expect gradients in sedimentary $\delta^{15}N$ along the trajectory of flow of the upwelled water.

Even though, as stated above, sedimentary $\delta^{15}N$ more correctly represents the balance between denitrification and N_2-fixation rather than denitrification alone, it may be assumed that during periods of intense denitrification in the past, the balance was similar to what exists today (caveat

34

1). Similarly, it may also be assumed that any diagenetic alteration of the isotopic signal in the sediments is time invariable (i.e. the offset of the sedimentary $\delta^{15}N$ from the corresponding value of sinking material at the time of its deposition is the same for a given site), so that changes observed within a record would still provide insights into denitrification variability (caveat 2). The qualitative similarity of the deep-sea records (e.g. from the core V34-101 raised from ~3 km depth and having a core top total nitrogen content of only 0.07%) to other records from the region justifies this assumption (Altabet et al., 1999a). With regard to caveat 3, Altabet et al. (1999a) argued that despite the large gradients in $\delta^{15}N$ of NO_3^- within the ODZ, the homogenous distribution of heavy $\delta^{15}N$ values just below the euphotic zone facilitates uniform preservation of the denitrification signal all over the Arabian Sea. This is analogous to the uniform distribution of high $\delta^{15}N$ in the suspended particulate material (SPM) observed by Montoya and Voss (2006) throughout the upper and intermediate water column in the Arabian Sea, although the processes that bring about such a homogenization are not understood.

Over the past decade or so, several sedimentary time series of $\delta^{15}N$ have been published from sites in the Arabian Sea representing diverse oceanographic settings and sedimentation rates (Altabet et al., 1995, 1999a, 2002; Ganeshram et al., 2000; Suthhof et al., 2001; Agnihotri et al., 2003a). These data show high enrichment of $\delta^{15}N$ throughout the Holocene as well as during all interglacial periods over the past 1 million years. In contrast, lower $\delta^{15}N$ values (~5-6‰), comparable to those occurring outside the ODZ's today are characteristic of sediments that accumulated during the glacial stages.

This suggests that, denitrification weakened or was absent during cold, glacial periods (Altabet et al., 1995, 1999a, 2002; Ganeshram et al., 1995, 2000; Suthhof et al., 2001). Sedimentary $\delta^{15}N$ has been found to exhibit a nearly normal distribution about a median of ~6.5‰, with the present day values being close to the upper end of the range, and without a long term trend (Altabet et al., 1999b). Spectral analysis of the records reveals cyclicities associated with the major orbital frequencies (100, 41 and 23 kyr), significantly coherent with records of $\delta^{18}O$ in foraminifera (a proxy of ice volume) for all three frequencies, and lithogenic grain (representing the SWM strength) for all but the eccentricity one. These points to the importance of both hydrography and productivity in controlling Arabian Sea denitrification (Altabet et al., 1995, 1999a). Higher resolution records reveal oscillations over the millennial time scale apparently linked with the climatic changes (Dansgaard/Oeschger oscillations and Heinrich events) inferred in ice cores (Suthhof et al., 2001; Altabet et al., 2002). For instance, the $\delta^{15}N$ records in two sediment cores from the Oman Margin analyzed by Altabet et al. (2002) reveal sharp maxima during Isotope Stage 3 that are remarkably similar in structure and timing to the ice core $\delta^{18}O$ excursions representing Dansgaard/Oeschger oscillations. When smoothened with a 3000y running average (note that the residence time of nitrogen in the sea is currently believed to be around 3000y; Codispoti et al., 2001), the two $\delta^{15}N$ curves are remarkably similar to the Antarctic temperature and CO_2 records. This prompted Altabet et al. (2002) to conclude that changes in denitrification in the ODZ of the Arabian Sea, and probably in other similar areas of the eastern

tropical Pacific, may have a major impact on global climate. Furthermore, it has been suggested that such changes probably also contributed to the variability in atmospheric N_2O content as recorded in polar ice (Altabet et al., 1995, 2002; Suthhof et al, 2001; Flückinger et al., 2002).

1.4.4 Trace metals as redox proxies

The solubility of trace metals in seawater and their partitioning between different phases are often determined by their oxidation states. For instance, iron (Fe) is one of the redox sensitive elements that have two oxidation states, Fe (II), and Fe (III), of which the reduced form is more soluble. In oxic waters Fe (III) gets precipitated as Fe-hydroxides into the sediments. Vanadium (V) on the other hand shows a completely opposite behaviour: its oxidized form [V (V)] is more soluble than the reduced form [V (IV)]. A great deal of attention has been paid to utilize other such metals which exhibit contrasting behavior under different natural redox conditions as proxies of the redox state of the environment at the time, deposition occurred. These tracers help to elucidate the mechanisms by which organic carbon–rich deposits and petroleum source rocks are formed (e.g.; Pedersen et al., 1992; Calvert and Pedersen, 1993), to constrain models of anoxia and associated reducing environment (Emerson and Huested, 1991; Calvert and Pedersen 1993; Hastings, 1994; Morford and Emerson 1999; Nameroff, 1996, Nameroff et al., 2002, 2004) and paleo-productivity (Dymond et al., 1992; Rosenthal et al., 1995a, Klump et al., 2000). However, before one utilizes the redox-sensitive trace metals as paleo–tracers, it is essential to comprehensively understand their

37

geochemistry in both oxidizing and reducing environments. Several problems exist concerning the interpretation of metal data with respect to past environmental variability. The most important of these is the diagenetic effect because of which concentrations in the sediments may not necessarily reflect redox conditions in overlying waters at the time of sediment deposition.

Unlike the application of $\delta^{15}N$ as a paleo-denitrification proxy, the application of trace metals as a tracer of paleo-redox conditions has been quite limited (Sarkar et al., 1993; Schenau et al., 2002; Pailler et al, 2002; Agnihotri et al., 2003a) in not only the Arabian Sea but Indian Ocean as a whole. Sarkar et al. (1993) reported the occurrence of deep-water anoxia based on the observed concomitant enrichment of organic carbon and authigenic uranium in the glacial sections of a core from the eastern Arabian Sea. This was attributed to a change in deep water circulation. However, the benthic carbon isotopic evidence presented later in this thesis suggests that, while the deep water oxygen concentrations did change with time, the change in benthic $\delta^{13}C$ is inconsistent with completely anoxic glacial deep water. This mismatch underscores the need to adopt a multi proxy approach in order to make the paleo-environmental reconstructions more reliable.

1.5 Significance, Objectives and Scope of the Study

Oceanographic processes in the Arabian Sea are to a very large extent controlled by the unique phenomenon of monsoon. Numerous previous studies have shown that the intensity of monsoon has fluctuated in the past on a variety of time scales, largely forced by changes in solar insolation (e.g., Prell, 1984b; Gupta et al., 2003). Moreover, the ongoing and future changes

in the Earth's climate are expected to affect the SWM (making it more intense) thereby impacting the regional biogeochemistry including the volume and intensity of the ODZ (e.g. Goes et al., 2005). The past holds the key to future; and so in order to predict these changes an understanding of paleo-denitrification and of the processes that controlled it, is essential.

Most of the earlier works on paleo-denitrification have focused on the western Arabian Sea, often utilizing $\delta^{15}N$ as the sole proxy. The ODZ is better developed in the north eastern Indian Ocean and a few published records of $\delta^{15}N$ are available from this region. Moreover, as already stated, apart from the open ocean sub-oxic zone, denitrifying conditions also develop over the Indian continental shelf on a seasonal basis. Changes in this shallow system in the past are yet to be investigated. Given these shortcoming in the available information, the present study strives to:

(1) provide new data from sites where denitrification is most intense (in northeastern Arabian Sea) following a multi-proxy approach

(2) addresses for the first time the important issue of, how the shallow water, seasonal ODZ change with time in recent past

The latter issue is of special significance, since it has more socio-economic relevance. The knowledge being sought is essential to evaluate the extent to which human activities are modifying the state of our coastal environment.

As the study focuses on both - the open Arabian Sea and the coastal region of India affected by water column oxygen deficiency, the results would give us insight on the behaviour of the two different environments during the

past and present. The results obtained from short coastal cores will help us in experiencing the behaviour of the coastal environment during the past. This in turn would provide us an understanding about the present day intensification of suboxia-anoxia occurring in the water column due to the anthropogenic activities correlated with the natural forcing.

The deep sea gravity core results would help us infer about the ventilation and presence of water masses with different oxygen concentration in the intermediate and bottom waters, especially from the sedimentary nitrogen isotope proxy (which is a denitrification indicator, and which infers about denitrification occurring in intermediate waters) and $\delta^{13}C$ of benthic fauna (*Cibicidoedes wuellerstorfi*, dwelling on seabed surface), together with redox sensitive elements which would record the changes occurring in the bottom waters at the time of its deposition.

The broad objectives of the study are:

i) To evaluate various proxies of paleo-productivity and redox conditions [stable carbon and nitrogen isotopes, organic matter and trace metals (*viz.* Mn, Co, Fe, Mo, V)].

ii) To distinguish signals of depositional environment from post-depositional diagenetic changes.

iii) To correlate these changes with those in the climate (particularly the Asian summer monsoon) and related physical and biological processes (such as upwelling, circulation, and biological productivity).

In order to fulfill these objectives, extensive measurements of various paleo proxies were carried out, the results of which are presented here.

Chapter 2 provides a description of the methods. Chapter 3 includes information on the hydrography and circulation that determine the state of the biogeochemical environment, including its redox status. Chemical and other ancillary data and a discussion of the relevant processes both in the open ocean and coastal ODZ are presented to serve as the background against which the paleo-data are interpreted and discussed in Chapter 4 (for the shallow ODZ) and Chapter 5 (for the deep ODZ). Finally, the major conclusions of the study are summarized in Chapter 6 and recommendations made for future works.

CHAPTER 2

Chapter 2

MATERIALS AND METHODS

2.1   Introduction

In order to achieve the scientific objectives identified in chapter 1, three short and two long gravity cores were collected from the coastal region (off Goa) along the western continental margin of India and open ocean denitrifying zone of Arabian Sea respectively. The geochemical measurements were carried out using various analytical techniques and instruments. Apart from core collection, water sampling was also done at the time of core collection and during other field trips, to have the water column data. The detailed descriptions of sampling and material including methods are given below.

2.2   Collection of Sediment Cores

Two short gravity cores were collected in October 2002, during the first trial cruise of a multi-corer on board the CRV Sagar Sukti. One more gravity core was collected in September 2005 on board the CRV Sagar Sukti during the SaSu-98 cruise, using the two meter long gravity corer on board. The other two long gravity cores were collected in February 2002, during the 42nd cruise of M/V A.A. Siderenko, a vessel chartered by the then Department of Ocean Development, now Ministry of Earth Sciences (MoES). Gravity cores were collected by the author while the short coastal cores were collected by the biogeochemistry group from NIO. Details of the core location, water depth

of collection and length of the sediment cores raised, are given in Table 2.1. Location of all the cores is shown in figure 2.1.

Colour and lithology of sediments were noted immediately after the recovery of the cores on board. Visual examinations was done for identifying the presence of turbidites and sediment slumping. All the cores were sub-sampled on board into 1 cm thick slices, throughout for the short cores and 2 cm slices for the long cores, using thin transparent knife shape acrylic plate. The sediment samples were then sealed in plastic zipped bags and stored. At shore based laboratory, required amount of all the samples were oven dried at 60°C and preserved in pre-cleaned plastic vials until further analyses.

2.3   Various proxies used in this study

Multi-proxy studies are common in reconstructing environmental changes. Particularly, anthropogenic eutrophication and the onset of anoxia have been examined in various estuarine systems by number of researchers (e.g. Cornwell et al., 1996; Zimmerman and Canuel, 2000; Chmura et al., 2004) through the multi-proxy approach. To decipher the past changes in biological productivity, sub-surface denitrification, terrestrial inputs and bottom water redox conditions at seabed, various proxies viz. biogenic constituents, stable carbon and nitrogen isotopes, trace metals, and stable oxygen and carbon isotopes of forams were measured. A detailed analytical scheme followed for the systematic sediment sample analyses is shown in figure 2.2. Details of all the proxy analyses done in this study and the different

Table 2.1

Locations and details of sediment cores collected from the Arabian Sea.

Cruise No.	Core No.	Latitude °N	Longitude °E	Water Depth (m)	Length of the Core (cm)	Collection date
SaSu - 98	CR-2	14°8.0'	74°2.0'	45	100	27/09/2005
SaSu Trial Cruise	SaSu-1	15°28.6'	73°27.5'	50	21	23/10/2002
SaSu Trial Cruise	SaSu-3B	15°28.4'	73°32.42'	35	43	23/10/2002
AAS - 42	AAS-42/15	17°13.0'	69°02.0'	2525	440	19/02/2002
AAS - 42	AAS-42/12A	15°4.0'	69°59.0'	2270	530	18/02/2002
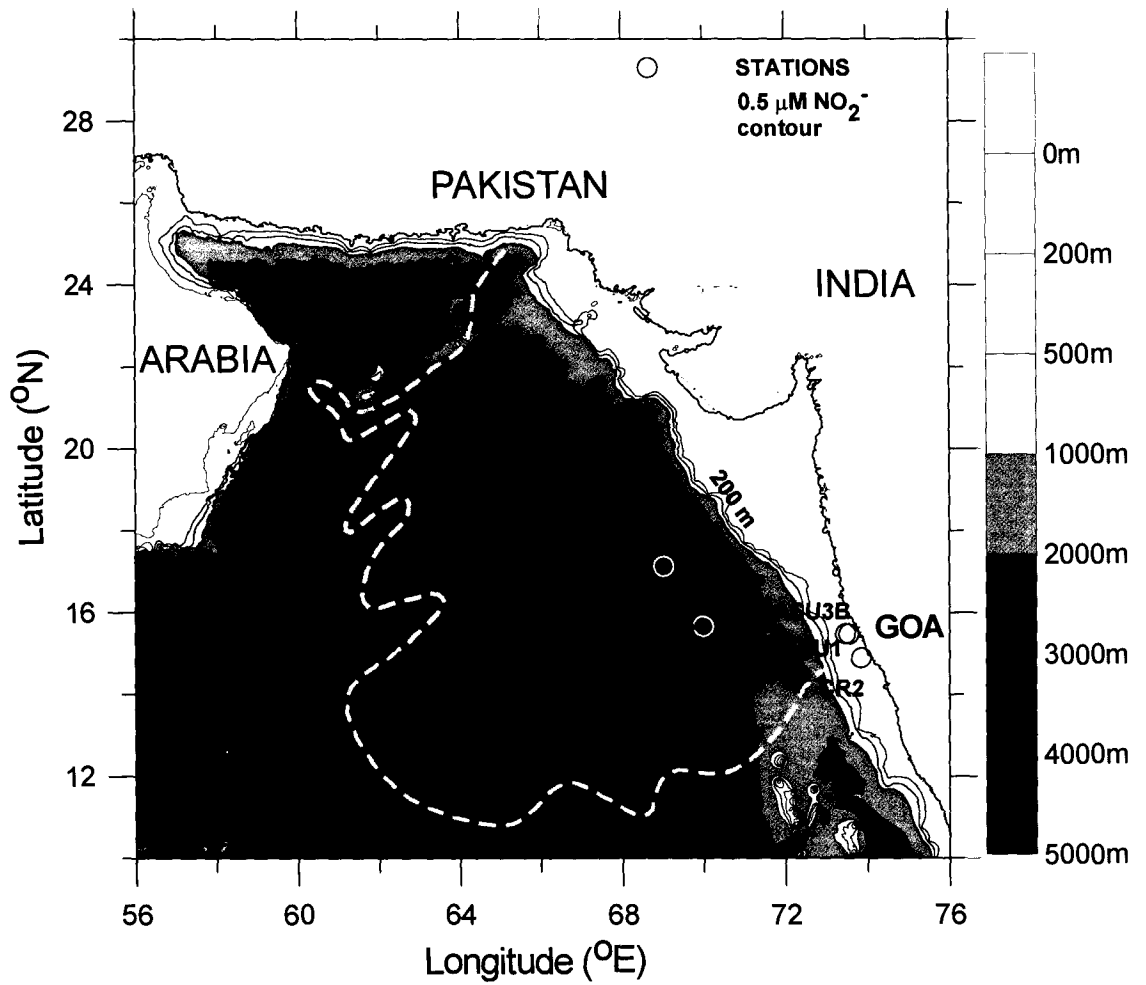
Figure 2.1: Location of cores collected from the shallow and deep water OMZ region of Arabian Sea. The extent of OMZ is demarcated by the secondary nitrite maxima (0.5μM). Figure modified from Naqvi (1991).
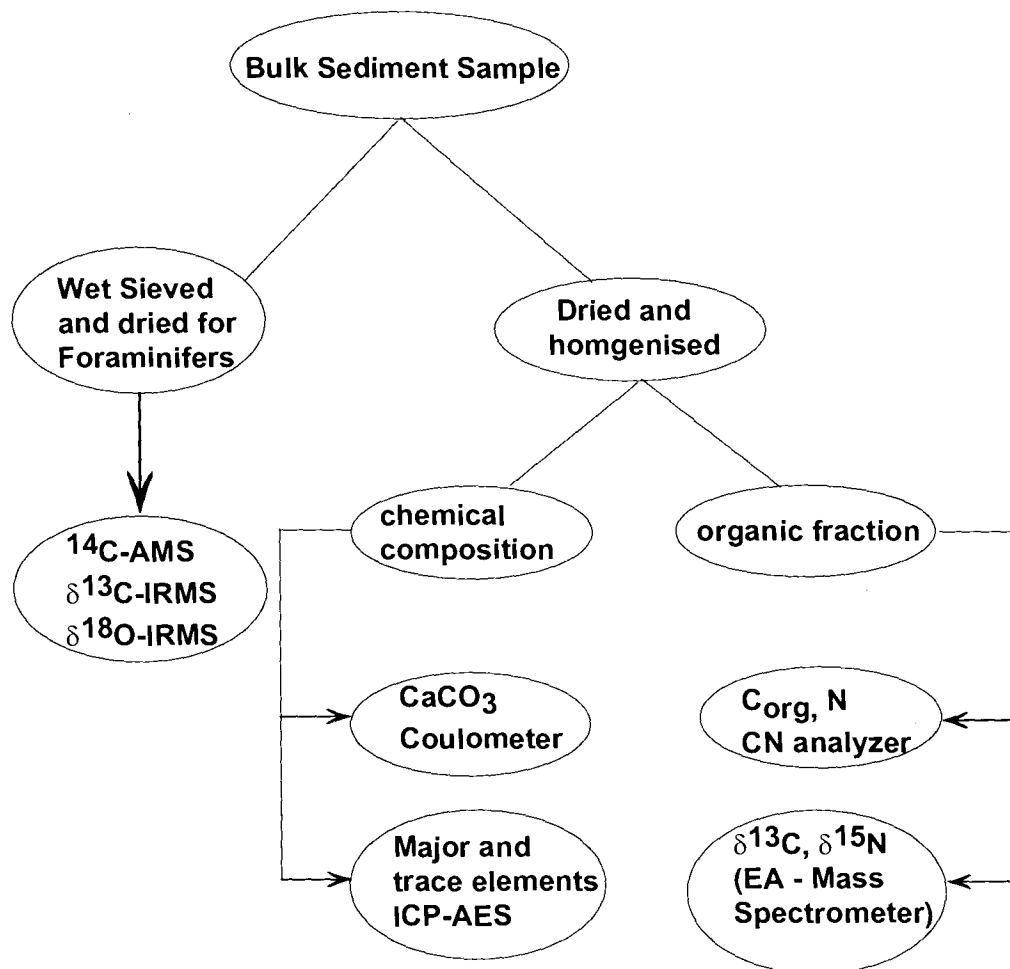
Figure 2.2: Analytical scheme for chemical and isotopic analyses of sediment samples

instruments used are discussed below, with the accuracies summarized in Table 2.4 in terms of precision.

2.3.1 ^{210}Pb and AMS ^{14}C dating

^{210}Pb dating

Chronology of short cores (SaSu-1, SaSu-3B and CR-2) was constructed by the ^{210}Pb dating technique, measured via its grand daughter nuclide ^{210}Po, at Physical Research Laboratory, Ahmedabad. About 2-3 g of ground dry sediment sample was leached with 8M HCl in presence of ^{209}Po spike. The solution was finally made in 50-60 mL of 0.6M HCl, and ascorbic acid was added to complex the Fe^{3+} ion present in the solution. The polonium (Po) isotopes were then autoplated onto a 1.5cm diameter silver disc suspended in solution. The plating was done for 3 hours by maintaining the temperature of the solution at ~65°C. After plating, silver disc was rinsed with distilled water, dried and the activities of the Po isotopes (^{209}Po and ^{210}Po) were measured for alpha counting using Si-surface barrier detectors coupled to a pulse height analyzer (Yadav et al, 1992; Sarin et al., 1992; Somayajulu et al., 1994, Sharma et al., 1994).

AMS ^{14}C dating

Chronology for the long gravity cores (AAS-42/15 and AAS-42/12A) was set up by ^{14}C dating of planktonic foraminiferal separates of *Globigerinoide ruber* species (>250 µm) employing Accelerated Mass Spectrometer (AMS). The AMS measurements were performed at the

National Ocean Sciences AMS Facility (NOSAMS), Woods Hole, MA (USA).

The samples were processed to derive the graphite form of carbon which was

then compressed by the target press and inserted into the cathode (Cs) of the

ion source. The sample was then accelerated and the carbon converted into a

positive ion and then, the separated C-12 and C-13 ions were measured in

Faraday Cups, where a ratio of their current was recorded. Simultaneously

the C-14 ions were recorded in a gas ionization counter so that ratios of C-14

to C-13 and C-12 were recorded instantly. These raw data signals were then

converted to radiocarbon ages using algorithms. Carrara Marble was used as

a blank, while Oxalic Acid was used as the standard. Based on repeat

standards analysis, the precision of the technique was found to be 5-7 per mil

(McNichol and Aluwihare, 2007), (http://www.nosams.whoi.edu). A single

sample (interval 97-99cm) from core CR-2 was also dated by AMS ^{14}C for

bulk organic matter, to ascertain the core age beyond the ^{210}Pb dating limits;

at the Institute of Physics (IoP), Bhubhaneshwar.

2.3.2 Organic Carbon and Nitrogen analyses

All the cores (SaSu-1, SaSu-3B, CR-2, AAS-42/15, and AAS-42/12A)

were analyzed for organic carbon and nitrogen proxies. Prior to analyses,

sediment samples were treated with 1M HCl to remove the carbonates,

washed thoroughly with de-ionized water, dried and homogenized except for

those analyzed in Germany. Analyses of sediment samples for organic carbon

(C_{org}) and nitrogen (N_{org}) were done on three different instruments as per their

availability to carry out the analysis. SaSu-1 and SaSu-3B core samples were

measured by *Fisons NA1500 NC Elemental Analyzer (Fisons Inc., Italy) at the Physical Research Laboratory (PRL), Ahmedabad.* About 10mg of the dried, decalcified samples were taken for analysis. The samples were packed in aluminium cups and introduced in the Elemental Analyzer through an autosampler. The samples were dropped into the combustion tube containing silver cobaltous cobaltic oxide and granular chromium oxide maintained at 1050°C. In the combustion tube, the samples were combusted readily due to flash combustion in presence of high purity oxygen at ~1800°C. All the halides and sulphur gases were removed in the combustion column and the evolved CO_2 and NO_x were then passed through a reduction column containing reduced Cu at 650 °C to yield finally purified CO_2 and N_2. The final pure CO_2 and N_2 were then separated in a GC column at 60 °C and measured by Thermal Conductivity Detector (Bhushan et al. (2001). A three point calibration sequence was made following linear-fit method using a Deer River Shale Standard as a reference material containing 2.53% carbon and 0.12% nitrogen (Sarin et al., 1997). The analytical precision for measurement of carbon and nitrogen was found to be ±1.0% and ±0.8% respectively based on repeat measurements of the sample and standard.

Organic carbon and nitrogen for AAS-42/15 core sediments were estimated by *NCS analyzer (CE Instruments, model NCS-2500; at NIO, Goa).* ~ 8mg of the samples were weighed in tin cups and introduced into the vertical quartz tube (filled with silver cobaltous cobaltic oxide and granular chromium oxide) and combusted completely at ~1000°C. The evolved CO_2 and NO_x were then passed through a reduction column containing Cu filings,

where nitrogen oxides got reduced to molecular nitrogen while the CO_2 remained unchanged. The gas mixture was then passed through an anhydrone trap, for the absorption of moisture. The resulting purified gas mixture was eluted and separated by a Porapack column and subsequently detected by a TCD detector. The precision of the analysis was found to be better than ±1% using Urea (NH_2CONH_2) as a standard.

Analysis of sediment samples from core AAS-42/12A for organic carbon and nitrogen were done by a *Carlo Erba NA 2100 elemental analyzer at Center for Tropical Marine Ecology - Bremen, Germany*. Organic carbon (C_{org}) and nitrogen was measured after removal of carbonate by adding 200 µL of 1M HCl and subsequent drying at 40 °C, by using ~10mg of sample taken into 9×10.5 mm silver cups. The decalcified samples then were combusted in an oxidation column at 1100 °C under the supply of oxygen. The gas mixture containing oxides of nitrogen, carbon, hydrogen and sulphur were then transported by Helium, to a column filled with silver to remove SO_2 if any. For reduction of nitrogen oxides (NO_x) the gases were passed through another column filled with copper. A trap was used to remove water. N_2 and CO_2 were then separated on a gas chromatographic column and measured by a thermal conductivity detector (TCD). Accuracy was monitored by measuring standards after every five samples. Standards used were 'Leco 1009' with 0.034 ±0.01 weight %N and 0.85 ±0.09 weight %C or 'Leco 1012' with 0.13 ±0.04 weight %N and 1.30 ±0.04 weight %C. Depending on sample sizes and compositions the combustion tube was cleaned for every 5-15 measurements.

The mean accuracy for nitrogen measurements were ±0.01%, while carbon was measured with accuracy of ±0.22%.

2.3.3 CaCO₃ analysis

Carbonate Carbon was determined for SaSu-1, Sasu-3B, CR-2, AAS-42/15 and AAS-42/12A cores by Coulometry using UIC Coulometer, model CM 5014 (UIC Inc., USA). CO_2 was evolved from the samples through acidification, by treating nearly 30mg of homogenized sediment sample with 5 mL of 1M HCl at 50 °C. CO_2 free air (air was stripped off CO_2 by passing through 45% KOH scrubber solution) was used as a carrier gas for flushing CO_2 in the system. The CO_2 liberated was flushed by the carrier gas and dried by passing it through a post scrubber solution of 50% KI maintained at pH=3 (pH adjusted to 3 with 50% Sulphuric Acid) and a column of activated silica gel and drierite (moisture absorbing zeolite). The dried CO_2 was then passed through the coulometer titration cell (with Platinum-cathode and Silver–anode) containing monoethanolamine solution and a self indicator (thymol blue) (Bhushan et al., 2001). Pure and dried CaCO₃ (suprapure grade MERCK) was used as a standard for calibration. The precision of CaCO₃ analysis was found to be <2.5% based on repeated standard and sample analysis.

2.3.4 Stable isotope studies

Stable oxygen and carbon isotope compositions of calcareous marine organisms have been widely used to reconstruct the paleo environmental conditions. For oxygen, $^{18}O/^{16}O$ ($\delta^{18}O$) ratio is used, while for carbon it was $^{13}C/^{12}C$ and denoted as $\delta^{13}C$. They were measured using Mass

Spectrometers with dual inlet system. In the present study, isotope measurements of forams were done using the Micromass (Isoprime) Dual Inlet, Mass Spectrometer of GV Instruments at National Institute of Oceanography, Goa.

Sample preparation

Samples of the open ocean gravity cores (AAS-42/15 and AAS-42/12A) were chronicled prior to analyses of other proxies. Stable isotope analysis of oxygen ($\delta^{18}O$) and carbon ($\delta^{13}C$) were used as proxies to find the chronology of the cores. Stable isotope studies were done on the foraminifera (forams) fossils from the sediment. For this, aliquots of sediment samples were wet sieved using a 63 micron mesh of diameter 12 inches, with tap water, dried and size fractionated for 250 and 125 µm using the respective sieves. The required species of planktonic and benthic forams were then hand picked using a simple stereo microscope with a resolution of 50X.

Basic principle of Mass Spectrometers

Mass spectrometers are the most effective and widely used means of measuring isotope abundances. In principle, a mass spectrometer deflects any moving charged particle under the influence of magnetic field and/or electric field. A mass spectrometer may be divided into four parts (Figure 2.3): (1) the inlet system, (2) the ion source and accelerator, (3) the mass analyzer, and (4) the ion detector (Hoefs, 1987). The whole system works under very high vacuum, which is essential for the stability of the ions produced and for their free flow.
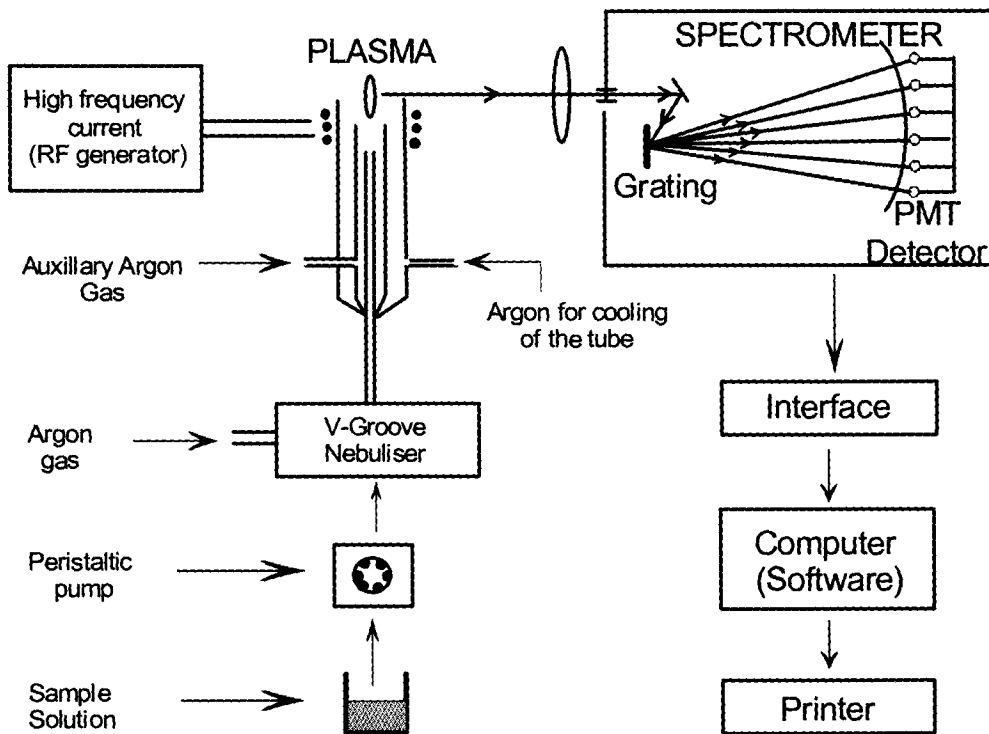
SCHEMATIC OF ICP-AES

Figure 2.5: Schematic diagram of an Inductively Coupled Plasma Atomic Emission Spectrometer (ICP-AES) for elemental analysis.

The *inlet system* provides a facility for purification of gas (CO_2 in case of carbonates – forams) before feeding to the mass spectrometer. This is done through a series of trapping systems (moisture trap along with cold fingers 1 and 2) which removes the moisture contents and other unwanted gases produced from the sample materials during the reaction with acid (phosphoric).

The *ion source* is an electrically heated metal coil (Thorium–Th) that gives off electrons. The atoms/molecules from the sample are bombarded with this stream of electrons (perpendicular to each other), during which some of the collisions are energetic enough to knock one or more electrons out of the atoms/molecules to make positive ions. These molecular positive ions are then repelled away form the very positive ionization chamber and accelerated into a finely focused beam.

The *mass analyzer* separates the ion beams emerging from the ion source based on their mass/charge ratio (mass/charge ratio is given the symbol m/z or sometimes m/e). This is done through a strong magnetic field. As the ion beam passes through the magnetic field, the ions get deflected into circular paths based on their masses (i.e. m/z ratio) as the charge on all ions is preferably assumed to be 1 and it requires a lot more energy to knock off the second electron from an already positive ion. The radii of the circular path are proportional to the square root of m/z ratio.

The ion detector (Faraday cups) collects the separated ion beam (coming from the analyzer) and converts it into electrical impulses, which are then fed into an amplifier. In case of oxygen and carbon isotope

measurements, there are separate Faraday cups to detect the different masses of ions simultaneously.

2.3.4.1 Stable Oxygen ($\delta^{18}O$) and Carbon ($\delta^{13}C$) Isotope analysis

Stable isotope measurements of both oxygen and carbon were performed on surface dwelling planktonic foraminifers - *Globigerinoide ruber* and benthic foraminifer - *Cibicidoides wuellerstorfi*, for both the open ocean gravity cores. For planktonic foraminifers, tests from >250 µm fraction were used for analysis to avoid the size fraction effect (Duplessy et al., 1981). Prior to analysis, the specimens were ultra sonicated for 5-10 seconds (taking care not to break the tests) to remove any fine material attached to the tests. The tests (mounted on special slides with holes) were then dried and preserved in a desiccator until analysis was done. The isotope (carbonates) measurements were carried out on the *GV- Micromass Spectrometer* coupled with an automated CO_2 preparation system (Gilson - multicarb). The isotopic composition of carbonate was measured on the CO_2 gas evolved by the treatment of foraminiferal shells with 102.6% pure, specific gravity $1.913g/cm^3$ ortho-phosphoric acid at a constant temperature of 90 °C through an auto-sampler. The ortho-phosphoric acid was purified by distillation in the laboratory from analytical grade 88% with specific gravity $1.75g/cm^3$. The standard CO_2 gas was then calibrated against the international carbonate standard – Pee Dee Belemnite (PDB), using National Bureau of Standards 19 (NBS-19). The denoted unit of isotope ratio measurements is the delta value (δ). The δ-value is defined in the same way as mentioned in equation (1) as:

T-385

$$\delta^{18}O = \{[(^{18}O/^{16}O)_{sample}/ (^{18}O/^{16}O)_{standard}] -1\} \times 1000 \text{------------------------} (1)$$

and

$$\delta^{13}C = \{[(^{13}C/^{12}C)_{sample}/ (^{13}C/^{12}C)_{standard}] -1\} \times 1000 \text{----------------------} (2)$$

The δ notation represents per mil (‰) deviations from the isotopic standard PDB, prepared from the rostrum of the belemnite - *Belemnitella Americana* from the Cretaceous Pee Dee formation of South Carolina. The PDB standard is defined as 0 per mil for carbon and oxygen. The isotopic composition of water was reported as per mil deviations of the sample, from Standard Mean Ocean Water (SMOW); a hypothetical water close to average ocean water (Craig, 1957). Since the supply of PDB is exhausted, calibrations are normally done through the analysis of NBS samples. The NBS 19 is a homogenized standard of Jurassic Solnhofen limestone form Southern Germany. The standard deviation, (i.e. the long term measurement precision) based on replicate analyses of internal laboratory standards and NBS19 for $\delta^{18}O$ were better than ± 0.06‰ and that for $\delta^{13}C$ was better than ± 0.04‰. The mean sample size was 3-5 shells for $\delta^{18}O$ measurements while for $\delta^{13}C$ measurements an approximate sample weight of 20-60µg was taken.

2.3.4.2 Analyses of $\delta^{13}C$ and $\delta^{15}N$ in sedimentary organic matter

Measurements of $\delta^{13}C_{org}$ and $\delta^{15}N$ were done in the organic fraction of the sediments for all the five cores (SaSu-1, SaSu-3B, CR-2, AAS-42/15, AAS-42/12A) using an isotope ratio mass spectrometer of *Thermo Finnigan Delta plus*, at the *Center for Tropical Marine Ecology - Bremen, Germany*. The

mass spectrometer was coupled with the *Flash EA 1112 elemental analyzer* in a continuous flow mode. Required amount of samples were weighed in silver cups and combusted. The gas mixture (N_2 and CO_2) was separated in a Flash EA 1112 elemental analyzer (same procedure as in the NA 2100 elemental analyzer mentioned in section 2.3.2). Carbon dioxide (CO_2) and Nitrogen (N_2) were ionized and transferred into a magnetic field, where they were separated by virtue of their different mass/charge ratio. The split ion beams were detected and the results were expressed as δ values in ‰, as deviation from composition of atmospheric nitrogen and V-PDB standard for carbon, $\delta^{13}C_{org}$ and $\delta^{15}N$ were calculated as follows:

$$\delta^{13}C_{org} \text{ and } \delta^{15}N = ((R_{samlpe}-R_{standard})/R_{standard}) \times 1000 \text{ ----------------- (3)}$$

Where $R = {}^{13}C/{}^{12}C$ and ${}^{15}N/{}^{14}N$.

Calibration for $\delta^{13}C_{org}$ and $\delta^{15}N$ contents was achieved using several international standards throughout the analyses. A sample from Brazil was frequently used as a reference and this standard was measured after every 7 samples (Pedersen et al., 1991, Ganeshram et al., 1995, Higginson et al., 2004). The standard deviation for $\delta^{13}C_{org}$ and $\delta^{15}N$ was found to be ±0.11 and ±0.17‰ respectively.

2.3.5 Elemental analysis of major and trace elements

Major and trace elements were analyzed for cores SaSu-1, Sasu-3B, CR-2, AAS-42/15 and AAS-42/12A using the Inductively Coupled Plasma - Atomic Emission Spectrometry (ICP-AES) technique. The spectrometry method required the sample to be introduced in solution form. For this, the

samples were digested using an appropriate acid mixture employing the closed vessel technique.

2.3.5.1   Sample preparation with MARS

The choice of digestion method depends on the requirement of extent of dissolution of the sample, quantities of acids, total digestion taken, and minimal analytical errors. Microwave-acid digestion utilizes lesser amounts of acids and is faster with minimal contamination than open vessel digestion. Also an important factor to be considered is the nature of the geological material (Totland et al., 1992). Keeping all these aspects in mind, microwave digestion technique was adopted for the dissolution of sediment samples. Schematic diagram of the digestion procedure is shown in figure 2.4. Dried, homogenized, sediment samples weighing ~500mg were taken in clean Teflon liners. To the liners then a mixture of concentrated, ultra pure (metal free) acids in the proportion of 5:3:2 mL of HNO_3: HF: HCl respectively was added (Morford and Emerson 1999; Crusius et al., 1996). However the acid combination was finalized after a series of laboratory experiments with different combination of all the acids (Rosenthal et al., 1995b; Reichart et al., 1998; Warnken et al., 2001). The Teflon vessels were then screw capped (fitted with rupture membrane for safety purpose) and placed in Microwave Accelerated Reaction System (MARS; model MARS5, CEM, USA). A two-step procedure as given in table 2.2 was followed to ensure complete digestion of the sediment samples. The final volume was made to 50 mL. For analysis of major elements, samples were accordingly diluted and measured

Table 2.2

Two step procedure for digestion of dried, homogenized sediment samples for elemental analysis on ICP-AES.

Step 1: Acid mixture (HNO_3, HF, HCl)

Microwave Power (watts)	No. of Vessels	Power (%)	Ramp Time (min)	Control Pressure (psi)	Control Temp. (°C)	Hold Time (min)
1200*	12	90	30.0	800	210	30.0

Step 2: Boric Acid (15-20mL for each sample)

1200*	12	85	20.0	800	180	30.0

*Microwave power is decided based on the number of vessels used for digestion as 1200W for 12; 600W for 6 and 300W for 3 vessels.
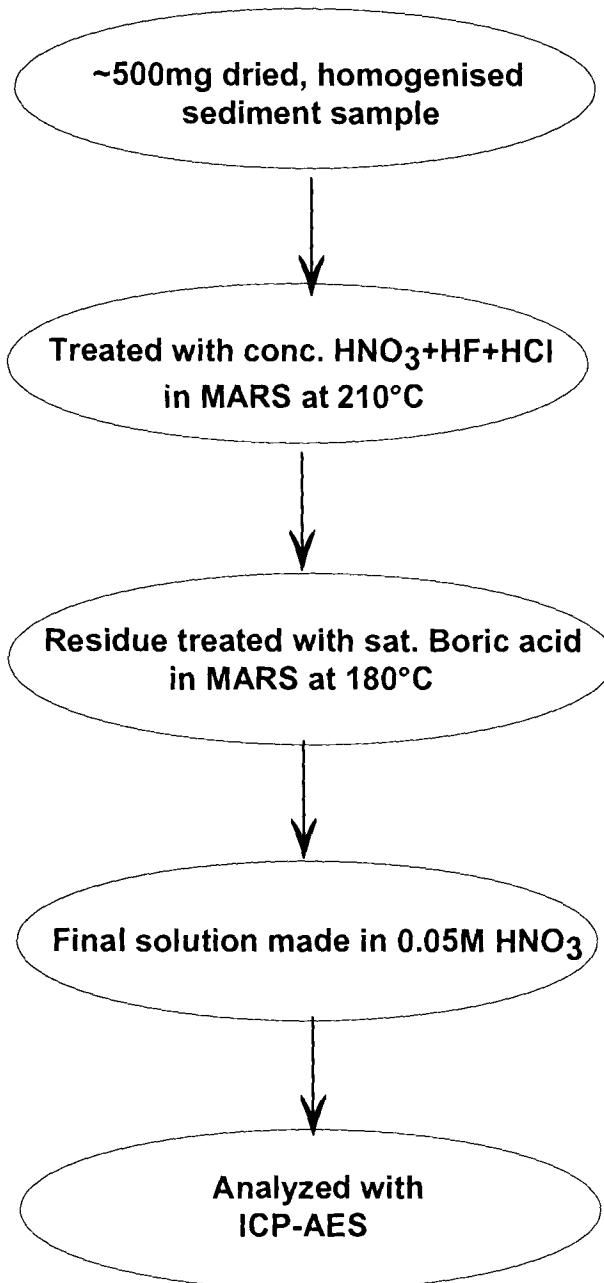
Figure 2.4: Schematic diagram of digestion procedure on MARS-5 for elemental analysis.

on ICP-AES. Standards (USGS) were also treated the same way as the samples.

2.3.5.2 Measurements on ICP-AES

The digested samples were measured for major and trace elements using the Liberty–Series II (Sequential mode) ICP-AES of Varian make. The major elements measured were Aluminium (Al), Magnesium (Mg), Iron (Fe), Strontium (Sr), Titanium (Ti) and Phosphorus (P) and among the trace elements, Manganese (Mn), Molybdenum (Mo), Vanadium (V), Cobalt (Co), Nickel (Ni), Copper (Cu), Barium (Ba) and Chromium (Cr). A schematic of the ICP-AES is shown in figure 2.5. The sample gets introduced into the nebulizer with the help of pneumatic peristaltic pump, where it is converted into an aerosol with the help of an inert Argon gas flowing perpendicular to the sample flow. The fine mist is then carried to the plasma flame (6,000-10,000°C) where the sample gets atomized, ionized and excited. The argon plasma works at very high radio frequency and in this instrument it is operated at 36MHz. The light emitted from the plasma is focused onto the holographic grating which resolves the light into its individual wavelengths specific for each element. The light signal is then taken up by the photomultiplier tube (PMT) detector, which generates a milli-volt signal proportional to incident light signal. The electrical signal then gets converted in terms of concentration with the help of a capacitor and a digital voltammeter. All the specifications and operating conditions of the ICP-AES are given in table 2.3.

Calibration of the spectrometer was achieved by means of multi-

Table 2.3

Specifications and operating conditions of ICP-AES.

ICP Spectrometer	Liberty Series II, Varian (sequential mode)
Power	1.2 KW
Plasma gas flow	12.0 L.min^{-1}
Auxillary gas flow	1.5 L.min^{-1}
Nebulizer	V-groove
Sample uptake rate	1 mL .min^{-1}
PMT voltage	700-800volts
Signal integration	3 seconds
Grating order	Default
Filter position	Default
Resolution	0.006 nm for Cd line at 228.8 nm
Detection limit	3 σ μg L^{-1}
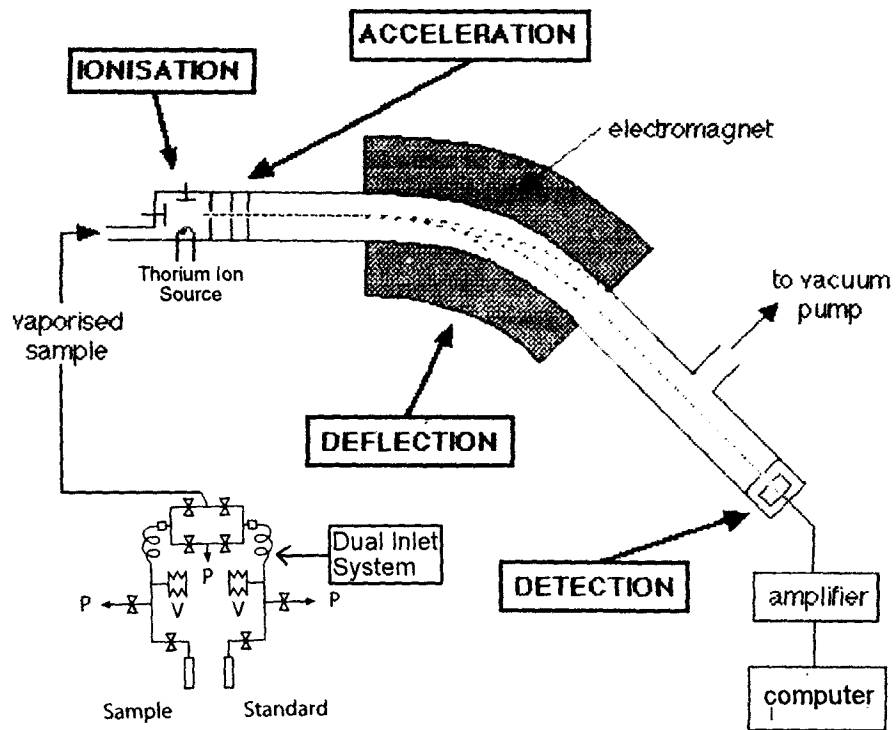
SCHEMATIC OF IR-MS

Figure 2.3: Schematic diagram of an isotope ratio mass spectrometer (IR-MS) for stable isotope measurements. The dual inlet (DI) section is modified from Hoefs, (1987) where 'P' denotes pumping system and 'V' a variable volume.

element standards in 0.5 M HNO_3 of varying concentrations at ppb and ppm levels as per the element requirement during analysis. Several USGS rock standards like MAG-1 (marine sediment), SCo-1(Cody shale/silty marine shale), and BIR-1(Icelandic Basalt) were analyzed to check accuracy and precision of the elemental analysis of sediment samples. Among all the standards, MAG-1 was analyzed extensively in this work as it closely matched the matrix of the sediment samples. Precision involved for the elements measured were 1-5%.

2.4   Water sampling and analysis

During the core collection from the deep sea, water samples were collected from selected (mostly standard) depths covering the entire water column (down to bottom) using either Go-flo or Niskin samplers (5/10 -litre capacity) mounted on rosette fitted to Sea-bird CTD (conductivity-temperature-depth, No. SBE 9/11). Temperature and conductivity sensors in the CTD units allowed continuous profiling of these properties. The salinity data derived from the in-situ sensor was calibrated through analysis of discrete samples in the laboratory. Temperature recorded by probe was occasionally verified by using reversible thermometers. While for the coastal sample collection, a portable CTD was generally used. Again the temperature profiling data from the CTD was checked with reversible thermometer readings and check for salinity was done by analyzing samples with an Autosal Salinometer (model 8400).

Once the CTD sampler was brought on the deck, samples were collected following a particular fashion. Firstly, salinity samples were collected in glass bottles after a thorough rinsing (three times) and filled up to the shoulder. The neck of the bottle was dried with a tissue paper so as to avoid salt deposition. The bottles were then capped tightly and kept in a temperature-controlled room until anlaysis. Salinity values are expressed as Practical Salinity Units (psu, Fofonoff, 1983).

The samples then collected for other chemical analyses, were first sampled for dissolved gases (O_2, H_2S, N_2O) in specialized glass bottles and then for nutrients in teflon plastic bottles. While sampling for dissolved gases, utmost care was taken to avoid any atmospheric contamination. Chemical analyses of discretely-collected water samples for O_2, hydrogen sulphide (H_2S), and nutrients (NO_3^-, NO_2^- and NH_4^+) were performed on board ships, whereas those samples collected during the coastal field trips were done in the shore laboratory. N_2O samples were preserved with $HgCl_2$ and analyzed either on board ship or in the shore laboratory.

2.4.1 Analyses of dissolved gases

2.4.1.1 Dissolved oxygen

Dissolved oxygen was estimated by the Winkler titration method as modified by Carpenter (1965). The principle of the method is as follows:

The dissolved oxygen in seawater was made to oxidize Mn (II) to Mn (III) to Mn (IV), under strongly alkaline medium. In the presence of excess iodide, reduction of Mn (III) and Mn (IV) liberates iodine upon acidification (either

H_2SO_4 or HCl). The iodine released was titrated against standard sodium thiosulphate solution using starch as the indicator. The amount of O_2 was calculated from sodium thiosulphate consumed.

2.4.1.2 Hydrogen Sulphide

Hydrogen sulphide was estimated spectrophotometrically by methylene blue method by Fonselius (1962). The method is based on dimethyl-p-phenylene diamine reaction in acidic medium with ferric chloride to form an indammonium salt (Bindshedler's green), an intermediate. The product then combines with hydrogen sulphide yielding a thiazine dye (methylene blue). This compound's maximal absorbance occurs at 670 nm and was measured at this particular wavelength.

2.4.1.3 Nitrous Oxide

The estimation of N_2O was carried out by multiple phase analysis using the equilibriation technique of McAuliff (1971). An aliquot of 25 mL of seawater sample was taken in 100mL air-tight syringe that was previously flushed with helium gas to avoid atmospheric contamination. An amount of 25 mL of helium gas was injected into the syringe. During the transfer of both, the water sample and helium gas utmost care was taken to avoid contact with atmosphere. The sample was equilibrated for 5 minutes by vigorous shaking on a mechanical shaker. The N_2O released from water into the headspace was dried by passing over a moisture trap (10cm long, 1cm wide). The sampled gas was then introduced in to the GC (via a 6-port valve) containing

a stainless steel column packed with Chromosorb (80/100 mesh) and maintained at 80 °C. The separated N_2O gas was then detected using Electron Capture Detector (ECD). The extraction was repeated twice, more on the same aliquot. The detector output was read in terms of peak area, by a data station. The precision of the method was ~ 4%. Standards were run at the beginning and end of each set of samples to check the drift in the instrumental conditions and response. Air was used as a working standard. Standardization was against a standard mixture of 510 ppb N_2O in nitrogen (Gas standards, Alltech Associated Inc, IL. USA). Calculations for getting the concentration of nitrous oxide were done by plotting the log of peak area of each extraction against the extraction number. The slope (z) and intercept (I) of each sample was computed and the initial concentration of nitrous oxide (N_2O) was then obtained from the following equation,

$$[N_2O] = I/(z-1) \text{ --- (4)}$$

The concentration unit used for Nitrous Oxide measurements was part per million (ppm).

2.4.2 Nutrient analyses

Nutrient analyses were done using an automated SKALAR segmented flow analyzer (Model 5100-1), following the principles discussed in Grasshoff et al. (1983). The primary standards for analysis were prepared in bulk and stored aseptically in ampoules to maintain uniformity.

2.4.2.1　Nitrite and Nitrate

The estimation of nitrite in seawater was based on its reaction with an aromatic amine that led to the formation of a diazonium compound, which on coupling with a secondary aromatic amine forms an azo dye (Bendschneider and Robinson, 1952). The absorbance of the pink colored azo dye was measured at 540 nm.

The nitrate in seawater was determined based on the reduction of nitrate to nitrite in a reductor column filled with copper-amalgamated cadmium granules following which, nitrite was determined via the formation of an azo dye (Grasshoff, 1969). The reduction conditions were maintained using ammonia-ammonium chloride buffer in such a way that nitrate was quantitatively converted to nitrite but not further. The principal reaction that takes place is

$$NO_3^- + Me_{(S)} + 2H^+ \rightarrow NO_2^- + Me^{++} + H_2O$$
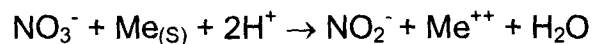
2.4.2.2　Ammonia ($NH_4^+ + NH_3$)

Ammonia estimation was based on the improved method given by Koroleff (1970). Ammonia dissolved in seawater reacts with hypochlorite under moderately alkaline conditions forming monochloramine, which in the presence of sodium nitroprusside (as catalyst), phenol and excess hypochlorite forms indophenol blue. The ratio of phenol:active chlorine must be constant and should be close to 25 w/v which otherwise will affect (bleach) the colour intensity. The blue colour of the indophenol was then measured at a wavelength of 630 nm.

2.4.2.3 Phosphate

Inorganic phosphate was estimated using the method given by Koroleff (1983). Phosphate ions in seawater were made to react with acidified molybdate to yield a phosphomolybdate complex, which was then reduced to highly coloured blue compound by ascorbic acid. The absorbance of formed phosphomolybdenum blue was measured at 880 nm. To avoid the interferences from silicate, the pH of the final reaction was less than 1 and the ratio of sulphuric acid to molybdate was maintained between 2 and 3.

Table 2.4

Summary of precision for the analytical instruments employed during analyses.

Instrument Name	Proxy analyzed	Precision
Scintillation Counter (RPL, Ahmedabad)	^{210}Pb	± 5%
Accelerator Mass Spectrometer (Woods Hole, USA)	^{14}C	5 - 7‰
NC Elemental Analyzer (PRL, Ahmedabad)	C_{org} N_{org}	±1.0% ±0.8%
NCS analyzer (NIO,Goa)	C_{org} N_{org}	±0.9% ±0.77%
Elemental analyzer (Bremen,Germany)	C_{org} N_{org}	±0.22% ±0.01%
Coulometer (NIO, Goa)	$CaCO_3$	±1.0%
IRMS (NIO, Goa)	$\delta^{18}O$ $\delta^{13}C$	± 0.06‰ ± 0.04‰.
EA - MS (Bremen,Germany)	$\delta^{13}C_{org}$ $\delta^{15}N_{org}$	±0.11‰ ±0.17 ‰
ICP-AES (NIO, Goa)	Fe & V , Mn & Mo, Co & Cd	<1%, <1.5%, <3%
GC (NIO, Goa)	N_2O	< 4%
Autoanalyzer (NIO, Goa)	NO_2^-, NO_3^-, NH_4^+, PO_4^{3-}	±0.006, 0.06, 0.06, 0.003 μM

CHAPTER 3

Chapter 3

HYDROGRAPHY AND BIOGEOCHEMICAL CHARACTERISTICS

OF THE CORING SITES

3.1 Introduction

This chapter provides the background information on oceanographic processes on the central and eastern Arabian Sea. Some of the information included is based on the published data for which appropriate references are made. The other data were generated by the biogeochemistry group of which the author was a participant. It may be added that collection of diverse data used in the study cannot be obtained by a single individual.

In order to understand the hydrographical and biogeochemical processes of the Indian Ocean, it is essential to consider its unique geographical setting and geomorphological features that have already been alluded to, in Chapter 1. The presence of land mass that limits the northern expanse of the Indian Ocean to a latitude $<\sim25$ °N, give rise to the monsoonal climate. The word "monsoon" is derived from the Arabic "mausam", meaning the climate. It is believed to have been used by the sailors in the context of the seasonally reversing winds and oceanic currents that they made use of, for sailing to and from India, from the middle-eastern and east African ports. There are actually two monsoons, the Northeast (NE) or winter monsoon and the Southwest (SW) or summer monsoon, both identified by the dominant direction, the winds blow from during December-March and June-September,
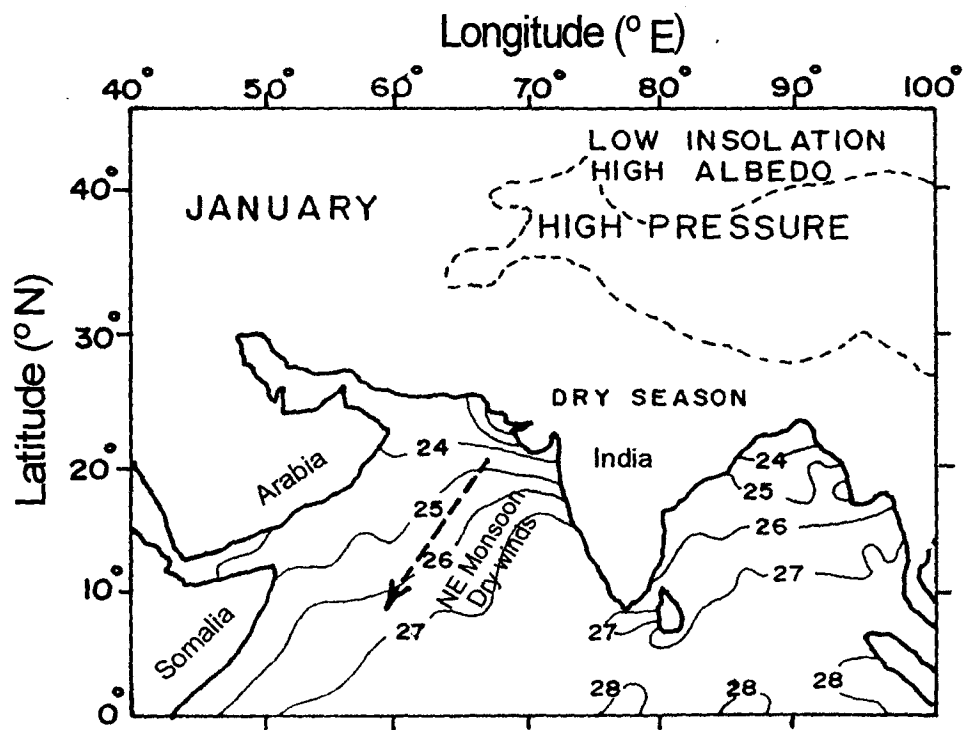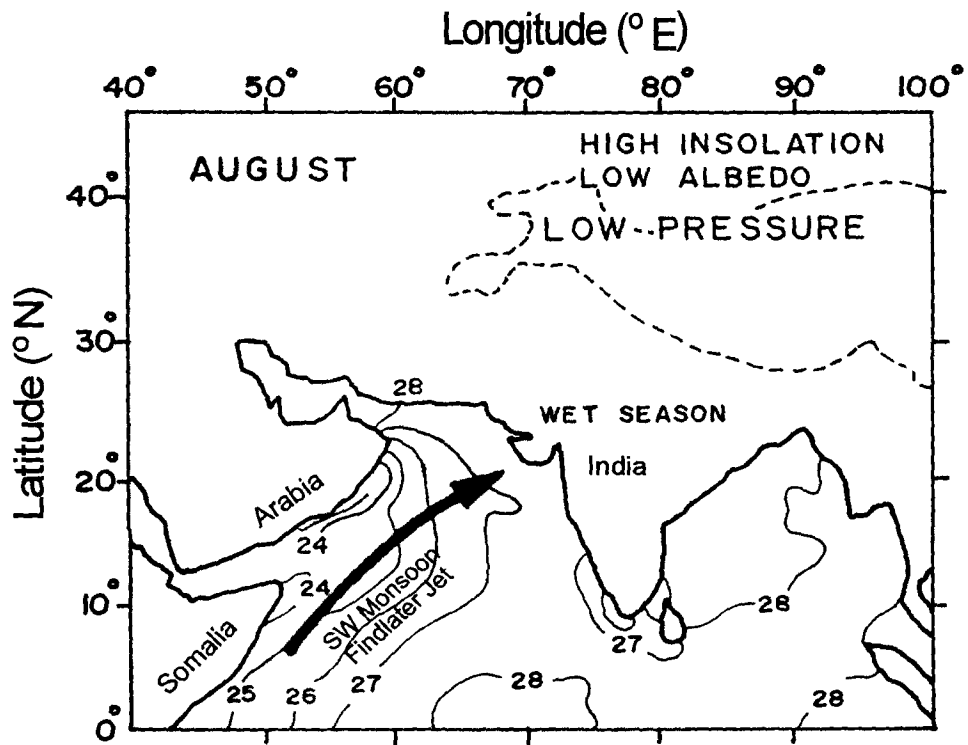
Figure 3.1: Modern sea surface temperature (°C) and general wind pattern during SW and NE monsoon period. The thick arrow represents the axis of Findlater Jet. The dashed line over Asia indicates elevations >3,000 meters. Dashed arrow indicates direction of relatively weak winds during NE monsoon period (modified from Prell, 1984a).

respectively. Following the scheme currently in use, the transition periods between the two monsoons are called the Spring Intermonsoon (April-May) and Fall Intermonsoon (October-November).

The winter (NE monsoon) season is characterized by high pressure over the Asian landmass which results in the northeasterly winds over the Arabian Sea (Figure 3.1). The formation of low pressure over the Asian landmass is due to the low seasonal insolation and relatively high albedo due to seasonal snow cover (Clemens et al., 1991). On the other hand in summer, as a result of the differential heating of the continent and oceanic regions, a low atmospheric pressure develops over the Asian landmass with relatively high atmospheric pressure over the cooler southern Indian Ocean. This drives southwesterly winds over the Arabian Sea including a strong low-level atmospheric jet, called the Findlater (or Somali) Jet (Smith et al., 1991) that extends from the Somali coast to the northwest coast of India (Figure 3.1). The moisture-laden winds bring about widespread rainfall over the whole of South Asia (Clemens et al., 1991).

Most of the rainfall over the Arabian Sea occurs during the SWM and along its eastern shores where it exceeds ~3000 mm y^{-1}. The precipitation declines towards the northwest. The balance between evaporation and precipitation is the highest off the Arabian coast and the lowest off Southwest India. The Arabian Sea receives much smaller river runoff than the Bay of Bengal with the combined discharges by the Indus, Narmada and Tapi being < 200 km^3 y^{-1}. However, there are numerous smaller rivers originating in the Western Ghats whose combined annual discharge (mostly during the SWM)

has been estimated to be about 150 km^3 (Naqvi et al., 2003). Due to the large rainfall and land runoff precipitation and runoff exceed evaporation over a narrow belt off the west coast of India. The net water balance is negative elsewhere in the Arabian Sea. Therefore, surface salinity shows a marked increase from the southeastern to the northwestern parts of the Arabian Sea (Wyrtki, 1971).

3.2 Circulation and water masses

The most remarkable feature of the surface circulation in the Arabian Sea, as indeed for the Indian Ocean as a whole, is the reversal of surface currents every six months. Because, the North Indian Ocean is a small ocean basin located essentially in the tropics, coastal and equatorial Kelvin waves and equatorial Rossby waves, that have both annual and sub-annual periods and are generated by changes in the monsoon winds, can propagate rapidly through the region, thereby strongly influencing circulation far away from their origins (Shetye and Gouveia, 1998). The combination of such remote forcing and local wind forcing produces features of surface circulation not observed in other regions.

Figure 3.2 shows the generalized surface circulation in the northern Indian Ocean during the two monsoon seasons. In general, surface currents in the Arabian Sea flow clockwise during the SWM and counter-clockwise during the NEM. The SWM currents are the most energetic in the western Arabian Sea, especially off Somalia, where the northbound seasonal Somali Current (SC) attains a volume transport which is comparable to that of the
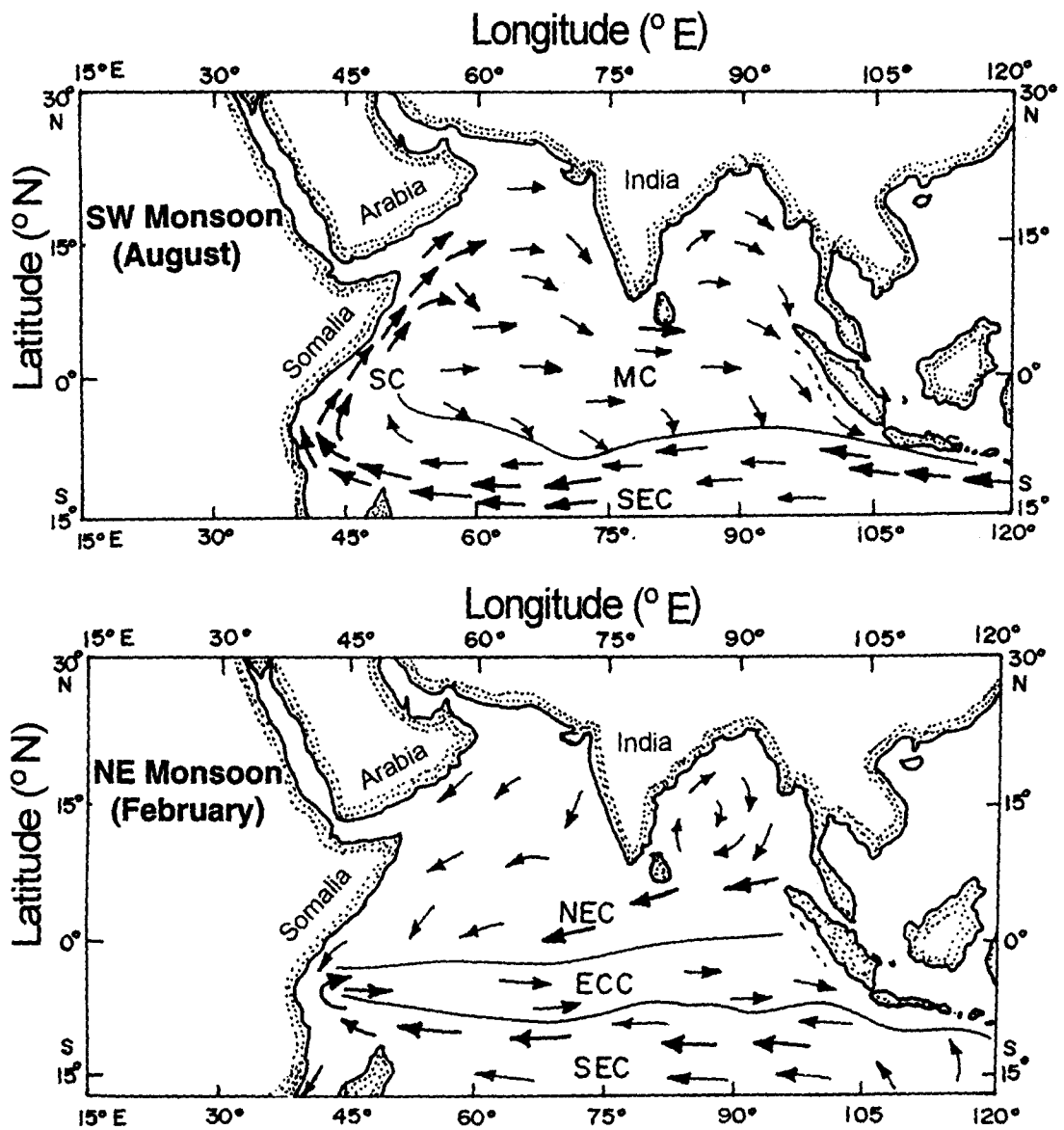
Figure 3.2: Surface circulations in the Indian Ocean during the SW and NE monsoon period (after Wyrtki, 1973). MC – Monsoon Current, SC – Somali Current, SEC – South Equatorial Current, NEC – North Equatorial Current, ECC – Equatorial Counter Current.

Gulf Stream (Schott and McCreary, 2001). The Somali Current system includes three major anticyclonic eddies - the Southern Gyre (SG), the Great Whirl (GW) and the Socotra Eddy (SE); because of which most of the northward coastal flow by the SC is deflected to the east and south around 4° and 10 °N latitudes to feed the Southwest Monsoon Current (SMC). The offshore divergence causes intense upwelling at these latitudes, especially around 10 °N. Even more widespread upwelling occurs further north off the Arabian coast, especially off Oman. However, the currents here do not exhibit an organized pattern and seasonality expected from the wind stress except close to the coast (e.g. the Ras-al-Hadd Jet off northwestern Oman). Instead, the flow is dominated by meso-scale eddies that account for the bulk of the kinetic energy (Flagg and Kim, 1998). The filaments and plumes carrying the cold, nutrient-rich upwelled waters extend up to ~1000 km from the coast, fertilizing a large volume of the surface layer and resulting in intense phytoplankton blooms (Naqvi et al., 2003).

Along the Indian coast, the southward flowing West India Coastal Current (WICC) induces upwelling, but this process is much weaker compared with the upwelling off Oman or Somalia and the upwelled water does not spread as far offshore. The thermocline does shoal up over a large area, though, all along the coast and in the region of the Lakshadweep Low (LL), a seasonal cyclonic eddy. Moreover, the upwelled water is overlain by a thin (~10 m) warm, fresher lens because of which the signatures of upwelling are not discernible in the satellite data. It may be noted that the upwelling period (May-November) extends well beyond the SWM season indicating that

the process cannot be forced entirely by local winds. This is supported by results of numerical modeling which shows that, remote forcing from the Bay of Bengal plays a major role in driving the WICC (McCreary et al., 1993).

During the NEM, the SMC is replaced by the Northeast Monsoon Current (NMC) that flows westward. Surface currents in the northern and western Arabian Sea are weaker and less organized, but circulation in the eastern Arabian Sea is best developed during this season. This current is the broadest off the SW coast of India, where the LL is replaced by the Lakshadweep High (LH), and gradually narrows as it flows northward (Shetye et al., 1991a). The warm, low-salinity waters of the WICC exert a major control on biogeochemical cycling as they do not allow convective mixing to occur along over most of the western continental shelf of India. This certainly is the case off Goa.

The subsurface water movement in the northern Indian Ocean is poorly known, but is also greatly impacted by the existence of the low latitude northern boundary. As the isotherms within the thermocline do not outcrop in the North Indian Ocean, the subsurface layers in the region are ventilated mostly from the south. The Arabian Sea does receive dense outflows from the Persian Gulf and Red Sea; however, their combined volume transport is only about 0.64×10^6 m^3 s^{-1}, an order of magnitude lower than the volume transport for intermediate waters of the southern origin (Warren, 1994). These waters enter the Arabian Sea only along its western boundary and during the SWM (Swallow, 1984) such that most of the mid-depth water renewal in the Arabian Sea (and in fact the entire North Indian Ocean) occurs in the western

region.

Based on the temperature and salinity distribution in the water column, three different kinds of water masses can be distinguished for the Indian Ocean; those that are generated within the open Indian Ocean by sub-duction, those that are mixing products of other water masses, and those that enters from outside (Wyrtki, 1971; Tomczak and Godfrey, 1994, Tomczak and Godfrey, 2003). Winter cooling in the northern Arabian Sea leads to the formation of a very shallow subsurface water mass called the Arabian Sea High Saline Water (ASHSW) (Shetye et al., 1994). Being denser, this water spreads as a salinity maximum just beneath the surface mixed layer (Morrison, 1997; Schott and Fischer, 2000). Another northern salty near-surface water mass, found at a depth of about 250–300 m which is clearly distinct from ASHSW, is the Persian Gulf Water (PGW). The influence of PGW does not extend very far beyond the northern Arabian Sea; it loses its identity due to mixing with waters of the southern origin as it moves southward (You and Tomczak, 1993; Kumar and Prasad, 1996). The third and the densest water formed in the region is the Red Sea Water (RSW) which is encountered at a water depth of 500-600 m; the salinity maximum corresponding to this water is rarely seen north of latitude 17 °N. Of the water masses coming from the Southern Hemisphere, the Subantarctic Mode Water (which has about the same density as the PGW) but is characterized by an oxygen maximum and a salinity minimum, is the most prominent (Sen Gupta and Naqvi, 1984). The oxygen maximum corresponding to this water vanishes at about 12 °N, the southern limit of the suboxic zone (Naqvi et al., 1993).

The Lower Circumpolar Deep Water (CDW) enters the deepest parts of central Indian Ocean (Toole and Warren, 1993). However its direct entry is generally obstructed by the deep ridges. The deepest water in the Arabian Sea is derived through a western boundary current that passes through a chain of western basins and enters the Arabian Basin through the Owen Fracture Zone (Naqvi and Kureishy, 1986). The Indian Deep water (IDW) mass which is presumably formed due to deep upwelling of the CDW flows just above the CDW. The IDW mass is oxygen-poor and has high salinity as a result of its mixing with older intermediate waters above while in the southwest, it has the characteristics of diluted North Atlantic Deep Water, which has higher oxygen and salinity (Mantyla and Reid, 1995).

3.3   Upwelling/vertical mixing, productivity and the oxygen minimum zone

The effect of monsoonal forcing in the Arabian Sea is evident in the seasonal sea surface temperature (SST) maps that also reflect the circulation pattern (Figure 3.1). The lowest SSTs in the Arabian Sea paradoxically occur in summer in the western Arabian Sea, obviously caused by upwelling. As already mentioned, upwelling also occurs along the west coast of India during the SWM, though far less vigorously than in the western Arabian Sea. This is because, the strong wind blowing with the Somali and Arabian coasts to its left results in rapid and large scale Ekman transport. The volume of water upwelled is very large as is the area of the Arabian Sea over which it spreads. In the eastern Arabian Sea, the process is much slower. The thermocline

shoals up to very shallow depths (with the upwelled water often prevented from reaching the surface by the low salinity cap) in response to the large scale circulation with the local winds contributing only part, to the upwelling. The process introduces copious amounts of nutrients to near-surface waters sustaining high primary productivity (PP).

Nutrient enrichment also occurs in the Arabian Sea during the NEM. This is because, the cold dry winds blowing from the continent over the ocean increase the density of surface waters resulting in convective overturning which reaches and erodes the upper portion of the thermocline over a large area in the northern and central Arabian Sea. The high biological productivity arising from the nutrient enrichment is accompanied by a high rate of organic matter input and its oxidation in the water column. As pointed out earlier, the renewal of intermediate waters is largely through advection from the south and these waters lose much of their oxygen content by the time they reach the Arabian Sea. The circulation in the equatorial Indian Ocean also plays an important role in maintaining low oxygen concentrations in the Arabian Sea. The flow of waters in the upper kilometer in the equatorial belt is mostly zonal, such that cross equatorial exchange of water is only confined to the western Arabian Sea (Swallow, 1984). According to Swallow, "The equatorial region between, say, 5 °N and 5 °S seems likely to act as a holding tank, in which the dissolved oxygen of the relatively new intermediate water decays and is reduced by mixing with the older water". Thus, the development of an intense and thick (150-1200 m) OMZ in the Arabian Sea is a result of the combination of limited oxygen supply to the intermediate layers through water renewal and

a moderately high rate of oxygen consumption (Swallow, 1984; Naqvi, 1987; Olson et al., 1993; Warren, 1994).

The acute oxygen depletion causes the heterotrophic bacterial population to switch over to alternate electron acceptors for organic matter degradation (Richards, 1965). The most abundant of such species in the water column is NO_3^-. For NO_3^- to be utilized as an oxidant, the dissolved oxygen concentrations must cross a threshold value which is probably well below 1 μM (Morrison et al., 1999; Codispoti et al., 2001; Naqvi et al., 2003). This threshold is deduced based on the observation that NO_2^- accumulation in oxygen-poor waters, taken as a diagnostic tool for denitrification, only occurs when the precisely measured oxygen concentrations are below this level. Note that the corresponding Winkler oxygen concentrations may be higher by 2-3 μM. The threshold oxygen levels appear to reach in only upper 1/3 or so of the OMZ in the Arabian Sea in the vertical within a zone that is well defined and does not seem to have changed much since it was first delineated by Naqvi (1991) from the climatology of NO_2^- data then available. It is remarkable that despite the presence of a large volume of water with oxygen levels just above the nitrate reduction threshold, the open-ocean denitrification (suboxic) zone remains fairly stable over decades, that too with the "global change" reportedly already underway (Goes et al., 2005).

3.4 Processes for the formation of coastal and open-ocean suboxic zones

The most intense OMZ, as inferred from the occurrence of the SNM is

located in the generally most productive northwestern part of the Indian Ocean. However, within the Arabian Sea itself, suboxic conditions are not associated with the upwelling systems of Somalia and Arabia; instead, the SNM zone extends toward the southwest into the central Arabian Sea from the northwestern Indian shelf, a region of relatively low PP (Figure 3.3). This is believed to arise from a more effective subsurface-water renewal along the Arabian Sea's western boundary through advection from the south (given that the cross-equatorial exchange of subsurface waters is largely confined in the western Indian Ocean – Swallow, 1984) as well as from the Red Sea and the Persian Gulf. Moreover, the dominance of upper-layer flow by meso-scale eddies, which account for the bulk of the kinetic energy (Flagg and Kim, 1998) and extend to the core of the suboxic zone, may facilitate greater downward diffusion of O_2 from the surface in the west. In contrast, the SNM coincides with the zone of the lowest kinetic energy and reduced vertical penetration of the eddy field (Kim et al., 2001). In addition to these physical factors, the availability and utilization of nutrients by phytoplankton and the subsequent vertical flux of organic matter must also contribute to the observed O_2 distribution. Kim et al. (2001) opined that the route of offshore transport of the nutrient-rich upwelled water (occurring predominantly through filaments and plumes) is such that the denitrification zone receives more nutrients/organic matter than the region located to its south and west. They emphasized the importance of the Ras al Hadd Jet that transports upwelled water first along the northeast Omani coast and then away from the coast off the cape, it has been named after. Nutrient distributions during the upwelling season (e.g. for
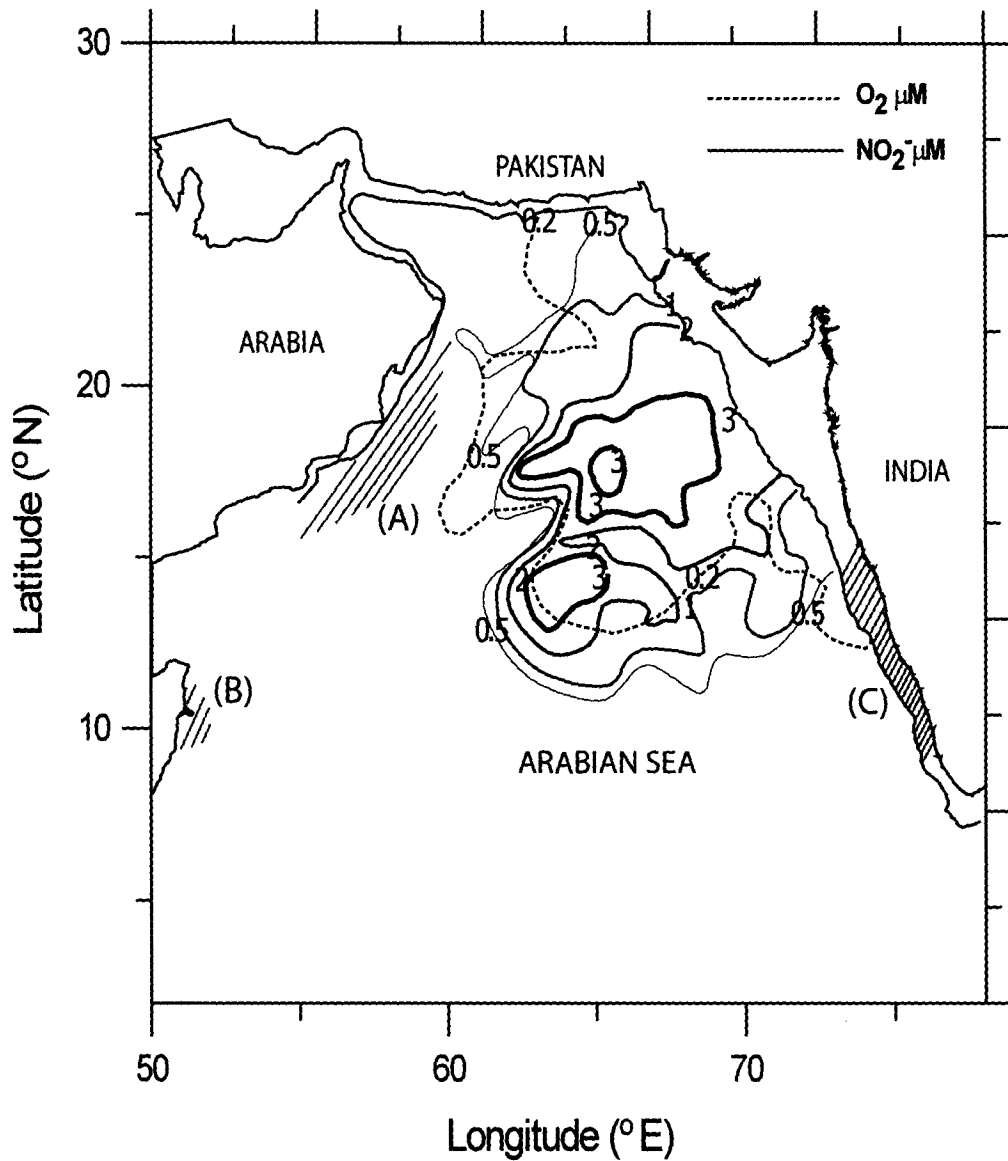
Figure 3.3: Map of Arabian Sea demarcating the OMZ region in terms of secondary nitrite (NO_2^-) maxima and oxygen (O_2) concentrations (μM). Hatched areas represent zones of upwelling off Arabia (A), Somalia (B) and Southwest India (C). Figure modified from Naqvi (1991).

NO_3^-; Figure 3.4) do indeed indicate long-distance ($\geq$1000 km) transport of the upwelled water reaching well within the region of the most intense O_2 deficiency, but the generally-observed gradual offshore decrease in surface nutrient concentration is not supportive of this view.

Recent results of modeling (Wiggert et al., 2006) as well as observations (Naqvi et al., submitted) suggest that, contrary to the prevalent belief, PP in the western Arabian Sea might sometimes be limited by iron (Fe) instead of nitrogen during the SWM. These results have important implications for the composition of phytoplankton and the vertical scale of organic matter degradation. Iron deficiency has been known to cause an increase in ratio of Si:N uptake by diatoms (Hutchins and Bruland, 1998) facilitating greater offshore transport of NO_3^-. A more rapid depletion of silicate is expected to cause a shift in phytoplankton community structure with increasing abundance of smaller autotrophs offshore, which is in accordance with observations (Garrison et al., 1998). During the northeast (NE) monsoon the central Arabian Sea experiences convective mixing that penetrates, at the most, to a depth of 125 m (Banse, 1984, 1987). The depthwise nutrient distribution in the region is such that vertical mixing brings up substantial amounts of NO_3^- to the euphotic zone but not much silicate, thereby limiting diatom productivity (Naqvi et al., 2002). Thus, PP in the open central Arabian Sea seems to be dominated by small, non-diatomaceous autotrophs during both the SWM and NEM. The organic matter produced by these organisms would be degraded at shallower depths relative to that produced by diatoms. Therefore, one would expect the average depth of remineralization of material
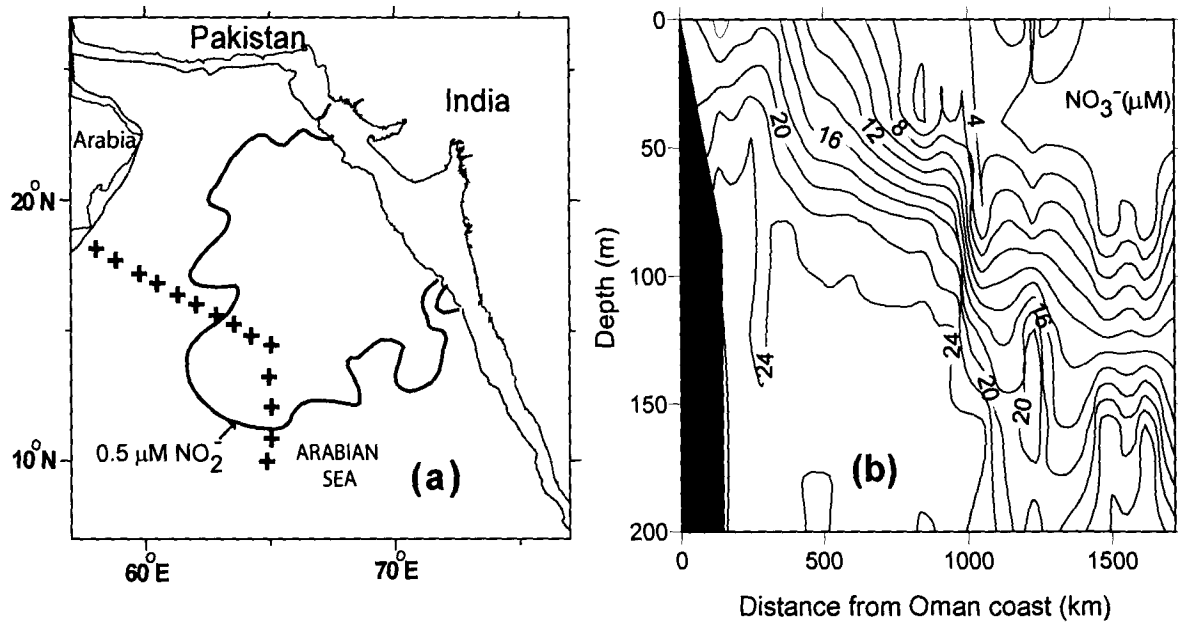
Figure 3.4: **(a)** Cruise track (+) of U.S. JGOFS cruise TN050 (August-September) **(b)** Distribution of NO₃⁻ (nitrate data from U.S. JGOFS cruise TN050) indicating long distance (>1000km) transport of upwelled waters reaching well within the OMZ region. (Figure adapted and modified from Naqvi et al., 2006b).

exported from the surface layer to shoal up with increasing distance from the coast, such that more material is degraded close to the core of the O_2 minimum zone in the offshore region. This is consistent with the observed O_2 distribution (Naqvi et al., submitted).

The development of suboxic conditions over the Indian shelf is related in a general way to the prevalence of large-scale, mesopelagic, open-ocean O_2 deficiency, because the latter is the source of water that upwells over the Indian shelf during the SWM. Nevertheless, the open-ocean and coastal suboxic zones are not contiguous. This is due to the presence of the West India Undercurrent (WIUC) that flows northward while the surface flow is toward the south. The WIUC may be identified just off the continental shelf/slope from the distribution of temperature (upward sloping of isotherms at the top of this feature and downward tilt close to its bottom; Figure 3.5a), and even more clearly from those of salinity and O_2 (Figure 3.5b,c). Note that the water derived from the south has lower salinity and slightly higher O_2 content. As judged by the 35.400 salinity contour, the influence of the undercurrent, at its peak, extends vertically down to approximately 400 m depth and horizontally up to 200 km from the continental slope at 15°N latitude (Figure 3.5b). Even though seasonally variable, the WIUC is very important for determining the redox status of subsurface waters since it is a source of O_2 to the otherwise suboxic mesopelagic zone that prevents the water from turning denitrifying off the continental margin probably as far north as 17 °N latitude. Consequently, as reflected by the distribution of NO_2^- (Figure 3.5d), denitrification intensifies away from the coast. This pattern is
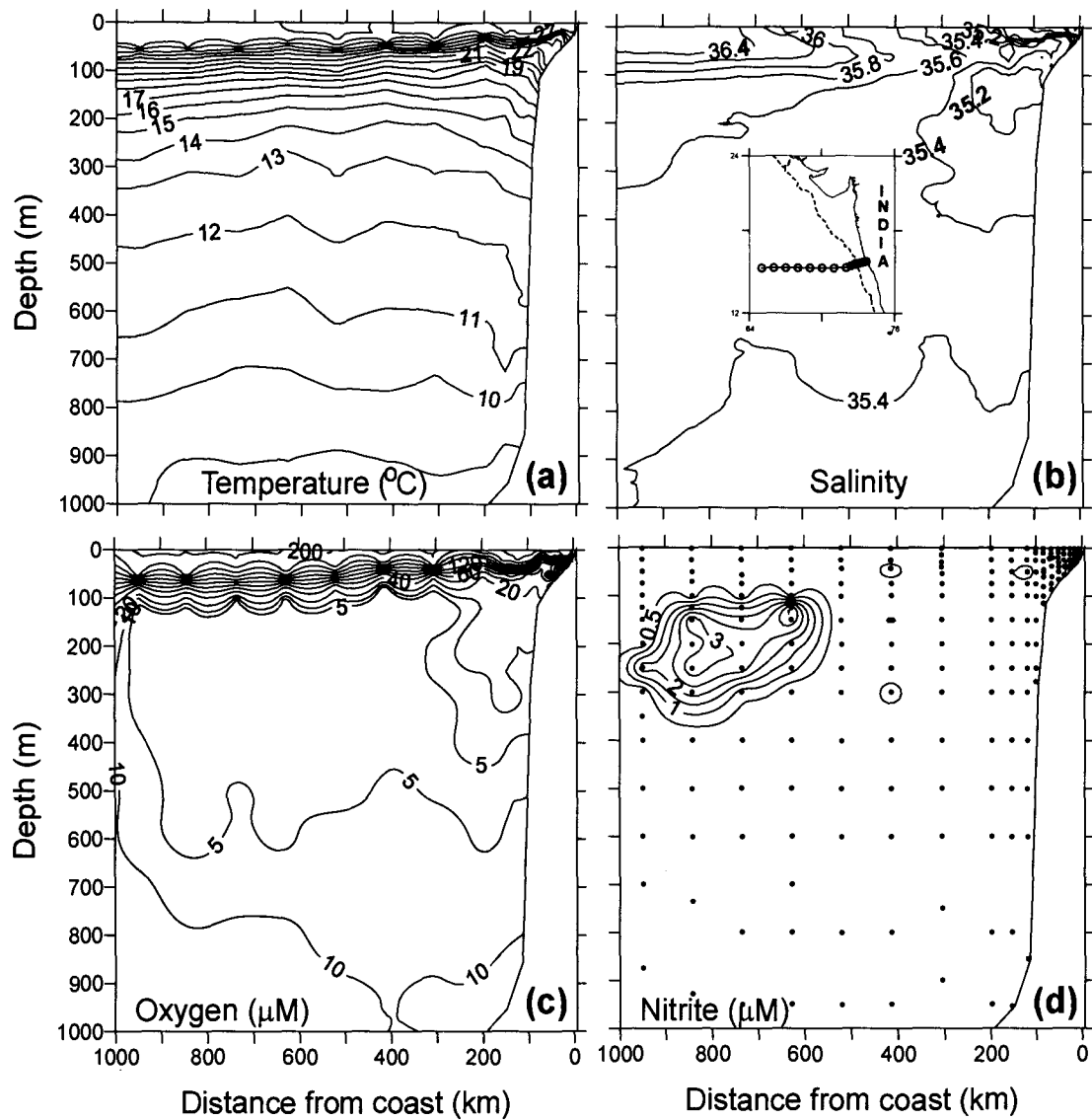
Figure 3.5: Distribution of (a) temperature, (b)salinity, (c)O_2, and (d) NO_2^- in the upper 1 km off Goa (see inset in (b) for station locations) during December 1998. Adapted from Navqi et al. (2006b).

opposite to that observed in the two other major oceanic suboxic zones, especially off Peru-Chile, where the poleward undercurrents, in fact, support bulk of the denitrification (Codispoti et al., 1989). This difference probably owes to a lower respiration rate within the WIUC, which, in turn, may be caused by two factors. First, unlike its counterpart off Peru-Chile the WIUC does not occur over the shelf but along the continental slope, and secondly, except in the most southern part, upwelling along the west coast of India is by and large confined to a narrow strip over the inner shelf such that surface waters directly overhead of the WIUC are not very productive. As the water upwells and moves shoreward, rapid increase in respiration depletes its already low O_2 content, culminating in the seasonal development of reducing conditions [denitrification followed by sulphate (SO_4^{2-}) reduction] over the mid- and inner-shelf regions (refer the following section of 3.5) covering a wide latitudinal range (between at least 12 °N – 20 °N, probably extending further north to the Pakistani coast).

3.5 Biogeochemical conditions prevailing over the shallow coring sites

Cores CR-2, SaSu-1 and SaSu-3B were raised from the inner- and mid-shelf regions off Goa (Figure 3.6). Hydrographic and chemical data along a coast-perpendicular section off Goa for the core sampling period (late SWM/early SI) are plotted in figure 3.7 whereas figure 3.8 provides the same information for the NEM season. In order to demonstrate the evolution and demise of the oxygen deficient conditions on an annual cycle, the data
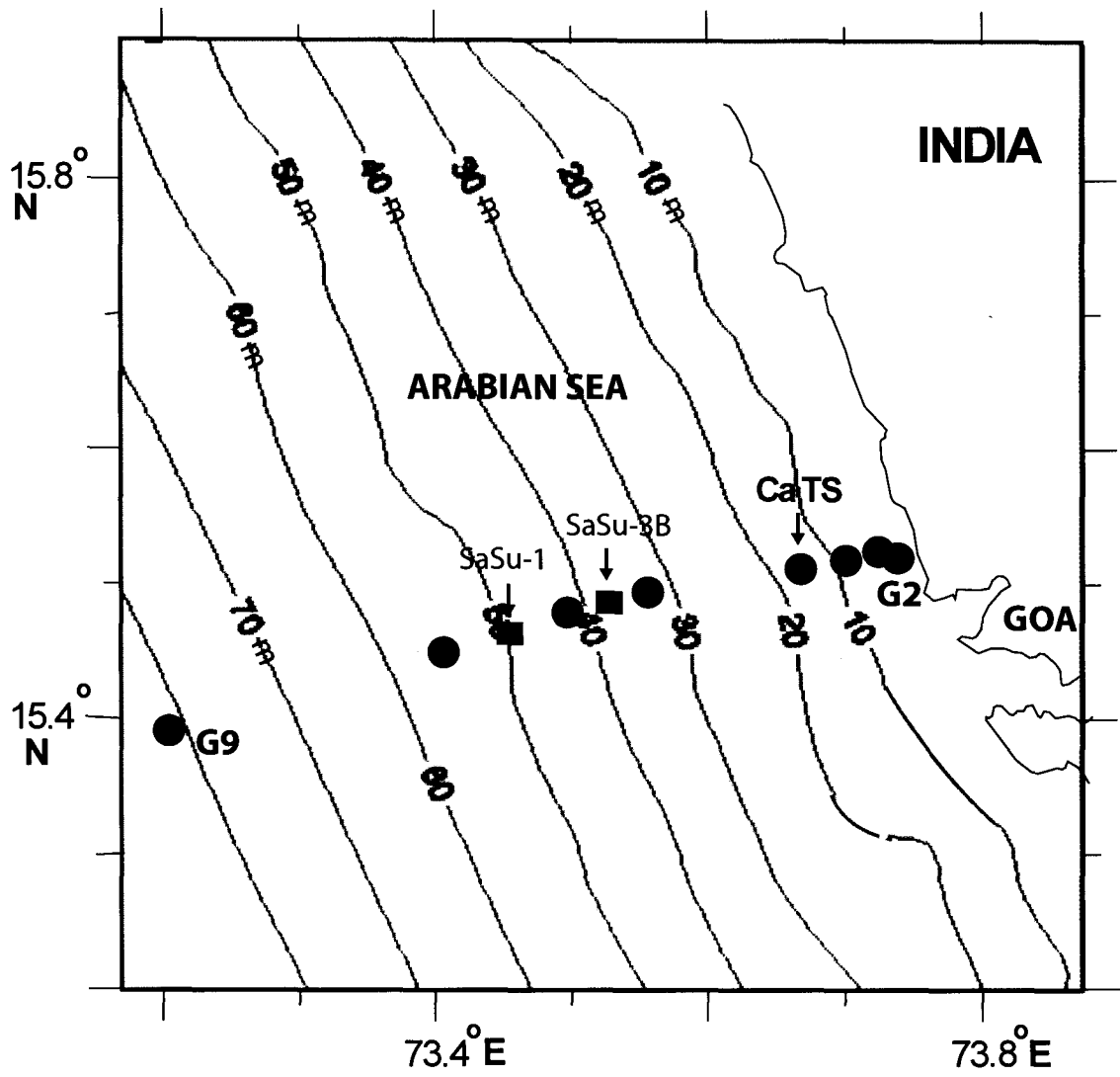
Figure 3.6: Section showing the sampling transect (G2-G9) off Goa, along with the CaTS and coastal core (SaSu-1, SaSu-3B) locations with bathymetry.

collected at the CaTS station are also presented and discussed.

3.5.1 Cross shelf sections off Goa during two seasons

As stated above, the southward flowing WICC induces upwelling along the west coast of India. Figure 3.7, based on measurements made in September 2002, shows this feature and also depicts the changes that occur in the upwelling water as it moves up the shelf. The upsloping of isotherms (Figure 3.7a) toward the coast are obviously due to upwelling which begins sometime in April-May and lasts till October/November. The other striking feature of the hydrographic data is the presence of the previously mentioned low-salinity lens that overlies the cold, saline upwelled water, especially near the coast (Figure 3.7b). This fresher water lens is produced as a result of intense rainfall in the coastal zone (in Goa, the annual rainfall is in the vicinity of 3000 mm, but most of it is concentrated during the SWM).

Around the shelf break, near-bottom water has low oxygen concentration, but it is oxidizing (DO is well above the detection limit of the Winkler procedure, NO_3^- content is high and NO_2^- is undetectable, see figures 3.7c,d,e). However, as this water ascends over the shelf, it quickly loses the residual oxygen that leads to sequential reduction of other oxidized chemical species: First, denitrification sets in over the mid-shelf region as evidenced by the depletion of NO_3^- and build up of NO_2^- (Figure 3.7e), and once NO_3^- and NO_2^- are fully consumed, SO_4^{2-} reduction is initiated over the inner-shelf, as reflected by the accumulation of H_2S (Figure 3.7f). These conditions are typical for the period (late summer/early autumn) although some variations do
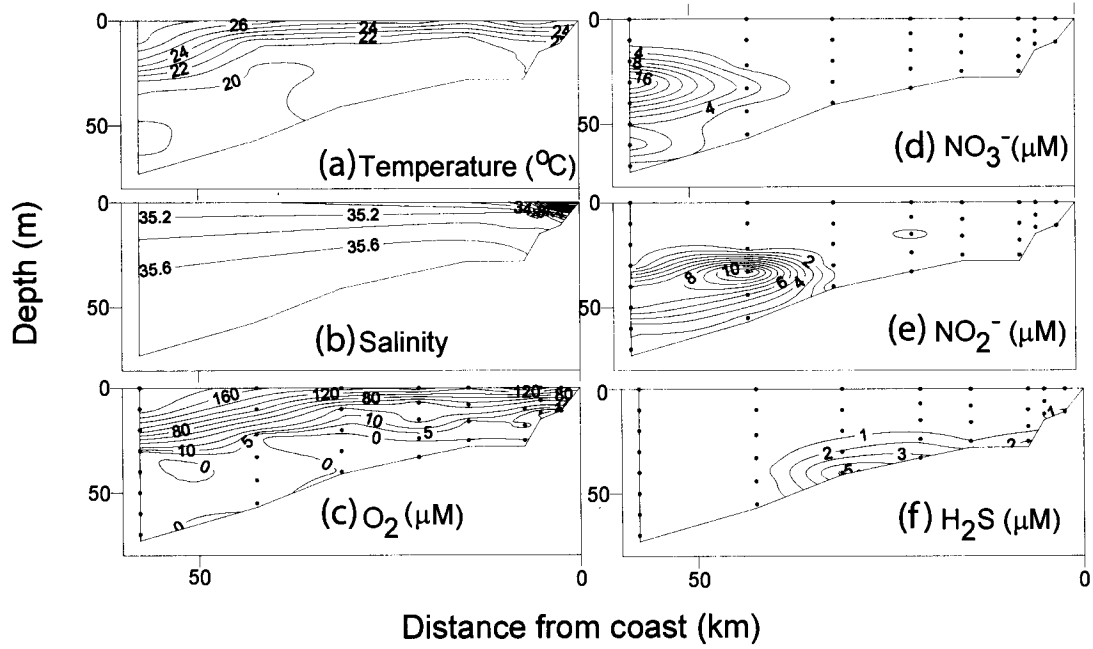
Figure 3.7: Vertical sections of temperature, salinity, oxygen (O_2), nitrate(NO_3^-), nitrite(NO_2^-) and hydrogen sulphide (H_2S) along a coast-perpendicular section off Goa (sampling transect as shown in figure 3.6) during late SWM (September 2002).

occur from one year to another (Naqvi et al., 2006a).

The conditions are quite different during the NEM when the WICC carries warmer, fresher waters of equatorial origin towards the north (Figure 3.8). The low concentrations of nutrients coupled with downwelling associated with this flow result in lower productivity and relatively deep mixed layers so that the shelf waters are generally well oxygenated. Observations made during the NEM season of 2002 accordingly show higher temperatures (~27-28 °C) than those observed during the SWM season (Figure 3.8a) while low salinity (< 34) persists to a depth of at least ~ 40m (Figure 3.8b). NO_3^- levels are much lower even when the denitrificaion does not occur due to the prevalence of high oxygen concentrations throughout the water column (Figures 3.8c).

3.5.2 Climatology at the CaTS site

The time-series station, named as the Candolim Time Series (CaTS), (15°31'N, 73°39'E) lies approximately 10 km off the coast from the village of Candolim (Figure 3.6). This site is being monitored since 1997. These observations are of great relevance to the present study because, the three short cores examined here come from the same general area and also because it is the most suitable data set to provide the background information on seasonal changes in the hydrographic and biogeochemical environment today with which, one can compare the core top proxy data and make inferences as to the past changes. The data for 7 years (1997-2004) have been pooled and averaged for various depth intervals on a fortnightly basis for
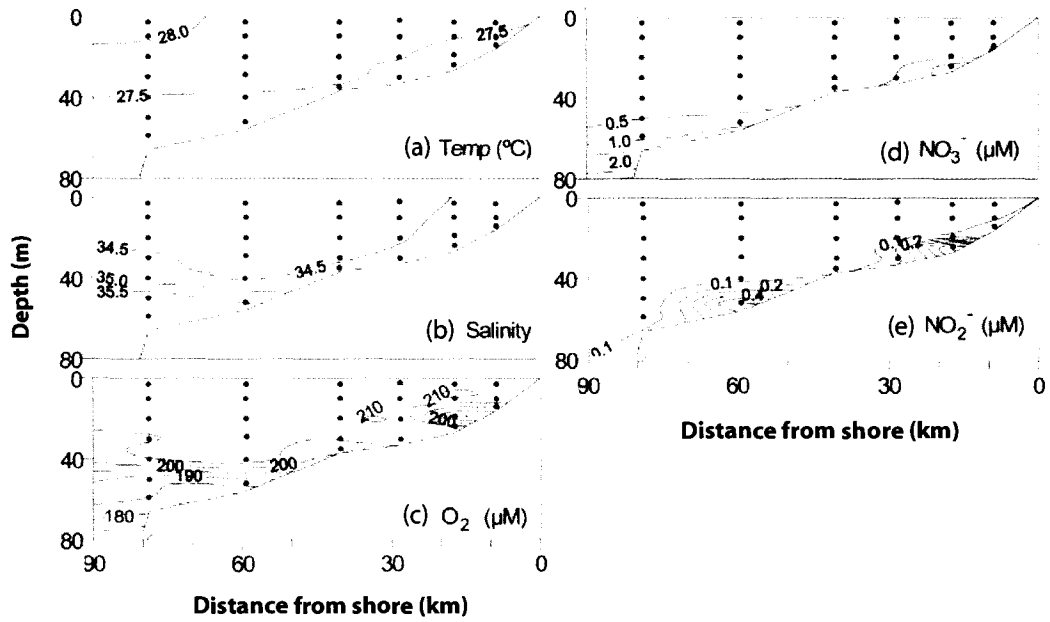
Figure 3.8: Vertical sections of temperature, salinity, oxygen (O_2), nitrate(NO_3^-), and nitrite(NO_2^-) along a coast-perpendicular section off Goa (sampling transect as shown in Figure 3.6), for the NEM season (February, 2002)

August-December and on a monthly basis for the remaining period. Figure 3.9 gives variations of various properties on a depth-time plot that reveals well-defined annual cycles of the measured variables.

The temperature record (Figure 3.9a) shows a bimodal distribution pattern that is well known to exist in this region (e.g. Banse, 1959). The highest values are recorded during the SI while the lowest values occur during the late SWM extending into the early FI, obviously due to upwelling. The water column during the NEM is homogenous but the salinity changes considerably (Figure 3.9b) presumably related to the northward flow of WICC that brings fresher waters from the south, especially in February. Like temperature, salinity also reaches its maximum ($\geq$ 36.000) during the SI season. With the onset of upwelling and almost simultaneous formation of the low salinity cap strong vertical gradients in salinity (and temperature) develop that persist from June/July to October/November (Figure 3.9).

The oxygen deficiency apparently persists for a much longer period than one would expect from the temperature record (Figure 3.9c). Naqvi et al. (2006a) speculated that the decay of *Trichodesmium* blooms during the SI could sometimes result in O_2 depletion in the near bottom water even before the onset of upwelling. However, near-bottom O_2 concentrations do not reach suboxic (< 10 μM) levels until July/August. NO_3^- concentrations increased during the early stages of upwelling, but decrease once suboxic conditions develop in near-bottom waters (Figure 3.9d). This is associated with the accumulation of NO_2^- (Figure 3.9e). Within about one month of its onset, denitrification reaches completion (i.e. NO_3^- and NO_2^- are fully consumed). It

77
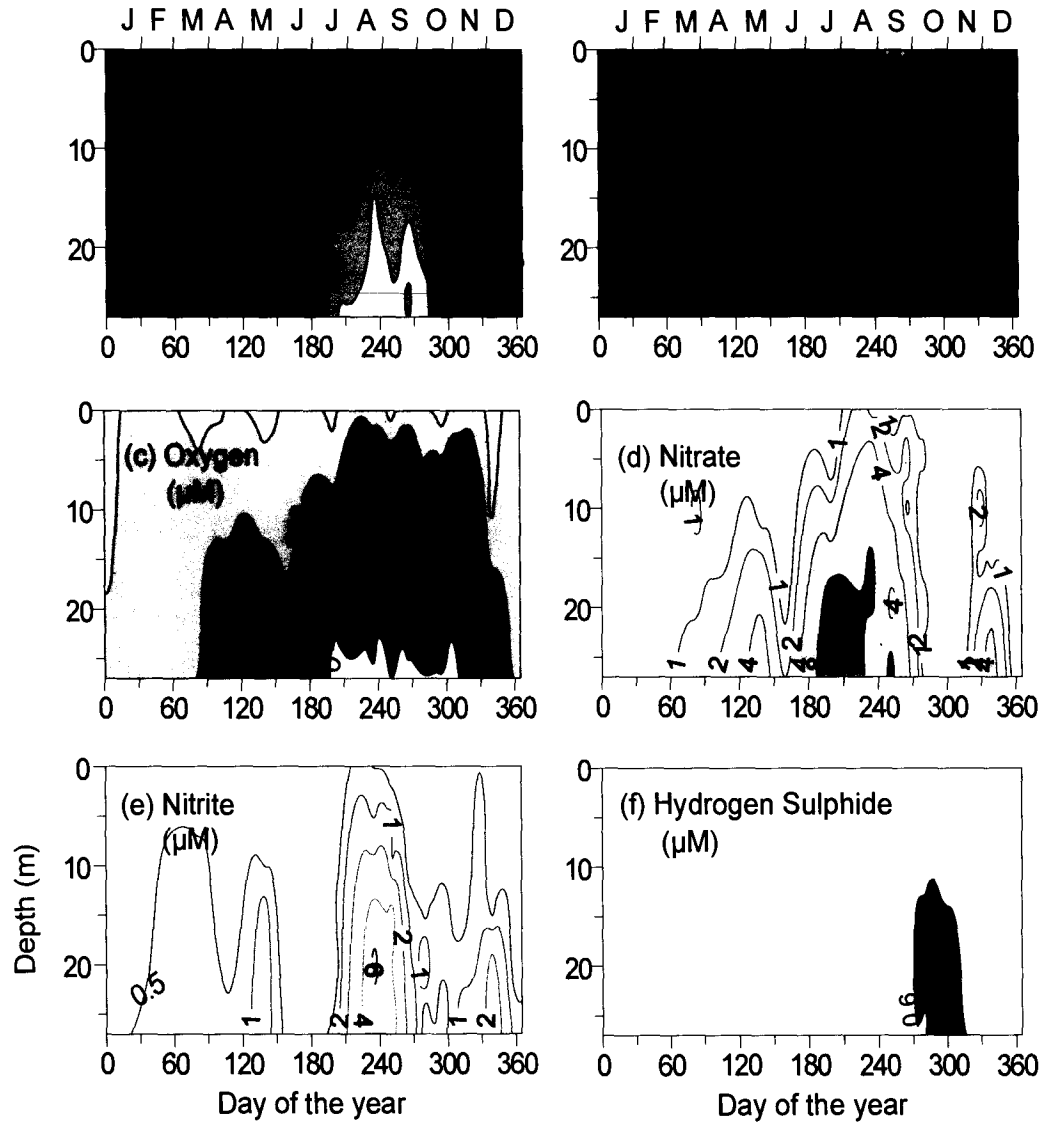
Figure 3.9: Monthly/fortnightly averaged records showing annual cycle of (a)Temperature (b)Salinity (c)Oxygen (d)Nitrate (e)Nitrite and (f)Hydrogen Sulphide at the Candolim Time Series (CaTS) site (15°31' N, 73°39' E) based on observations from 1997-2004. Figure modified from Naqvi et al. (2006a).

may be noted that in addition to the build-up of NO_2^- in suboxic waters during denitrification, some accumulation of NO_2^- also takes place at shallower depths in oxygenated waters (Figure 3.9e); this is due to assimilatory reduction of NO_3^- by phytoplankton, nitrification or denitrification in sediments (Naqvi et al., 2006a).

Reduction of SO_4^{2-} as indicated by the appearance of H_2S (Figure 3.9f) begins only after the complete removal of the oxidized N species from the water column. Such (anoxic) conditions prevail during the months of September and October (Figure 3.9). During this period, cross-shelf sections north of about 12°N latitude (e.g. Figure 3.10), exhibit all three types of redox environments (oxic over and beyond the outer shelf, suboxic over the mid-shelf and anoxic over the inner shelf). Such a well-organized sequence with a remarkable regularity is not known to occur along any other open coast. However, it is believed that a few decades ago complete anoxia in this region was not as frequent, if it existed at all, as it is now (at the CaTS site it has been recurring every year since 1998). For the region off Karwar and during the upwelling period, Naqvi et al. (2006a) compared oxygen data generated in recent years (1997-2004) with those collected in the 1970s, and found the recent values to be significantly lower. According to these authors, oxygen deficiency in this region seems to have intensified as a consequence of enhanced nutrient loading and this might account for the development of completely anoxic conditions.
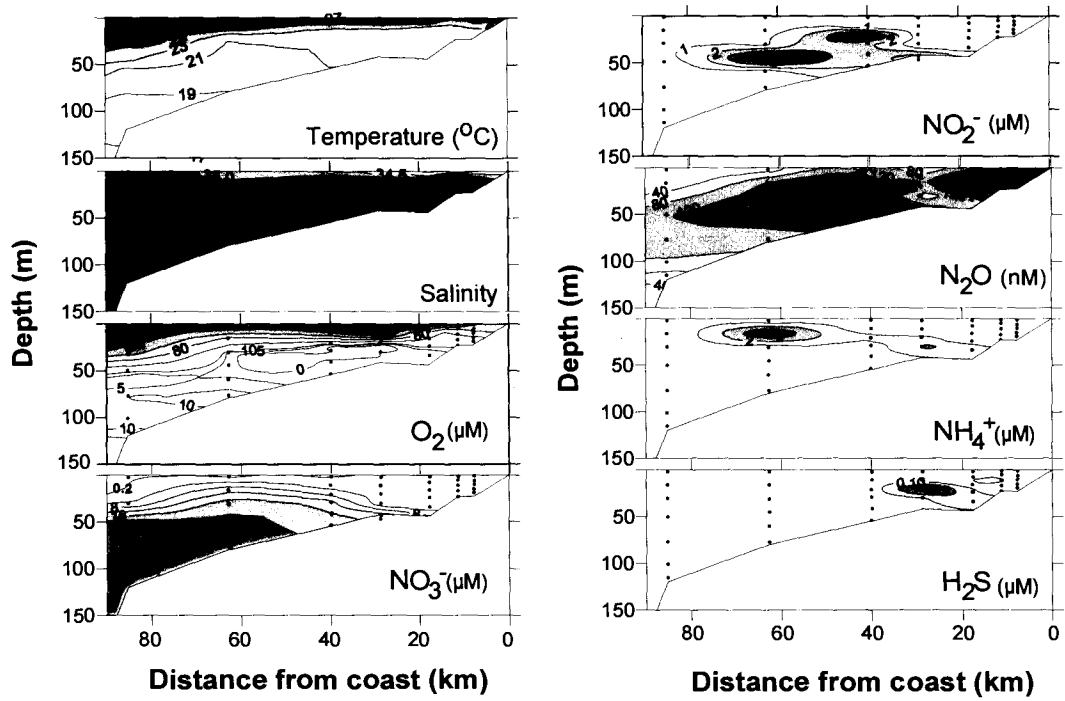
Figure 3.10: Vertical sections of temperature, salinity, oxygen, inorganic species and hydrogen sulphide off Goa during October 1999. Station locations are the same as shown in figure 3.6.

3.6 Biogeochemical conditions prevailing within the suboxic zone of the open ocean

As already stated, the seasonal suboxic zone over the western continental shelf of India is not contiguous with the perennial deeper suboxic zone of the open ocean. In figure 3.11, the boundaries of the perennial suboxic zone along with the climatological maximal nitrite concentrations reported by Naqvi, (1991) are shown along with the locations of the two open ocean coring sites (AAS-42/15 and AAS-42/12A). The two sites are clearly in the region that experiences intense denitrification today. A brief account of the hydrographic and biogeochemical attributes of the water column at this site is as follows:

Three stations were selected to provide representative profiles of hydrographic and chemical parameters. Two of them (3201 and 3202), occupied during the FORV *Sagar Sampada cruise* SS119 in April 1994, and are very close to the location of the core AAS-42/15 (17.07'997°N, 68.01'016°E). Station 3201 was sampled down to ~1.5 km, but 3202 was sampled down to 3 km. However, since the T, S and O_2 profiles converge at ~1.5 km, the profiles at 3202 can be taken to apply, to the core-top at this coring site and to the AA-42/12A site as well (horizontal gradients in properties at depths > 2 km are negligible between the two locations).

Vertical profiles of temperature, salinity and oxygen and of oxygen, nitrate and nitrite at the two stations are presented in figure 3.12a and 3.12b, respectively. A pronounced OMZ is conspicuously seen at both the sites between 150-1000 m, with the lowest oxygen values occurring in the upper
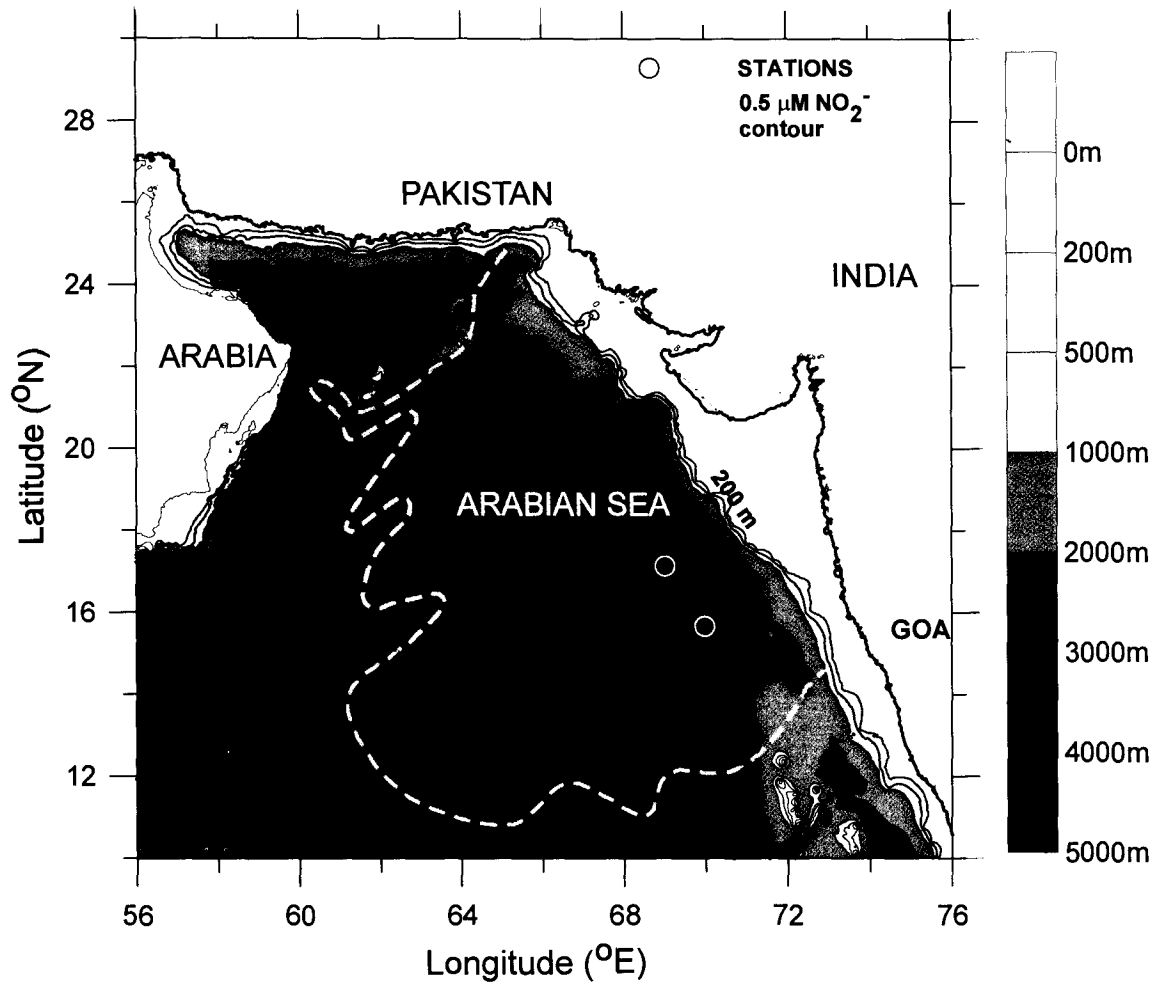
Figure 3.11: Geographical limits of the perennial suboxic zone, demarcated by 0.5 μM nitrite contour, along with location of open ocean cores (denoted with empty circles) and bathymetry.

Oxygen (μM)

0   50   100   150   200   250

Temperature (°C)

0   10   20   30

Oxygen
Salinity
Temperature

34.4   34.8   35.2   35.6   36.0   36.4   36.8
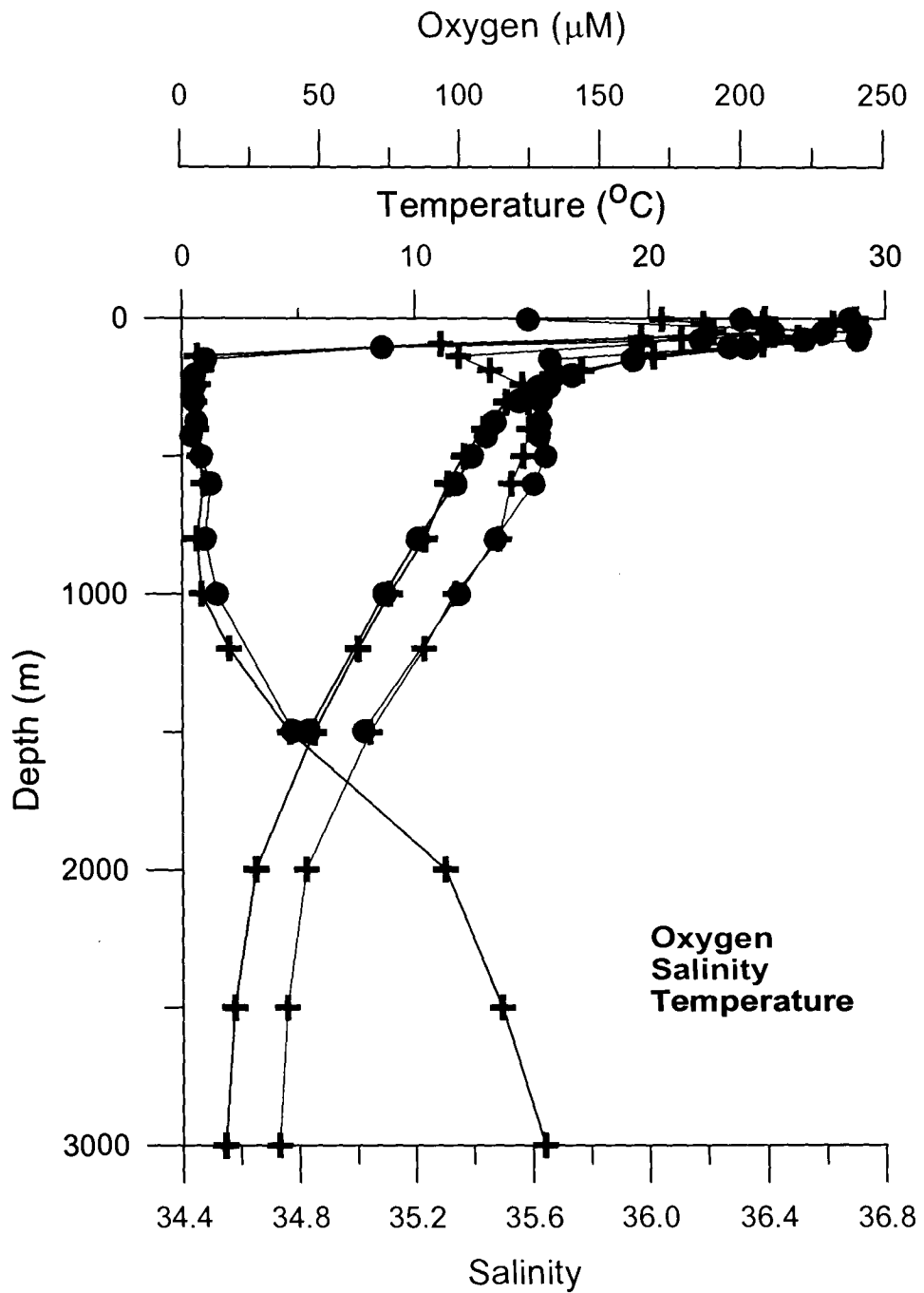
Salinity

Figure 3.12a: Vertical profiles of temperature, salinity and oxygen at the two stations 3201 and 3202 sampled during the FORV Sagar Sampada cruise SS119 in April 1994. Station 3201 was sampled down to ~1.5 km [data points marked with plus (+)], but 3202 was sampled down to 3 km [data points marked with filled circles (●)].
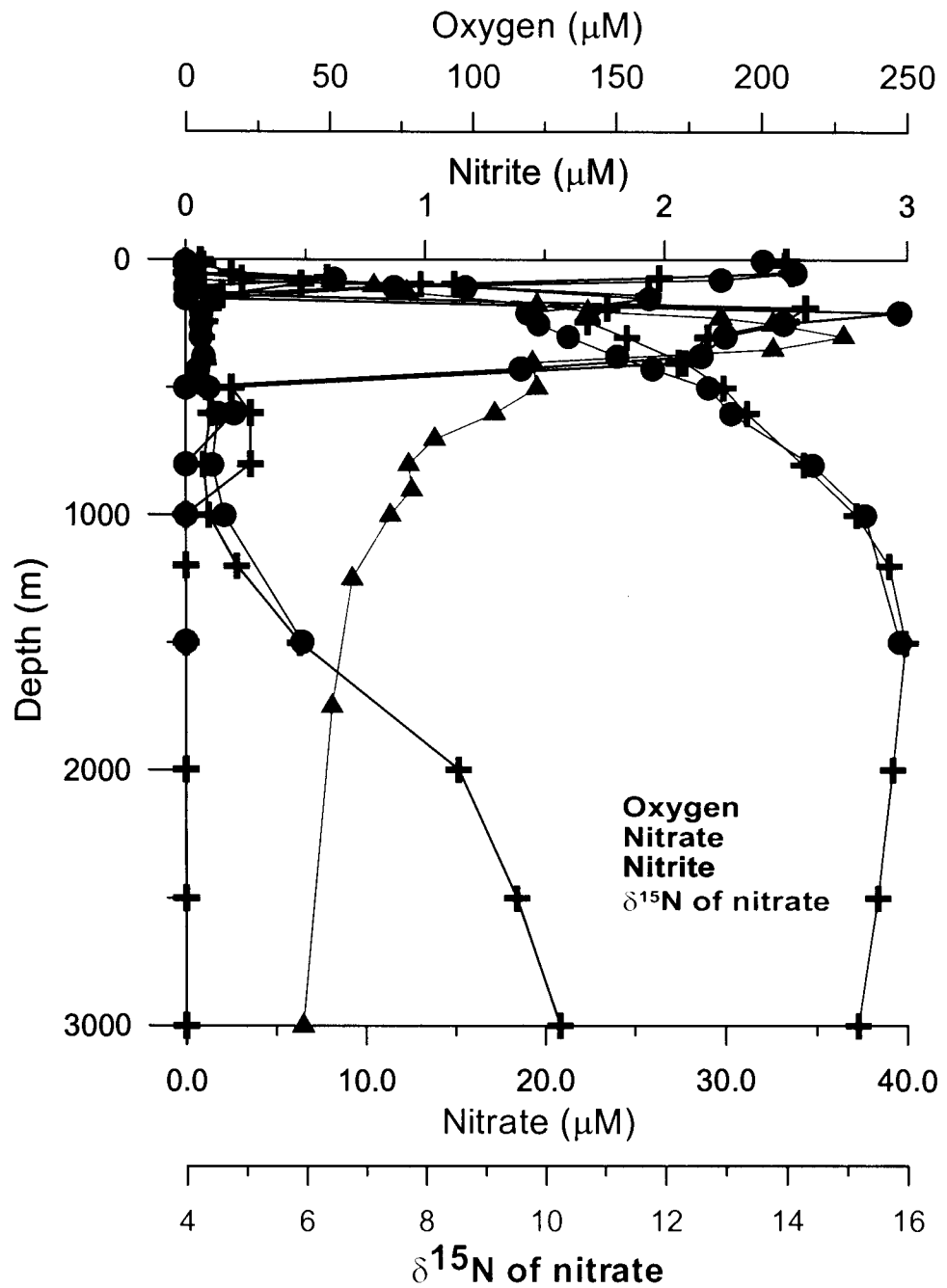
Figure 3.12b: Vertical profiles of oxygen, nitrate and nitrite at the two stations 3201 and 3202 sampled during the FORV Sagar Sampada cruise SS119 in April 1994. Station 3201 was sampled down to ~1.5 km [data points marked with plus (+)], but 3202 was sampled down to 3 km [data points marked with filled circles (●)].

portion of the OMZ, as already mentioned. It is within this layer that the main secondary nitrite maximum is located and also nitrate profiles exhibit a pronounced minimum, indicative of denitrification. Note that the nitrite maximum is not confined to a specific water mass. At 3201, salinity remains high and relatively invariable throughout the nitrite maximum whereas at 3202 the most intense nitrite maximum includes the transition from a salinity minimum to a salinity maximum. The oxygen concentration rises at depths exceeding 1 km where both T and S decreases steadily. At the depths, the two cores were raised from the oxygen concentrations are >100 μM. In other words, both core sites are presently bathed by fairly oxygenated waters.

Similar results are also observed at another location slightly (by 2°Latitude) to the north of the coring sites. This location (19°N, 67°E) was sampled repeatedly during the United States Joint Global Ocean Flux Studies (U.S. JGOFS) Arabian Sea Process Study (1994-95) and thereafter during cruises conducted by the National Institute of Oceanography. The oxygen data collected during the US JGOFS cruises following either the automated Winkler titration or colorimetric procedures are more accurate, as the nitrite build-up was almost always noticed when oxygen fell below 1 μM (Figure 3.13a). This was also where nitrous oxide (N_2O) concentrations were the lowest indicating that like NO_3^- and NO_2^-, N_2O was also being used by bacteria as an electron acceptor (Figure 3.13a, b). At the boundaries of the secondary nitrite maximum, however, N_2O accumulates in high concentrations due to production by nitrification, denitrification or a coupling between the two processes (refer Figure 4 from Naqvi and Noronha, 1991).

Figure 3.13: Vertical profiles of oxygen (O_2), nitrate (NO_3^-), nitrite (NO_2^-) and nitrous oxide (N_2O) at 19°N, 67°E (data from TN039 cruise of U.S. JGOFS – station 18; during October 1994). **(a)** O_2 (circles) and NO_3^- (triangles); **(b)** N_2O (circles) and NO_2^- (triangles); **(c)** NO_3^- deficit according to Codispoti et al. (2001) are shown with dots connected by solid line, "excess nitrogen (N_2)" calculated from the N_2/Ar ratio (larger unconnected symbols –crosses for the data collected on two different cruises from this station and triangles for those from other stations also located within the denitrification zone) and N* according to Gruber and Sarmiento (2002) (small filled triangles connected by dashed line). N/Ar data are from Devol et al. (2006a).

In addition to the routine hydrographic and chemical data, specialized measurements made at this site included the N_2/Ar ratio. This ratio exhibits a strong increase within the secondary nitrite maximum zone, and by subtracting the background ratio (at the same density level but outside the suboxic zone), it is possible to calculate the excess nitrogen biologically produced in these waters. Surprisingly at its maximum, the excess nitrogen far exceeds even the most generous estimates of nitrate deficit (Figure 3.13c). Some of this discrepancy might be accounted by the contribution by anammox, with the rest mostly caused by the non-Redfieldian (N:P >> 16) composition of organic matter, produced by nitrogen fixers, that is supplied to and degraded within the OMZ (Codispoti et al., 2001; Devol et al., 2006). In any case, it would appear that the current estimates for N_2 production in the open-ocean suboxic zone should be conservative.

3.6.1 Nitrogen Isotope composition

Discrimination by denitrifying bacteria between the two stable isotopes of nitrogen (^{14}N and ^{15}N) has been known for quite some time (Wada and Hattori, 1991, and references therein). Brandes et al. (1998) were the first to demonstrate that, this effect leads to marked enrichment of the heavier isotope in residual nitrate in the open-ocean suboxic zone of the Arabian Sea. Their data came from the one of the stations (3201) for which the hydrographic and chemical data have been presented and discussed above (see Figure 3.12). Deep waters (2500 to 3000 m) at this site are found to have $\delta^{15}N$ ($^{15}NO_3^-$) of ~6‰ which is close to the values (~5‰) observed in other

areas (Wu et al., 1997; Sigman et al., 1997). However the $\delta^{15}N$ values

increases to 15‰ within the core of the denitrifying layer (Naqvi et al., 2006b;

Brandes et al., 1998; Figure 3.12) because of the preferential reduction of

$^{14}NO_3^-$ over $^{15}NO_3^-$ in seawater (Cline and Kaplan, 1975). Concurrently, the

$\delta^{15}N$ of N_2 was found to decrease from ~0.6‰ to ~0.2‰ in the denitrifying

layer of the central Arabian Sea (Brandes et al., 1998). Brandes et al. (1998)

computed the isotope fractionation factor (ε) using the measured $\delta^{15}N$ in NO_3^-

and the nitrate deficits computed following Naqvi and Sen Gupta (1985). The

estimated values for ε for the Arabian Sea (22 - 25‰) were similar to those

calculated for the eastern tropical North Pacific. These estimates were also

well within the range (ε = 17 to 29‰) obtained by Delwiche and Steyn, (1970),

Mariotti et al. (1981) and Barford et al. (1999) in laboratory cultures of

denitrifying bacteria.

The isotopic distribution pattern observed in the coastal suboxic zone is

quite different, and more variable, from that described above, even though the

data are rather limited (Naqvi et al., 2006b). These data come from two sets

of observations - in August 1997 off Mangalore (Station SS 3939; isotopic

analysis carried out following Brandes et al., 1998) and in September 2000 off

Goa (Stations G3, G4 and G5; isotopic analysis carried out following Tanaka

and Saino, 2002). On both occasions the sub-pycnocline water column had

experienced significant losses of NO_3^-. The NO_3^- profile at Station 3939

exhibited a mid-depth maximum below which concentrations decreased while

the NO_2^- concentrations showed a concomitant increase with depth (Naqvi et

al., 2006b). NO_3^- deficit also increased with depth, reaching the peak value of

just under 15 μM in the deepest sample (27 m). While all the above parameters exhibited expected depth wise changes, the profile of $\delta^{15}N$-NO_3^- deviated greatly from the expected one. That is, given the high NO_3^- deficit in subsurface waters, the $\delta^{15}N$-NO_3^- values should have ranged between 17 and 26‰ if the isotopic fractionation factor reported for the open ocean suboxic zone (~25‰) was also applicable to the shallow suboxic zone. The values measured were consistently lower. In fact, all samples taken from within or below the pycnocline yielded $\delta^{15}N$-NO_3^- values (6.65 to 7.41‰) that were quite close to the oceanic average with no depth wise variability. NO_3^- in the only sample taken from the surface layer was even lighter (3.43‰).

Several possibilities could be invoked to explain the above observations: (1) Processes responsible for the observed NO_3^- losses in the coastal suboxic zone may be different from those in its open ocean. A likely scenario is that a substantial fraction of the loss may occur within the sediments, and the much smaller isotopic fractionation associated with sedimentary denitrification (Brandes and Devol, 2002) could then account for the low $\delta^{15}N$-NO_3^- values. The few data on sedimentary denitrification, measured mostly during the upwelling period following the acetylene block technique, have yielded values ranging from 0.23 to 1.25 mmol NO_3^- m^{-2} d^{-1}, which are generally within the range of values from other areas (Naik and Naqvi, 2002). Estimates based on the isotope pairing method are comparable with these values (Naqvi et al., manuscript in preparation). These rates by themselves appear to be inadequate to account for the observed NO_3^- loss in the water column. The other processes that may bring about NO_3^- removal are

anammox, dissimilatory reduction of NO_3^- to NH_4^+ (which may also be coupled to anammox) and/or autotrophic denitrification (e.g. reduction of NO_3^- by species such as S^{2-}/HS^-, Fe^{2+} and Mn^{2+}; Luther et al., 1997). Of these at least anammox is expected to be quite important in view of the above-mentioned results from other regions, more so over the Indian shelf where very high NO_2^- concentrations (maximum 16 µM) are expected to be matched by a high rate of diffusive supply of NH_4^+ from the sediments (Naqvi et al., 2000). (2) Apparently low $\delta^{15}N\text{-}NO_3^-$ relative to the NO_3^- deficit could be produced by mixing involving anoxic water. (3) It has been found recently that the reduction of NO_3^- to NO_2^- involves huge isotopic discrimination, such that $\delta^{15}N$ of NO_2^- in the suboxic zone of the eastern tropical North Pacific is quite low (Casciotti, in press). The procedures followed to measure isotopic composition of NO_3^- did not differentiate between NO_3^- and NO_2^-, and therefore the measured values would be dependent on the ratio between NO_2^- and NO_3^- concentrations. This ratio is generally much higher in the coastal zone than in the open ocean, and that could contribute to lower $\delta^{15}N$ of the combined NO_3^- and NO_2^- pool. (4) Finally, it is also possible that if and when the NO_3^- loss is through heterotrophic denitrification, the fractionation factor associated with the process may not be the same in the coastal and offshore regions.

Unlike the observations off Mangalore, isotopic data off Goa do show substantial enrichment of the heavier isotope in residual NO_3^- (Naqvi et al., 2006a). For these samples the fractionation factor was calculated using a simple advection-reaction model that ignores diffusion. The ε value so obtained was 7.7‰. Inclusion of data from Sta. SS 3939 led to little change in

ε (7.21‰). At the first glance these results appear to support the notion of lower fractionation factor in the coastal suboxic zone. However, as discussed above, the possibility of other factors being also responsible for pulling down the $\delta^{15}N$ value of NO_3^- of coastal waters cannot be ruled out. In fact, it is quite likely that all the factors mentioned above may be in operation, their relative importance varying in space and time. Such a dynamic environment which contrasts the relatively more stable conditions of the open ocean system offers both challenges and opportunities to gain further insights into the pathways of oceanic nitrogen cycling.

3.7   Conclusions

The water column data along the off Goa transect clearly indicates the existence of an enhanced suboxia turning to anoxia. This leads to the inference that the coastal cores (SaSu-1 and SaSu-3B) collected along the same transect and the core (CR-2) just below this transect were all overlain with low oxygen waters during the time of collection. For the open ocean gravity cores, from the data presented in vicinity to core locations, confirms the bottom waters to be oxygenated with denitrification occurring in the intermediate water column.

CHAPTER 4

Chapter 4

RECONSTRUCTION OF PALEO - CHEMICAL ENVIRONMENT
ON DECADAL TO CENTENNIAL TIME SCALES

4.1   Introduction

The mid- and inner-shelf segments of the eastern Arabian Sea (west coast of India) are affected seasonally by intense O_2 deficiency in near-bottom waters, as has already been described and discussed in Chapter 3. This process has been known since the 1950s, but the early works were concentrated in the regions off Bombay (Carruthers et al., 1959; Gogate, 1960) and off Cochin (Banse, 1959). The latter study deserves special mention because it involved the first systematic time series measurements of biogeochemical parameters. Banse monitored two stations located over the shelf (at water depths of 25 and 55-60 m) from August 1958 to January 1960, and another deeper station over the continental slope (depth ~2000 m) from November 1958 to May 1959. Combining these measurements with the other available data, he provided a comprehensive description, on a seasonal basis, of hydrography of the eastern and northern parts of the Arabian Sea that also covered O_2 distribution (Banse, 1959, 1968, 1984). A similar time series from the central western shelf was made available much later by Naqvi and coworkers (example Naqvi et al., 2006a) at the CaTS (Candolim Time Series) site (Chapter 3). The similarity between the temperature and O_2 data published by Banse (1968) with the climatological record at CaTS is quite striking. For example, the lowest temperature (~21 °C) and the lowest bottom-water O_2 occur during September-October in both records. The O_2 deficiency

observed off Goa is far more intense, however. A northward intensification of the O_2 deficiency is to be expected from physical considerations. Specifically, the waters upwelling over the Indian shelf are derived from the poleward-flowing West India Under Current (WIUC; Naqvi et al., 2000). The core of the WIUC has slightly higher O_2 than the surrounding waters, but it is still fairly O_2 depleted (Naqvi et al., 2006a). The O_2 content of the WIUC should fall northward making it easier for the upwelling waters to turn suboxic/ anoxic.

In addition to the natural processes, it is likely that human activities are also contributing to coastal hypoxia/suboxia/anoxia through enhanced riverine inputs and atmospheric deposition of nutrients (especially DIN). For the North Indian Ocean as a whole potential human induced alterations are more important than in other regions for two reasons: (1) The countries bordering the North Indian Ocean account for roughly 25% the world's human population, a great majority of which (about 1.4 billion people) lives in India, Pakistan and Bangladesh. There are large requirements of food and energy for such a large population. For example, the current rate of synthetic fertilizer consumption the South Asian exceeds 15 million tonnes of nitrogen (N) per year. This is roughly 46-times the amount consumed in 1960-61. Similarly, oil consumption, which accounts for roughly a third of all commercial energy sources in the region, is about 2.5 billion barrels per day (http://www.eia.doe.gov/emeu/cabs/topworldtables34.html) (to put this in a perspective, India consumes roughly the same amount of oil annually as that produced by Kuwait). Thus, large quantities of nitrogen from both the food and energy sectors are expected to be "leaked" and introduced to the

environment, including coastal waters. Coastal waters in this region therefore face a larger risk of eutrophication. (2) Due to the widespread mesopelagic O_2 deficiency and a much lower area-to-coastline ratio (515 km) than the global ocean (888 km), the North Indian Ocean contains about 2/3 of the continental margin area exposed to waters with O_2 content below 0.2 mL/L (Helly and Levin, 2004).

In fact, the human induced O_2 deficiency in coastal waters is being noticed with increasing frequency all over the globe. The best known of the 'dead zones' (named so because of the exclusion of many organisms including commercially important fishes arising from the O_2 deficiency) is the one occurring in the inner Gulf of Mexico; this develops every summer due to fertilizer runoff by the Mississippi (Diaz and Rosenberg, 1995; Malakoff, 1998; Rabalais and Nixon, 2002). However, these zones are different from those found along the eastern boundaries of the Pacific and the Atlantic Oceans and along the northern boundary of the Indian Ocean (Kamykowski and Zentara, 1990; Helly and Levin, 2004), in that the latter are primarily of natural origin. However, for reasons mentioned above, it is quite possible that some of the naturally formed coastal O_2 deficient zones are also undergoing intensification, and the coastal O_2 deficient system of the eastern Arabian Sea is perhaps the most affected by such a change.

Naqvi et al. (2000) were the first to suggest that seasonal O_2 deficiency over the Indian shelf has been intensifying over the past few decades due to enhanced fertilizer loading. The principal argument being used to support this view is that the complete anoxia distinguished by the presence of H_2S

completely has been recurring in near-bottom waters at the CaTS site every year since 1998. There is no indication for the occurrence of sulphate reduction in the historical data sets, though. It may be argued that anoxia may be occurring in the past as well but it was not noticed because it was not specifically looked for. However, it should be realized that H_2S, if present even in sub micromolar concentrations, can be easily detected by its unpleasant odour, and a Winkler O_2 analyst would have easily noticed this phenomenon, if it had occurred in the past. An extensive data set was gathered in the 1970s along numerous cross-shelf sections under the UNDP/FAO sponsored Integrated Fisheries Project (IFP) during 1971-1975. The sections were repeated in different seasons. When these data are compared with recent measurements in the region off Karwar, a general decrease in subsurface O_2 appears to have occurred over the past three decades (Naqvi et al., 2006a). Whether or not the observed change is human-induced cannot be established with absolute certainty, though. One cannot, for example, rule out the possibility that the shift may be a part of the natural variability on decadal/centennial time scales, related to subtle shifts in hydrography and circulation (upwelling and/or stratification). Indeed, analyses of biomarkers of biological productivity has revealed that the latter varied with time in unison with solar irradiance and is currently higher than ever before during the past seven centuries (Kurian et al., submitted). How the redox environment changed over the same time period is not known. This question is of considerable importance in the context of future evolution of the coastal biogeochemical environment and ecosystems in response to the impending

global warming, given its potentially large impact on both socio-economics of coastal communities (e.g. effect on fisheries – Naqvi et al., 2006a) and on climate [possible positive feedback through enhanced production of nitrous oxide (N_2O), Naqvi et al., 2000]. The work carried out to address this issue is described in this chapter.

4.2 Sedimentary Records

Rapidly accumulating sediments of the continental margin that are exposed to the OMZ are expected to catalogue overhead productivity in the form of higher sedimentary organic carbon (C_{org}) content due to better preservation of C_{org} under oxygen deficient conditions (Paropkari et al., 1987, 1991, 1992, 1993a; Schulz et al., 1998; Van der Weijden et al., 1999; Bhushan et al., 2001). Agnihotri et al. (2002) found the C_{org} variations in sediment cores from the northeastern Arabian Sea to mimic variations in surface productivity as well as monsoon intensity (the latter controlling the former through upwelling-induced surface water nutrient enrichment). Accordingly, downcore C_{org} variations in sediments from the northeastern Arabian Sea have been used to infer paleomonsoon intensity that seems to have varied in unison with the climatic oscillations deduced from the Greenland ice cores for the past 110,000 years (Schulz et al., 1998). Isotope records of carbon in sediments are affected by global, regional, or local carbon cycle change. The $^{13}C/^{12}C$ ratio in marine sediments provides a measure of terrestrial inputs (on account of the fact that the terrestrial organic matter is significantly more depleted in ^{13}C as compared to the marine organic

90

matter; refer paragraph 3 from now). The terrestrial organic matter is also generally depleted in ^{15}N. But a more common application of the sedimentary nitrogen isotope composition ($\delta^{15}N$) has been for reconstructing the history of N cycle processes on time scales from 100's to millions of years. As already stated, $\delta^{15}N$ has been found to be a useful tool for inferring past changes in water column denitrification (Ganeshram et al., 1995, 2000; Pride et al., 1999; Altabet et al., 2002; Thunell and Kepple, 2004) in areas where NO_3^- gets fully consumed by phytoplankton from the surface layers and near-surface NO_3^- drawdown by phytoplankton, where it is partially utilized (Francois 1997; Sigman et al., 1999).

Due to the high sedimentation rates coastal environments commonly preserve thick sequences of the Holocene sediments that are best suited to investigate past climate and sea-level changes as well as local environmental changes. Since coastal sediments are repositories of large quantities of inorganic and organic carbon (Bauer and Druffel, 1998), they have been subjected to extensive studies in the recent past (e.g. Fry and Sherr, 1989; Andrews et al., 2000). Knowledge of the sources of organic matter in estuarine and coastal sediments and factors controlling their distribution is important to the understanding of global biogeochemical cycles.

In this chapter, an attempt is made to examine the temporal variability of various paleo-proxies such as C_{org}, total nitrogen (N_{org}), calcium carbonate ($CaCO_3$), weight ratios of carbon and nitrogen (C/N), isotopic compositions of carbon ($\delta^{13}C_{org}$) and nitrogen ($\delta^{15}N$) and redox sensitive trace elements, on a decadal to centennial scale. Three sediment cores covering the past few

hundred years (maximum ~700 years) retrieved from the tropical coastal environment off Goa are utilized for this purpose. The observed proxy variations are interpreted to decipher past changes in productivity and redox environment.

Before the presentation of results related to this study, a brief discussion of the various proxies employed will be in order. Distribution of organic matter in estuarine and marine sediments has been a subject of considerable interest and a large number of investigations have been performed on this aspect. The sedimentary organic matter is comprised of both, the material produced in the sea as well as that derived from land, the fraction of the latter obviously becoming more important in continental margin sediments than in the abyssal basins. The conventional methods used to trace terrestrial organic matter in marine environment include the lignin content, and the C/N, H/D and $^{13}C/^{12}C$ ratios (Sackett, 1964; Gardner and Menzel, 1974; Nissenbaum, 1974; Pocklington, 1976; Hedges and Parker, 1976). The carbon isotope method is based upon a general depletion of ^{13}C in terrestrial organic matter compared with marine organic matter (Craig, 1953; Sackett, 1964; Smith and Epstein, 1971). In general the average $\delta^{13}C$ values of the organic matter produced by the land plants and marine plants differ by 8‰ (Sackett, 1964). This difference is retained in the sedimentary organic carbon. As a result gradients are observed for the sediments deposited in near-shore environments where there is a mixing of terrestrial and marine derived materials. This technique has been used extensively to investigate the origin and extent of terrestrial organic matter in the marine environment

(Eckelman et al., 1962; Sackett, 1964; Parker et al., 1972; Newman et al., 1973; Fontugne and Duplessy, 1986).

The C/N ratio is normally measured along with $\delta^{13}C_{org}$. This ratio has long been used to evaluate the relative contributions from terrestrial and marine sources (Bordovskiy, 1965; Tyson 1995). The weight ratio in the organic matter produced by marine plankton is ~5.6 (Redfield et al., 1963), much lower than in the terrestrial organic matter which is more than 20 (Bordovskiy, 1965). Although due to differential mineralization of C and N, the ratio in the sediments is higher, values lower than 10 are generally taken to indicate a largely marine origin whereas values around 10 or higher represent both marine and terrestrial organic components (Stein, 1991). The sedimentary C_{org} can serve as a proxy of surface productivity only, if it is of marine origin and well preserved in the sediment after deposition. It's absolutely not clear if these criteria are met in the sediment cores examined by us. Nevertheless C_{org} has been used as productivity proxy by previous workers in the Eastern Arabian Sea (Agnihotri et al., 2003a,b, Thamban et al., 2001, Bhushan et al., 2001).

The use of organic matter signatures in isolation may not be adequate to investigate processes responsible for its production and consumption; instead a much better understanding of these processes can be achieved by combining the C/N data with information on $\delta^{13}C$ (Andrews et al., 1998; Matson and Brisnon, 1990) and $\delta^{15}N$ (Talbot, 2001; Thornton and McManus, 1994). Andrews et al.(1998), Muller and Voss (1999), Maksymowska et al. (2000), Bhushan et al. (2001) and Agnihotri (2002), among others, have used

C/N ratios and $\delta^{13}C_{org}$ as potentially useful indicators for identifying the sources of sedimentary organic matter. It may be pointed out that, diagenesis of sediments could alter the isotopic composition of sedimentary organic matter and should this take place the use of this parameter for investigating the deposition history of sediments becomes more complicated. However, on the time scale covered by this study and given the high sedimentation rate in the cores examined this effect can be ignored (Sackett, 1964).

The application of nitrogen isotopic ratio ($\delta^{15}N$) as a proxy of N cycling processes in sediments owes to the discrimination between the two isotopes during various biogeochemical transformations. The major source of new nitrogen to the euphotic zone is the vertical transport of NO_3^- (McCarthy and Carpenter, 1983), with biological nitrogen fixation and atmospheric input making only minor contributions (Knap et al., 1986). The nitrogen isotopic composition has been used to investigate its sources and transformations in the ocean (e.g., Saino and Hattori, 1980, 1987; Altabet and McCarthy. 1985; Wada and Hattori, 1991). Altabet (1988) found that for a site near Bermuda the $\delta^{15}N$ of particles sinking from the euphotic zone was, on average, 4‰ higher relative to the suspended matter, indicating that only certain components of the suspended pool were selectively transformed into sinking particles. $\delta^{15}N$ has also been used to deduce the sources of particulate matter to the sediment (Peters et al., 1978; Sweeney and Kaplan, 1980). Although the isotopic composition is modified as the material passes through the food web and before the particles produced are eventually deposited on the seafloor, downcore $\delta^{15}N$ changes are widely used to infer past changes in the

oceanic N cycle (Rau et al., 1987; Altabet and Curry, 1989; Altabet et al., 1995, 2002; Deutsch et al., 2004).

Apart from recording changes in denitrification in the subsurface waters and partial NO_3^- utilization in the euphotic zone (Altabet and Francois, 1994), $\delta^{15}N$ also helps to determine the sources of organic matter (Sweeney and Kaplan, 1980; Kerherve et al., 2001). The $\delta^{15}N$ values of terrestrial vascular plants are typically within the range -5‰ to +18‰ with an average value ~3‰, while the marine POC is characterized by $\delta^{15}N$ ranging between 3‰ and 12‰ with a mean of ~6‰ (Wada and Hattori, 1991; Muller and Voss, 1999; Makshymowska et al., 2000). Although there are several complications caused by the existence of a variety of potential source pools (Meyers, 1997; Talbot, 2001), and by processes such as denitrification (Seitzinger, 1990), $\delta^{15}N$ has been still used to differentiate between terrestrial and marine sources of organic matter.

The abundance of various elements in sediments relative to sedimentary rocks can also provide valuable information in regard to the conditions under which the deposition occurred or the changes that have occurred thereafter. Concentrations of trace elements in sediments reflect the various physical, chemical and biological controls on their supply to, their distribution in, and their removal from the ocean. Many of the trace elements that have been studied in sediments and sedimentary rocks are polyvalent with their oxidized and reduced forms having different solubilities. They are therefore partitioned between the solid and solution phases to different extents under varying redox conditions, and their accumulation in or

mobilization from the sediments is controlled by either a change in redox state (as in case of Fe, Mn, Re and U) and/or speciation (as happens for Mo). Other metals such as Cd have a single stable oxidation state in aqueous solution but their concentrations may be are regulated by solubility of the least soluble salt; most metal sulphides are sparingly soluble in water, and so under fully anoxic conditions such metals are removed from interstitial waters to the solid phase. The differential solubility of the oxidized and reduced metal forms, has led to their use as paleo-environmental proxies (Rosenthal et al., 1995a,b; Crusius et al., 1999; Dean et al., 1999; Yarincik et al., 2000; Adelson et al., 2001; Pailler et al., 2002; Ivanochko and Pedersen, 2004). For example, changes in the intensity of the oxygen minimum zone, over the north eastern margin of the Pacific have been inferred from variations in the sedimentary concentrations of redox-sensitive trace metals (Dean et al., 1997; Zheng et al., 2000a; Nameroff et al., 2004; Mckay et al., 2005). However, the application of redox-sensitive trace metals as paleo-proxies requires an understanding of their geochemical behaviours under different conditions. For this purpose, several researchers have focused their attention to the permanently anoxic systems such as the Black Sea and Cariaco Basin (Calvert, 1990; Dean et al., 1997; Morford and Emerson, 1999; Nameroff et al., 2002; Sundby et al., 2004; McKay et al., 2007). One important factor that must be taken into consideration while interpreting the sedimentary record of trace metals is diagenesis. That is, since the redox conditions in subsurface sediments are quite different from those in the overlying waters, changes can occur after sedimentary burial and it is critical to separate the diagenetic and
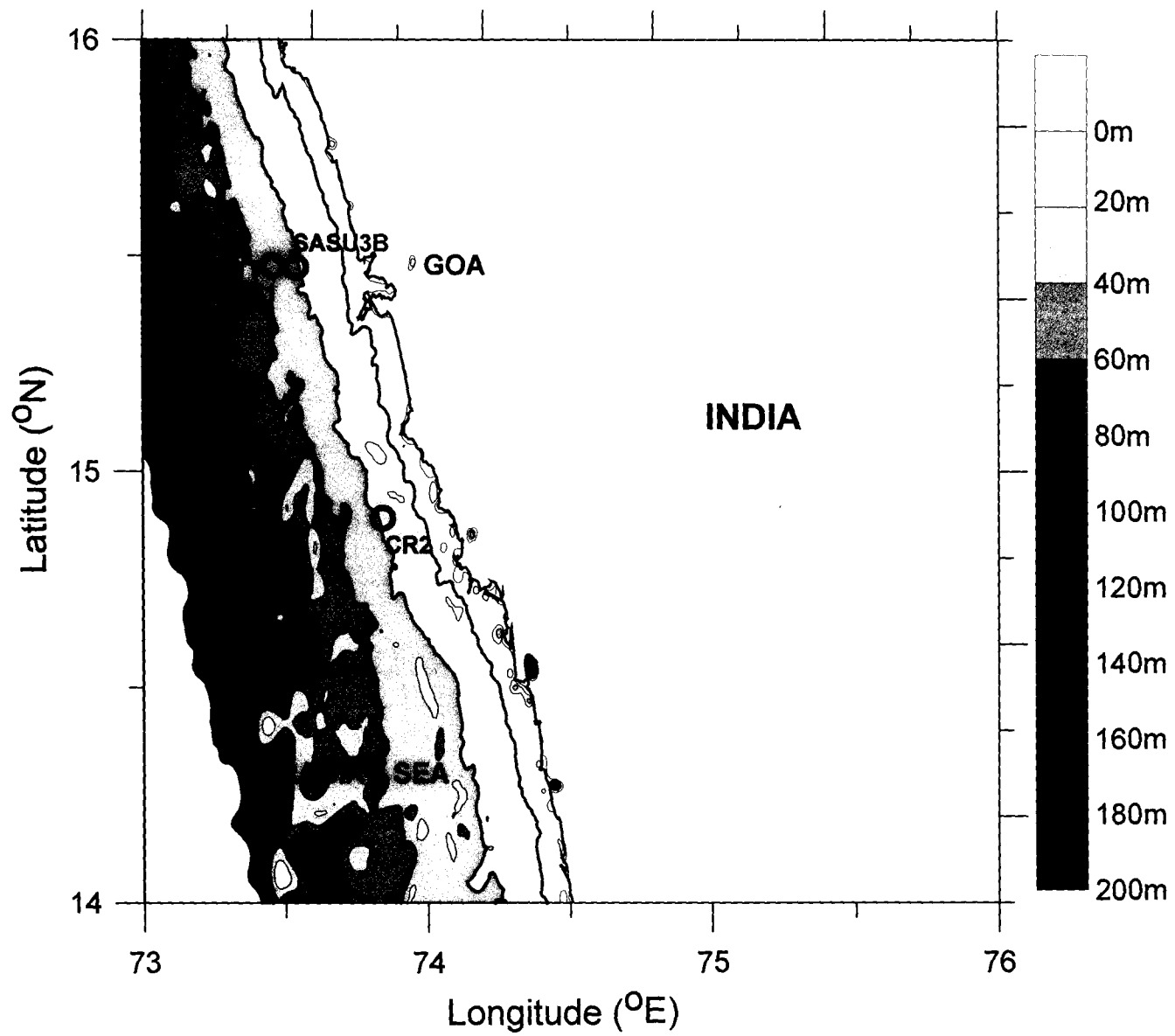
Figure 4.1: Core locations of three shallow cores raised from the inner and mid shelf region off Goa.

depositional signatures.

4.2.1 Age Models

Three cores raised from the inner- and mid-shelf regions off Goa are utilized here for gaining insights into past changes in surface productivity and subsurface denitrification on the decadal to centennial time scales. The core locations are shown in figure 4.1 and the details are provided in table 4.1.

Two of the cores analyzed (SaSu-1 and SaSu-3B) were collected using a multi-corer and were < 0.5 m long. The third, CR-2, was a 1-m long gravity core. Since the coring sites were expected to have high sedimentation rates, they were dated using the $^{210}Pb_{xs}$ method (Sarin et al., 1992; Sharma et al., 1994). ^{210}Pb has a half-life of 22.5 years, and so this method is useful for dating only very recent sediments (<~100 years old). Linear ^{210}Pb decay was seen from 4 to 15 cm depth in case of SaSu-1, and from 4.5 to 17 cm in case of SaSu-3B. The sedimentation rates for the two cores were calculated to be 1.14 mm/y and 1.78 mm/y, respectively. Uniform ^{210}Pb activity in the upper 4 - 4.5 cm of the two cores was presumably due to bioturbation. The computed sedimentation rates were applied to the period beyond 100 years. The dated records extend up to ~175 years before present (B.P.) for SaSu-1 and ~240 years B.P. for SaSu-3B (Figure 4.2a,b). The temporal resolutions in the two cores is quite high (<10 y). A few quantitative estimates made by Stackelberg (1972) and ZoBell (1973) in the inner shelf region along the western continental margin of India suggested a maximum rate of sedimentation of 15–19 cm/100y which agrees very well with the sedimentation rates in the

Table 4.1

Details of core intervals dated for ^{210}Pb, sedimentation rates and total core age for cores SaSu-1, SaSu-3B and CR-2.

Sr. No.	Core No.	^{210}Pb Dated Core depths (cm)	Sedimentation Rate (mm/y)	Total Core Age (Y B.P.)
1.	SaSu-1	4 – 15	1.14	175
2.	SaSu-3B	4.5 – 17	1.78	240
3.	CR-2	0.0 – 22	1.5	900
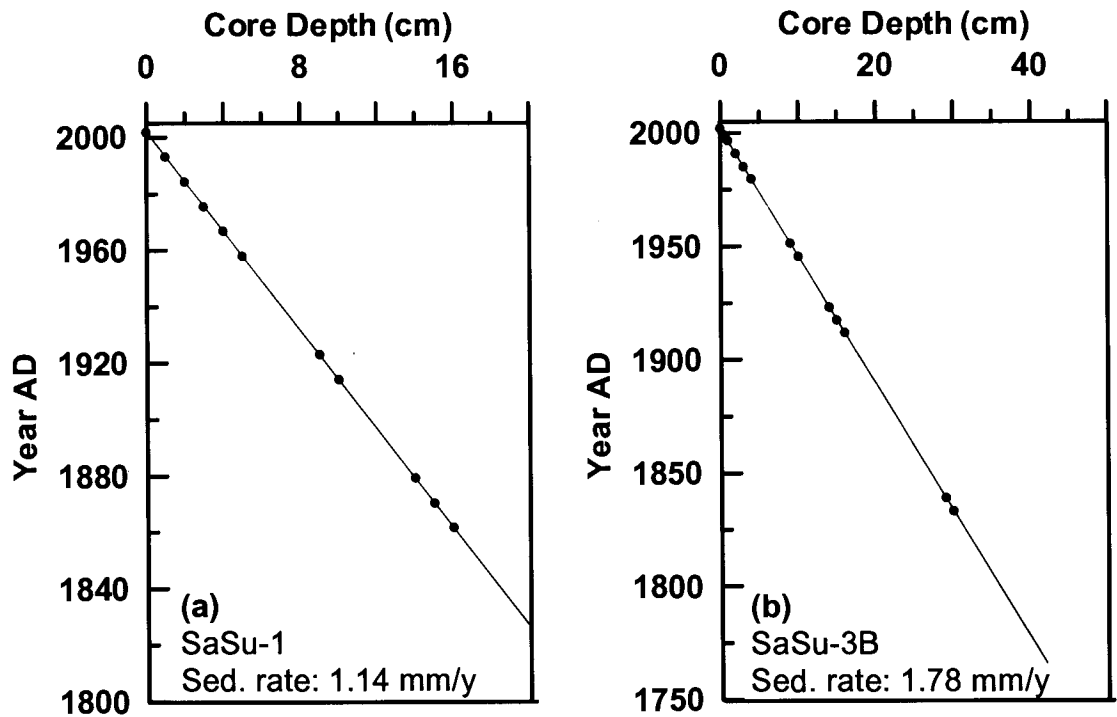
Figure 4.2: Age Curves for cores SaSu-1 and SaSu-3B based on measurements of ^{210}Pb dates. Data points with blue filled circles (●) are experimental ^{210}Pb dates. The calculated Sedimentation (Sed.) rates rates are indicated. The age curves shown in above plots are for full length of the cores sampled.
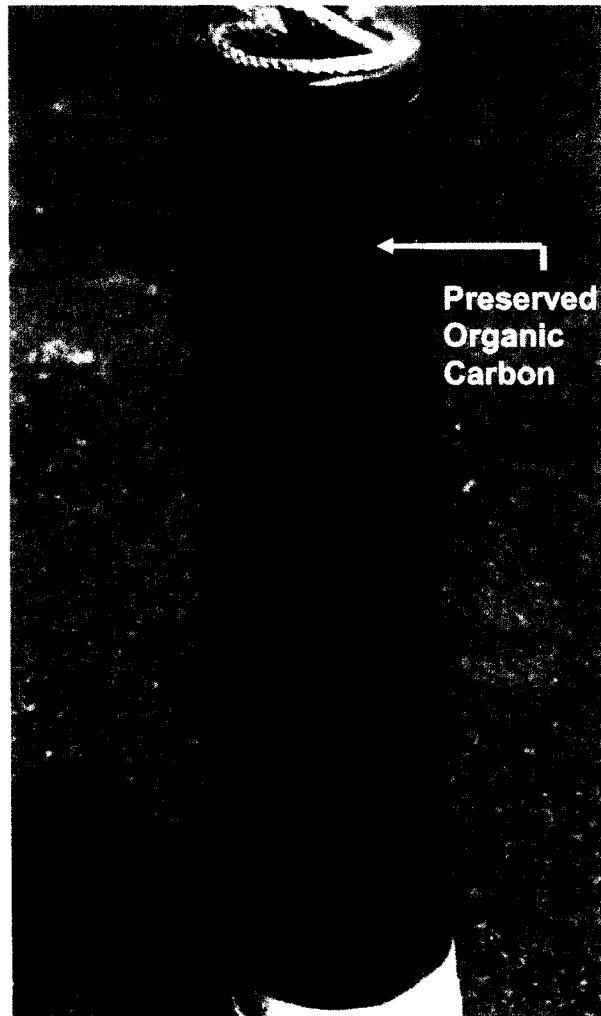
Plate 4.1: Photograph of SaSu-3B core. Jet dark colour sediment at the top of the core indicates preservation of organic carbon.

cores examined in the present study.

In case of the CR-2, the upper portion of the core was also dated by the $^{210}Pb_{xs}$ method (Sharma et al., 1994). A systematic decrease of normalized excess i.e. $^{210}Pb_{xs}/Al$ with depth was found between core top to 20-22 cm depth-interval, yielding a linear sedimentation rate of 1.5 mm/y (Figure 4.3). Assuming the core top to correspond to the year of collection (2005 AD) and using a linear sedimentation rate of 1.5 mm/y, an age-depth model was constructed for the last ~150 years. If one extends this age-depth model to the entire core length, the time period covered would be ~660 years with an average sampling resolution of ~13 years. AMS ^{14}C dating of bulk organic matter from the 97-99 cm level yielded an age of 900±66 (1σ) Calendar y BP (Figure 4.3). Given the uncertainties involved in both techniques, this agreement is quite good.

CR-2 has also been analyzed for biomarkers (dinosterol, phytosterol, stigmasterol and ß-sitosterol) (Kurian et al, submitted). An excellent covariance was found between the downcore records of the major biomarker and organic proxies (based on ^{210}Pb derived age model), especially dinosterol, and the Sunspot number time-series during the last ~250 years [adapted from www.ncdc.noaa.gov/paleo/forcing.html]. In addition, at deeper levels, beyond the range of ^{210}Pb dating (last ~150 years), the dinosterol record is remarkably similar to that of reconstructed total solar irradiance (TSI) (Bard et al., 2000) except that the extrema in the former appear to be a little younger. The ^{210}Pb-derived age model has therefore been revised by matching the extrema in two records and assigning the TSI-based ages to the
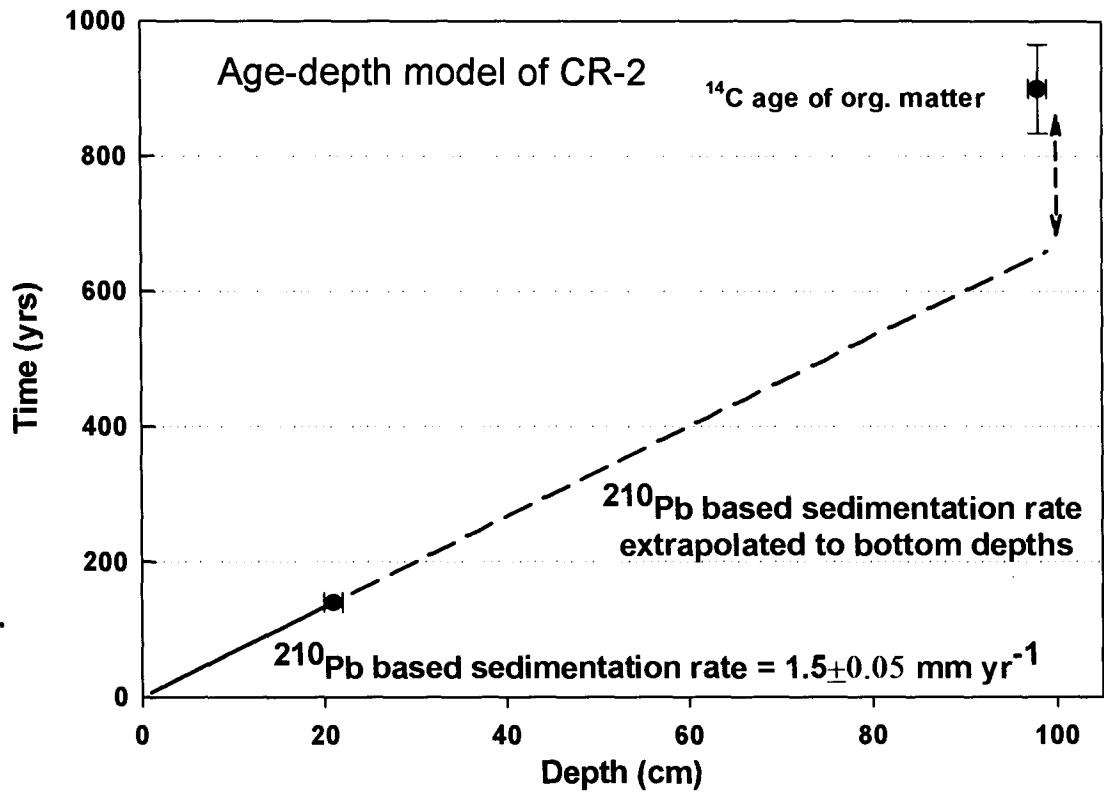
Figure 4.3: Age-depth model for core CR-2.

major dinosterol extrema. Using a binomial best-fit (r^2= 0.98) to the depth versus TSI-derived age, ages were recalculated for the entire core. The estimated age of the deepest sample was thus found to be ~720 yr, which is intermediate of the ^{210}Pb and ^{14}C based ages, providing further confidence in the tuned age-depth model.

4.2.2 Changes over the past 700 years – proxy records from CR-2

Data on the established productivity proxies and stable isotope ratios in core CR-2 are presented in table 4.2, while major and trace element data are listed in table 4.3. The $\delta^{13}C_{org}$ values vary within a narrow range, from –21.4 to –20.5‰, while $\delta^{15}N$ values range from ~6 to 7.8‰. C_{org} and N contents vary from 2.32 to 3.4% and from 0.24 to 0.40%, respectively. C/N ratios are between 8.5 and 10.5, well within the reported range for marine sedimentary organic matter in the northeastern Arabian Sea (8±2; Reichart, 1997; Bhushan et al., 2001). Changes in inorganic and siliceous productivity were inferred from $CaCO_3$ and BioSi contents that vary from ~4 to13.5% and from 1.18 to 2.67%, respectively. The observed concentration ranges for major elements supplied predominantly by continental detritus are rather narrow (e.g. 6.4-8.1% for Al, 5.3-6.3% for Fe and 2.1-2.5% for Mg).

Since abundances of most trace elements are controlled by both biogenic and detrital components, in order to investigate changes that are not caused by variations in detritus supply, concentrations of these elements are normalized with that of Al (Calvert and Pedersen, 1993; Reichart, 1997; Agnihotri et al., 2003a). Non-detrital /authigenic component of any element

can also be calculated as elemental excess (or depletion) (Ele_{xs}) over its natural shale abundance using the following equation:

$$Ele_{xs} = Ele_{total} - [Al_{measured} \times (Ele/Al)_{shale}] \text{------------------------(1)}$$

4.2.2.1 Surface productivity and sub-surface denitrification variations during the last ~700 years

Figure 4.4 shows downcore records of the productivity-related variables, viz. C_{org}, N_{org}, $CaCO_3$ and BioSi contents, C/N ratio, and C and N isotopes of sedimentary organic matter, with the depth scale transformed to the scale of time of sediment deposition i.e. year AD; using the tuned age-depth model described above. Kurian et al. (submitted) have shown that surface productivity, supported by monsoon upwelling, varied in unison with the Sunspot activity/Solar irradiance forcing during the last ~700 years. Downcore changes in $CaCO_3$ closely follow those in C_{org} and N_{org} (Figure 4.4a,b,c) suggesting a close covariance of the organic and inorganic (calcareous) productivity in the region during the deposition period. Both records display prominent minima during ~1650-1750 AD within the time span of the Little Ice Age (LIA, from ~1500 to 1750 AD). Biogenic silica, however, exhibits much greater short-term oscillations, but decreased productivity during the LIA is still discernible in its record (Figure 4.4g).

The $\delta^{15}N$ of sedimentary OM is a well-tested tool for tracking past changes in water column denitrification, especially in the rapidly accumulating sediments that experience high surface productivity (Altabet et al., 1999b, 2002; Ganeshram et al., 2000; Suthhof et al., 2001; Agnihotri et al., 2003a,
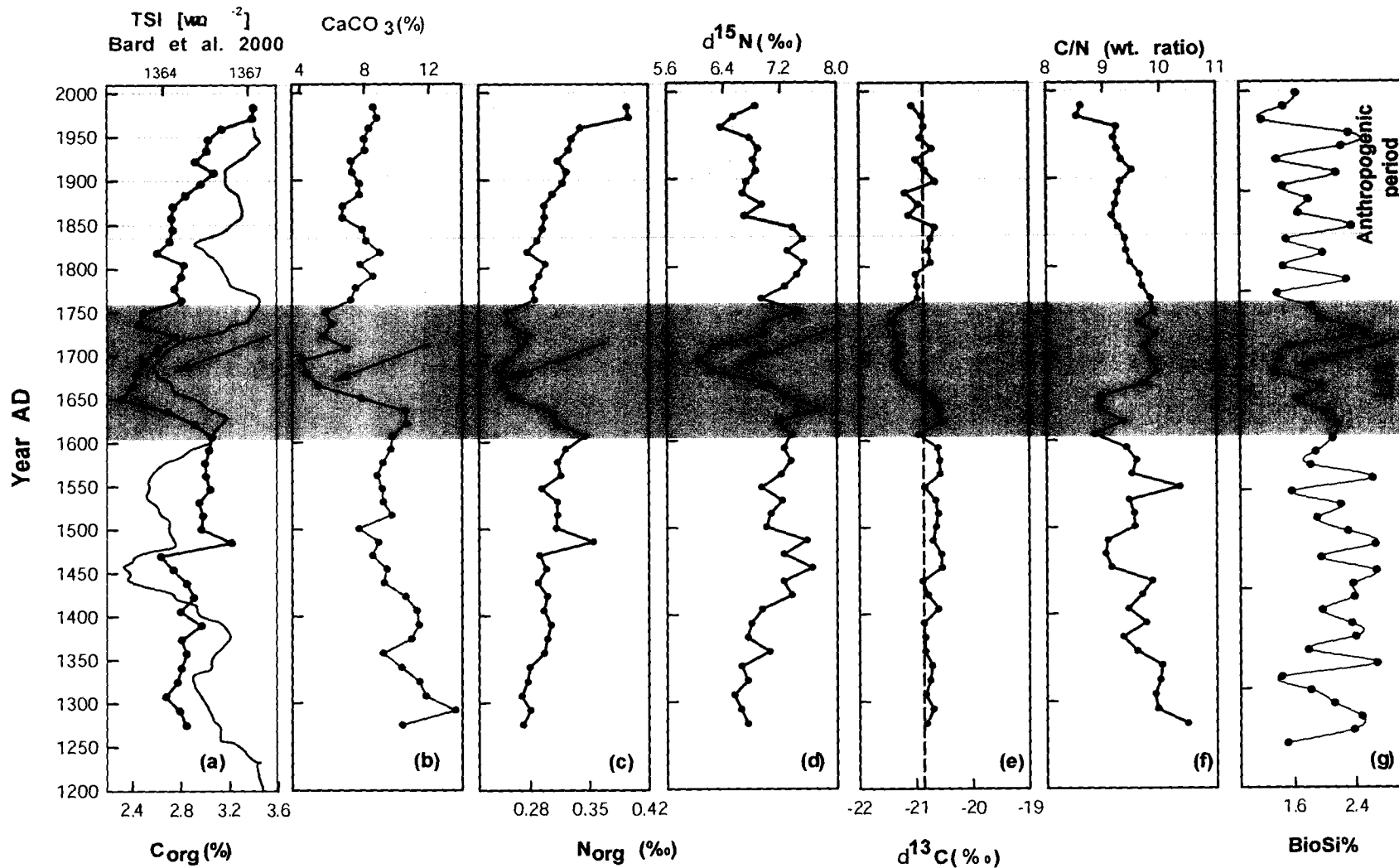
Figure 4.4: Temporal variability of major productivity proxies, C & N isotopes of sedimentary organic matter along with C/N weight ratio in core CR-2. A conspicuous decrease in δ^{15}N can be seen during ~ 1650-1750 AD, representing Little Ice Age (LIA).

2006). The $\delta^{15}N$ of particulate organic matter (POM) is a function of the $\delta^{15}N$ of source NO_3^- and fractionation that occurs during its uptake by phytoplankton (provided that NO_3^- is not fully utilized). The $\delta^{15}N$ of dissolved NO_3^- in the seawater is on an average ~5‰ (Altabet, 2006), but in the perennial suboxic zone of the central Arabian Sea (~150-600 m; Naqvi, 1987), denitrification results in $\delta^{15}N$ values as high as 15-18‰ (Brandes et al., 1998). As most of the new nitrogen fuelling primary production in the euphotic zone is derived from the subsurface layers (Naqvi et al., 2007), the suspended and sinking organic matter as well as surficial sediments are characterized by elevated $\delta^{15}N$ values all over the Arabian Sea where the upwelled NO_3^- is fully consumed on an annual basis (Schäfer and Ittekkot, 1995; Gaye-Haake et al., 2005; Montoya and Voss, 2006). Variations in $\delta^{15}N$ in numerous cores raised from the continental slope, seamounts or abyssal plain in the Arabian Sea have revealed that, large enrichment of $\delta^{15}N$ in sediments has been prevalent not only throughout the Holocene, but also all interglacial periods over the past 1 Ma. In contrast, lighter isotopic values (~5-6‰), comparable to those found in non-reducing environments today, characterize sediments that accumulated during the glacial stages indicating that denitrification weakened or was absent during such periods (Altabet et al., 1995, 1999a, 2002; Ganeshram et al., 1995, 2000; Suthhof et al., 2001). Higher resolution records indicate variations on an even shorter (millennial) time scale, closely linked with the climatic changes recorded by the Greenland ice cores (Suthhof et al., 2001; Altabet et al., 2002). For example, the $\delta^{15}N$ records in two sediment cores from the Oman Margin generated by

Altabet et al. (2002) show oscillations that are remarkably similar in structure and timing to the Dansgaard/Oeschger events recorded in the Greenland (GISP2) ice cores. High resolution records of the Holocene, such as those recently analyzed by Altabet (2007) are not available from the Arabian Sea. The data presented here are, in fact, the first from the continental shelf anywhere in the Indian Ocean.

The CR-2 site is presently affected by intense denitrification, albeit seasonally; however, this is not reflected in the near core-top $\delta^{15}N$ that averages only 6.6‰ in the upper 5 cm (Table 4.2, Figure 4.4). Sedimentary $\delta^{15}N$ at this location appears to have decreased slightly but steadily over the last century (the upper shaded portion in Figure 4.4). This is inconsistent with the trend exhibited by the productivity proxies (e.g. C_{org}, Figure 4.4, and even more so dinosterol – Kurian et al., submitted) that suggest an increase in productivity over the same period (Kurian et al., submitted). There are several possible explanations of this anomaly: (i) Dilution of the $\delta^{15}N$ signal by inputs of terrestrial organic matter containing isotopically lighter nitrogen; (ii) Inputs of lighter inorganic combined nitrogen of anthropogenic origin leading to the production of organic matter with lower $\delta^{15}N$. Note that possibility (i) also requires a decrease in the $\delta^{13}C_{org}$ and an increase in C/N, which are not observed, whereas possibility (ii) only requires a decrease in $\delta^{15}N$; (iii) The sedimentary $\delta^{15}N$ may not proportionately reflect the degree of water column denitrification because the isotopic fractionation factor in coastal suboxic zone may be significantly different (lower) than in the perennial suboxic zone in the open ocean (Naqvi et al., 2006b) and/or as denitrification often leads to

complete removal of NO_3^- from the water column (Naqvi et al., 2000, 2006a,b), the impact of the process on the sedimentary $\delta^{15}N$ may not be very large; and (iv) the region is well known for the occurrence of *Trichodesmium* blooms. Fixation of light nitrogen by these and possibly other diazotrophs would compensate for the heavy isotope enrichment by denitrification. It may be pointed out that denitrification and N_2-fixation are coupled since the latter produces excess phosphate that is expected to stimulate the growth of diazotrophs (Deutsch et al., 2007; Naqvi, 2007); moreover, other limiting elements for N_2-fixation (mainly iron) are expected to be present in high concentrations in the coastal waters. The available data sets do not allow an evaluation of the relative importance of these possible factors.

Despite the above-mentioned complexities, that limit the application of sedimentary $\delta^{15}N$ as a reliable paleo-denitrification tool in coastal marine environments, the $\delta^{15}N$ record does, nevertheless, show overall similarities with those of the productivity proxies and TSI curve during much of the time period covered by the core barring the Anthropocene. The most prominent feature of the $\delta^{15}N$ record is the conspicuous decrease in $\delta^{15}N$ concurrent with a decrease in organic productivity during the period from ~1650 to 1750 AD, within the time span of the LIA (~1500 to 1750 AD) (Figure 4.4d). Contemporaneous $\delta^{13}C_{org}$ values vary within narrow range (~20.86±0.23‰) that is typical of marine sedimentary OM in the Arabian Sea (Fontugne and Duplessy, 1986; Reichart, 1997) and show no obvious decrease (Figure 4.4e). Similarly, the absence of an increase in the C/N ratio (Figure 4.4f) indicates that the negative $\delta^{15}N$ excursion during ~1650 to 1750 AD could not

have been due to dilution by terrestrial OM. Taken together these results strongly suggest that denitrification over the Indian shelf substantially weakened, probably due to a less intense upwelling and weaker stratification in response to weaker southwest monsoon, during this period. Significantly, this event is reflected in marked changes in most of the properties examined here (Figures 4.4 and 4.5).

Given the previously reported weakening of winds in the Arabian Sea during the LIA, it is also possible that water column denitrification in the Arabian Sea as a whole (coastal as well as open ocean) became less vigorous and thus the observed signal could represent a regional decrease in $\delta^{15}N$ in NO_3^- and ultimately in the sedimentary OM. It may be pointed out that the coastal hypoxic zone only accounts for ~10% of the overall water column denitrification in the region (Naqvi et al., 2007). However, the open ocean and coastal suboxic zones are not contiguous in the region of the present study and the upwelled water is derived from the WIUC that originates in the southeastern Arabian Sea/Laccadive Sea. The oxygen concentrations in the undercurrent water are not low enough for denitrification to occur (Naqvi et al., 2006a,b), and so the effect of open ocean denitrification is not expected to dominate that of local denitrification over the shelf at the sites chosen in the present study.

Another noteworthy feature of figure 4.4d is an apparent absence of a long term change in sedimentary $\delta^{15}N$. The above mentioned uncertainties in the interpretation of the $\delta^{15}N$ data not withstanding, the lack of a long-term trend probably implies a fairly stable balance between the nitrogen input and
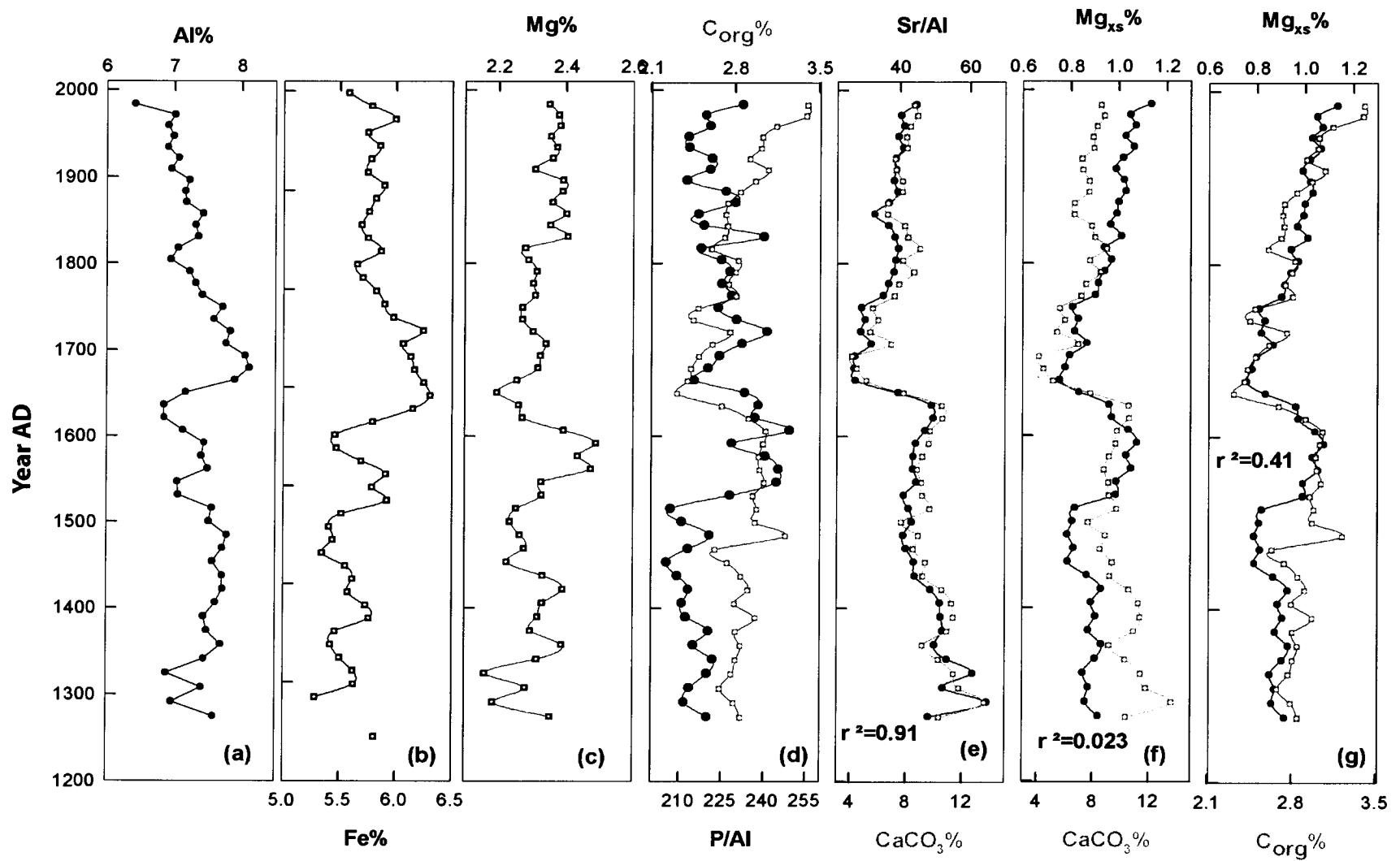
Figure 4.5: Downcore records of selected major and minor elements (Al, Fe, Mg, P and Sr) and their inter-relationships with major productivity indicators measured in core CR-2. Mg_{xs} is calculated by subtracting detrital component using average shale value of Mg/Al (~0.19) from total Mg content.

removal processes over the last seven centuries. This is consistent with the results of Altabet (2007) who also found little secular trends in sedimentary $\delta^{15}N$ variations in other areas over the past few millennia; as discussed by him these results have important implications for the N budgets that seem to be grossly out of balance in today's oceans.

4.2.2.2 Temporal variability of major elements

In continental margin sediments, Al is mainly present in clay minerals carried by the air and continental runoff, and therefore it is predominantly of continental origin. This also applies to two other major elements, Fe and Mg (Calvert and Pedersen, 1993). Though Fe is known to undergo redox changes, its close covariance with typical continental lithogenic tags such as Al and Ti indicates that its temporal variability is mainly due to changes in the detrital supply (Agnihotri et al., 2003a). A plausible reason for the observed tight covariance between Fe and other detrital tags (non-redox sensitive elements such as Al and Ti) is that the majority of reactive (redox-sensitive) Fe is mobilized within the suboxic water columns. Close covariance of Fe with Al in core CR-2 (Figure 4.5a,b) can be interpreted in a similar way. Thus the variability in concentrations of both Fe and Al may be brought about by dilution with the major biogenic components such as C_{org} and $CaCO_3$. Mg is another major element supplied mainly by continental detritus; however, downcore changes in Mg do not appear to follow those in Al and Fe (Figure 4.5c), a feature discussed later in the section.

In order to investigate changes in the non-detrital component of

phosphorus (P), a major macronutrient, the P content was normalized with Al. In CR-2, P/Al ratio (by weight) varies from 130 to 348 × 10^{-4} consistently higher than its average shale value (~88 x 10^{-4}; Turekian and Wedepohl, 1961) thereby suggesting dominant presence of non detrital P. A visual covariance can be seen in P/Al and C_{org} records of CR-2 (Figure 4.5d).

The Sr/Al ratio varies from 27 to 65 x 10^{-4} with a mean (±SD) of 43±8 x 10^{-4}, which is close to its average shale value (38 x 10^{-4}; Turekian and Wedepohl, 1961). Nonetheless, downcore variability of Sr/Al is very similar to that of $CaCO_3$ (r^2= 0.91; Figure 4.5e), suggesting their close association as observed in other late-Quaternary and Holocene paleo records from the eastern Arabian Sea (Agnihotri et al., 2003a,b).

Mg_{xs} estimated using equation 1 varies from 0.75 to 1.13%; thus, this element is substantially (~40%) enriched in CR-2 sediments relative to shale. The Mg_{xs} could be present in sediments as $MgCO_3$ (dolomite and palygorskite) mainly supplied by atmospheric dust and/or as fragmented continental weathered material from basaltic terrain of western India which is known to be Mg rich (Rao and Wagle, 1997, Sirocko et al., 2000). It is less likely that calcite contributes to the observed Mg_{xs} because Mg_{xs} and $CaCO_3$ do not show statistically significant correlation (r^2= 0.023; Figure 4.5f). In contrast, the depth profile of Mg_{xs} shows statistically significant positive correlation with C_{org} (r^2= 0.41; Figure 4.5g). Specific analysis of Mg-bearing minerals such as palygorskite / dolomite could provide further insights into Mg speciation in shelf sediments of this region.

4.2.2.3 Temporal variability of redox-sensitive and nutrient type elements

Downcore records of redox-sensitive elements Mn, Cr, V, and Ba have been plotted in figure 4.6. Mn concentrations vary from 283 to 354 $\mu g\ g^{-1}$, whereas the corresponding ranges for Cr and V are 111-151 and 59-107 $\mu g\ g^{-1}$, respectively (Table 4.3). Ba content oscillates between 109 and 139 $\mu g\ g^{-1}$ (Table 4.3). The average Mn/Al ratio in the core is $44\pm4 \times 10^{-4}$, which is less than half of the average shale value ($\sim106 \times 10^{-4}$; Turekian and Wedepohl, 1961). Observed lower Mn/Al ratios throughout the deposition period of the core (Figure 4.6a) suggests that Mn is mobilized out of the sedimentary column, a process commonly observed in reducing sediments (Somayajulu et al., 1994).

Elements such as Cr and V are known to precipitate out from seawater under reducing conditions (Piper and Isaacs, 1996). The Cr/Al and V/Al ratios remain within very narrow ranges, 16-20 and 8-14 $\times 10^{-4}$, respectively. The average value for Cr/Al ($18\pm1 \times 10^{-4}$) is slightly higher than the average shale value of 11×10^{-4} but the average V/Al ($12\pm1 \times 10^{-4}$) is lower than the shale value (16×10^{-4}; Figure 4.6b,c). Thus, the expected enrichment in the solid phase is seen only in case of Cr. A slow long-term increasing trend in both ratios appears to exist, the reason for which is not clear, with no consistent excursions during the TSI extrema. It would thus appear that the changes in productivity and the redox status of the overlying water had little effect on sedimentary redox cycling; while the sedimentary environment continued to remain reducing throughout the deposition period. Evidently, post depositional
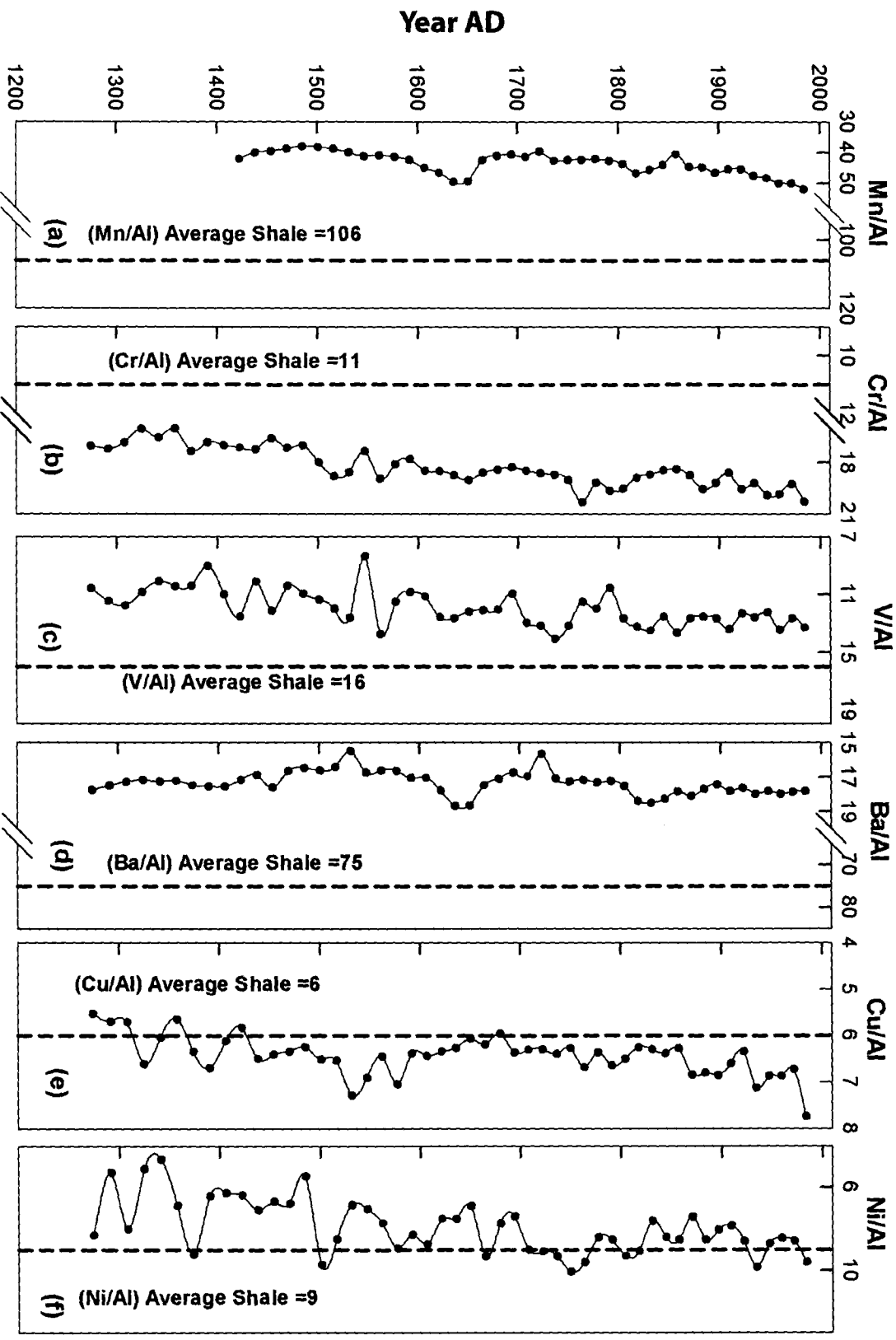
Figure 4.6: Downcore records of minor element(s)/Al ratios in core CR-2

diagenetic alterations have not been large since such changes would drive Mn/Al and Cr/Al in opposite directions, and an anti-correlation between the downcore records of these ratios are not observed (Figure 4.6a,b).

Ba is used as a reliable paleo-productivity proxy in sediments where (i) amount of its terrestrial contribution is much smaller compared with its biogenic component (Dymond et al., 1992); and (ii) sediments are deposited under oxic condition (i.e. beyond OMZ in case of eastern Arabian Sea) (Prakash Babu et al., 2002; Agnihotri et al., 2003b). In rapidly accumulating and reducing shelf sediments where contribution of Ba supplied by detritus is significant, considerable amount of Ba could be mobilized into water column from the underlying sediments (McManus et al., 1998). Ba concentrations in core CR-2 show significant depletion (factor of ~4) relative to its average shale abundance (Figure 4.6d), suggesting strong reducing conditions of water column throughout the deposition period. Under such persistent reducing environment with almost constant sedimentation rate, sedimentary C_{org} content serves as a reliable proxy for surface productivity and hence monsoon intensity in the region.

In addition to $CaCO_3$, C_{org}, N_{org} and BioSi, non-detrital components of Cu and Ni can be used as productivity proxies. These elements act as micronutrients which are removed from surface waters during plankton growth and liberated from settling organic debris in the sub-surface waters (Calvert and Pedersen, 1993). In anoxic (sulfidic) sedimentary conditions, these elements also precipitate as their respective sulfides (Sirocko et al., 2000). In CR-2, however, Cu and Ni do not show any significant excess over their

detrital components (Figure 4.6e,f). This may be because the free sulphide concentrations in pore waters, in the inner shelf off Goa are surprisingly low (S.W.A. Naqvi, unpublished data). Nevertheless, some accumulation of these nutrient-like elements in sediments should be expected during periods of high productivity, such as the last ~150 years. The Cu record does provide some evidence for this phenomenon (Figure 4.6e).

4.2.3 Changes over the past ~200 years – proxy records from SaSu-1 and SaSu-3B

The two shorter cores facilitate a better focus on the changes that have occurred in the coastal environment in the eastern Arabian Sea in more recent times (over the last two centuries), and hence these records are discussed in greater detail below. Data on the established proxies of productivity and stable isotope ratios in core SaSu-1 and SaSu-3B are presented in table 4.4 and table 4.5 respectively, while major and trace element data are listed in table 4.6 and table 4.7 for SaSu-1 and SaSu-3B respectively.

4.2.3.1 Organic carbon, total nitrogen and $CaCO_3$

The C_{org} and TN concentrations for SaSu-1 vary from 4.1 to 4.7% and from 0.47 to 0.57%, respectively (Figure 4.7a,b). In both cases, the minima occurred approximately 60 y BP after which the concentrations have risen steadily with the present values being the highest recorded in the core. This is consistent with the record from CR-2 discussed above. In the lower half of the
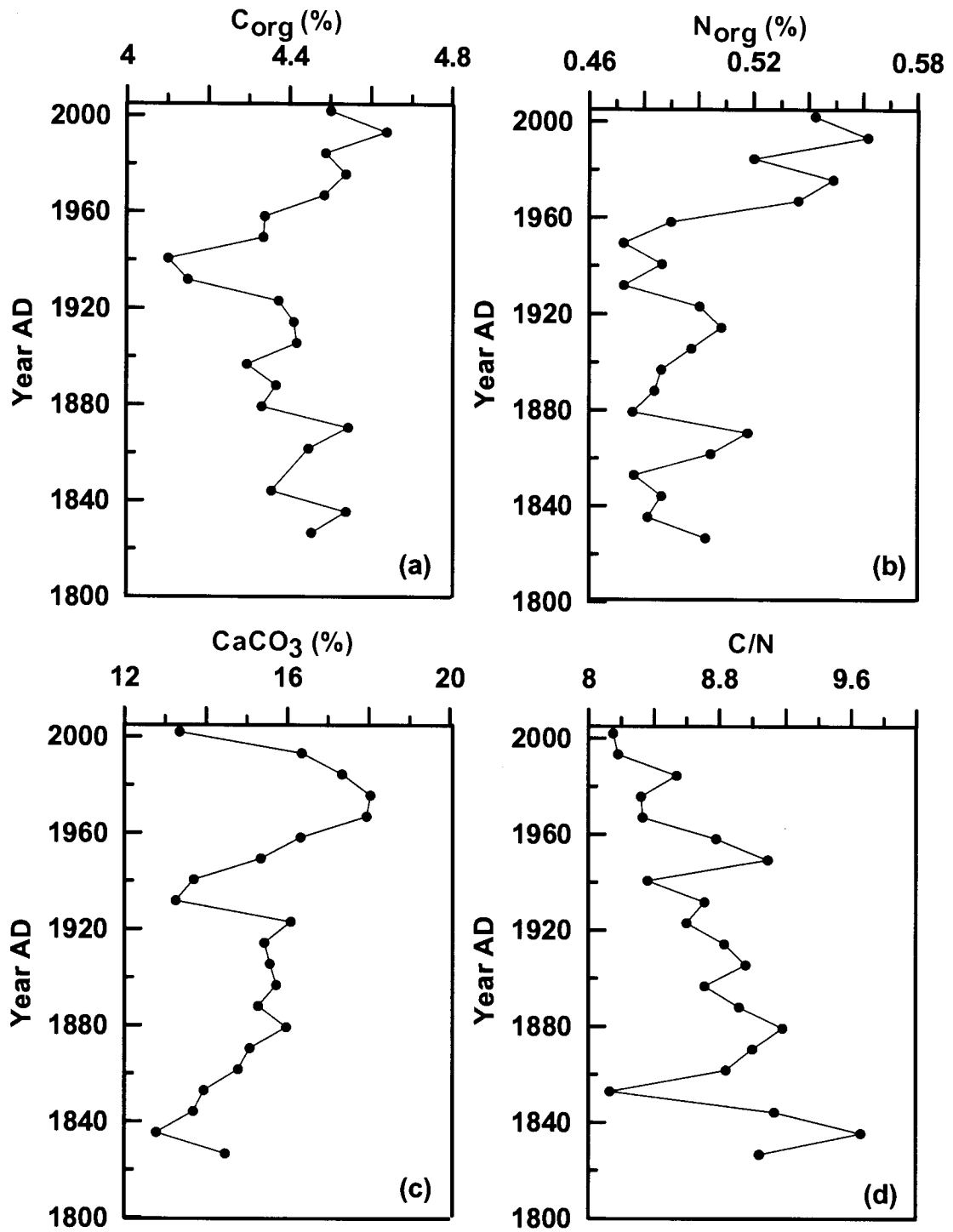
Figure 4.7: Downcore variation of (a)C_{org} (b)N_{org} (c)$CaCO_3$ and (d)C/N in core SaSu-1.

core, the ranges of variability are quite narrow. The average C_{org} and TN contents are 4.41 and 0.50%, respectively. The $CaCO_3$ content is found to fluctuate between 12.5 and 18% with an average of ~15% (Figure 4.7c). The highest value of ~18% is observed ~40 yrs BP and the lowest ~70 yr BP for $CaCO_3$, coinciding with minima in C_{org} and TN, and in the oldest and the youngest samples. Thus, $CaCO_3$ shows a more or less parallel correlation with C_{org} and TN except for the most recent past where a divergence between the organic and inorganic proxies is noticed. The C/N weight ratio varies between 8 and 9.6 with a generally downcore increasing trend (Figure 4.7d). The mean C/N ratio in this core is 8.7.

In SaSu-3B, C_{org} and TN contents range from 3.5 to 5.3%, and from 0.36 to 0.58% (Figure 4.8a,b). As in the case of SaSu-1, the C_{org} and TN concentrations exhibit rapid increase over the past 50-60 years. In older samples, the values remain relatively uniform (a slight longer term decreasing trend with depth is discernible for TN, though). The average values for the whole core are ~3.9% for C_{org} and 0.41% for TN. The $CaCO_3$ content varies between 4 to 8% with an average value of ~6% (Figure 4.8c). A prominent long term decreasing trend with lowest values at the present time distinguishes this record. Weight ratios of C/N range between 8 and 11 also showing an increasing trend down core, except for an anomalously high value close to the core top (Figure 4.8d). The mean ratio for the entire core is 9.7. The long term trend for the C/N ratio in this core is similar to that in SaSu-1, but such is not the case for $CaCO_3$.
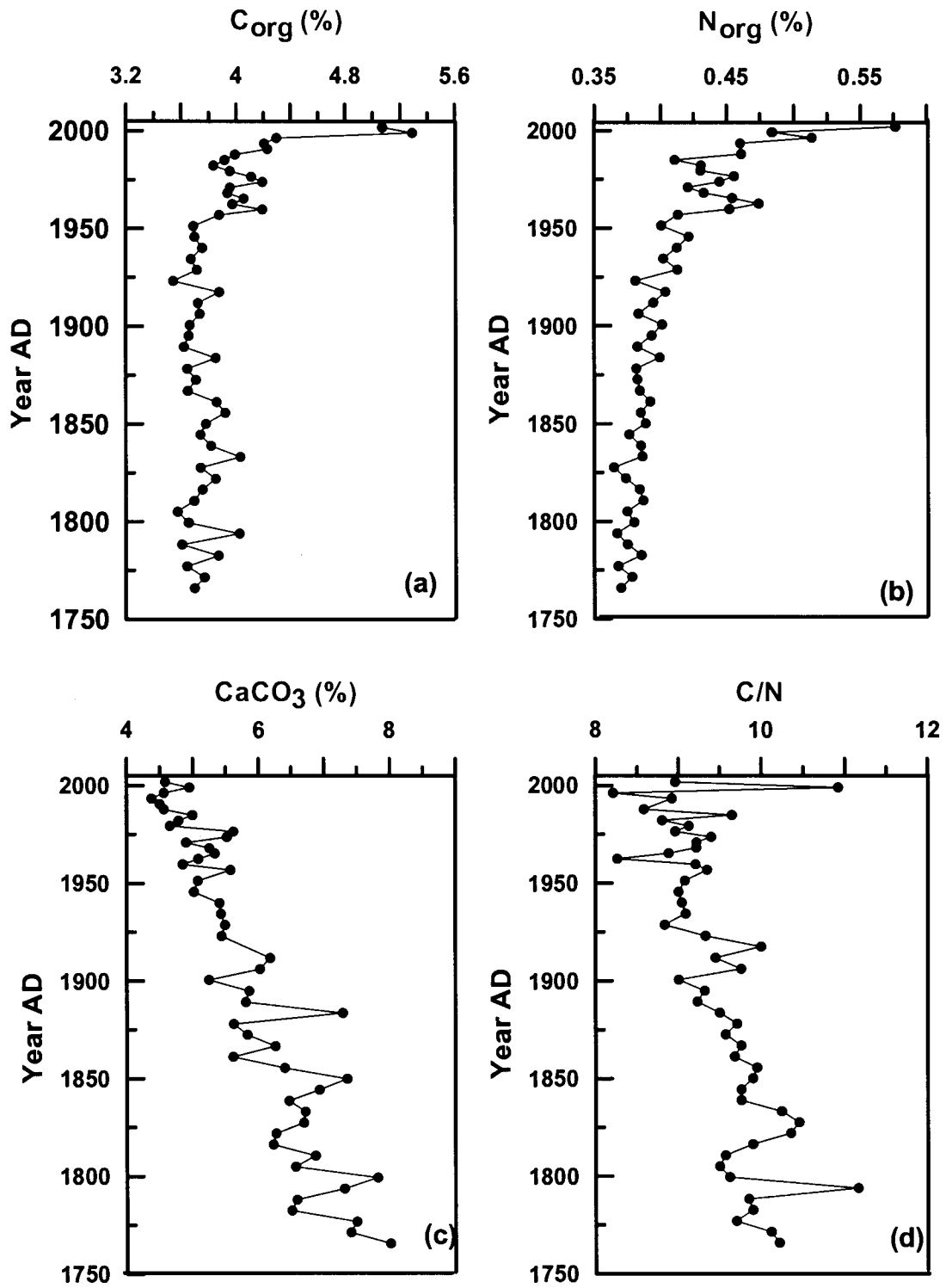
Figure 4.8: Downcore variation of (a)C_{org} (b)N_{org} (c)$CaCO_3$ and (d)C/N in core SaSu-3B.

4.2.3.2 Sedimentary Carbon ($\delta^{13}C_{org}$) and Nitrogen ($\delta^{15}N$) isotopes

Sedimentary $\delta^{13}C_{org}$ and $\delta^{15}N$ values for SaSu-1 vary from -21.0 to -20.5‰ and from ~7.0 to 7.7‰ respectively (Figure 4.9a). In both cases the lightest values occur in the upper portion of the core although in the case of $\delta^{13}C_{org}$ the decrease occurred much later (i.e, in younger samples) as compared to $\delta^{15}N$, which declined abruptly ~60 yr BP. Variations in older samples are within a narrow range.

In case of Core SaSu-3B also, similar trends as in SaSu-1 are observed for both proxies, albeit with larger oscillations. The $\delta^{13}C_{org}$ and $\delta^{15}N$ values range from -21.3 to -20.5‰ and from ~7.0 to 8.2‰, respectively (Figure 4.9b). The amplitude of the oscillations is particularly large in the lower 2/3 of this core.

4.2.3.3 Temporal variations in carbon sources and denitrification inferred from concentrations and isotopic composition of organic carbon and Nitrogen

A compilation of the available data on organic carbon content of sediments in the Arabian Sea by Paropkari et al. (1987) revealed high (1-4%) C_{org} enrichment in the inner shelf region. The slope sediments have even higher C_{org} (4-6%), but the outer shelf sediments are conspicuously depleted in C_{org} (<1%). Possible causes for the enrichment of organic carbon in the slope region have been examined in detail for the last two and half decades, and is intensely debated, with one group of researchers supporting the production hypothesis (Parrish, 1982; Pedersen and Calvert, 1990; Calvert
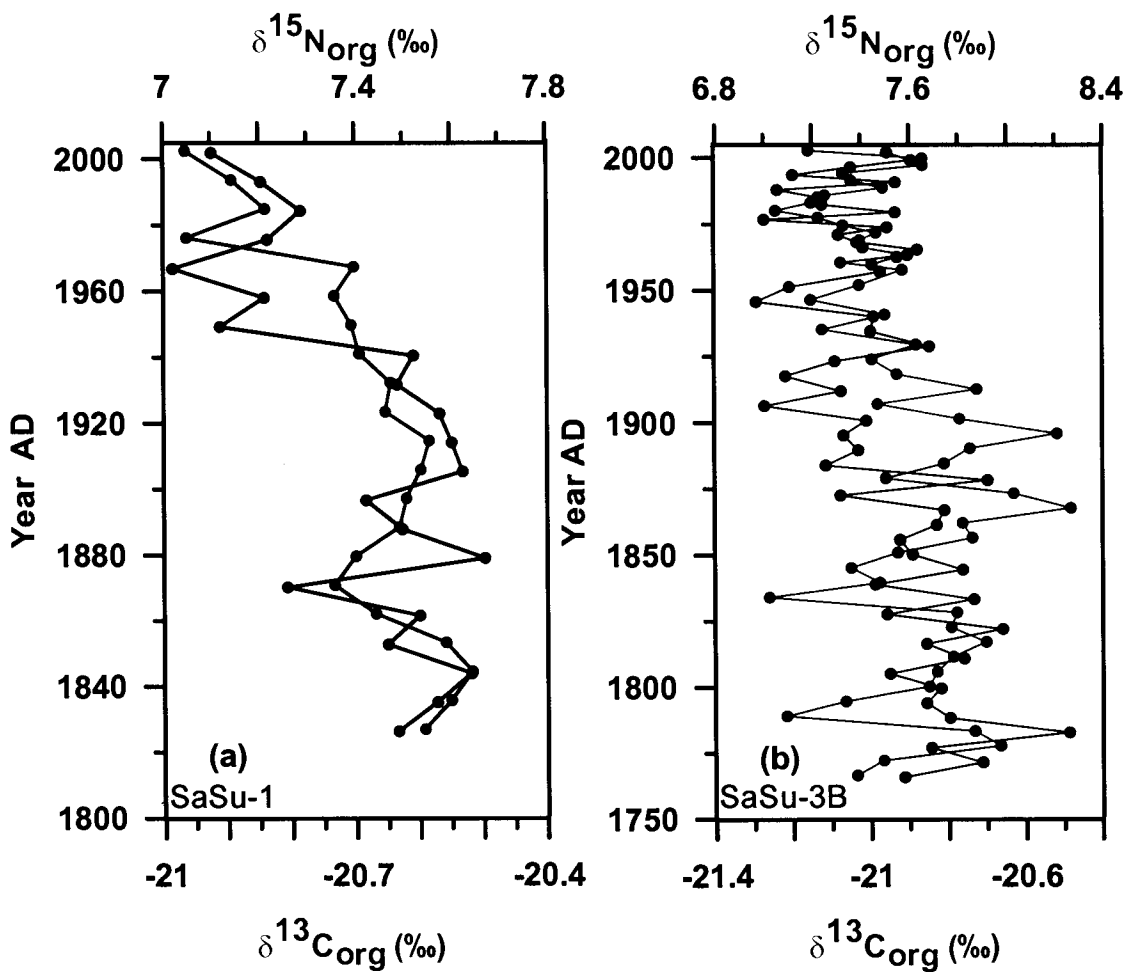
Figure 4.9: Downcore variation of $\delta^{13}C_{org}$ and $\delta^{15}N_{org}$ in cores (a)SaSu-1 and (b)SaSu-3B.

and Pedersen, 1992; Calvert et al., 1995), while the other favouring the preservation hypothesis (Dow, 1978; Demaison and Moore, 1980; Bralower and Thierstein, 1987; Summerhayes, 1987; Paropkari et al., 1991, 1992, 1993a). Paropkari et al. (1992) emphasized that productivity does not exert the dominant control on organic carbon distribution in the sediments; instead it is the bottom water anoxia that, in conjunction with various depositional parameters, determines the degree of preservation. Calvert et al. (1995), on the other hand, concluded that the distribution of organic matter on the western continental margin is controlled by variation in supply, dilution by other sedimentary components, and the texture of sediments. Cowie et al. (1995) concluded that along with productivity and anoxia, other factors such as sedimentation rates, local productivity, water depth, sediment mineralogy, texture, particle winnowing, biological mixing and irrigation also contribute to the preservation of organic carbon.

The high organic carbon concentrations observed in both the shorter cores analyzed in this study are generally in accordance with previous reports from the Indian margin (Marchig, 1972; Paropkari et al., 1987; Rao and Rao, 1989; Naidu et al., 1992). However, the large increase in the near surface sediments occurring in the past few tens of years was not recorded previously. To be more specific, the C_{org} contents (4.1-4.7% for SaSu-1 and 3.5-5.3% for SaSu-3B) observed in these cores are close to the upper end of the range (0.35 – 3.53%) reported by Paropkari et al. (1987). These authors found the average C_{org} for the inner shelf regions between Ratnagiri and Quilon to be ~2%, almost half the average C_{org} value of ~4.2% for the SaSu

cores. The TN content in both cores (0.36-0.58%) is within the range (0.1-1.25%) observed by Paropkari et al. (1987). More recently, Gaye-Haake et al. (2005) reported a local maximum in TN of ~0.5% in surficial sediments over the western Indian continental margin. These authors found sedimentary nitrogen to be generally higher, closer to the coast in the Arabian Sea than in the Bay of Bengal, due to the dilution caused by the river-derived sediments in the latter region. Surface values in the cores examined here are thus also consistent with Gaye-Haake et al's (2005) data.

An interesting one-to-one correlation is observed between TN and C_{org} with the depth profiles of the two parameters being almost identical in both cores (Figure 4.10a,b). A striking feature of records of both parameters is the aforementioned increase occurring over the latter half of the last century. This change seems to be more pronounced in SaSu-3B than in SaSu-1 presumably because of proximity of the former to the coast. The top few centimeters of the core had a distinctly different appearance (the sediment was distinctly much darker; plate 4.1), which also suggests that an abrupt change occurred in this region in the most recent past. It is within this layer that the highest C_{org} (5.3%) and TN (0.58) contents were recorded. The exact reason of this increase i.e. whether it is due to higher production (through eutrophication or intensification of upwelling) or preservation (through intensifying coastal oxygen deficiency) is not clear, but it is most likely that both causative mechanisms are in operation (given that oxygen deficiency itself is related to nutrient enrichment).

The reported mean C/N weight ratio for marine organic matter in the
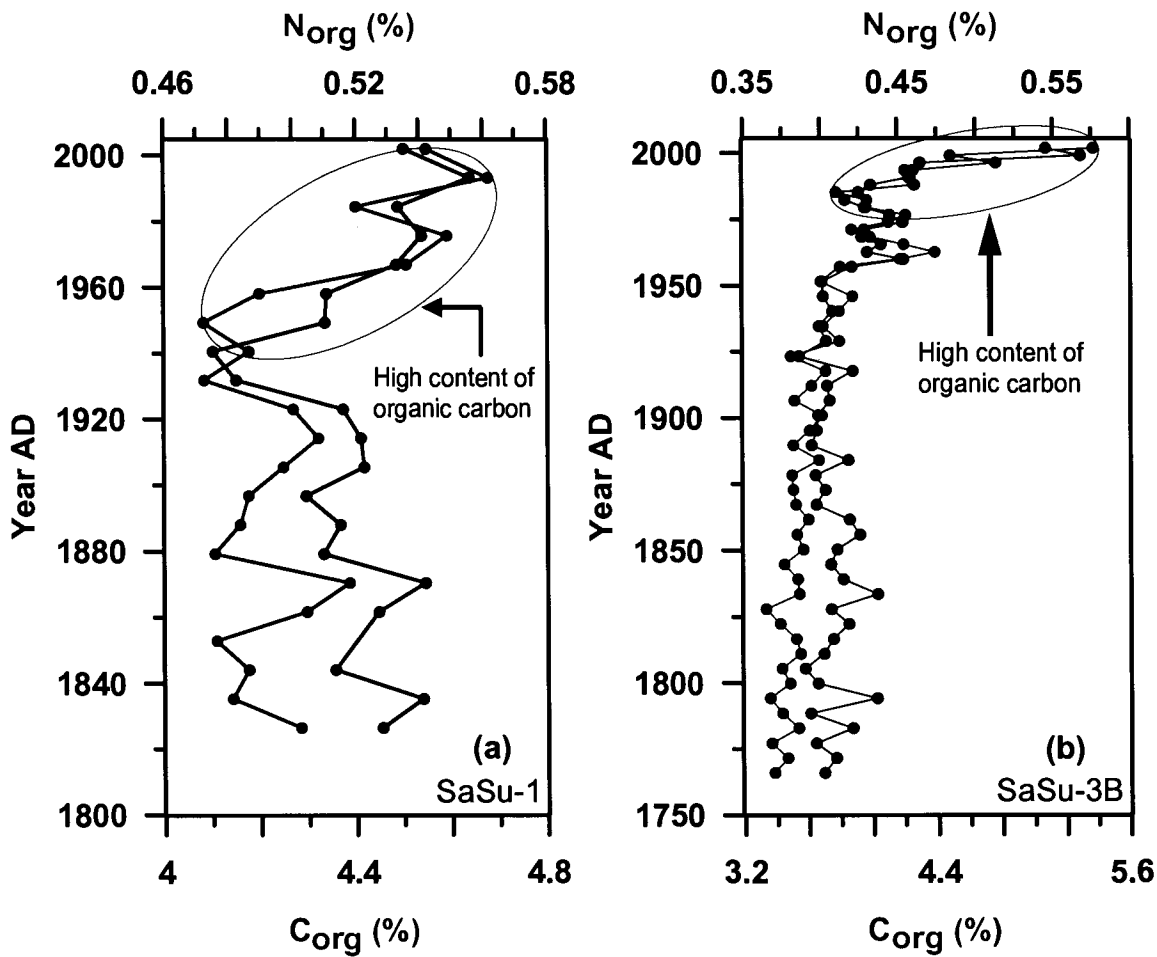
Figure 4.10: Downcore variation of C_{org} and N_{org} in cores (a)SaSu-1 and (b)SaSu-3B.

Eastern Arabian Sea is 8±2 (Calvert et al., 1995; Bhushan et al., 2001; Agnihotri, 2002). The mean C/N weight ratio (8.7) in SaSu-1 is therefore consistent with the earlier data and indicates the largely marine origin of organic matter. The mean C/N weight ratio (9.7) in SaSu-3B is slightly towards the higher side, which again can be explained by the shallower depth. Intriguingly, there exist distinct long-term decreasing trends in C/N with time (i.e. core top values being the lowest) in both the cores. This would imply a decreasing supply of organic carbon from land over the past 200 years (which is against the expectation, given the well known change in land use, and an intensification of the monsoonal rainfall as has already been discussed earlier). It would appear that the C/N change could have been caused by other processes (e.g. differential remineralization of carbon and nitrogen or changes in food web structure especially among the benthic community). Note, however, that there is one very high value of C/N (Figure 4.8d) near the core top within the black, distinctly different layer mentioned above. This portion of the sediment probably contains substantial terrigenous component.

As stated earlier, the $\delta^{13}C_{org}$ provides valuable clues as to the source of the organic matter as the carbon isotopic composition of coastal sediments is determined by the relative contributions from marine phytoplankton (typically with $\delta^{13}C_{org}$ of -20 to -22‰ vs PDB), and marine plants (largely C3 with an average $\delta^{13}C_{org}$ of around -27‰) (Meyers, 1997; Tyson, 1995 However the $\delta^{13}C_{org}$ of phytoplankton signature can also vary as a result CO_2 uptake caused by high primary productivity, which in turn may re
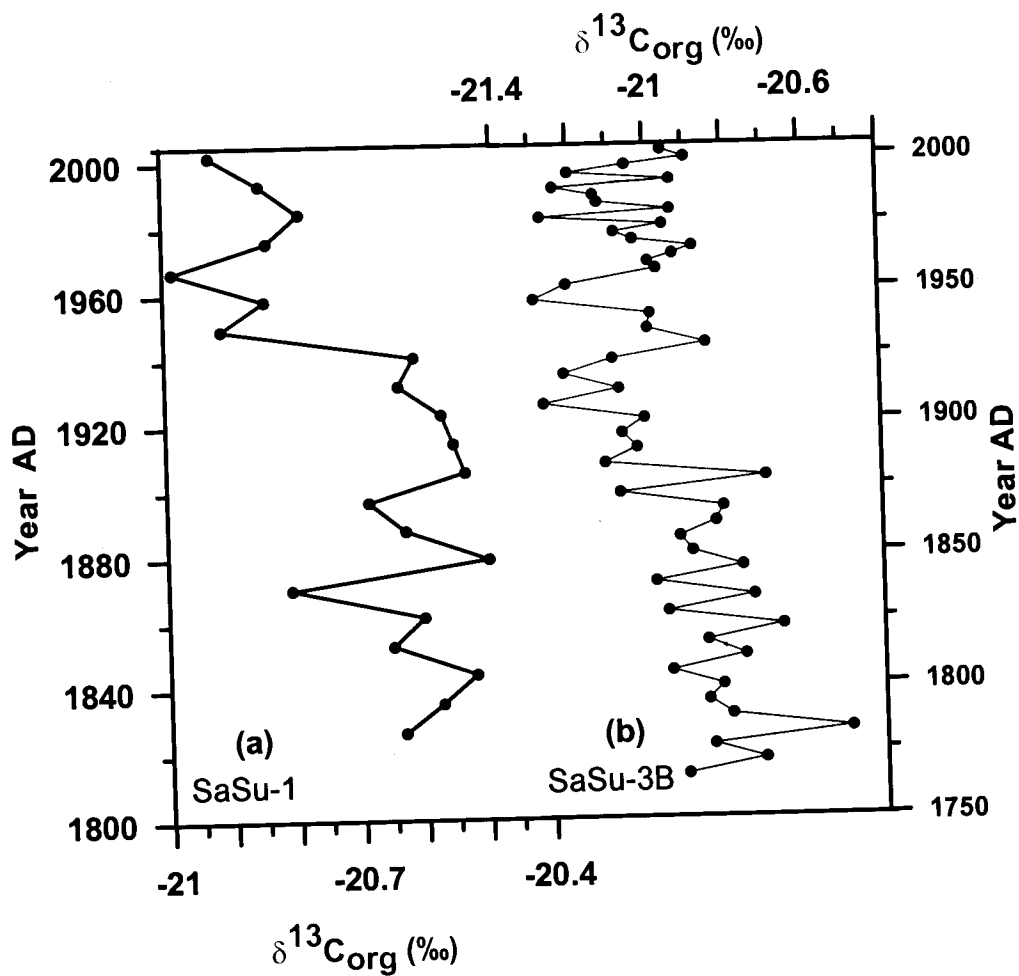
Figure 4.11 : Downcore variation of $\delta^{13}C_{org}$ in cores (a)SaSu-1 and (b)SaSu-3B.

nutrient loading (Schelske and Hodell, 1995). In this case, $\delta^{13}C_{org}$ values may vary by as much as -13 to -29‰ (Andrews et al., 1998). There is also a possibility of slight fractionation through food chain (Peterson et al., 1985) and during degradation of organic matter (Thornton and McManus, 1994). The mean $\delta^{13}C_{org}$ (versus PDB) based on 21 measurements in SaSu-1 is -20.70‰; the corresponding mean of 47 analyses in SaSu-3B is -20.96‰. The range of $\delta^{13}C_{org}$ values in both the cores is thus typical for the marine organic matter. Nevertheless, the $\delta^{13}C_{org}$ profiles in both the cores show a distinct relative upcore decrease in values over the last 4-5 decades (Figure 4.11a,b). This is not consistent with the C/N data discussed above. However, this conforms to expectations as the monsoonal strength (and thus presumably terrigenous supply of organic matter) has been higher in the region than ever before in the past 700 years. Moreover, sterol biomarkers (stigmasterol and β-sitosterol produced by terrigenous plants although not exclusively) are also most concentrated in the upper portion of core CR-2 representing the same time period (Kurian et al., submitted).

The $\delta^{15}N$ in SaSu-1 and SaSu-3B are ~7 and 7.2‰, respectively. These values are higher than those (<6‰) reported by Gaye-Haake et al. (2005) for surficial sediments over the western Indian shelf. These are also higher than the average $\delta^{15}N$ of oceanic NO_3^- (5‰ - Altabet, 2006), but lower than the $\delta^{15}N$ of sedimentary nitrogen in areas of open ocean underlying zones of denitrification (up to 9‰ in the central Arabian Sea; Gaye-Haake et al., 2005; also see Chapter 5). The value for the core CR-2 is even lower

(6.6‰), as discussed in 4.2.2.1. This is a rather unexpected finding because as discussed in Chapter 3, the inner- and mid-shelf regions experience intense denitrification in late summer and autumn. In fact, the relatively lower $\delta^{15}N$ persist throughout the upper portions of the cores representing the past few decades. High quality NO_3^- data from the shelf region available for over two decades show that denitrification did occur during this period (see supplementary in Naqvi et al, 2000). The $\delta^{15}N$ in the sediments older than 40-60 years are generally higher (reaching up to ~8.2‰ in the middle part of SaSu-3B), and the average $\delta^{15}N$ for the entire cores (7.41‰ for SaSu-1 and 7.55‰ for SaSu-3B) also reflect the occurrence of denitrification in the region. But for the most recent past (last two decades) for which the water column data are available, the sedimentary nitrogen isotope data, does not seem to track accurately the denitrification intensity.

Over the last few decades, expanding human populations in coastal regions, land use changes by the increasing use of synthetic nitrogenous fertilizers in agriculture and combustion of fossil fuel (that releases NOx), have resulted in increased nutrient inputs to estuarine systems (Howarth et al., 2002). These inputs have led to eutrophication in many coastal systems (Naqvi et al., 2000; Turner and Rabalais, 1994, 2003) and it is feared that, this trend will continue. The Chesapeake Bay is one of such systems that receive large anthropogenic nutrient loads and experiences bottom water suboxia during summer. Bratton et al. (2003) have reconstructed the history of suboxic events in this system using stable N isotopes based on the observed increase in $\delta^{15}N$ in sediment cores (by up to 4‰ during periods of

suboxia). Similar results were also obtained by Eadie et al. (1994) over Louisiana shelf off the mouth of the Mississippi River, where the heavy $\delta^{15}N$ signatures were linked to nutrient enhancement of productivity and denitrification. As in the case of area of the present study, these two regions experience seasonal suboxia, and so the absence of a very heavy $\delta^{15}N$ signal cannot be linked to the lack of perennial denitrification. Moreover, these regions also receive terrestrial matter with its characteristically lower $\delta^{15}N$. Keeping in view, the above discussion on terrestrial dilution, it is highly unlikely that the dilution by terrestrial inputs can overwhelm the denitrification signal. The possible causes of the lower than expected sedimentary $\delta^{15}N$ over the Indian shelf have already been mentioned earlier (see Section 4.2.2.1). The favoured explanation is that denitrification presently does not lead to very high enrichment of ^{15}N in NO_3^- over the Indian shelf. Water column data on $\delta^{15}N$ of NO_3^- lends observational support to this view. As described in Chapter 3, the $\delta^{15}N$ of NO_3^- is highly variable (ranging from 3.4 to 22.5‰). However, even the highest value is substantially lower than that expected from the observed NO_3^- deficit and the fractionation factor computed for the open ocean denitrification zone (Naqvi et al., 2006b). The possible causes of this anomaly are described in Chapter 3. In addition, as stated in Section 4.2.2.1, there is also the possibility of N_2-fixation, which occurs in the region during the oligotrophic intermonsoon seasons (especially during the spring intermonsoon – Devassy et al., 1978), may dilute the N isotopic signal produced by denitrification.

The mismatch between productivity and denitrification-produced $\delta^{15}N$

enrichment may, however, be a recent phenomenon arising from the intensified productivity and denitrification in the last few decades in response to human induced changes. This is because; in the older sediments of the two SaSu cores as well as in CR-2 the sedimentary $\delta^{15}N$ does exhibit higher values and (in the longer record) tracks the productivity proxies. In other words, the relationship between sedimentary $\delta^{15}N$ and productivity/extent of denitrification may not always co-vary. This is to be expected because once denitrification reaches completion, $^{15}NO_3^-$ is also fully consumed such that the period over which denitrifying bacteria can afford the luxury of discriminating between the two N isotopes is relatively short (about 1 month). In any case, the results of the present study clearly demonstrate for the first time the limitation of $\delta^{15}N$ as a proxy of denitrification in coastal waters.

4.2.3.4 Variability among the cores

Some differences are observed in terms of organic matter signatures between the two cores though both core locations are quite close to each other (Table 4.8). In general, all parameters show smaller variations in SaSu-1 as compared to SaSu-3B. Located farther from land, the sedimentation rate is lower for SaSu-1 compared with SaSu-3B, and it is probably for this reason, the C_{org} content is higher. Often spatial variability reflects water depth (and proximity to shorelines). For example, the C/N ratio in cores generally increases, as water depth decreases (Owen and Lee, 2004). The same is observed here too, with somewhat higher C/N values occurring at 35 m (SaSu-3B) as compared to 50m (SaSu-1) water depth.

The average $\delta^{15}N$ as well as its range are significantly larger in SaSu-3B compared to SaSu-1. This may be because near-bottom suboxia over the Indian shelf is limited to a very narrow belt (Chapter 3). As a result the inner shelf experiences this phenomenon longer than the middle shelf. It is quite likely that there were times in the past when this process did not occur at the site of SaSu-1.

Distribution of $CaCO_3$ is quite different in the two cores; while the $CaCO_3$ content decreased almost monotonously in SaSu-3B by a factor of 2 from the oldest to the youngest sample, its profile has a greater structure in SaSu-1, where the overall amplitude of oscillations is smaller but the $CaCO_3$ content is higher. In addition to dilution by terrigenous material (which accounts for the shoreward decrease in $CaCO_3$ in the region), one other factor to be considered is the intensity of oxygen minimum. Anoxic conditions would prevent the growth of benthos with calcareous shells and intensifying anoxia might account for the decline in the $CaCO_3$ content in recent times. The changes in benthic ecology are also expected to affect the C/N ratio, and this is an aspect that future research should focus on.

4.2.3.5   Co-variability of proxies

Figures 4.12 and 4.13 show scatter plots between various organic proxies. Significant correlation is observed between C_{org} and TN in both cores, especially in SaSu-3B. This suggests that the two are largely bound together. Statistically significant correlations also exist between $\delta^{13}C_{org}$ and $\delta^{15}N$, and $\delta^{15}N$ and C/N in SaSu-1, apparently in contradiction with one
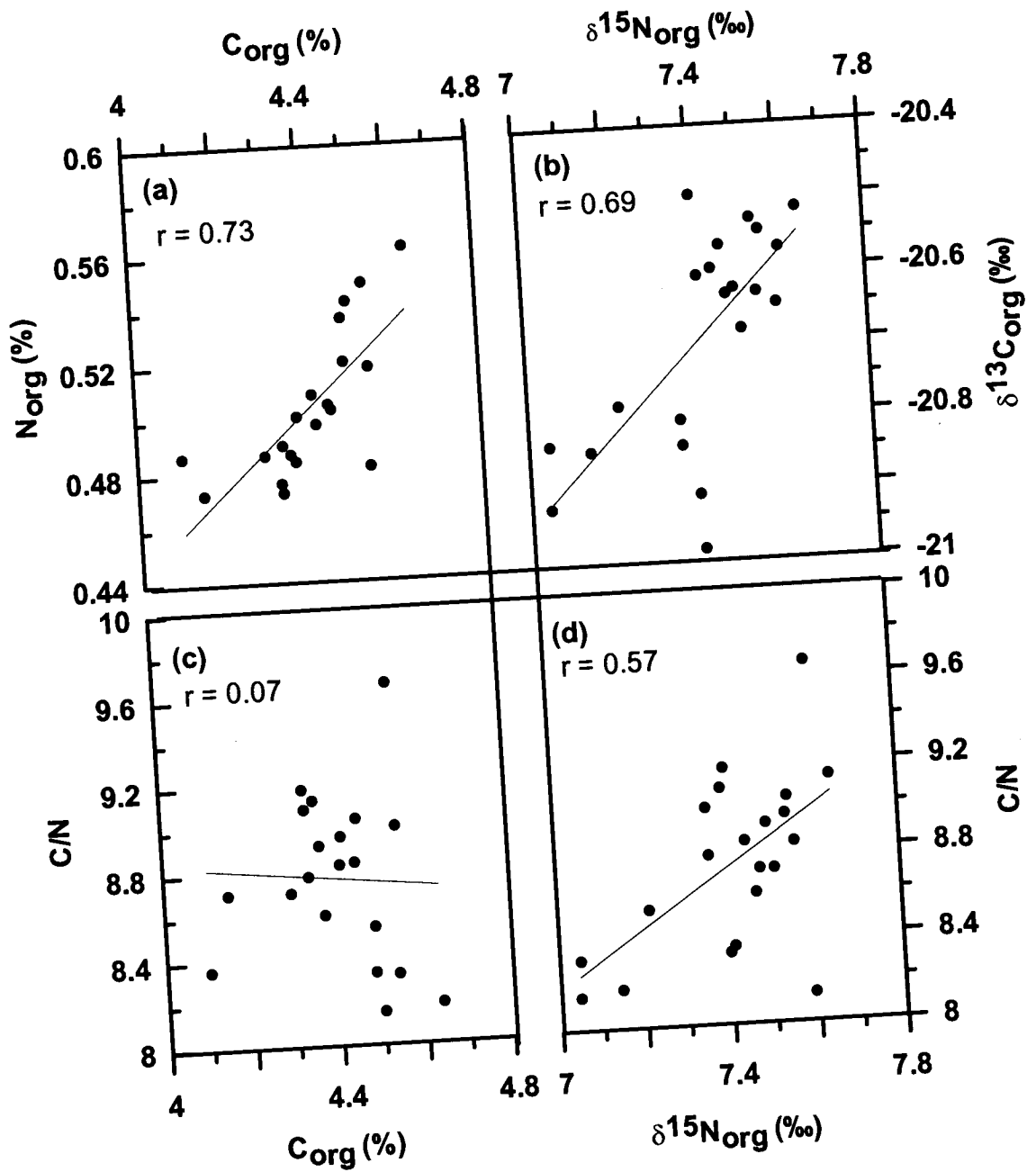
Figure 4.12: Cross plots of elemental and isotopic data with trend lines for core SaSu-1. (a)C_{org} vs N_{org} (b)$\delta^{13}C_{org}$ vs $\delta^{15}N_{org}$ (c)C_{org} vs C/N (d)$\delta^{15}N_{org}$ vs C/N.
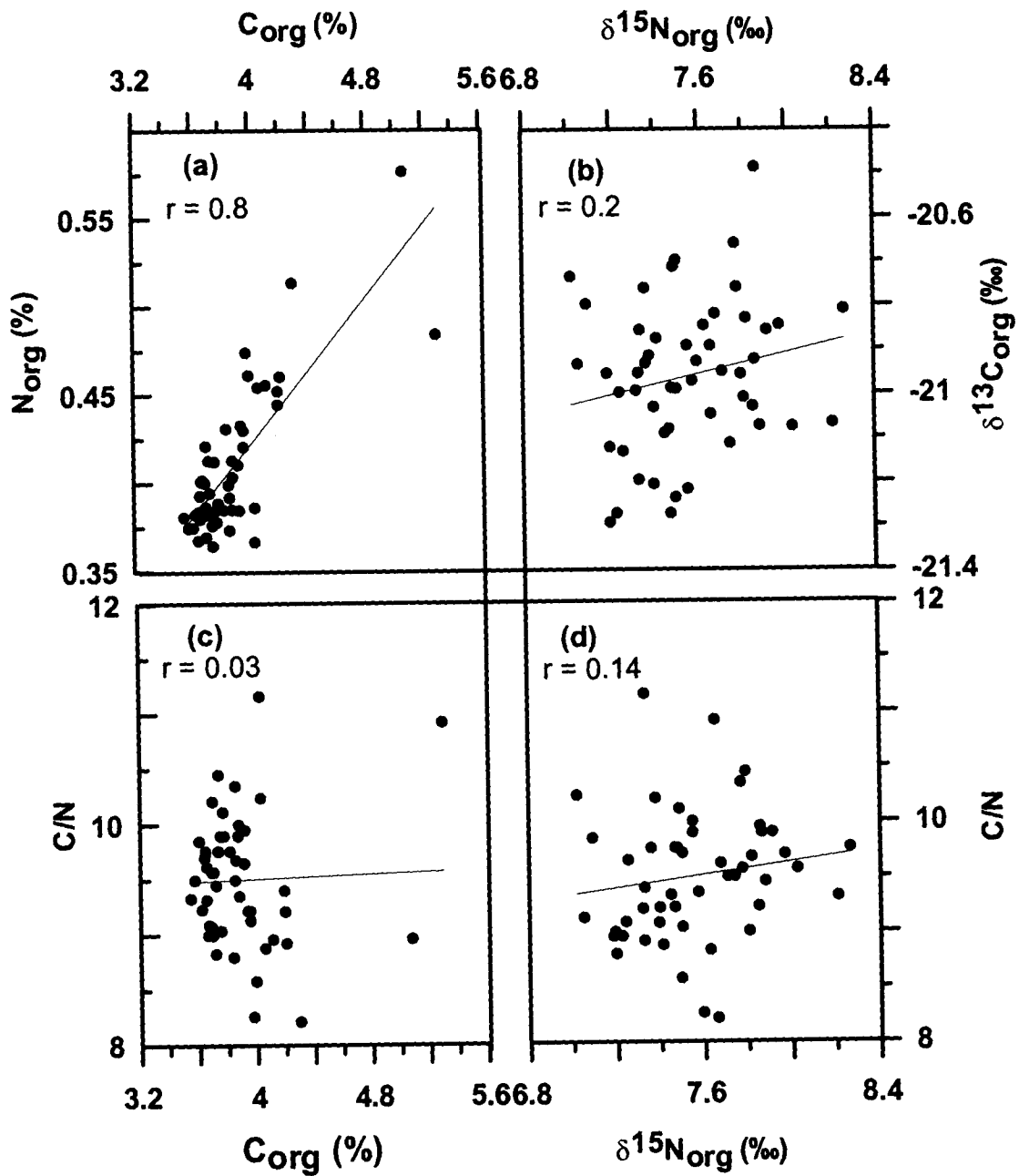
Figure 4.13: Cross plots of elemental and isotopic data with trend line for core SaSu-3B. (a)C_{org} vs N_{org} (b)$\delta^{13}C_{org}$ vs $\delta^{15}N_{org}$ (c)C_{org} vs C/N (d)$\delta^{15}N_{org}$ vs C/N.

another. It means that either $\delta^{13}C_{org}$ or C/N does not accurately track the terrestrial inputs of organic matter. Assuming it to be C/N, some dilution of the $\delta^{15}N$ signal arising from denitrification by terrestrial organic matter occurs at this site. However, such a dilution should have been more pronounced in SaSu-3B, since it is located closer to land. Such is not the case. Correlations between $\delta^{13}C_{org}$ and $\delta^{15}N$, $\delta^{13}C_{org}$ and C/N, and $\delta^{15}N$ and C/N are statistically insignificant in this core.

Downcore records of C_{org} and $CaCO_3$ exhibit visual similarity in SaSu-1, especially in the middle portion of the core (Figure 4.14a). For example, coincident minima in both variables about 60 y BP suggest lower organic and inorganic productivity. However, this co-variabilty is not seen in SaSu-3B (Figure 4.14b) where, as mentioned above, C_{org} remains fairly invariant for most parts except for the increase observed in the past few decades, while the $CaCO_3$ content decreases monotonously with time. This difference is probably caused by the proximity of SaSu-3B to land and the resultant environmental conditions that probably drive different food webs in the benthic realm. Bhushan et al. (2001) also observed a lack of parallel trend between $CaCO_3$ and C_{org} in cores collected off Goa.

Records of BioSi and C_{org} should show similar trends as the diatoms are the principal group of phytoplankton in this region. Surprisingly, however, there seems to be an anti-correlation between the two for most parts, except for the last few decades, in SaSu-1. This also applies to the relation between BioSi and $CaCO_3$ in this core (Figure 4.15a). In SaSu-3B, the BioSi shows a long term declining trend similar to that of $CaCO_3$ although with more
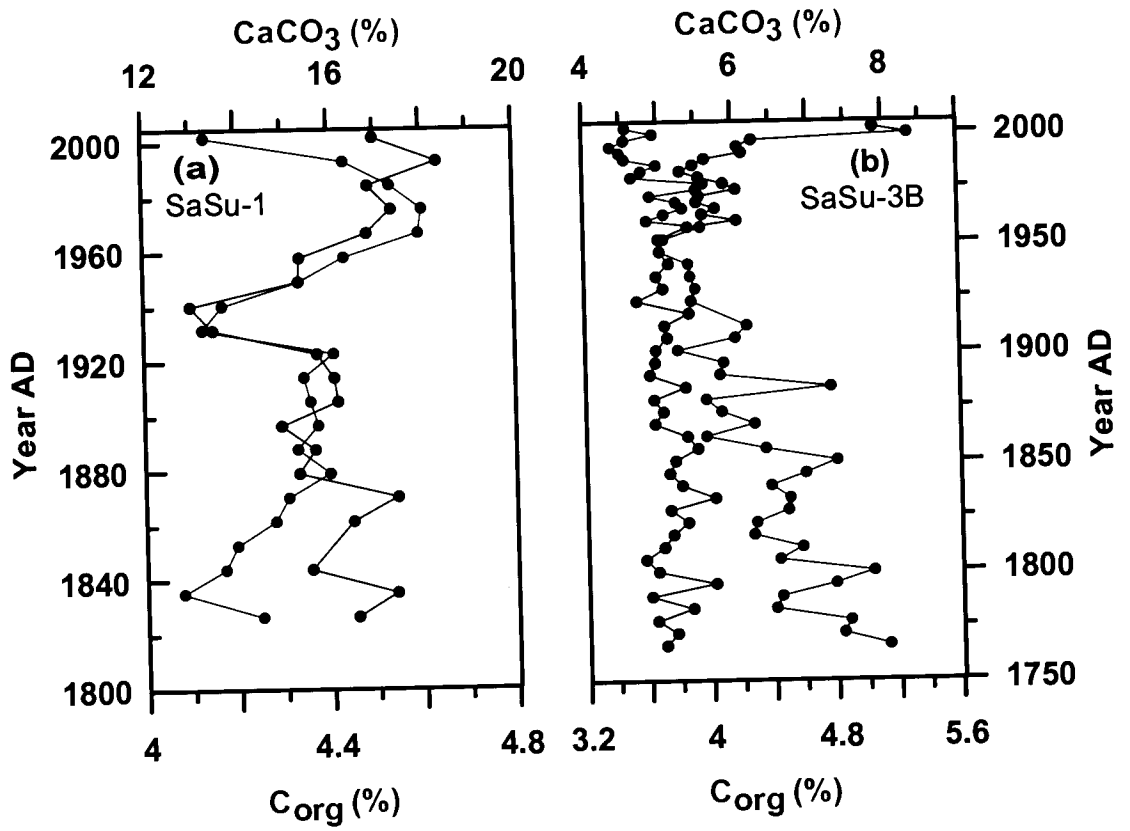
Figure 4.14: Downcore variation of $CaCO_3$ and C_{org} in cores (a)SaSu-1 and (b) SaSu-3B.
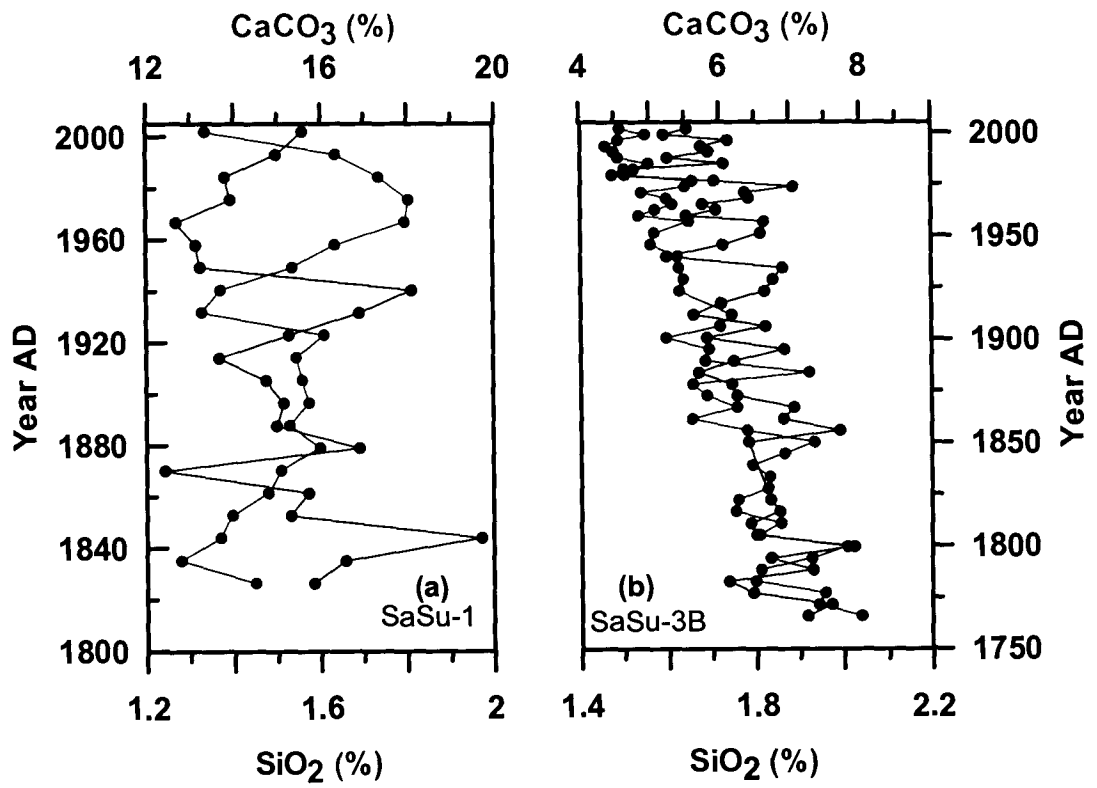
Figure 4.15: Downcore variation of $CaCO_3$ and biogenic silica (SiO_2) in cores (a)SaSu-1 and (b)SaSu-3B.

fluctuations (Figure 4.15b).

4.2.3.6 Burial fluxes and past productivity changes

Burial fluxes (also called the mass accumulation rates, MAR) for C_{org}, TN and $CaCO_3$ were calculated by multiplying the respective concentrations (g/g) with sedimentation rate (cm/kyr) and dry bulk densities (DBD, g/cm^3). Fluxes of C_{org} range from 19 to 23 g m^{-2} y^{-1}, and from 26 to 32 g m^{-2} y^{-1} (except for two values which are as high as 38 g m^{-2} y^{-1} for surface samples) in SaSu-1 and SaSu-3B, respectively. The flux ranges observed for TN are 2.2-2.8 g m^{-2} y^{-1} and 2.4-4.0 g m^{-2} y^{-1} for SaSu-1 and SaSu-3B, respectively. The variations in fluxes observed in both the cores are similar to those observed by Bhushan et al. (2001).

It is readily apparent from the profiles [Figure 4.16 (SaSu-1) and Figure 4.17 (SaSu-3B)], that the flux patterns for all the three parameters mirror their original proxy distribution pattern in both the cores. Note, however, that the relative values for the two, change substantially. For example, the C_{org} content is lower in SaSu-3B compared with SaSu-1, but reverse is the case for the C_{org} burial fluxes. This, of course, is due to higher sedimentation rate at the shallower site. In SaSu-1, C_{org}, TN and $CaCO_3$ exhibit a similar downcore trend, as pointed out earlier, and the same holds good for their respective flux profiles as well. In SaSu-3B, $CaCO_3$ content as well as its burial flux do not show any covariation with the corresponding C_{org} and TN values. As the variations in C_{org} flux are identical to those in case of TN in both the cores indicating the absence of any preservation bias. This is in
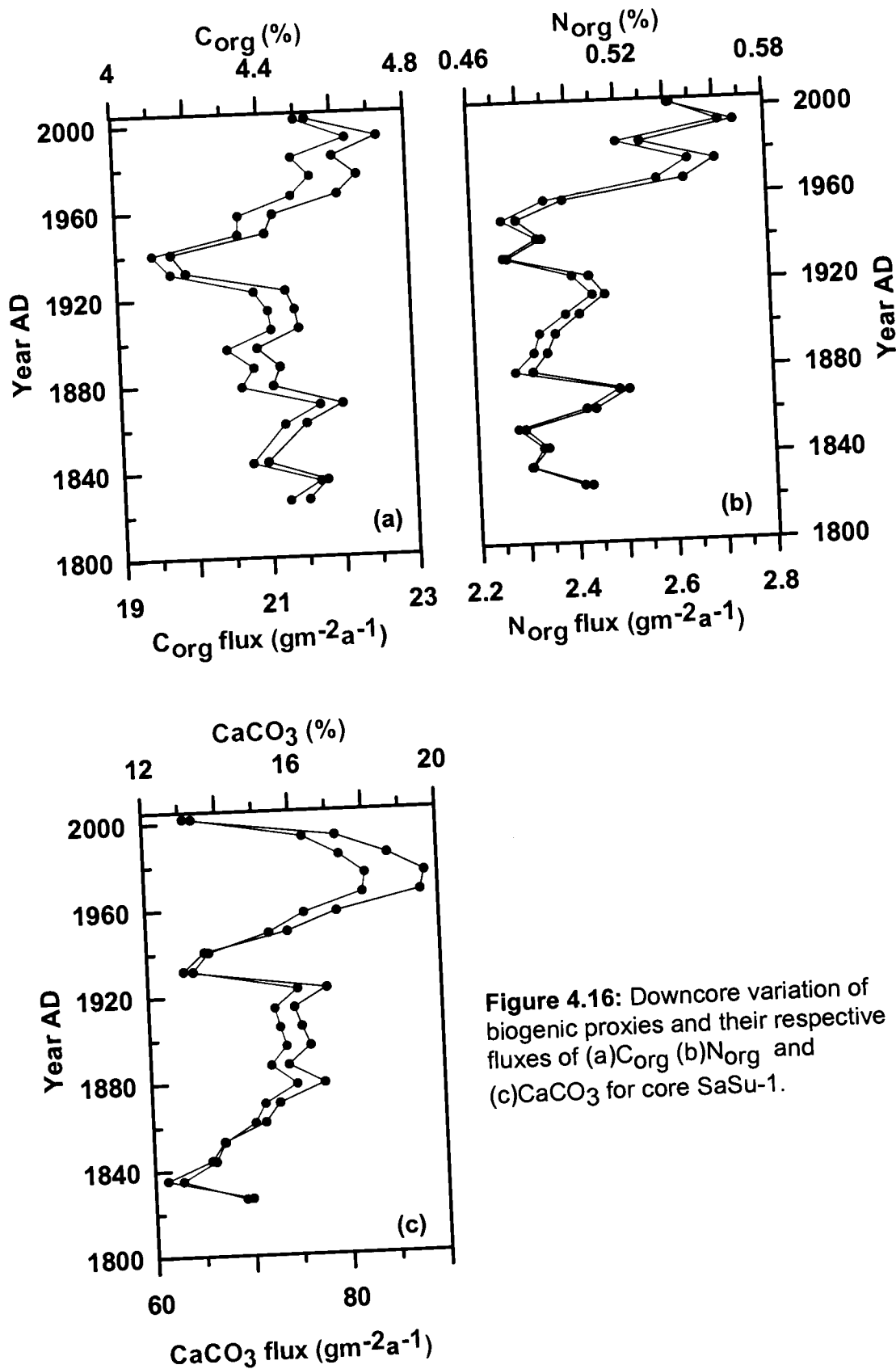
Figure 4.16: Downcore variation of biogenic proxies and their respective fluxes of (a)C_{org} (b)N_{org} and (c)$CaCO_3$ for core SaSu-1.
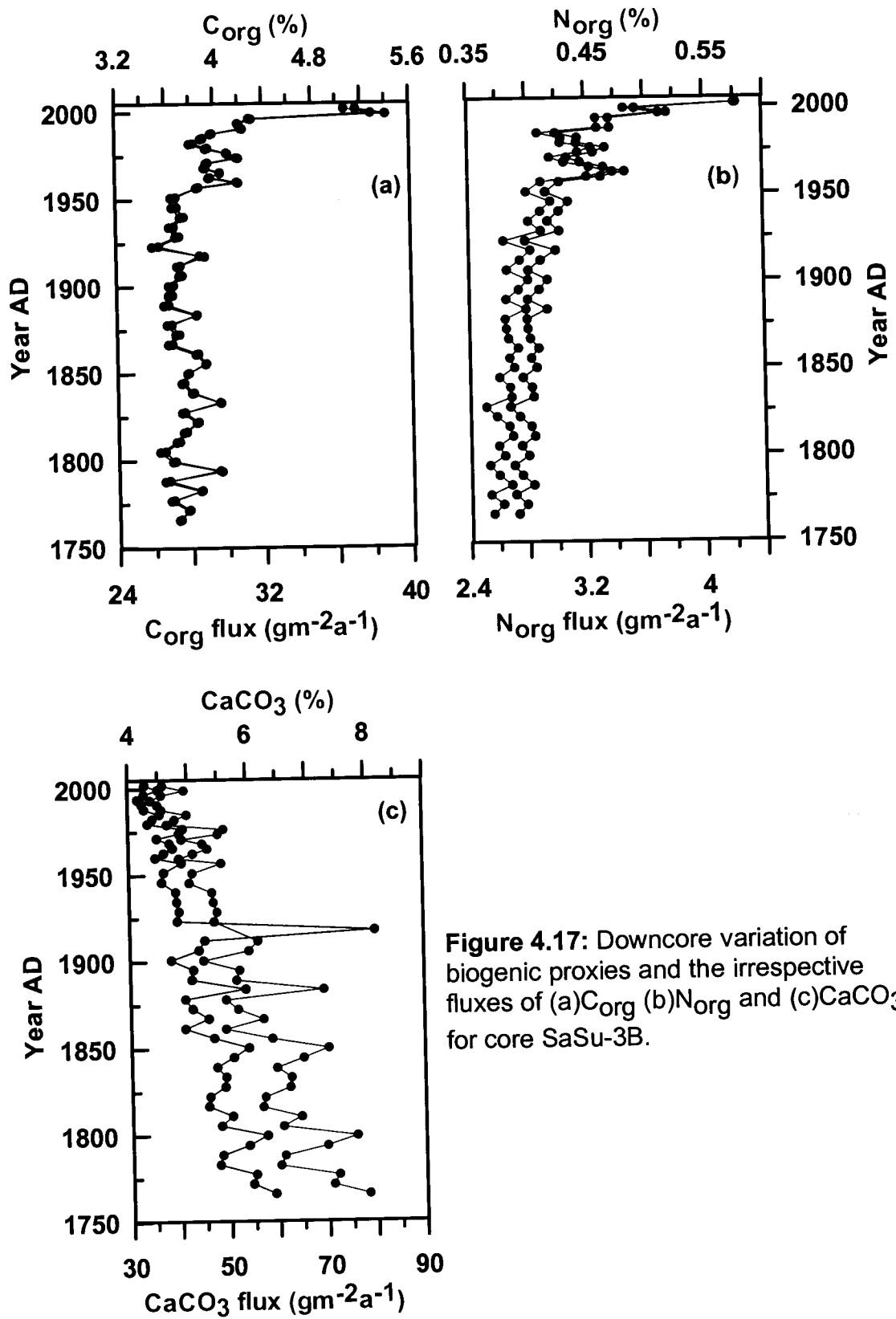
Figure 4.17: Downcore variation of biogenic proxies and the irrespective fluxes of (a)C_{org} (b)N_{org} and (c)$CaCO_3$ for core SaSu-3B.

contrast with the results of Bratton et al. (2003) from the Chesapeake Bay where the TOC flux pattern did not mirror the TN flux. Instead the TN fluxes rose steadily over the 20th century whereas TOC fluxes peaked at ~1950 and declined thereafter.

4.2.3.7 Major and Trace Elements

Geochemistry of surface sediments in the region have also been a subject of several past studies (Murty et al., 1978; Shankar et al., 1987; Kolla et al., 1976b, 1981a,b; Prakash Babu et al., 2002). Sirocko et al. (2000) analyzed thirty seven sediment cores from the deep Arabian Sea for investigating past variations in the intensity of the monsoon-driven atmospheric circulation and the associated oceanographic processes in surface waters. His comprehensive work allowed tracking past monsoon changes with century-scale resolution. But most of these records are from sites away from the area of our study. Over the western Indian continental margin Agnihotri (2002) carried out a fairly detailed study using trace metals as proxies of paleo-chemical environment. However, the material examined by him did not include cores from the inner shelf region with modern records of seasonal anoxia. The records presented in Sections 4.2.2.2 and 4.2.2.3 and below are thus the first of their kind from the eastern Arabian Sea.

4.2.3.7.1 Temporal variability of major elements

The Al content of sediments in SaSu-1 and SaSu-3B ranged from 6 to 7.3% (mean 6.5%), and from 7.7 to 9.5% (mean 8.56%), respectively. The

generally higher Al content in SaSu-3B is evident due to its proximity to land. The average values are almost half of the corresponding shale value [~17; Wedepohl (1971, 1991)]. In SaSu-1, Al concentrations appear to have been rising since the beginning of the last century along with those of Fe and Mg (Figure 4.18a,b,c), and that like Al also appear to have a dominant land source, as discussed above. This can be explained by the increasing supply from land, both due to increase in rainfall (and consequently land runoff) and changes in land use (deforestation in the Western Ghats as well agricultural practices). This trend was not so well marked in SaSu-3B for Al (where two rising trends interrupted by a sharp discontinuity 80-100 y BP are observed), but the Fe and Mg contents (Figure 4.19a,b,c) in this core still show general upcore increase. Mg content in SaSu-1 varied from 2.03 to 2.55% (mean 2.2%), whereas for SaSu-3B it was between 2.12 and 2.36% (average 2.24%). The Sr/Al weight ratio varied from 53 to 80 x 10^{-4} (average 64 x 10^{-4}), and from 22 to 30 x 10^{-4} (average 25 x 10^{-4}) for SaSu-1 and SaSu-3B cores, respectively. The average value of Sr/Al in SaSu-1 core is higher than the average shale value (38 x 10^{-4}; Turekian and Wedepohl, 1961), but in case of SaSu-3B this value is lower. The downcore profile of Sr/Al shows similarity with that of $CaCO_3$. The similarity was more pronounced for SaSu-1 (r=0.92; Figure 4.18e) than in SaSu-3B (r=0.63; Figure 4.19e). This similarity seems to persist throughout the late-Quaternary and Holocene (Agnihotri et al., 2003a,b; Agnihotri and Dutta, 2003) suggesting a close association between the Ca and Sr.

The P/Al weight ratio varied from 199 to 225 x 10^{-4} (average 210 x10^{-4}),
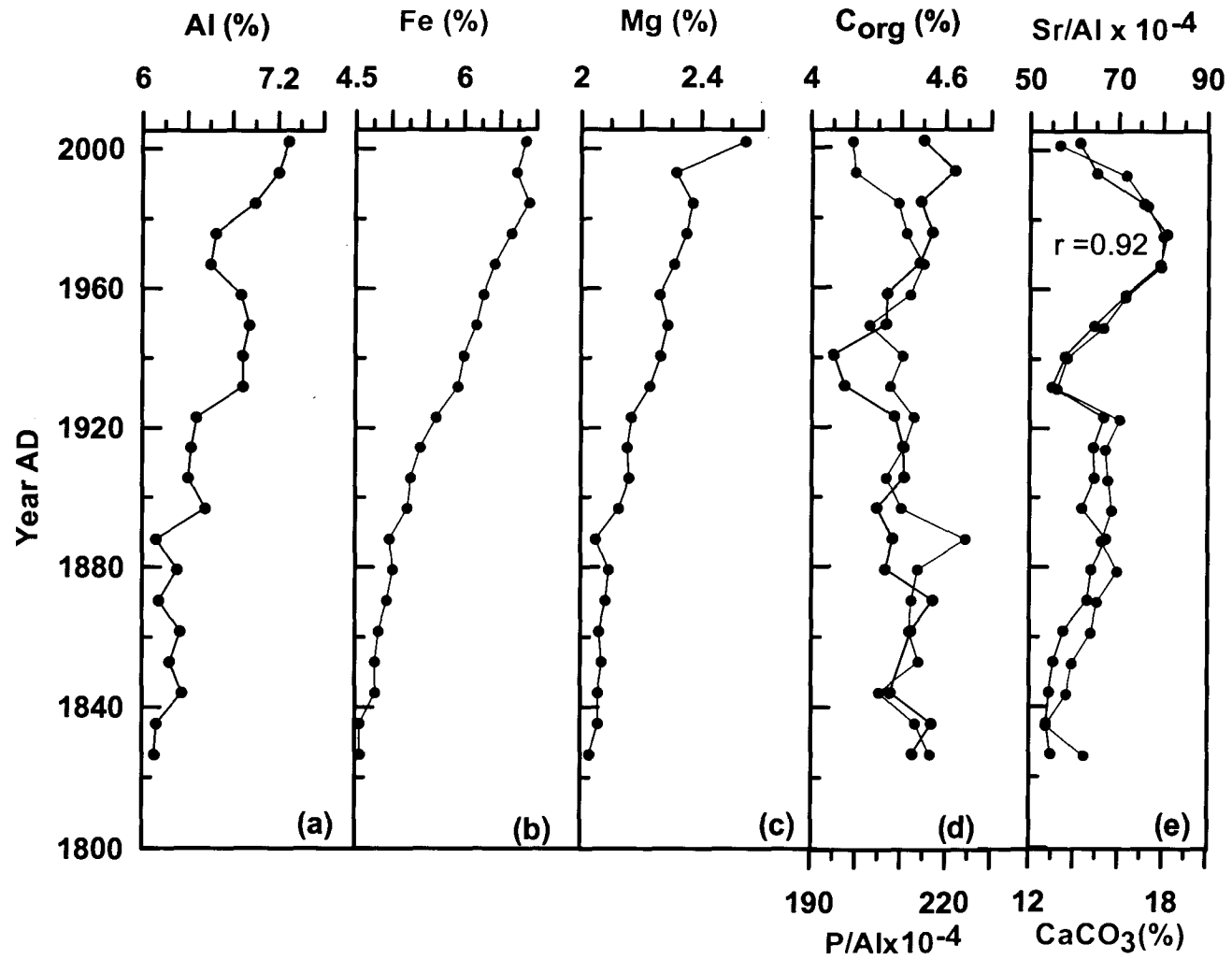
Figure 4.18: Vertical profiles of organic carbon in comparision with major elements in core SaSu-1. (a)Al (b)Fe (c)Mg (d)C_{org} and P/Al (e)Sr/Al and CO_3.
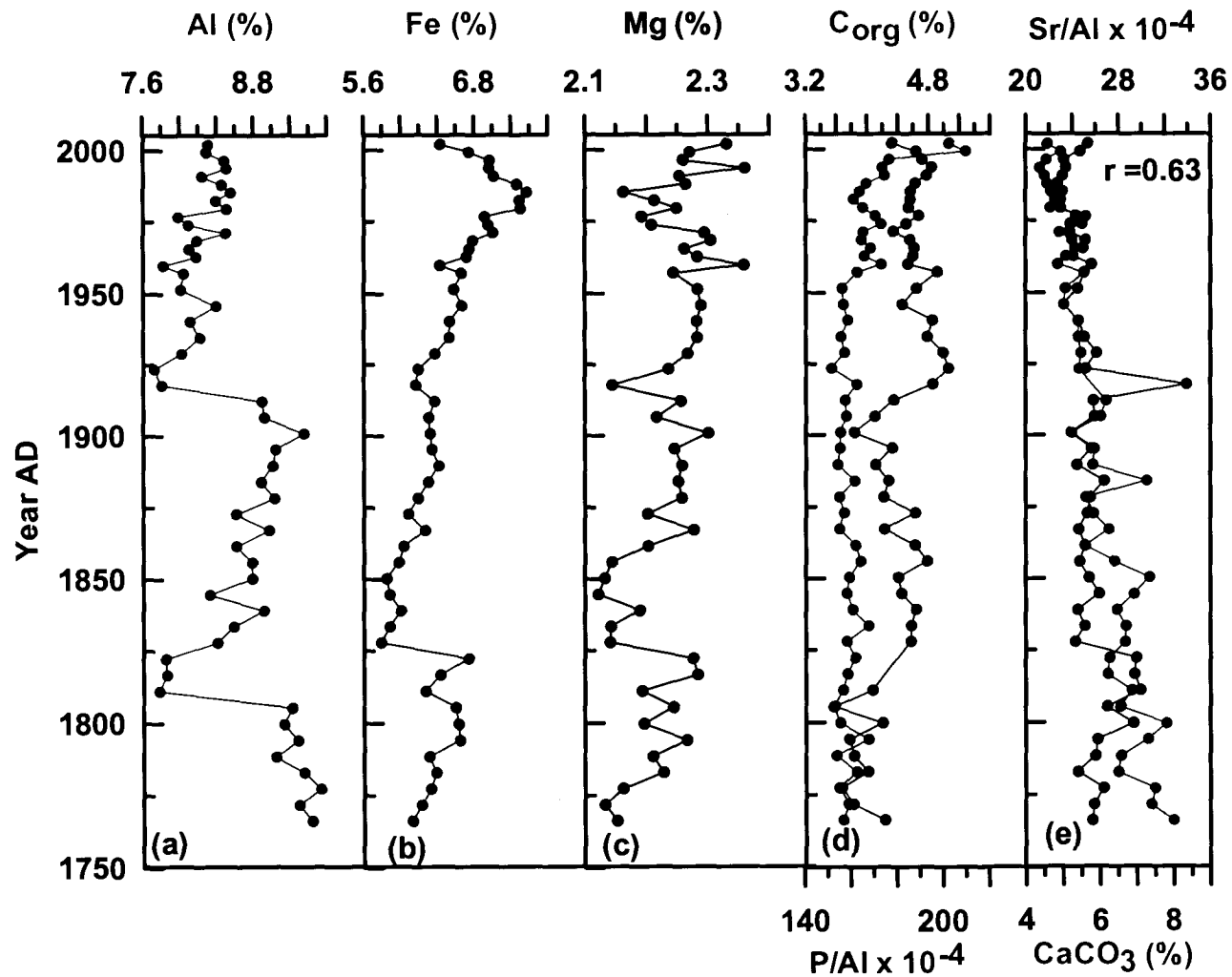
Figure 4.19: Downcore profiles of major elements and organic carbon in core SaSu-3B. (a)Al (b)Fe (c)Mg (d)C_{org} and P/Al (e)Sr/Al and $CaCO_3$.

and from 153 to 202 x 10^{-4} (average 182 x 10^{-4}) for SaSu-1 (Figure 4.18d) and SaSu-3B (Figure 4.19d), respectively. For both the cores, the values observed are considerably higher than the average shale value of 88 x 10^{-4}; (Turekian and Wedepohl, 1961) suggesting the presence of large amounts of non detrital P. When the downcore profiles of P/Al and C_{org} are superimposed on each other (Figure 4.18d, Figure 4.19d) no visible co-variance occurs in SaSu-3B but the two profiles exhibit substantial similarity in SaSu-1. A correlation also seems to exist among the P/Al and C_{org} records of core CR-2. Its absence in SaSu-3B may be due to a disturbed Al record in this core.

4.2.3.7.2 Temporal variability of redox sensitive elements

The sites of both SaSu-1 and SaSu-3B are presently overlain within the zone of seasonal anoxia (DO = 3 μM; 0.06 mL/L). Variations in redox status of bottom waters in the past should have influenced the behaviour of redox-sensitive metals and also the C_{org} preservation. To investigate this effect, depth profiles of redox sensitive elements Fe, Mn, Mo, Cr, Co, and V are examined here.

In SaSu-1, bulk Fe and Mn concentrations vary from 4.56 to 6.92% and from 284 to 491 μg/g with average values of 5.6% and 369 μg/g, respectively (Figure 4.20b,c). The concentration ranges for Mo, V, Cr and Co are 62.2-71.5, 3.4-78, 40-116 and 17.3-39.6 μg/g, with average values of 66.44, 27.7, 79 and 24.05 μg/g, respectively (Figure 4.20d,e,f,g).

In SaSu-3B, bulk Fe and Mn concentrations vary from 5.79 to 7.38%
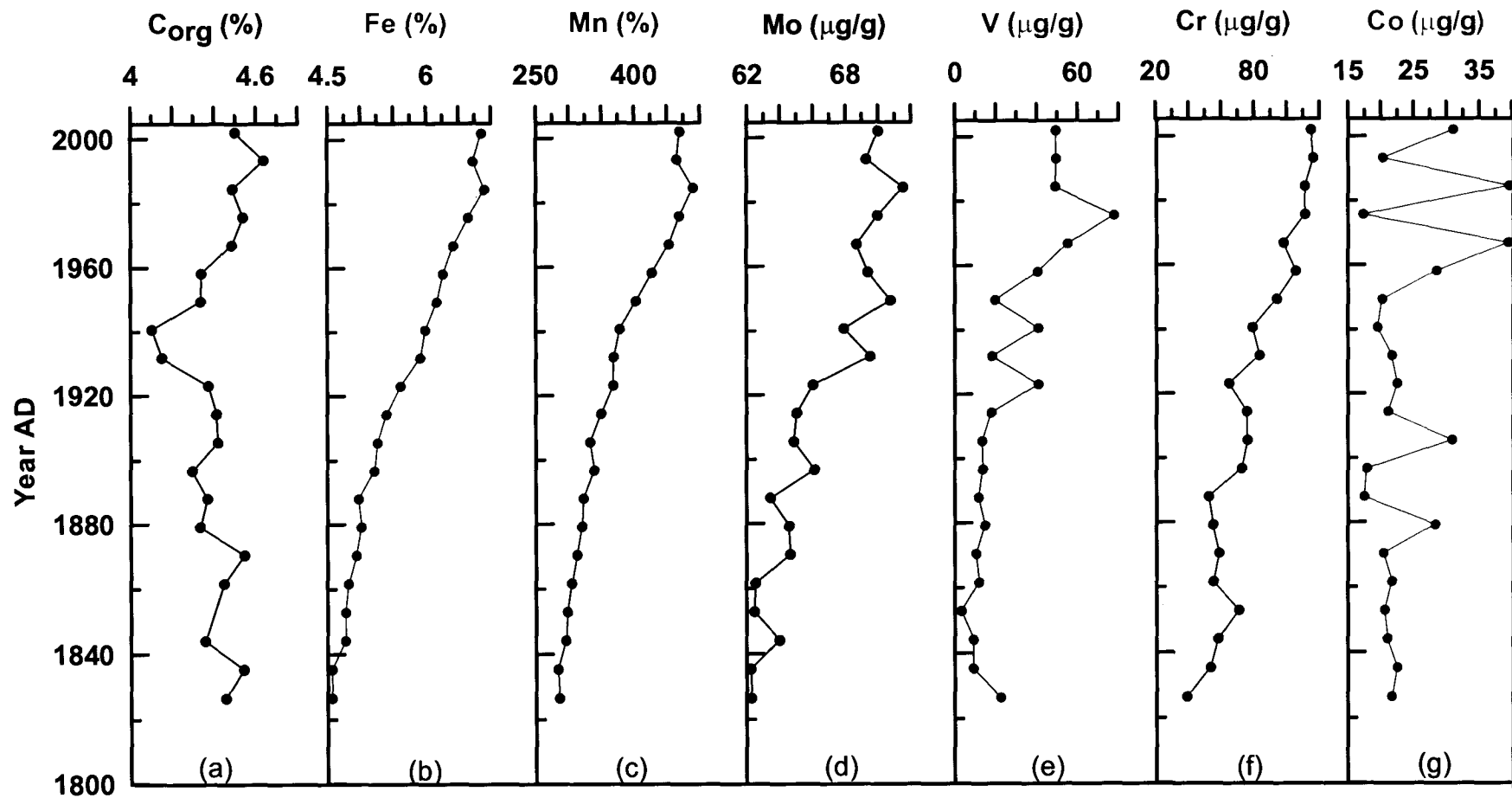
Figure 4.20: Downcore variations of selected redox sensitive trace metals and their inter-relationship with major productivity indicator (C_{org}) in core SaSu-1. (a)C_{org} (b)Fe (c)Mn (d)Mo (e)V (f)Cr (g)Co.
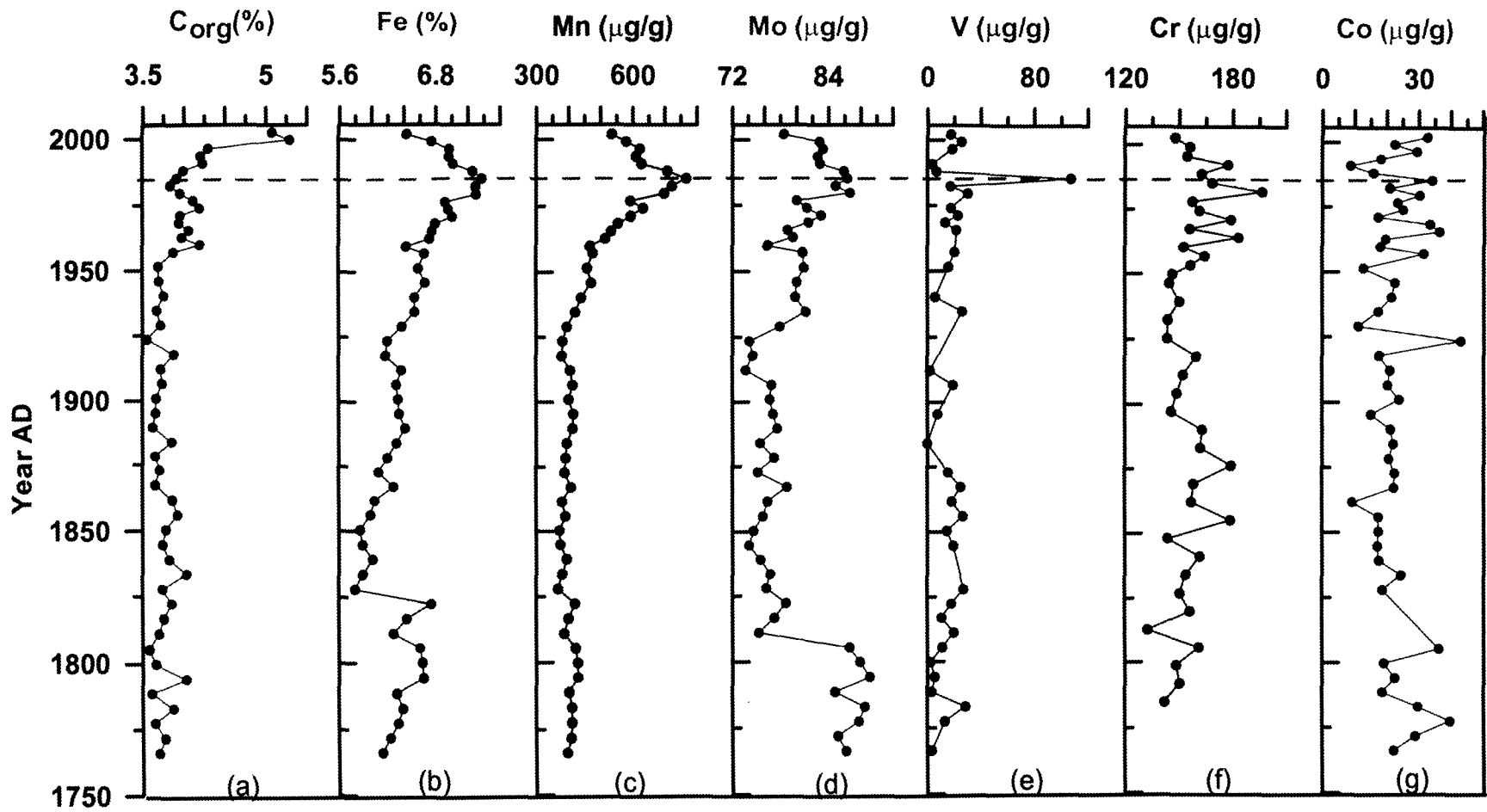
Figure 4.21: Downcore variations of selected redox sensitive trace metals and their inter-relationship with major productivity indicator (C_{org}) in core SaSu-3B. (a)C_{org} (b)Fe (c)Mn (d)Mo (e)V (f)Cr (g)Co.

and from 372 to 768 µg/g with average value of 6.5% and 471 µg/g, respectively (Figure. 4.21b,c). Concentration ranges for other elements are from 73.7 to 89.2 µg/g for Mo, from 2.3 to 30.3 µg/g for V, from 142 to 196 for Cr µg/g, and from 8.78 to 43.23 µg/g for Co, with corresponding average values being 80.26, 15.46, 158 and 22.88 µg/g (Figure 4.21d,e,f,g). A single point maximum value of 107 µg/g was observed in the V profile; this value was excluded from the calculation of the mean. Interestingly, maxima in several other metals also occurred at this level which seems to correspond to a strong monsoonal activity in the recent past. Concentration and element/Al ratio, average shale values are given in table 4.9 for reference.

Coming from shallow coastal sites, the two cores are more likely to be influenced by terrigenous inputs, which would affect metal concentrations. In order to account for this effect, the metal data have been normalized with Al. If the bottom waters at the core site have undergone changes in redox conditions during the past, this is expected to be reflected by the redox-sensitive metal data. In natural aquatic systems, Mn and Fe are present as Mn(II), Mn (III), Mn(IV), Fe (II), and Fe (III). Mn concentrations are controlled by the detrital phase because reactive Mn oxyhydroxides deposited on the sea floor are reduced to soluble Mn(II), which diffuses out into the overlying waters. The redox behaviour of Mn plays a central role in the cycling of other metals that can adsorb onto Mn hydroxides (e.g. Mo, V, and Cr) (Shaw et al., 1990). The geochemistry of Mn and Fe are similar, both responding to oxidative precipitation and reductive dissolution (Moffett, 1990). Dickens and Owen (1994) have suggested that the redox-sensitive Mn oxyhydroxide

particulates get dissolved upon entering an OMZ. The Mn (II) so produced is redirected by the circulation eventually to precipitate in oxygenated environments. The average values of the Mn/Al ratio for SaSu-1 and SaSu-3B cores are 56 x 10^{-4} and 55 x 10^{-4} respectively which is almost half of the average shale value (~106 x 10^{-4}; Turekian and Wedepohl, 1961). The observed low values of Mn/Al ratios throughout the cores (Figure 4.22a & 4.23a) suggest the mobilization of reactive redox sensitive Mn out of the sedimentary column, which normally occurs in reducing sediments (Somayajulu et al., 1994). This is similar to the trend observed in CR-2.

Cr, Mo, Co and V are known to precipitate out from seawater under reducing conditions (Calvert and Pedersen, 1993; Piper and Isaacs, 1996). The profiles for the ratios of Cr/Al, Mo/Al, Co/Al and V/Al are shown in figure 4.22b,c,d,e (SaSu-1) and 4.23b,c,d,e (SaSu-3B). All the above ratios Cr/Al, Mo/Al, Co/Al and V/Al exhibit a narrow range of variation between 6-17, 9-11, 3-6, 1-12 x 10^{-4} for SaSu-1 and 16-23, 8.5-10, 1-6, 0-12 x 10^{-4} for SaSu-3B respectively. The average value of Cr/Al is found to be substantially higher in SaSu-3B (19 x 10^{-4}) but marginally higher in SaSu-1 (12 x 10^{-4}) than its average shale value of 11 x 10^{-4}. Similarly, as expected, the average values of Co/Al and Mo/Al are also found to be on the higher side in both the cores as compared to their average shale values (Table 4.9). However, the average V/Al values of 4 x 10^{-4} and 2 x 10^{-4} in SaSu-1 and SaSu-3B, respectively, are much lower than the relatively high average shale value of 16 x 10^{-4}. Thus, the expected enrichment in the solid phase was not observed contrary to the trends for Cr, Mo and Co. Nonetheless, a slow long-term upcore trend

appears to exist in all ratios which is also reflected in the increasing upcore trend for C_{org} (Figure 4.22f and 4.23f). It would thus appear that changes in productivity and reducing conditions in the overlying water had very little effect on the sedimentary cycling of redox elements and that the sedimentary environment was reducing all the time during the deposition time of the cores. Evidently there has been no significant post diagenetic change since these alterations would then have resulted in opposite trends in the Mn/Al and rest of the ratios (Cr, Co, Mo, and V) discussed above, which is not observed (Figure 4.22 and 4.23). A similar observation has also been made for CR-2.

4.2.3.7.3 Temporal variability of nutrient type elements- Barium and its significance for paleo-productivity studies

Ba concentrations in both SaSu-1 and SaSu-3B show significant depletion (factor of ~4.5, in this study that favourably compares with the factor of ~4 depletion observed in CR-2) relative to its average shale abundance (Figure 4.24a,b), suggesting the occurrence of suboxic conditions throughout the deposition period of the cores. Under such continuous reducing conditions with almost constant sedimentation rate, sedimentary C_{org} content rather than Ba should be used as a reliable surface productivity proxy.

4.2.3.7.4 Micronutrient elements as paleo-productivity proxies

Cu and Ni did not show any significant excess over their average shale values (Figure 4.25), except to some extent for Cu in SaSu-1 (Figure 4.25c). As mentioned earlier, the lack of pronounced enrichment of these elements in
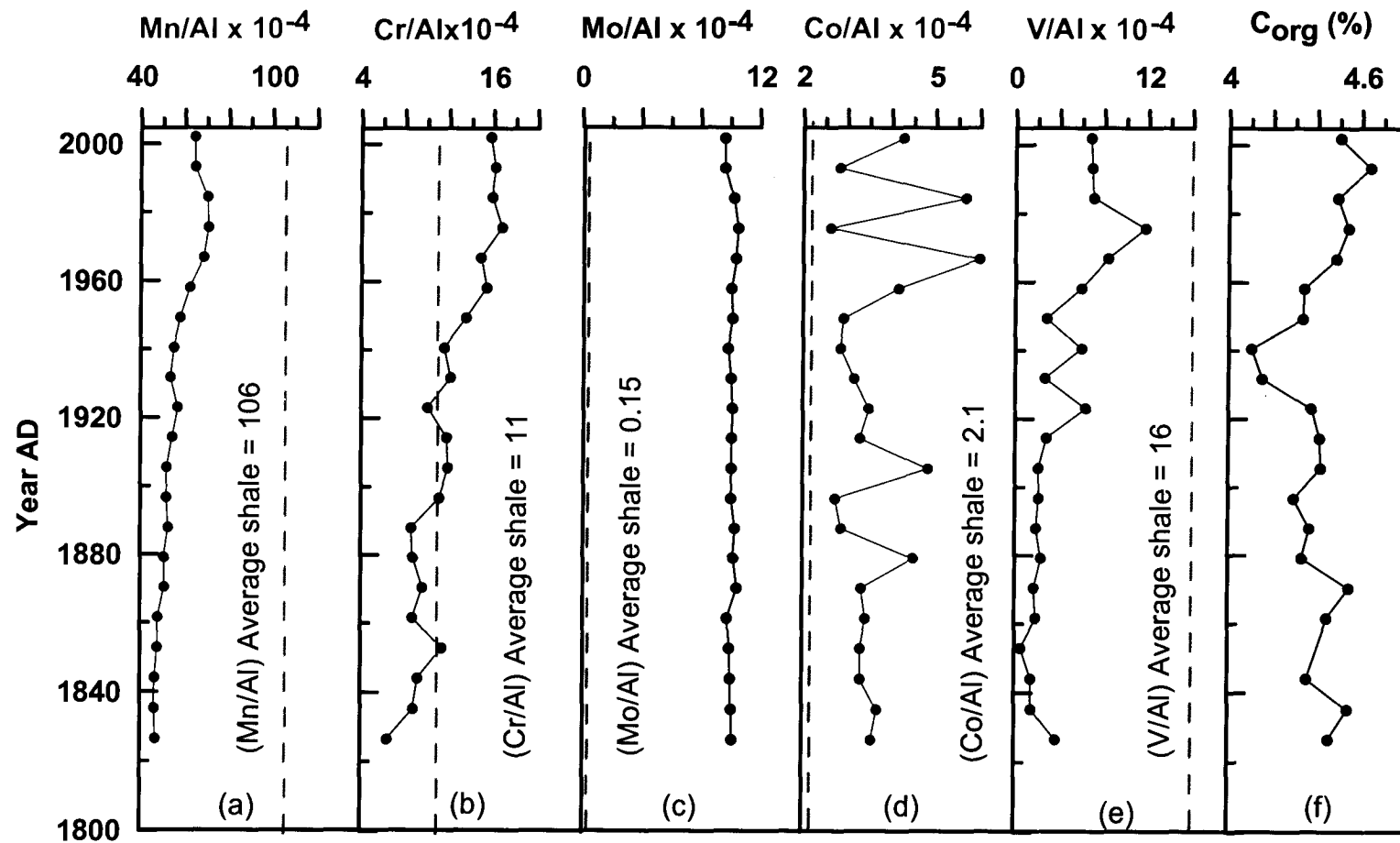
Figure 4.22: Downcore variations in Element/Al ratios of selected redox-sensitive trace metals in relation with their respective average shale values for core SaSu-1. Also shown is vertical profile of C_{org} for comparison. (a)Mn/Al (b)Cr/Al (c)Mo/Al (d)Co/Al (e)V/Al (f)C_{org}.
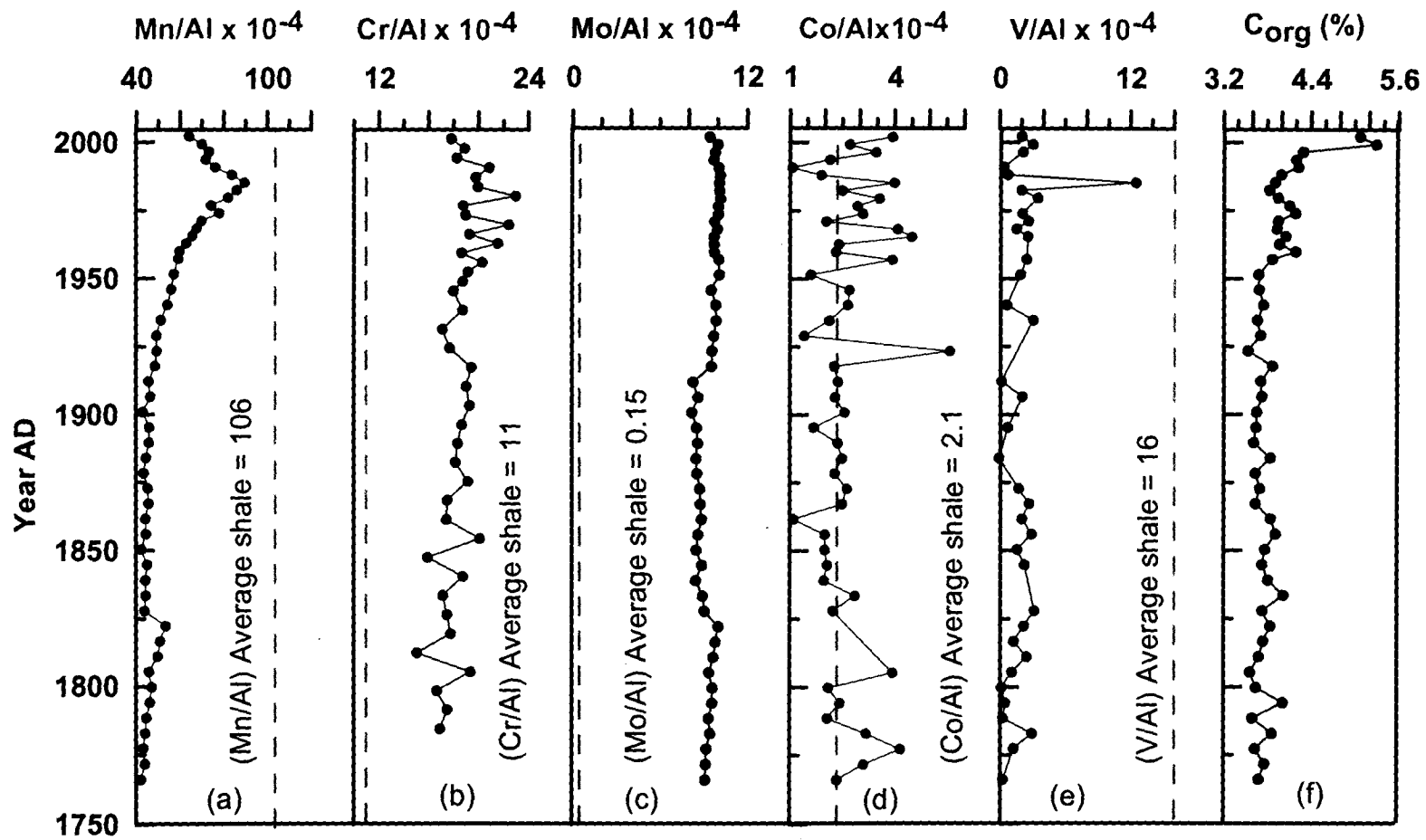
Figure 4.23: Downcore variations in Element/Al ratios of selected redox-sensitive trace metals in relation with their respective average shale values for core SaSu-3B. Also shown is vertical profile of C_{org} for comparison. (a)Mn/Al (b)Cr/Al (c)Mo/Al (d)Co/Al (e)V/Al (f)C_{org}.
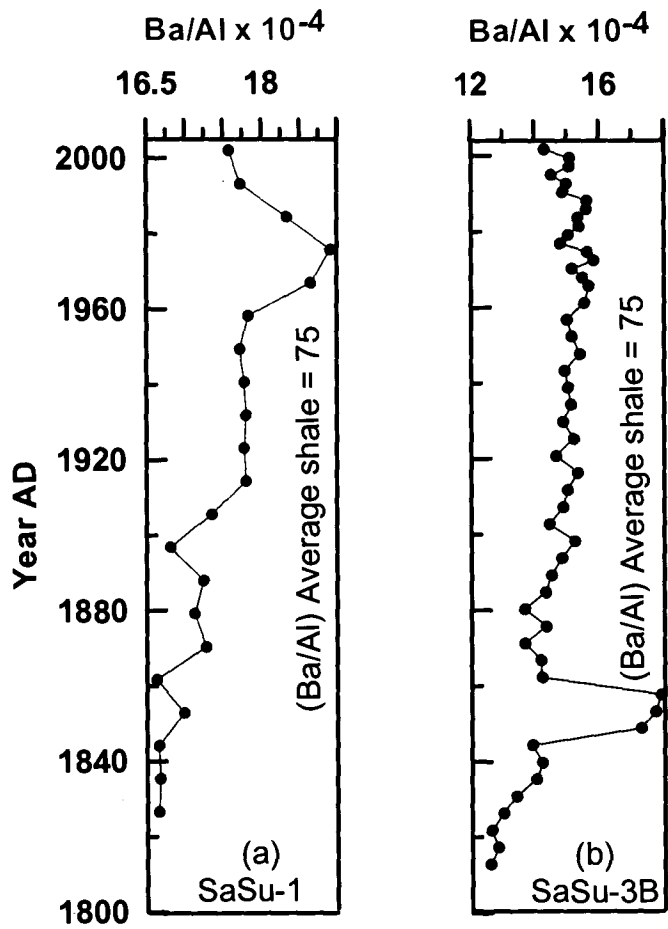
Figure 4.24: Downcore records of Ba/Al as productivity proxy in variation with its average shale value for cores (a)SaSu-1 and (b)SaSu-3B.
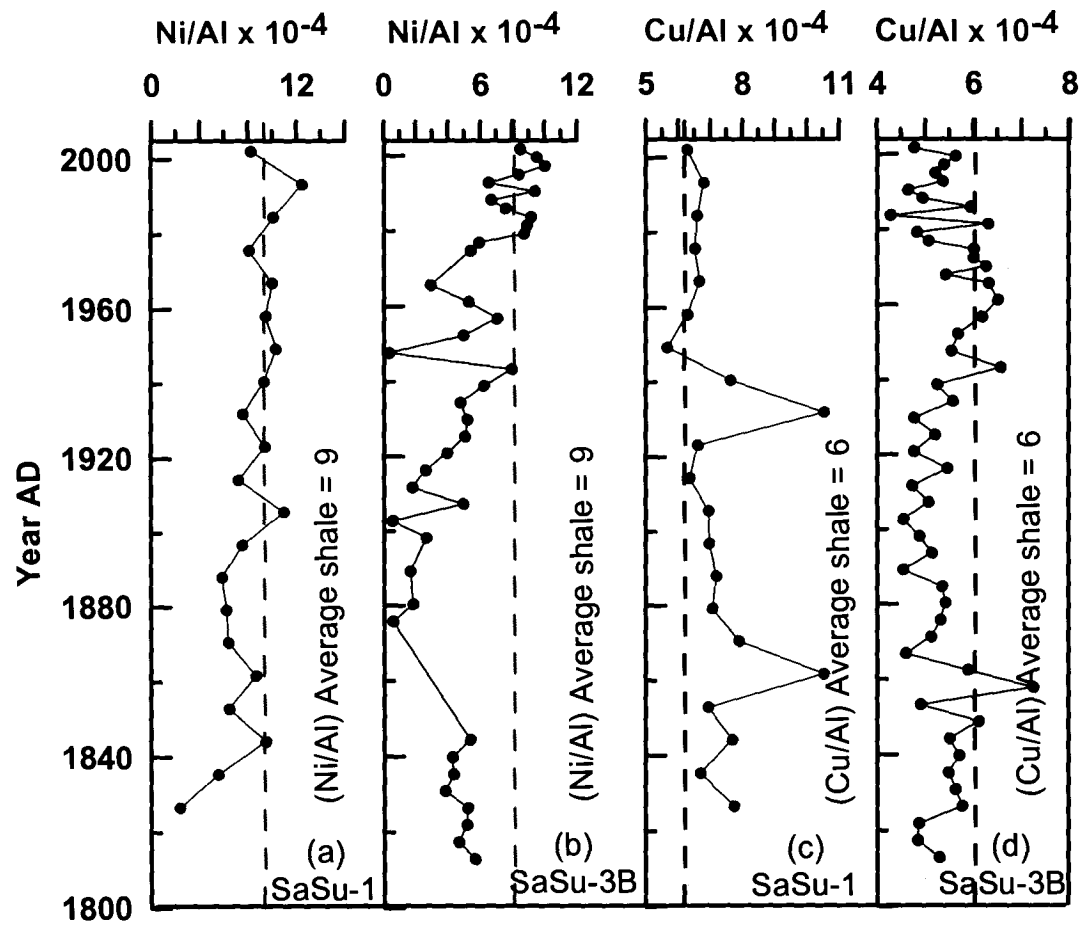
Figure 4.25: Downcore records of Element/Al ratio for micro nutrient type elements (Ni and Cu) in variation with its average shale value. (a)Ni/Al for SaSu-1 (b)Ni/Al for SaSu-3B (c)Cu/Al for SaSu-1 (d)Cu/Al for SaSu-3B.

reducing sediments is perhaps due to the non-availability of free sulphide in high concentrations in interstitial waters for their precipitation. However, accumulation of these elements in sediments should still be expected to some extent at least during period of high productivity. The Ni/Al record in SaSu-3B (Figure 4.25b) does show a general trend of increase in the last few decades, the period of the highest productivity as inferred from several other proxy records discussed above. Such an increase is not readily evident in the case of the Cu/Al ratio in this core (Figure 4.25d). In SaSu-1, although the ratios (Figure 4.25a,c) are closer to their respective average shale values, the downcore changes are not consistent with the trends in other proxies of productivity (which appears to be at its all time maximum over the past few decades).

4.3 Conclusions

Various proxies analyzed in the three shallow cores raised from the inner- and mid-shelf areas that are seasonally overlain by suboxic/anoxic waters today, exhibit significant downcore variations.

1. The consistent increasing trend observed for various biogenic proxies viz. C_{org}, $CaCO_3$, N_{org} in all the three cores, indicate enhanced productivity over the past few decades. In most probability, this increase is the consequence of human activities (fertilizer inputs from land).

2. However, despite this increase in, and possibly because of, the higher productivity that should be expected to support a higher rate of near-bottom denitrification (the evidence of which is provided by the water column

measurements); the sediments do not seem to reflect an enhancement of the $\delta^{15}N$ signal (especially during the last few decades for all three cores). In deeper sediments (core CR-2) though, particularly during the Little Ice Age, $\delta^{15}N$ might still serve as a proxy of (reduced) denitrification.

3.   Ba concentrations did not exhibit any significant increasing trends during the last few decades in all the three cores as indicated by the biogenic proxies. Instead the Ba/Al average values were depleted by a factor of 4 when compared with its average shale value, indicating removal of Ba from the sediments due to strong reducing environments. Thus Ba acted more as a redox proxy rather than productivity proxy.

4.   The micronutrient elements - Cu and Ni, did not show any enrichment compared to its average shale values, for the corresponding increased productivity during the last few decades in any of the three cores.

5.   For all the three cores, the redox sensitive elements – Fe, Mn, Co, Cr, Mo and V indicated the persistence of reducing conditions throughout the depositional periods of the cores. Evidently, no significant post diagenetic changes were detected, as these alterations would have resulted in opposite trends in the Mn/Al, Fe/Al and rest of the ratios (Cr, Co, Mo and V) which was not observed.

Table 4.2
Major bulk carriers of productivity measured in core CR-2 along with C and N isotopes of sedimentary organic matter.

Mean depth (cm)	C_{org} (%)	N (%)	$CaCO_3$ (%)	BioSi(%)	$\delta^{13}C$(‰)	$\delta^{15}N$(‰)	C/N
1	3.40	0.39	8.55	1.63	-21.1	6.9	8.6
3	3.39	0.40	8.77	1.47	-20.9	6.5	8.5
5	3.14	0.34	8.26	1.19	-20.9	6.4	9.2
7	3.03	0.33	7.98	2.32	-20.9	6.8	9.2
9	3.02	0.33	8.03	2.22	-20.7	6.9	9.3
11	2.92	0.31	7.18	1.38	-21.0	6.8	9.3
13	3.07	0.32	7.24	2.15	-20.8	6.9	9.5
15	2.97	0.32	7.70	1.45	-20.7	6.7	9.3
17	2.84	0.31	7.69	1.79	-21.2	6.7	9.3
19	2.74	0.30	6.66	1.66	-20.9	6.9	9.2
21	2.72	0.30	6.64	2.35	-21.1	6.7	9.2
23	2.74	0.30	7.87	1.50	-20.7	7.4	9.3
25	2.71	0.29	8.10	1.98	-20.7	7.5	9.4
27	2.60	0.28	8.96	1.46	-20.8	7.3	9.4
29	2.83	0.30	7.74	2.28	-20.7	7.5	9.5
31	2.80	0.29	8.52	1.38	-21.0	7.4	9.6
33	2.75	0.28	7.46	1.83	-21.0	7.3	9.7
35	2.81	0.29	7.14	1.97	-21.0	6.9	9.8
37	2.50	0.25	5.59	2.51	-21.3	7.4	9.9
39	2.45	0.25	5.98	1.55	-21.4	7.0	9.6
41	2.76	0.28	5.42	1.42	-21.3	7.0	9.9
43	2.61	0.27	6.91	1.36	-21.3	6.3	9.7
45	2.50	0.25	4.12	1.94	-21.3	6.1	9.9
47	2.43	0.24	4.45	1.63	-21.3	6.2	10.0
49	2.41	0.25	5.14	2.00	-21.2	7.0	9.7
51	2.32	0.26	7.79	2.17	-20.7	7.3	9.0
53	2.69	0.30	10.52	2.10	-20.6	7.8	8.9
55	2.91	0.31	10.57	1.88	-20.5	7.2	9.3
57	3.06	0.35	9.70	1.81	-21.0	7.4	8.9
59	3.03	0.32	9.60	2.62	-20.6	7.3	9.4
61	3.00	0.31	9.13	1.57	-20.6	7.4	9.6
63	3.01	0.32	8.76	2.20	-20.6	7.2	9.5
65	3.04	0.29	9.08	1.90	-20.8	6.9	10.4
67	2.95	0.31	9.13	2.30	-20.7	7.2	9.5
69	2.98	0.31	9.67	2.65	-20.6	7.1	9.5
71	2.97	0.31	7.63	1.95	-20.6	7.0	9.6
73	3.22	0.35	8.85	2.66	-20.7	7.6	9.1
75	2.63	0.29	8.47	2.36	-20.6	7.2	9.0
77	2.74	0.30	9.36	2.38	-20.5	7.6	9.1
79	2.85	0.29	9.18	1.96	-20.9	7.2	9.9
81	2.91	0.30	10.54	2.35	-20.8	7.4	9.7
83	2.80	0.30	11.22	2.39	-20.6	6.9	9.4
85	2.97	0.30	11.34	1.78	-20.9	6.8	9.8
87	2.81	0.30	10.88	2.67	-20.8	6.7	9.3
89	2.85	0.30	9.14	1.43	-20.8	7.0	9.6
91	2.80	0.28	10.28	1.81	-20.7	6.7	10.0
93	2.77	0.28	11.37	2.12	-20.8	6.7	10.0
95	2.68	0.27	11.76	2.47	-20.8	6.5	9.9
97	2.79	0.28	13.58	2.37	-20.7	6.6	10.0
99	2.85	0.27	10.33	1.51	-20.8	6.7	10.5

Table 4.3
Major and minor element measured in core CR-2. P and minor element concentrations are presented in µg/g (ppm).

Mean depth (cm)	Al (%)	Fe (%)	Mg (%)	P	Mn	Ba	Sr	Cr	Cu	Ni	V
1	6.41	5.58	2.35	1489	333	114	286	130	50	61	85
3	7.01	5.78	2.38	1536	351	125	282	135	47	60	89
5	6.91	5.99	2.38	1525	345	124	285	137	47	58	93
7	6.99	5.75	2.35	1489	338	125	275	139	48	61	85
9	6.9	5.85	2.37	1472	329	124	282	133	49	68	87
11	7.06	5.78	2.36	1564	322	125	274	138	45	61	87
13	6.95	5.75	2.31	1534	316	124	270	129	47	54	93
15	7.22	5.89	2.39	1533	337	126	275	139	49	58	91
17	7.16	5.82	2.39	1620	321	127	281	140	49	61	90
19	7.17	5.76	2.36	1648	320	130	264	135	49	53	91
21	7.42	5.7	2.4	1608	301	133	242	137	47	63	101
23	7.31	5.75	2.35	1598	322	134	268	135	47	61	92
25	7.35	5.87	2.41	1763	336	136	283	137	46	56	99
27	7.05	5.65	2.28	1533	330	130	278	133	44	64	93
29	6.95	5.71	2.29	1562	303	122	269	136	45	65	88
31	7.23	5.83	2.31	1646	308	125	276	142	48	62	76
33	7.31	5.9	2.3	1644	308	127	268	140	46	61	88
35	7.41	5.98	2.31	1693	314	127	260	151	49	71	85
37	7.71	6.24	2.27	1724	327	133	223	147	48	78	102
39	7.58	6.07	2.27	1746	323	130	227	142	48	71	107
41	7.83	6.13	2.3	1887	310	123	225	146	49	71	103
43	7.76	6.17	2.34	1802	321	132	246	144	49	70	101
45	8.05	6.25	2.32	1803	327	135	218	147	51	59	88
47	8.11	6.3	2.32	1785	333	139	218	149	48	63	98
49	7.89	6.15	2.25	1699	336	138	215	147	49	73	96
51	7.17	5.79	2.2	1672	354	134	283	137	43	49	87
53	6.85	5.46	2.26	1629	339	128	335	128	43	51	87
55	6.85	5.47	2.27	1622	319	122	339	127	43	51	86
57	7.13	5.69	2.39	1776	321	122	336	132	46	62	79
59	7.44	5.91	2.49	1701	316	127	331	133	47	62	81
61	7.4	5.79	2.44	1779	307	123	324	134	52	66	85
63	7.49	5.92	2.48	1837	306	125	327	142	48	58	103
65	7.05	5.52	2.33	1723	290	118	315	122	49	50	59
67	7.06	5.41	2.33	1609	283	110	290	131	51	48	89
69	7.56	5.44	2.25	1563	294	124	321	142	49	64	91
71	7.51	5.34	2.23	1584	287	125	325	135	49	73	85
73	7.78	5.55	2.26	1717	296	128	318	132	49	42	85
75	7.71	5.61	2.28	1644	299	129	322	132	49	52	80
77	7.57	5.57	2.23	1554	299	133	332	126	48	50	92
79	7.71	5.73	2.33	1613	309	130	341	133	50	55	78
81	7.72	5.76	2.39	1645	325	133	376	132	45	49	97
83	7.61	5.46	2.33	1606	na	134	391	130	47	48	84
85	7.44	5.42	2.32	1579	na	131	384	125	50	48	67
87	7.49	5.5	2.3	1649	na	131	390	130	47	69	78
89	7.69	5.62	2.39	1654	na	133	383	123	43	53	80
91	7.44	5.63	2.32	1651	na	129	398	123	45	34	75
93	6.89	5.28	2.16	1514	na	118	418	111	46	35	75
95	7.41	na	2.28	1583	na	128	388	125	42	59	87
97	6.97	na	2.18	1475	na	122	452	120	40	37	80
99	7.58	5.81	2.35	1667	na	135	365	129	42	63	80

Table 4.4
Major bulk carriers of productivity, sedimentary C and N isotopes of organic matter measured in core SaSu-1 along with fluxes for carbon, nitrogen and $CaCO_3$.

Core (cm)	C_{org} (%)	N_{org} (%)	C/N	$CaCO_3$ (%)	$\delta^{15}N$ (‰)	$\delta^{13}C_{org}$ (‰)	SiO_2 (%)	C_{org} flux $(gm^{-2}a^{-1})$	N_{org} flux $(gm^{-2}a^{-1})$	CO_3 flux $(gm^{-2}a^{-1})$
0	4.50	0.54	8.15	13.35	7.05	-20.92	1.56	21.64	2.61	64.20
1	4.64	0.56	8.18	16.35	7.14	-20.85	1.50	22.61	2.74	79.73
2	4.49	0.52	8.54	17.35	7.21	-20.79	1.38	22.00	2.55	85.00
3	4.54	0.55	8.32	18.04	7.05	-20.84	1.39	22.32	2.70	88.72
4	4.49	0.54	8.33	17.95	7.40	-20.99	1.27	22.05	2.64	88.26
5	4.34	0.49	8.78	16.33	7.36	-20.84	1.31	21.15	2.39	79.61
6	4.34	0.47	9.09	15.35	7.39	-20.91	1.32	21.03	2.29	74.47
7	4.10	0.49	8.36	13.70	7.41	-20.61	1.81	19.75	2.34	65.97
8	4.15	0.47	8.71	13.26	7.48	-20.64	1.69	19.95	2.27	63.74
9	4.37	0.50	8.60	16.09	7.46	-20.57	1.53	21.29	2.44	78.31
10	4.41	0.51	8.83	15.44	7.56	-20.55	1.37	21.41	2.47	74.92
11	4.42	0.50	8.96	15.57	7.54	-20.53	1.47	21.45	2.42	75.61
12	4.30	0.49	8.71	15.73	7.51	-20.68	1.52	20.88	2.36	76.43
13	4.37	0.48	8.92	15.28	7.49	-20.63	1.50	21.18	2.35	74.11
14	4.33	0.48	9.18	15.98	7.40	-20.50	1.69	21.08	2.32	77.74
15	4.55	0.52	9.00	15.08	7.36	-20.81	1.24	22.02	2.51	73.04
16	4.45	0.50	8.84	14.79	7.44	-20.60	1.57	21.52	2.44	71.54
17		0.48	8.13	13.95	7.59	-20.65	1.53		2.30	67.25
18	4.36	0.49	9.13	13.69	7.65	-20.52	1.97	20.98	2.34	65.90
19	4.54	0.48	9.66	12.78	7.60	-20.57	1.66	21.78	2.31	61.29
20	4.45	0.50	9.04	14.47	7.55	-20.63	1.58	21.52	2.43	69.92

Table 4.5

Major bulk carriers of productivity, sedimentary C and N isotopes of organic matter measured in core SaSu-3B along with fluxes for carbon, nitrogen and $CaCO_3$.

Core (cm)	C_{org} (%)	N_{org} (%)	C/N	$CaCO_3$ (%)	$\delta^{15}N$ (‰)	$\delta^{13}C_{org}$ (‰)	SiO_2 (%)	C_{org} flux gm^{-2}a^{-1}	N_{org} flux gm^{-2}a^{-1}	$CaCO_3$ flux gm^{-2}a^{-1}
0.0	5.07	0.58	8.96	4.59	7.19	-20.95	1.64	37.15	4.22	33.59
0.5	5.29	0.48	10.92	4.95	7.65	-20.89	1.59	38.78	3.55	36.30
1.0	4.30	0.51	8.21	4.56	7.66	-21.05	1.74	31.46	3.76	33.42
1.5	4.20	0.46	8.92	4.38	7.33	-21.20	1.68	30.78	3.37	32.05
2.0	4.23			4.50	7.36	-20.93	1.69	30.98		32.95
2.5	3.99	0.46	8.58	4.57	7.49	-21.24	1.60	29.24	3.38	33.44
3.0	3.92	0.41	9.65	5.00	7.25	-21.13	1.73	28.69	3.01	36.63
3.5	3.83	0.43	8.80	4.79	7.20	-21.12	1.50	28.08	3.15	35.09
4.0	3.95	0.43	9.13	4.66	7.05	-20.93	1.47	28.96	3.15	34.10
4.5	4.11	0.46	8.96	5.62	7.23	-21.27	1.71	30.16	3.34	41.24
5.0	4.19	0.44	9.40	5.52	7.33	-20.95	1.89	30.74	3.26	40.49
5.5	3.95	0.42	9.22	4.90	7.46	-21.08	1.78	28.97	3.08	35.91
6.0	3.94	0.43	9.22	5.25	7.40	-21.03	1.79	28.86	3.17	38.51
6.5	4.06	0.45	8.88	5.34	7.41	-20.88	1.68	29.74	3.33	39.13
7.0	3.97	0.47	8.26	5.09	7.59	-20.93	1.71	29.11	3.47	37.28
7.5	4.19	0.45	9.21	4.85	7.32	-20.99	1.64	30.72	3.31	35.57
8.0	3.88	0.41	9.35	5.57	7.57	-20.97	1.82	28.43	3.03	40.89
9.0	3.69	0.40	9.08	5.08	7.39	-21.21	1.81	27.02	2.93	37.21
10.0	3.70	0.42	9.00	5.02	7.19	-21.29	1.73	27.08	3.09	36.80
11.0	3.75	0.41	9.04	5.41	7.50	-20.99	1.60	27.52	3.02	39.64
12.0	3.67	0.40	9.09	5.43	7.24	-21.00	1.86	26.91	2.95	39.80
13.0	3.71	0.41	8.83	5.49	7.63	-20.85	1.84	27.24	3.03	40.27
14.0	3.54	0.38	9.33	5.44	7.44	-21.09	1.82	25.98	2.79	39.86
15.0	3.88	0.40	10.00		7.55	-21.22	1.72	28.83	3.00	80.10
16.0	3.72	0.39	9.45	6.18	7.88	-21.07	1.66	27.32	2.90	45.37
17.0	3.73	0.38	9.76	6.02	7.47	-21.27	1.82	27.42	2.81	44.20
18.0	3.66	0.40	9.00	5.25	7.81	-21.01	1.69	26.85	2.94	38.46

Core (cm)	Corg (%)	Norg (%)	C/N	CaCO$_3$ (%)	δ^{15}N (‰)	δ^{13}C$_{org}$ (‰)	SiO$_2$ (%)	C$_{org}$ flux gm^{-2}a^{-1}	N$_{org}$ flux gm^{-2}a^{-1}	CaCO$_3$ flux gm^{-2}a^{-1}
19.0	3.65	0.39	9.32	5.86	8.21	-21.07	1.87	26.82	2.88	42.99
20.0	3.62	0.38	9.23	5.81	7.85	-21.03	1.75	26.57	2.80	42.60
21.0	3.85	0.40	9.50	7.29	7.74	-21.11	1.67	28.34	2.94	53.64
22.0	3.64	0.38	9.71	5.62	7.50	-20.70	1.75	26.74	2.80	41.22
23.0	3.71	0.38	9.57	5.83	8.03	-21.08	1.76	27.20	2.81	42.75
24.0	3.65	0.38	9.76	6.26	8.27	-20.81	1.89	26.80	2.82	45.95
25.0	3.86	0.39	9.68	5.61	7.82	-20.83	1.86	28.29	2.88	41.16
26.0	3.92	0.38	9.95	6.40	7.86	-20.92	1.99	28.81	2.83	47.01
27.0	3.78	0.39	9.90	7.35	7.55	-20.89	1.78	27.81	2.86	54.14
28.0	3.74	0.38	9.76	6.93	7.36	-20.76		27.50	2.77	50.96
29.0	3.82	0.38	9.76	6.47	7.48	-20.99		28.05	2.83	47.52
30.0	4.03	0.39	10.24	6.72	7.02	-20.73		29.63	2.84	49.37
31.0	3.74	0.36	10.45	6.69	7.79	-20.96		27.50	2.68	49.17
32.0	3.85	0.37	10.35	6.27	7.77	-20.66	1.83	28.29	2.74	46.03
33.0	3.75	0.38	9.90	6.23	7.91	-20.86	1.85	27.57	2.82	45.72
34.0	3.69	0.39	9.57	6.87	7.78	-20.76	1.79	27.17	2.84	50.55
35.0	3.57	0.37	9.50	6.57	7.71	-20.95	1.80	26.27	2.75	48.25
36.0	3.66	0.38	9.62	7.81	7.68	-20.82	2.02	26.94	2.80	57.60
37.0	4.02	0.37	11.16	7.31	7.33	-20.86	1.83	29.63	2.70	53.83
38.0	3.61	0.37	9.85	6.59	7.09	-20.80	1.93	26.52	2.75	48.42
39.0	3.87	0.39	9.90	6.51	7.86	-20.49	1.74	28.45	2.83	47.81
40.0	3.64	0.37	9.70	7.50	7.97	-20.85	1.79	26.83	2.71	55.24
41.0	3.77	0.38	10.12	7.41	7.49	-20.71	1.97	27.75	2.78	54.55
42.0	3.70	0.37	10.21	8.01	7.38	-20.91	1.92	27.26	2.73	59.07

Table 4.6

Major and minor element measured in core SaSu-1. Minor element concentrations are presented in µg/g.

Core (cm)	Al (%)	Mg (%)	Fe (%)	P	Mn	Ba	Sr	Cr	Cu	Ni	V	Co	Mo
0	7.3	2.5	6.9	1453	470	128	447	115	46	60	49	31	70
1	7.2	2.3	6.7	1439	466	128	469	116	49	90	50	20	69
2	7.0	2.4	6.9	1465	491	128	530	111	46	71	49	40	72
3	6.6	2.4	6.7	1403	470	126	538	112	43	54	78	17	70
4	6.6	2.3	6.4	1420	453	123	525	98	44	66	55	40	69
5	6.9	2.3	6.3	1457	428	123	492	106	43	65	41	29	69
6	6.9	2.3	6.2	1411	403	123	449	94	39	72	20	20	71
7	6.9	2.3	6.0	1449	379	122	399	80	53	64	41	20	68
8	6.9	2.2	5.9	1431	369	123	379	84	73	52	18	22	70
9	6.5	2.2	5.6	1380	369	115	433	65	43	61	41	23	66
10	6.4	2.2	5.4	1356	350	115	414	76	41	47	18	21	65
11	6.4	2.2	5.3	1326	333	111	414	76	45	70	14	31	65
12	6.6	2.1	5.2	1378	339	110	405	73	46	50	14	18	66
13	6.1	2.1	5.0	1375	323	106	413	53	44	36	12	18	63
14	6.3	2.1	5.0	1349	321	108	403	55	45	39	15	28	65
15	6.1	2.1	4.9	1306	313	106	388	59	49	39	11	20	65
16	6.3	2.1	4.8	1342	305	105	365	56	67	55	12	22	63
17	6.2	2.1	4.8	1336	298	106	346	71	43	40	3	21	62
18	6.4	2.1	4.8	1304	296	106	346	59	49	60	9	21	64
19	6.1	2.1	4.6	1307	284	102	330	54	41	34	9	23	62
20	6.1	2.0	4.6	1323	287	102	335	39	47	14	23	22	62

Table 4.7
Major and minor element measured in core SaSu-3B. Minor element concentrations are presented in µg/g.

Core (cm)	Al (%)	Mg (%)	Fe (%)	P	Mn	Ba	Sr	Cr	Cu	Ni	V	Co	Mo
0	8.3	2.3	6.4	1481	535	119	211	148	40	71	17	33	78
0.5	8.3	2.3	6.8	1565	581	125	205	156	47	79	26	23	83
1	8.5	2.3	7.0	1623	623	128	198	155	46	85	19	30	83
1.5	8.5	2.4	7.0	1663	611	124	200	178	45	72		18	83
2	8.2	2.3	7.0	1592	628	124	191	163	44	54	4	9	83
2.5	8.5	2.3	7.3	1592	709	126	192	169	39	80	7	16	86
3	8.6	2.2	7.4	1595	768	134	190	197	42	58	107	34	86
3.5	8.4	2.2	7.3	1564	723	131	194	158	50	64	17	21	85
4	8.5	2.2	7.3	1579	699	131	196	162	37	79	30	30	87
4.5	8.0	2.2	6.9	1516	594	123	195	179	51	71		23	80
5	8.1	2.2	7.0	1493	632	122	193	156	39	71	17	25	81
5.5	8.5	2.3	7.0	1520	595	126	203	183	43	51	23	17	83
6	8.2	2.3	6.8	1525	554	128	207	153	49	45	13	34	82
6.5	8.1	2.3	6.8	1523	533	129	203	165	49		22	37	79
7	8.2	2.3	6.7	1533	514	124	197	157	51			20	80
7.5	7.8	2.4	6.4	1448	468	121	201	146	43			18	76
8	8.0	2.2	6.7	1590	477	126	202	145	51	24	21	32	81
9	8.0	2.3	6.6	1516	459	125	197	150	52	43	16	13	81
10	8.4	2.3	6.7	1536	471	126	196	144	52	60		23	80
11	8.1	2.3	6.5	1588	441	123	199	143	46	40	6	22	80
12	8.2	2.3	6.5	1593	421	127	207	160	46	3	26	18	81
13	8.0	2.3	6.4	1607	396	120	210	152	53	64		11	78
14	7.7	2.2	6.2	1566	382	116	195	149	41	48		43	74
15	7.8	2.1	6.2	1530	380	118	266	146	44	37		18	75
16	8.9	2.3	6.4	1592	406	133	230	163	43	47	2	21	74

Core (cm)	Al (%)	Mg (%)	Fe (%)	P	Mn	Ba	Sr	Cr	Cu	Ni	V	Co	Mo
17	8.9	2.2	6.3	1523	414	136	232	162	47	45	19	20	77
18	9.4	2.3	6.3	1515	402	137	224	179	45	37		24	77
19	9.0	2.2	6.3	1613	415	139	233	158	50	24	8	15	77
20	9.0	2.3	6.4	1541	413	136	220	157	43	16		21	78
21	8.9	2.3	6.3	1572	396	133	238	179	45	44	0	22	76
22	9.0	2.3	6.2	1577	392	131	231	144	41	5		21	77
23	8.6	2.2	6.1	1621	389	132	218	162	42	23	16	23	75
24	9.0	2.3	6.3	1571	410	134	221	154	46		25	22	79
25	8.6	2.2	6.0	1621	381	125	217	151	39	15	18	9	76
26	8.8	2.1	6.0	1700	391	126	217	156	47		27	18	76
27	8.8	2.1	5.9	1592	372	121	224	133	48	16	15	18	75
28	8.3	2.1	5.9	1519	375	120	220	161	44	5	20	17	74
29	8.9	2.2	6.0	1682	395	122	219	148	46			18	76
30	8.6	2.1	5.9	1604	381	122	216	150	40			25	77
31	8.4	2.1	5.8	1567	369	120	204	142	50		27	19	76
32	7.9	2.3	6.7		421	141	232		57		18		79
33	7.9	2.3	6.4		400	140	232		39		11		77
34	7.8	2.2	6.3	1321	387	135	233		48		20		75
35	9.2	2.2	6.6	1416	423	129	250		51	50	11	36	87
36	9.1	2.2	6.6	1591	430	130	268		52	39	2	19	88
37	9.3	2.3	6.7	1483	430	131	244		51	41	6	23	89
38	9.1	2.2	6.3	1464	403	122	236		51	35	3	19	85
39	9.4	2.2	6.4	1571	412	122	230		54	49	29	30	89
40	9.5	2.2	6.3	1491	411	121	255		47	49	13	40	88
41	9.3	2.1	6.2	1502	409	120	241		45	44		29	85
42	9.4	2.2	6.1	1654	397	119	243		50	54	3	22	86

Table 4.8

Statistical summary for organic matter signatures and sedimentation rates from the two study cores.

Sr. No.	Core No. Latitude, Longitude.	Location	C_{org} (% range)	C/N (ratio range)	$\delta^{13}C_{org}$ (‰ range)	$\delta^{15}N$ (‰ range)	Sedimentation rate
1.	SaSu1 15.28.6°N 73.27.5°E	Mid-shelf Region	4.1 – 4.7	8 – 9.6	-21 to -20.5	7 – 7.7	1.14 mm/y
2.	SaSu3B 15.28.4°N 73.32.4°E	Inner shelf Region	3.5 – 5.3	8 - 11	-21.3 to -20.5	7 – 8.2	1.78 mm/y

Table 4.9

Average shale values of major and minor elements and element/Al ratios.

Element	Average shale	Element/Al	Average shale
Al	16.7	Fe/Al	0.59
Fe	7	Mg/Al	0.19
Mg	2.6	Ti/Al	575
P	0.16	P/Al	88×10^{-4}
Sr	300	Sr/Al	38×10^{-4}
Mn	850	Mn/Al	106×10^{-4}
Ba	580	Ba/Al	75×10^{-4}
Cr	90	Cr/Al	11×10^{-4}
Cu	45	Cu/Al	06×10^{-4}
Ni	68	Ni/Al	09×10^{-4}
V	130	V/Al	16×10^{-4}
Co	19	Co/Al	2.4×10^{-4}
Mo	1	Mo/Al	0.15×10^{-4}

CHAPTER 5

Chapter 5

RECONSTRUCTION OF PALEO-CHEMICAL ENVIRONMENT ON

TIME SCALE OF CENTENNIAL TO TENS OF

KILO YEARS

5.1 Introduction

The Arabian Sea is an area of high biological productivity driven by the

summer monsoon upwelling and winter monsoon convection (Barber et al.,

2001). Since changes in monsoon forcing are expected to be recorded by the

sediments, it is not surprising that sediment cores from the Arabian Sea have

been widely studied to reconstruct past climate variability in response to

orbital changes in insolation (Prell, 1984b; Clemens and Prell, 1990; Murray

and Prell, 1992; Emeis et al., 1995; Reichart et al., 1997). Despite these

extensive efforts, a complete consensus is yet to emerge on past

climate/environment variability as inferred from the analyses of various

proxies in many well-dated sediment records from the region. Over several

glacial-interglacial cycles, for instance, Reichart et al. (1997), Rostek et al.

(1997), and Schubert et al. (1998) have shown that the accumulation of

organic carbon in the Northeast Arabian Sea has been strongly dominated by

a 23 ky cycle, with maxima in organic carbon content corresponding to

periods of low summer insolation in the northern hemisphere. In contrast,

Prell (1984b), Murray and Prell (1991), Shimmield, (1992), Sirocko et al.

(1993) and Emeis et al. (1995) observed different patterns in the western Arabian Sea and attributed the observed variations in their proxies to maxima in productivity during periods of high boreal summer insolation. Furthermore, Sarkar et al. (1993) attributed the elevated organic carbon and uranium contents of sediments during the last glacial maximum (LGM) in the eastern Arabian Sea to increased preservation of organic carbon and reduction of uranium caused by deep-water anoxia, a view not supported by other data as will be discussed later.

In this study, a number of proxies have been measured in the same cores to circumvent the potential problem relating to one single proxy not accurately recording ambient conditions in various areas or at different times. Another novel approach adopted here is to compare the $\delta^{13}C$ record in benthic foraminifera with the $\delta^{15}N$ record in bulk sediments to infer conditions prevailing at two different depths, since the former is a proxy of ambient nutrient levels (and by extension the oxygen concentration) in near-bottom waters (the bathypelagic) and the latter reflects the intensity of denitrification (or the severity of the OMZ) at depths of few hundred metres (the mesopelagic). The results are expected to improve our understanding of variability and response of the subsurface reducing environment in the Arabian Sea to global and regional changes in climate and oceanographic processes (productivity and circulation). In this chapter, variations in these proxies are examined in two gravity cores collected from seamounts that lie well below but directly underneath the mesopelagic layer experiencing intense denitrification in the open ocean (Figure 5.1). Details of the cores are given in Chapter 2, Table

2.1. Core AAS-42/15 was retrieved from the Raman Seamount (water depth 2525m), while core AAS-42/12A came from the Wadia Seamount (water depth 2270m). Both cores were carefully checked and found free from any slumping activities. The sediments were also devoid of any turbidites as one would expect for cores from the seamounts.

5. 2 Results

5.2.1 Stratigraphy and sedimentation rates

Studies on stable isotope composition of carbonaceous remains of marine organisms are extensively used to reconstruct environmental conditions over the geological time scale. These studies were started in the early 1950's on different organisms [e.g. by Epstein et al. (1953) on molluscs; Emilliani (1955) on planktonic foraminifera; and Shackleton (1977) on benthic foraminifera]. Variations in oxygen isotopic composition of foraminifera have been found to provide valuable information on oceanic paleotemperature, paleosalinity and past fluctuations in sea level and glacial ice volumes (Duplessy, 1982; Shackleton, 1987; Wefer and Berger, 1991; Sirocko et al., 1993). Studies on carbon isotopes provide insights into the changes of past ocean biological productivity, circulation patterns and global carbon budget (Shackleton, 1977; Berger et al., 1978; Shackleton and Vincent, 1978; Altenbach and Sarnthein, 1989).

The planktonic oxygen isotope data were used to establish the chronologies of the two cores. For this purpose downcore records of planktonic $\delta^{18}O$ were tuned with the standard low latitude oxygen isotope
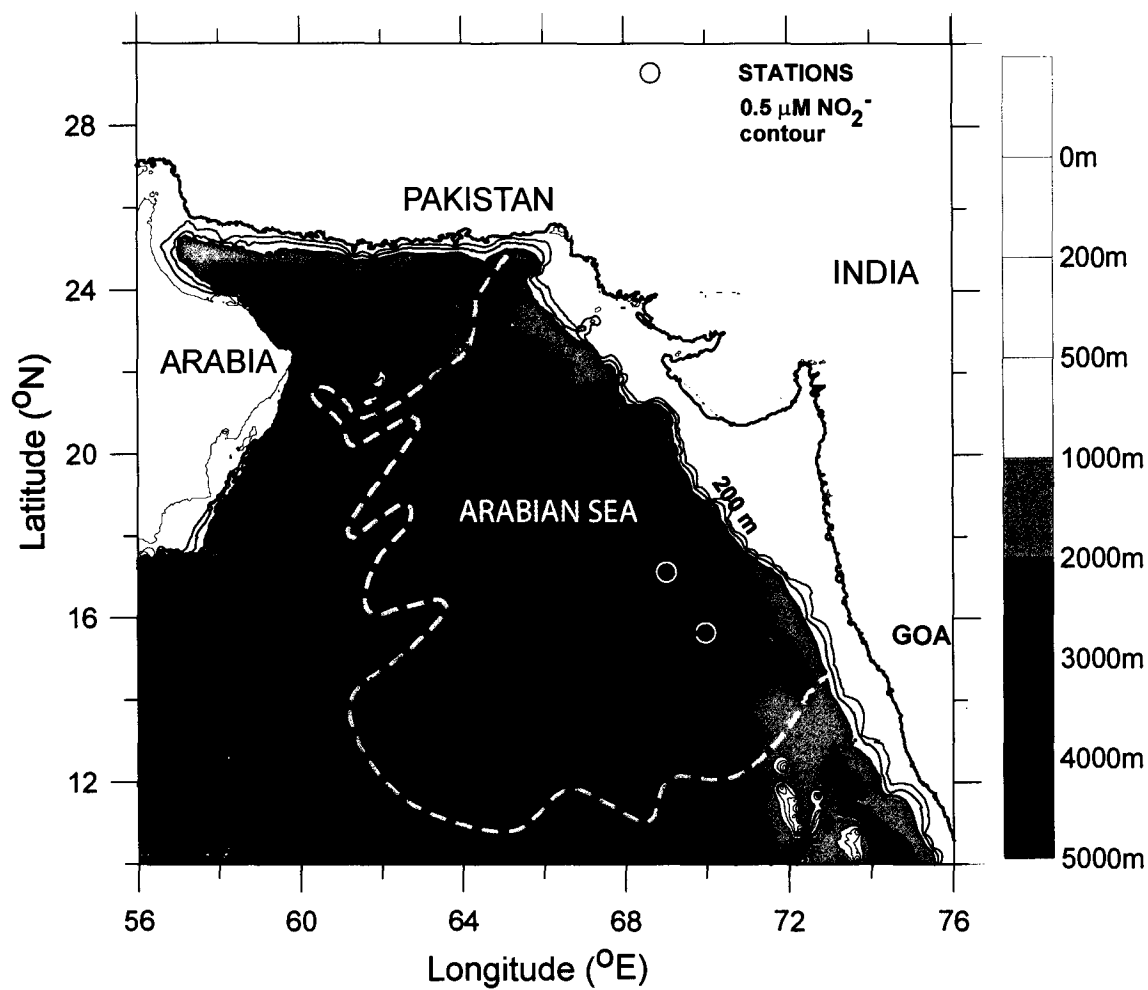
Figure 5.1: Locations of open ocean gravity cores (denoted with open white circles) raised from the OMZ region of Arabian Sea.

curve of Bassinot et al. (1994). This low-latitude $\delta^{18}O$ reference record has been developed by stacking and tuning the $\delta^{18}O$ records from core MD900963 and ODP site 677 with the SPECMAP stack of Imbrie et al. (1984). Based on the oxygen isotope stratigraphy, Core AAS-42/15 extended to Oxygen Isotopic Stage (OIS) 6 whereas core AAS-42/12A extended to OIS 8 and the beginning of OIS 9. In both the cores the isotopic stages could be readily identified. The oxygen isotope record for the two cores along with the curve of Bassinot et al. (1994) are shown in Figure 5.2a,b. Several tie points were identified for both cores to get the best fits.

In order to achieve a better stratigraphic control for the period within the radiocarbon dating, the upper parts of the two cores were subjected to AMS ^{14}C analysis. Hand-picked specimens of *Globigerinoide ruber* were used for this purpose. The AMS ^{14}C ages were calibrated to reservoir-corrected calendar ages before present (1950) using the CalPal software [CalPal, The Cologne Radiocarbon Calibration and Palaeoclimate Research Package (for more details see - http://www.calpal.de/)], which provides calibration back to 50 ky BP. Estimated AMS ^{14}C age, described as ky BP (thousands of years before present) and appropriately corrected ages in calendar years (as ca ky BP) are given in table 5.1. The sedimentation rates varied considerably over time in the same core and more so between the two cores despite their geographical proximity to each other. Core AAS-42/15 covered a period of ~160 Ky BP, while core AAS-42/12A extended to ~320 Ky BP. Details of ^{14}C dates, tie points taken (in terms of core depth in cm) and sedimentation rates calculated for both the cores are given in table 5.2. It may be noted that the

Table 5.1

Estimated AMS ^{14}C age and corresponding age in calendar years.
Calendar years are calculated using the CalPal software.

Core AAS-42/15

Depth interval in core (cm)	Estimated [14]C Age (Ky-BP)	Age in calendar Years (cal-Ky-BP)
0-2	5.76 ± 0.050	~ 6.6 ± 0.062
20-22	11.05 ± 0.070	~13.0 ± 0.110
30-32	13.35 ± 0.055	~16.5 ± 0.519
50-52	17.70 ± 0.085	~21.1 ± 0.389
80-82	21.10 ± 0.110	~25.3 ± 0.356
130-132	33.40 ± 0.510	~38.8 ± 1.212

Core AAS-42/12A

Depth interval in core (cm)	Estimated [14]C Age (Ky-BP)	Age in calendar Years (cal-Ky-BP)
0-2	6.44 ± 0.050	~7.4 ± 0.047
30-32	18.05 ± 0.100	~22.0 ± 0.460
80-82 cm	38.40 ± 0.370	~43.0 ± 0.460

Table 5.2

Sedimentation rates calculated based on AMS ^{14}C dates (marked with asterisks) and tie points taken from Bassinot et al., (1994).

Core AAS-42/15 (Raman Seamount, off Bombay)			Core AAS-42/12A (Wadia Seamount, off Goa)		
Core Depth (cm)	Estimated Age (Kyr)	Sedimentation Rates (cm/Kyr)	Core Depth	Estimated Age (Kyr)	Sedimentation Rates (cm/Kyr)
0	6.6*	OIS 1	0	7.4*	OIS 1
20	13.0*	3.13 OIS 1	30	22.0*	2.05 OIS 2
30	16.5*	2.86 OIS 2	80	43.0*	2.38 OIS 3
50	21.1*	4.35 OIS 2	140	66.0	2.61 OIS 4
80	25.3*	7.14 OIS 3	160	80.0	1.43 OIS 5
130	38.8	3.70 OIS 3	170	88.0	1.25 OIS 5
150	52.0	1.52 OIS 3	230	122.0	1.76 OIS 5
180	64.0	2.50 OIS 4	310	194.0	1.11 OIS 7
230	78.0	3.57 OIS 5	340	224.0	1.00 OIS 7
258	88.0	2.80 OIS 5	400	234.0	6.00 OIS 7
270	98.0	1.20 OIS 5	410	250.0	0.63 OIS 8
280	106.0	1.25 OIS 5	470	288.0	1.58 OIS 9
312	120.0	2.29 OIS 5	490	296.0	2.50 OIS 9
352	134.0	2.86 OIS 6	520	310.0	2.14 OIS 10
386	152.0	1.89 OIS 6			
424	158.0	6.33 OIS 6			
440	164.29	2.54 OIS 6			

(a)

δ¹⁸O (‰)
G. ruber
(Low latitude Isostack)

$\delta^{18}O$ (‰)
G. ruber (AAS - 42/15)

(b)

δ¹⁸O (‰)
G. ruber
(Low latitude Isostack)

$\delta^{18}O$ (‰)
G. ruber (AAS - 42/12A)
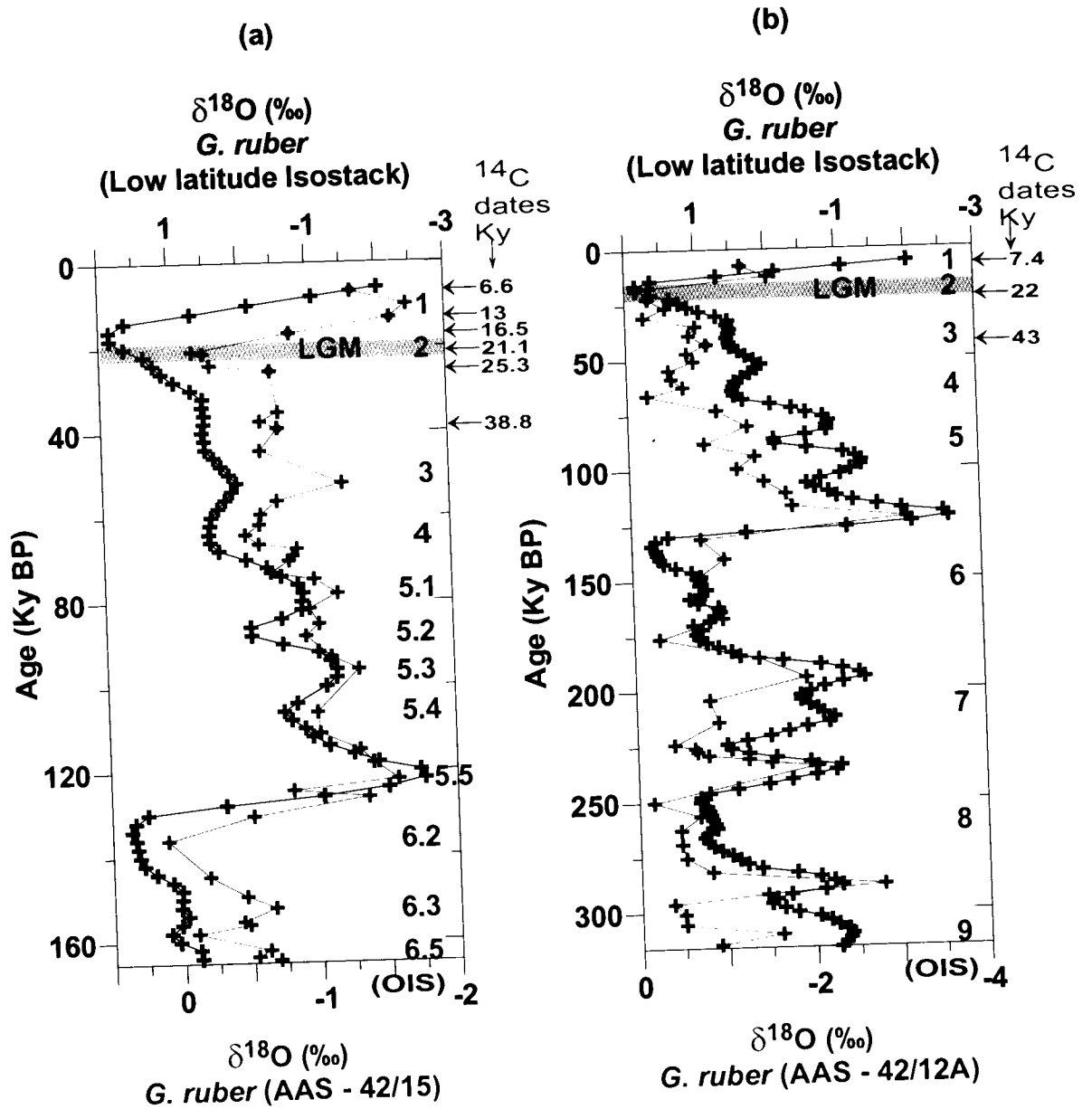
Figure 5.2: Time frame for (a)AAS-42/15 (Raman Seamount) and (b)AAS-42/12A (Wadia Seamount). The plots are stacked over the Low Latitude Isostack Plot from Bassinot et al. (1994). Oxygen Isotope Stages (OIS) and AMS ¹⁴C dates indicated.

those parts of the cores that were dated by the radiocarbon method, the oxygen isotope records do not exactly match with the standard $\delta^{18}O$ curve (that is essentially used for the stratigraphic purpose in older sediments) in that the $\delta^{18}O$ maxima corresponding to the LGM appear to be older. The age-depth profiles and sedimentation rates for both the cores are shown in figure 5.3. The average sedimentation rate calculated for core AAS-42/15 was 3.16 cm/Ky whereas for core AAS-42/12A it was 2.06 cm/Ky. The sedimentation rate of core AAS-42/12A is in good agreement with sedimentation rates previously reported for nearby locations (2.1 cm/Ky by Paropkari et al., 1992; and 2.8 cm/Ky by Prabhu et al., 2004).

5.2.2 Oxygen isotope ($\delta^{18}O$) variations

Variations in oxygen isotopic composition ($\delta^{18}O$) of calcareous shells are caused by either temperature or salinity, with the latter often being the predominant factor. During the process of evaporation of seawater, there is fractionation of isotopes because of the relative ease of $H_2^{16}O$ going to the vapour phase than $H_2^{18}O$ (Dawson, 1992). Therefore, during times when the salinity of the oceans was higher than today (e.g. the LGM when large volume of water was locked up into ice sheets on the continents and in the sea), the $\delta^{18}O$ value of water (and of the $CaCO_3$) biologically precipitated by the organisms was higher (by 1.2‰ often referred to as the ice volume effect due to ~120 m lower sea level; Fairbanks, 1989).

Figure 5.3: Age-depth model based on AMS^{14}C dates along with tie points from low latitude isostack of Bassinot et al. (1994), used to develop chronology. The tie points marked with red asterisks are reservoir corrected radiocarbon dates in sequential order as given at the side of each plot. Average Sedimentation (Av. Sed.) rates are indicated.
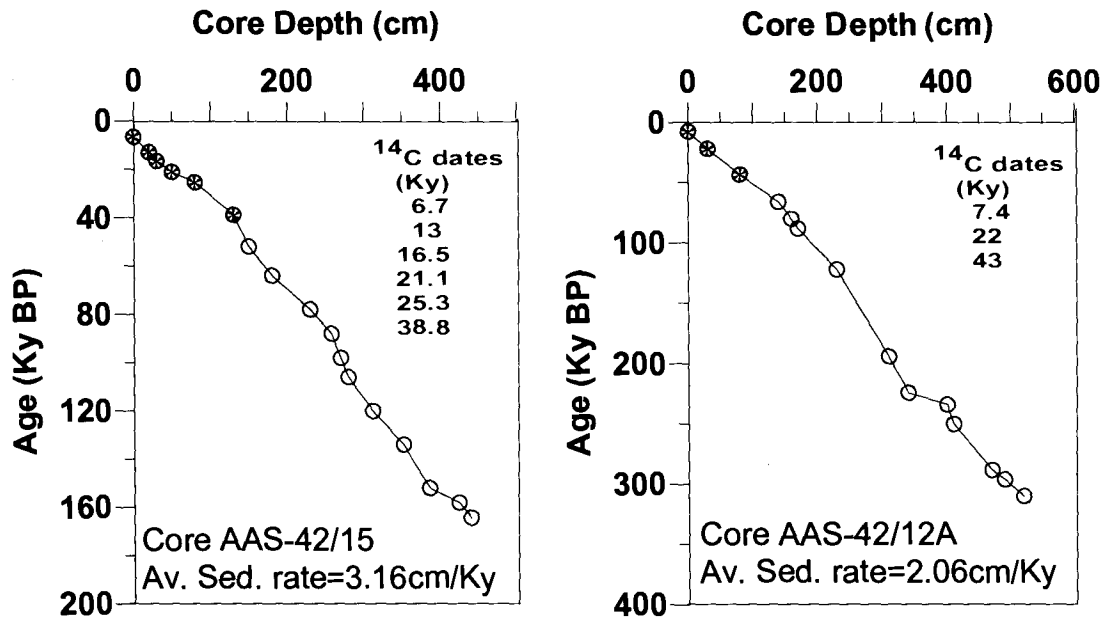
5.2.2.1 $\delta^{18}O$ records of planktonic foraminifera

Downcore $\delta^{18}O$ values of the planktonic species - *G. ruber* varied between -1.73 and +0.10‰ in AAS-42/15 and between -3.15 and -0.17‰ in AAS-42/12A with more negative (lighter) values occurring during the interglacial times (warmer periods) and relatively heavier (less negative) values found during glaciations (colder periods) (Figure 5.4a,b; Table 5.3). For core AAS-42/15 steep decreases in $\delta^{18}O$ are documented at ~13-9 Ky (OIS 1), ~55-50 (OIS 3) and again at ~125–120 Ky (OIS 5), whereas gradual enrichments are evident in between these intervals and also beyond 125 Ky. Within the ~125 and 55 Ky interval depleted $\delta^{18}O$ values occur corresponding to the warm sub-stages of OIS 5 i.e. 5.5, 5.3 and 5.1, and enriched values corresponding to colder sub-stages 5.4, 5.2 and 4. In core AAS-42/12A decreases are seen between ~13-9, ~125-120, ~240-230 and ~295-290 cal Ky for OIS 1, 5, 7 and 8.5 respectively. However the decrease in $\delta^{18}O$ during OIS 3 is not very pronounced in this core. The amplitude of $\Delta\delta^{18}O$ (difference between the last glacial and interglacial $\delta^{18}O$ values) is 1.55‰ and 1.43‰ for cores AAS-42/15 and AAS-42/12A, respectively.

5.2.2.2 $\delta^{18}O$ records of benthic foraminifera

Oxygen isotope record of *Cibicidoides wuellerstorfi* in core AAS-42/12A was observed to be very absurd showing no proper trend and fluctuated irregularly. These data are regarded as suspect and will therefore be excluded from discussion. The $\delta^{18}O$ record for the other core (AAS-42/15) did show a
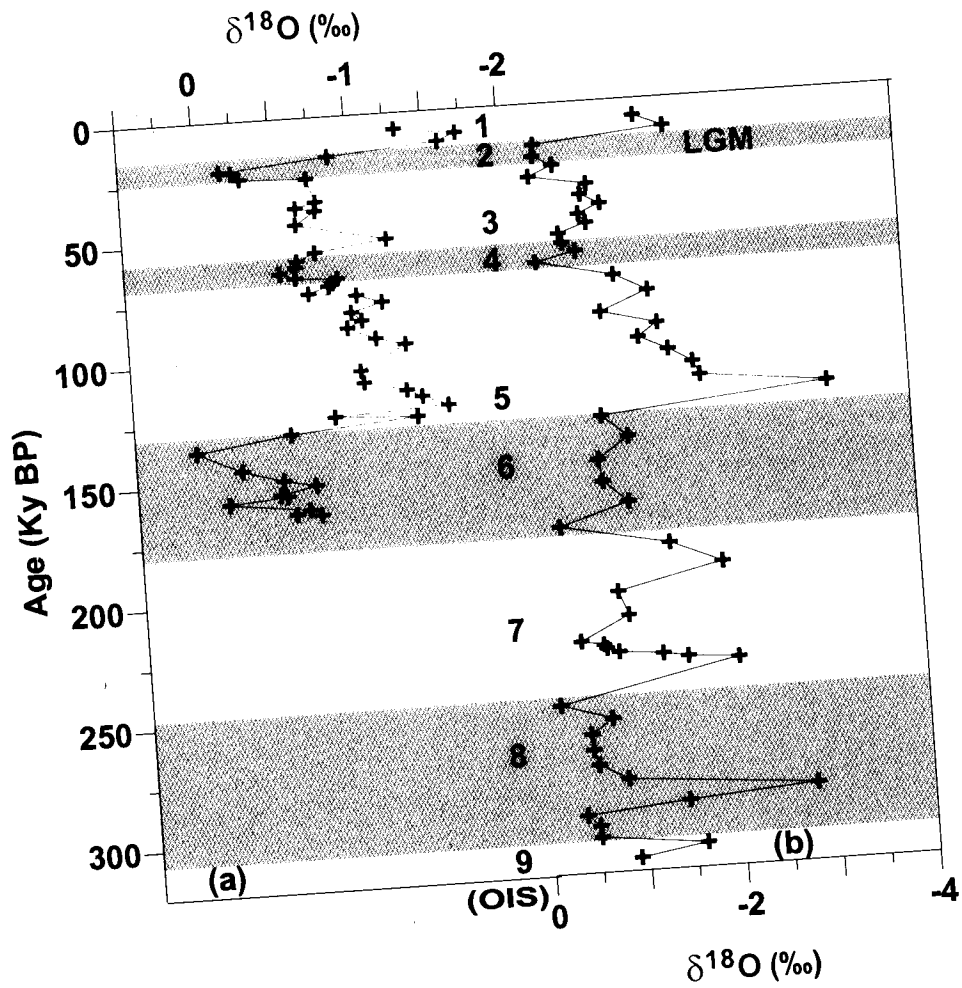
Figure 5.4: Downcore variation of $\delta^{18}O$ with planktonic species *Globigerinoide ruber* in cores (a)AAS-42/15 and (b)AAS-42/12A. Oxygen Isotope Stages (OIS) are indicated in numbers (1-9). Shaded areas represent glacial periods.

trend consistent with the planktonic record for the same core and the OIS 1 to 6, could be marked (Figure 5.5a). In this core, $\delta^{18}O$ values varied between 2.36 to 4.06‰ (Table 5.4) with a LGM to Holocene shift of 1.70‰ that substantially exceeds the ice volume effect.

5.2.3 Carbon isotope ($\delta^{13}C$) variations

The carbon Isotope composition of marine fossil carbonates is more complicated compared to oxygen isotopes. This is because the composition of $CaCO_3$ shells secreted by foraminifera depends on the $^{13}C/^{12}C$ ratio of dissolved HCO_3^- (Wefer and Berger, 1991). The $^{13}C/^{12}C$ ratio, in turn, varies within the water column as a result of the photosynthetic carbon fixation and oxidation of organic matter (Kroopnick, 1974). The $\delta^{13}C$ of calcite is relatively less sensitive to changes in temperature (~0.035‰ /°C – Emrich et al., 1970). Hence the down core variation in $\delta^{13}C$, though complex, is indicative of the variations in the $\delta^{13}C$ of dissolved HCO_3^- in the environment. The dissolved HCO_3^- is also affected by the air-sea exchange of CO_2 (Hoefs, 1987).

5.2.3.1 $\delta^{13}C$ record of planktonic foraminifera

The $\delta^{13}C$ values for *G. ruber* are found to range between 0.05 and 1.33‰, in AAS-42/15, while in AAS-42/12A the range is 0.02-1.55‰ (Figure 5.6a,b; Table 5.5). The $\delta^{13}C$ shows large oscillations in AAS-42/15 with relatively higher values occurring during the interglacial times compared to the glacial periods. In core AAS-42/12A, values are less variable and no
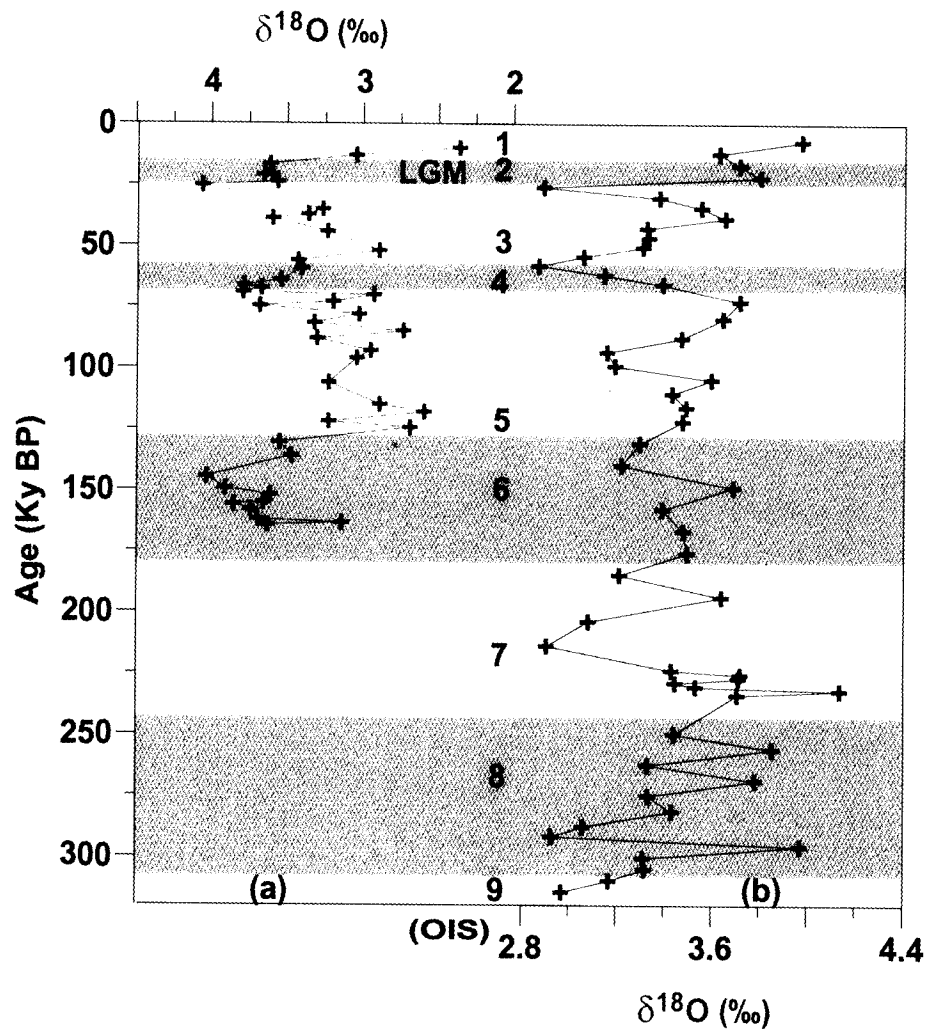
Figure 5.5: Downcore variation of $\delta^{18}O$ with benthic species *Cibicidoides wuellerstorfi* in cores (a)AAS-42/15 and (b)AAS-42/12A. Oxygen Isotope Stages (OIS) are indicated in numbers (1-9). Shaded areas represent glacial periods.
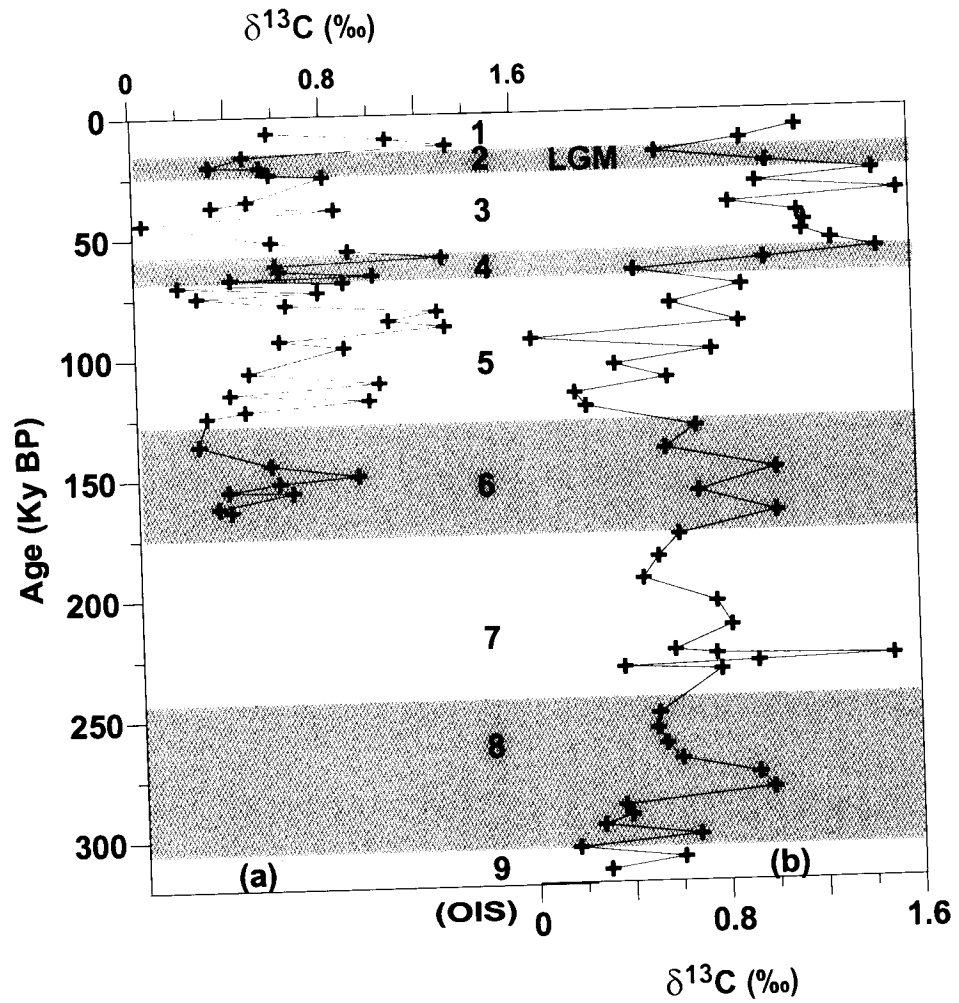
Figure 5.6: Downcore variation of $\delta^{13}C$ with planktonic species *Globigerinoide ruber* in cores (a)AAS-42/15 and (b)AAS-42/12A. Oxygen Isotope Stages (OIS) are indicated in numbers (1-9). Shaded areas represent glacial periods.

systematic trend is observed among various OISs.

5.2.3.2 $\delta^{13}C$ records of benthic foraminifera

The $\delta^{13}C$ of *C. wuellerstorfi* in core AAS-42/15 varies from -0.6 to 0.31‰, while in core AAS-42/12A, the variation is between -0.38 and 0.25‰ (Figure 5.7a,b; Table 5.6). Like the planktonic and benthic oxygen isotope records of AAS-42/15, the benthic carbon isotope record also distinguishes all the 6 marine isotopic stages very neatly. Unlike the $\delta^{18}O$, the $\delta^{13}C$ profile of *C. wuellerstorfi* in AAS-42/12A is reasonable distinguishing the 9 marine isotopic stages.

5.2.4 Organic carbon, nitrogen and CaCO₃ variations

All the data for organic carbon (C_{org}), nitrogen (N), C/N weight ratio and $CaCO_3$ are listed in table 5.7 for core AAS-42/15 and in table 5.8 for core AAS-42/12A. Downcore plots for all the proxies are presented in figure 5.9 for AAS-42/15 and in figure 5.10 for AAS-42/12A. C_{org} varies from 0.65 to 3.67% in ASS-42/15, and from 0.7 to 3.5% in core AAS-42/12A, except for one very high value (5.2%) at the core top. Nitrogen content varies between 0.02 and 0.37% in core ASS-42/15, and between 0.1 and 0.35% in core ASS-42/12A, except for one very high value of 0.58% in the surface sample as in the case of C_{org}. The $CaCO_3$ content varied over broad ranges, from 30 to 60% in core AAS-42/15 and from 40 to 69% in core AAS-42/12A. The surface sample in the latter core was distinguished by a high value of 74% for $CaCO_3$ as well. The C/N weight ratio ranged between 4.5 and 12.0 for core AAS-42/15 with one high value of 25 at ~136 Ky and in core AAS-42/12A it ranged between
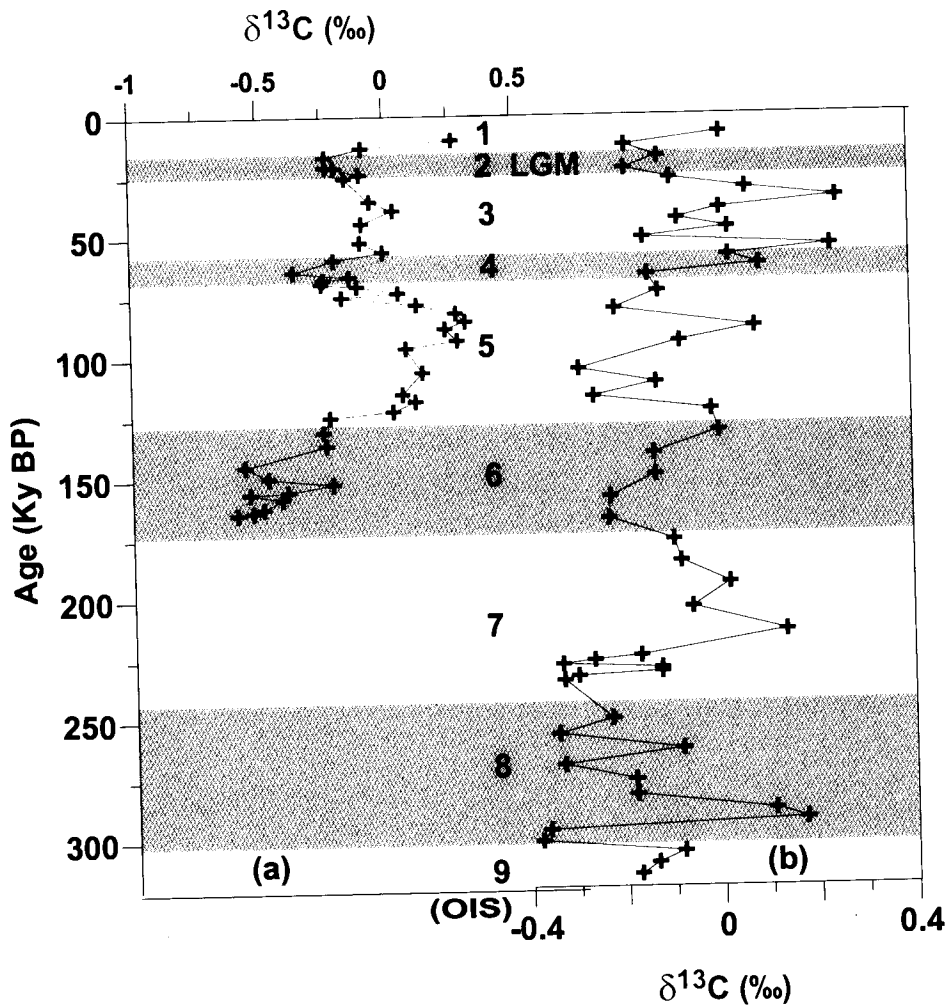
Figure 5.7: Downcore variation of $\delta^{13}C$ with benthic species of *Cibicidoes wuellursturfii* in cores (a)AAS-42/15 and (b)AAS-42/12A. Oxygen Isotope Stages (OIS) are indicated in numbers (1-9). Shaded areas represent glacial periods.
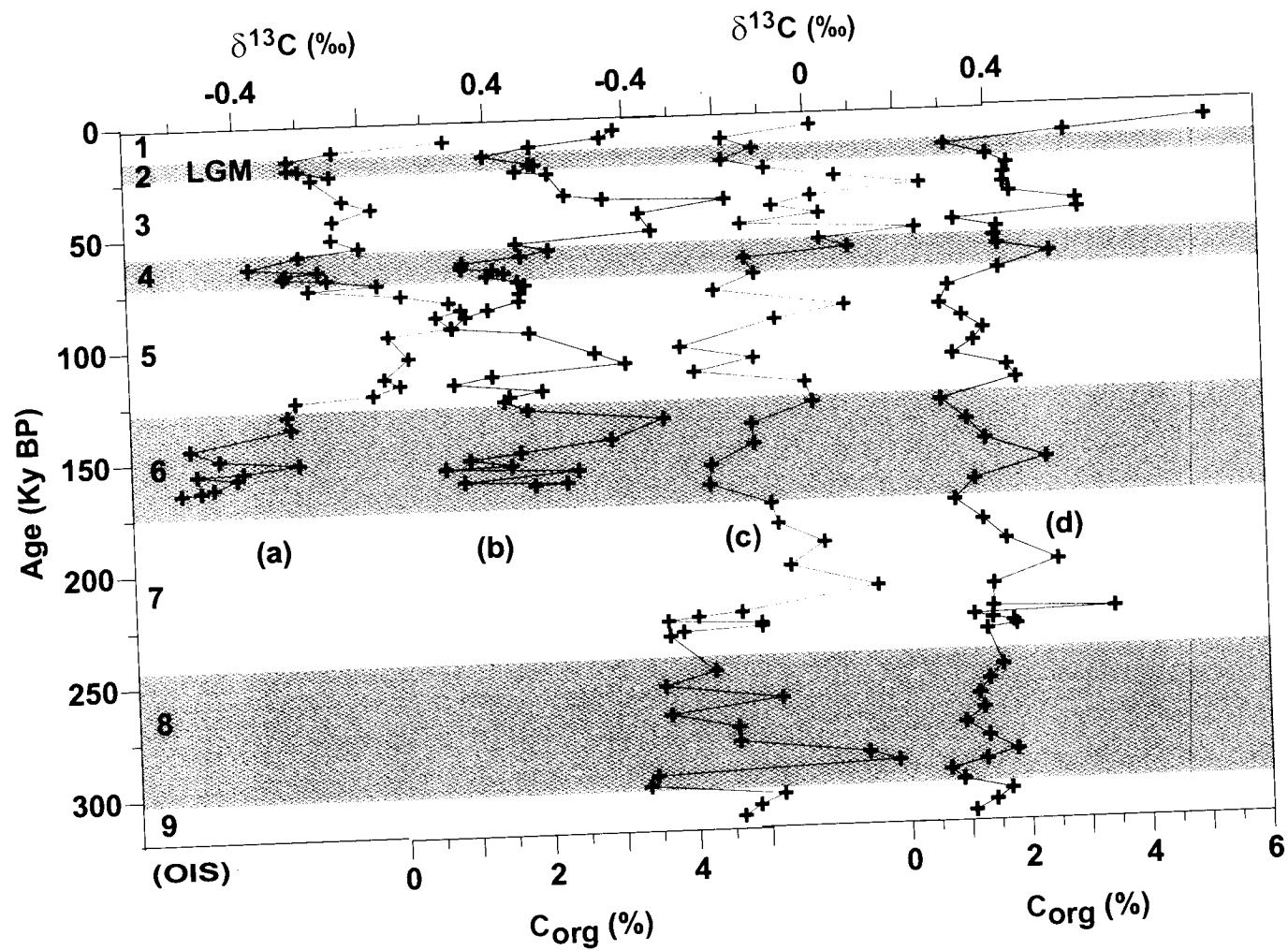
Figure 5.8: Downcore variations of (a)$\delta^{13}C$ (b)C_{org} in core AAS-42/15 and (c)$\delta^{13}C$ (d)C_{org} in core AAS-42/12A. The $\delta^{13}C$ variation of benthic *Cibicidoides wuellerstorfi* is compared with C_{org} in both the cores. Oxygen Isotope Stages (OIS) are indicated in numbers (1-9). Shaded areas represent glacial periods.

6.2 and 10.2 with a high value of 18.5 at ~225 Ky. As expected, the results for all the organic proxies showed relatively high values during the interglacial periods and low values during the glacial periods.

5.2.5 Sedimentary organic $\delta^{13}C$ and $\delta^{15}N$ variations

Figures 5.11a,c depict variations in $\delta^{13}C_{org}$ in the two cores whereas the corresponding profiles of $\delta^{15}N$ are shown in figures 5.11b,d. Both cores showed large changes in $\delta^{15}N$ of bulk sedimentary organic matter with values ranging from 6.5 to 9.5‰ in AAS-42/15 and from 5.5 to 8.9‰ in AAS-42/12A (refer Table 5.8). $\delta^{13}C_{org}$ oscillated between -22.7 and -18.25‰ in core AAS-42/15 with large number of values around -20 and -19‰. The range observed in core AAS-42/12A was from -21.0 to -18.7‰, but again most data fell within a very narrow range of -19.75 to -18.75‰.

5.3 Discussions

5.3.1 Variations in planktonic $\delta^{18}O$ records

As expected, large excursions of $\delta^{18}O$ of *G. ruber* are observed in both the cores (Figure 5.4a,b) during the transition from OIS 6 to OIS 5 (Termination II) and from OIS 2 to OIS 1 (Termination I). However in both cores, the Younger Dryas event (excursion to lighter $\delta^{18}O$ around ~11 Ky BP; Fairbanks, 1989) could not be seen. This is probably because the sample resolution is poor in both the cores. Furthermore, in core AAS-42/12A the excursion of $\delta^{18}O$ corresponding to the transition from OIS 9 and to OIS 8 was
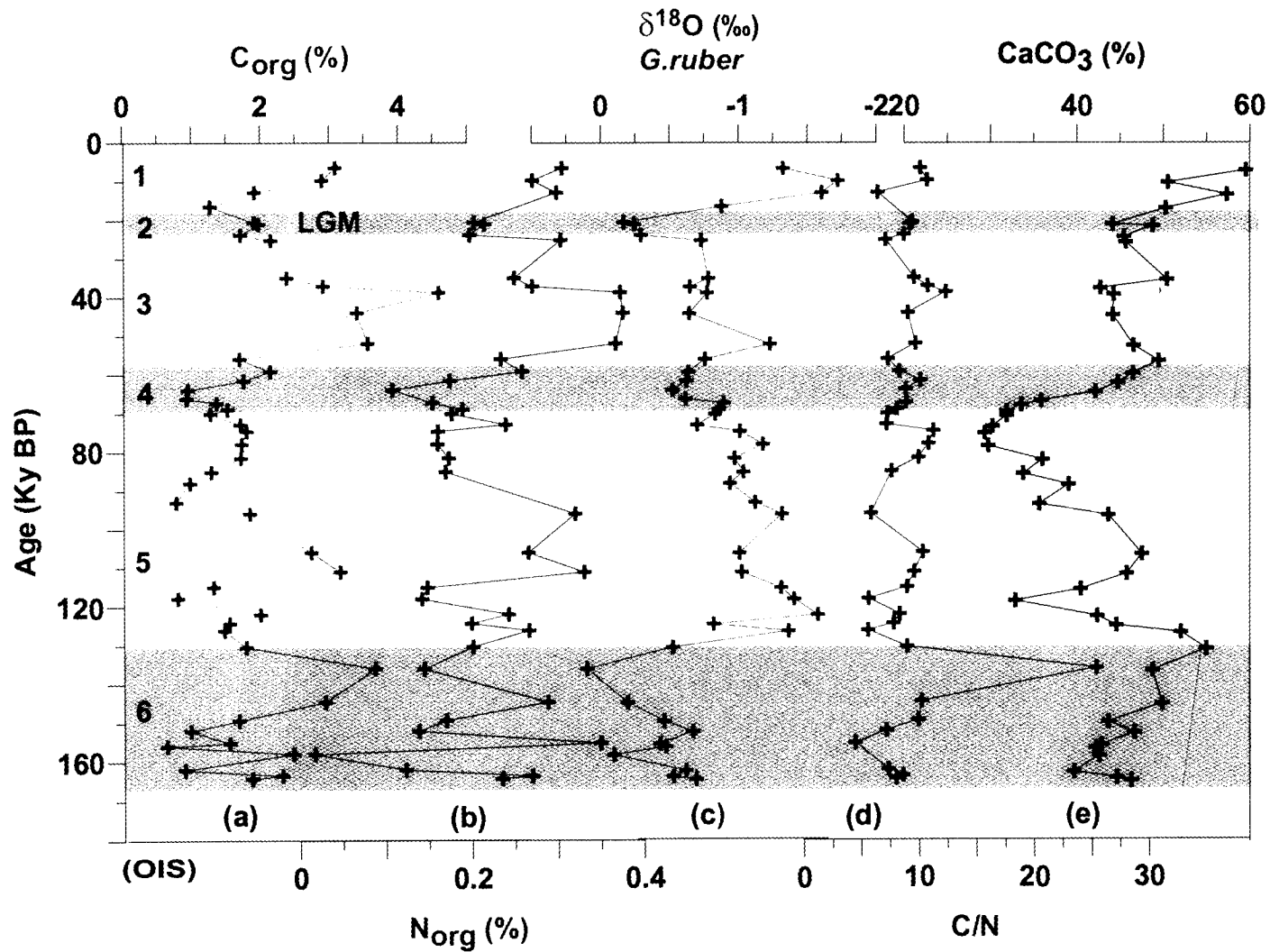
Figure 5.9: Downcore variations of (a)C_{org} (b)N_{org} (c)$\delta^{18}O$ (d)C/N (e)$CaCO_3$ in core AAS-42/15. Oxygen Isotope Stages (OIS) are indicated in numbers (1-6). Shaded areas represent glacial periods.
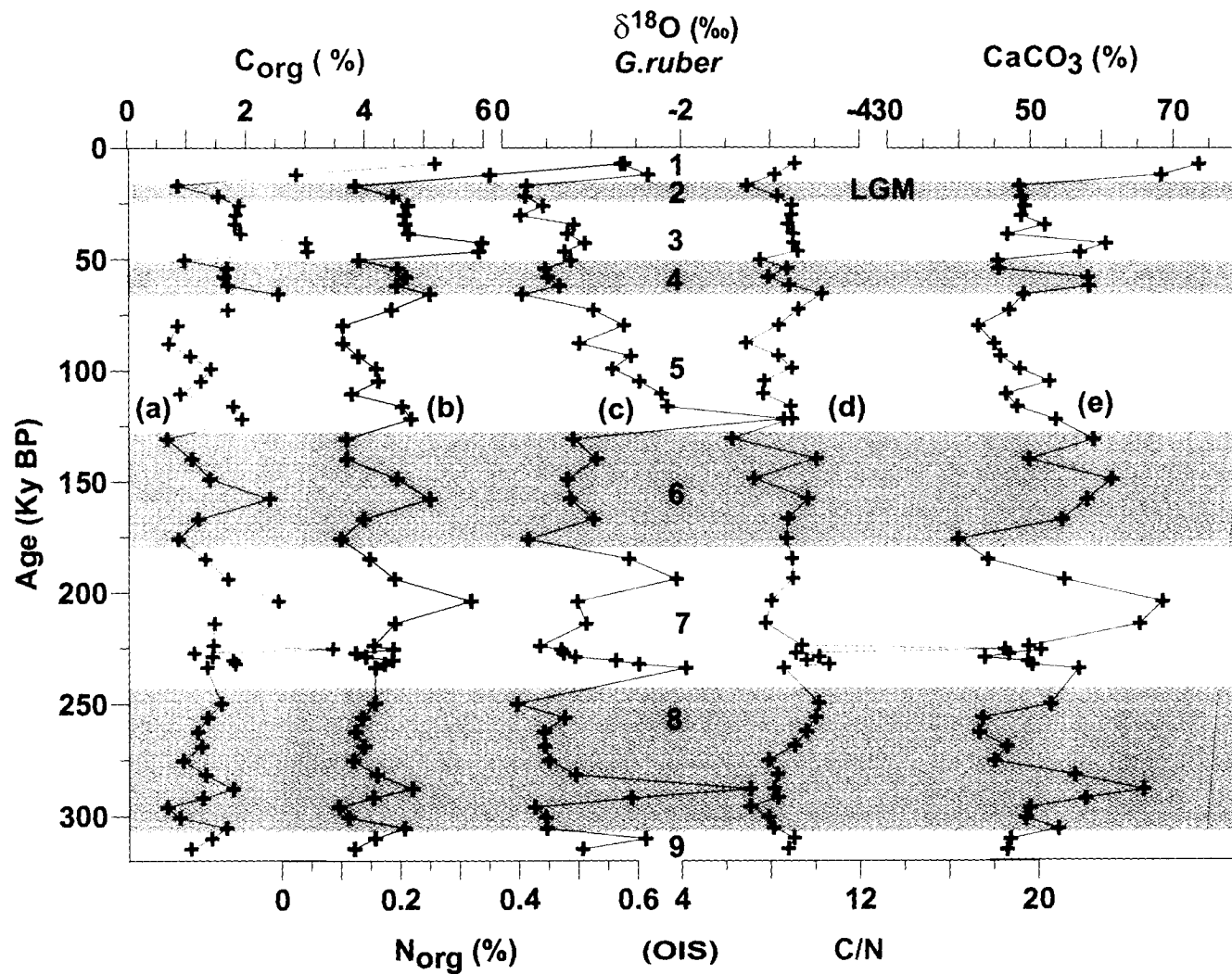
Figure 5.10: Downcore variations of (a)C_{org} (b)N_{org} (c)$\delta^{18}O$ (d)C/N (e)$CaCO_3$ in core AAS-42/12A. Oxygen Isotope Stages (OIS) are indicated in numbers (1-9). Shaded areas represent glacial periods.
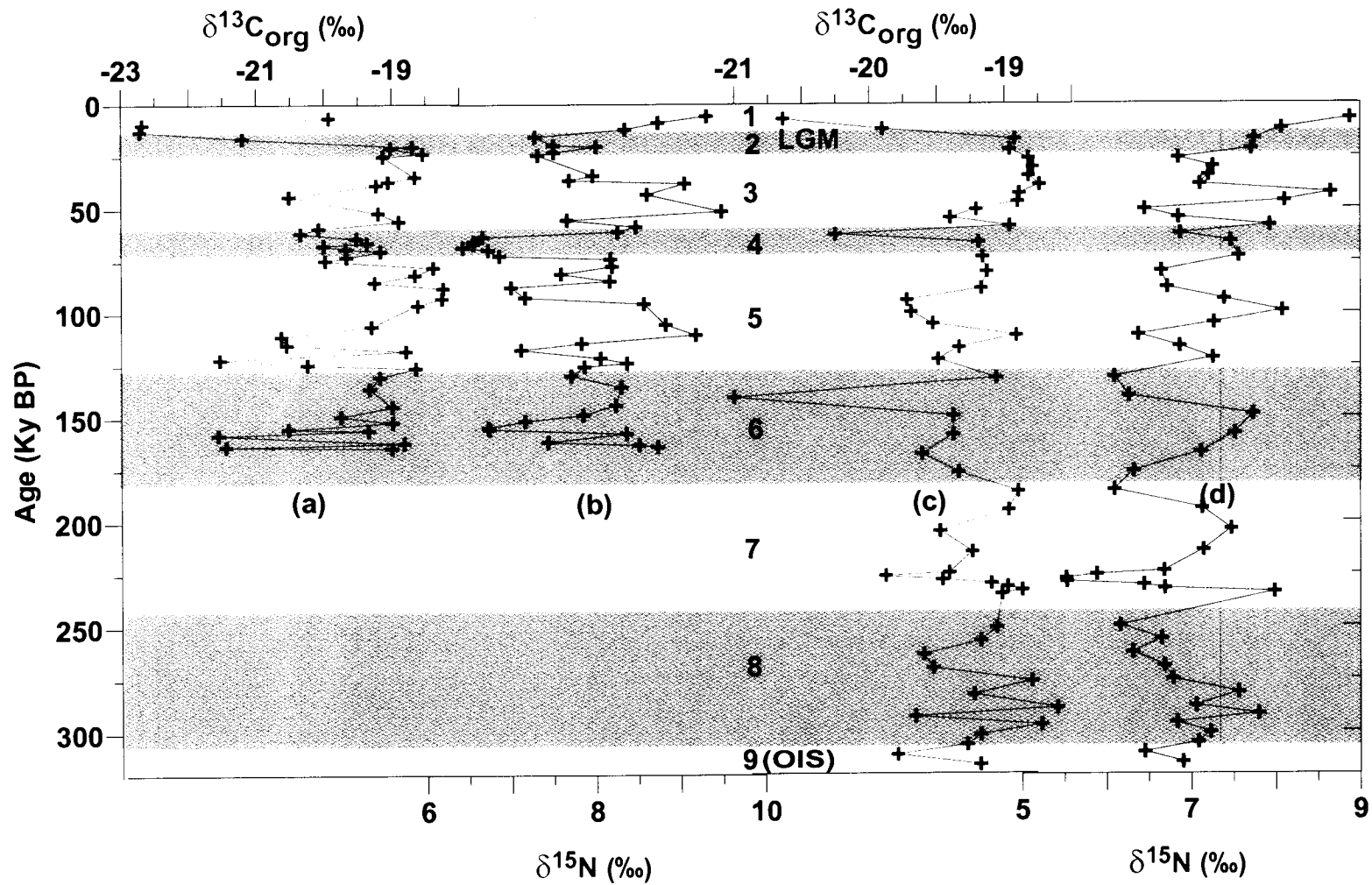
Figure 5.11: Downcore variations of (a)$\delta^{13}C_{org}$ (b)$\delta^{15}N$ in core AAS-42/15 and (c)$\delta^{13}C_{org}$ (d)$\delta^{15}N$ for core AAS-42/12A. Oxygen Isotope Stages (OIS) are indicated in numbers (1-9). Shaded areas represent glacial periods.

also observed. Two more quite prominent excursions of $\delta^{18}O$ are noticeable in this core representing the warm interstadial OIS 7.5 and 7.1.

The oxygen isotopic composition of seawater is determined by changes in global continental ice volume and regional or local changes in SST and salinity (Broecker, 1986). Processes such as evaporation, precipitation, freezing and mixing can affect the $\delta^{18}O$ values of surface waters locally (Savin and Yeh, 1981). A number of reports have been published form the Arabian Sea on fluctuations in $\delta^{18}O$ of planktonic foraminifera covering the last glacial-interglacial transition (e.g., Duplessey, 1982; Sarkar et al., 1990; Rostek et al., 1993; Sirocko et al., 1993; Thamban et al., 2001; Prabhu et al., 2004). These studies revealed enrichment of $\delta^{18}O$ substantially in excess of the ice volume. The glacial-interglacial shifts ($\Delta\delta^{18}O$) of 1.55‰ (in AAS-42/15) and 1.43‰ (in AAS-42/12A) are accordingly higher than the global ice volume effect (1.2‰; Labeyrie et al., 1987; Fairbanks, 1989). The high $\delta^{18}O$ values during the LGM have been ascribed by previous workers to: (1) lower glacial SST, a larger excess of evaporation over precipitation resulting in higher salinity, (2) mixing of water masses and (3) changes in habitat of foraminifers (Sirocko et al., 1993).

The $\Delta\delta^{18}O$ amplitudes observed in the present study are nevertheless lower than those reported previously (~2‰; Sonzogni et al., 1998, Thamban et al., 2001; Prabhu et al., 2004). According to Epstein et al. (1953), and Ganssen and Sarnthein (1983), a decrease in SST by 1°C leads to an increase in $\delta^{18}O$ by ~0.2‰. Assuming no salinity change other than the ice

volume effect ($\delta^{18}O$ = 1.2‰), the excess $\Delta\delta^{18}O$ (by ~0.35 and ~ 0.25‰ for cores AAS-42/15 and AAS-42/12A respectively), would require a glacial SST decrease by 1-2°C. Previous studies based on oxygen isotopic data have also inferred SST change of comparable magnitude (Duplessy, 1982; Sarkar et al., 1990). The analysis of alkenones in a sediment core from southeastern Arabian Sea led to the suggestion that SST's were lower during the LGM as compared to today by 2°C (Sonzogni et al., 1998; Rostek et al., 1997). Also using alkenone data Banakar et al. (2005) reported a mean SST decrease of 1°C for the period 24Ka – 12Ka. The lowest SST was found to occur at 12Ka, which cast doubts on the SST reconstructions of these authors (Ramesh and Tiwari, 2007). Quantification of tropical temperatures based on pollen studies (Bonnefille et al., 1990, 1992) indicates that the continental temperatures in East African highlands were lower by 3-4°C during the LGM than today. However, Thamban et al. (2001) found a significant shift in $\delta^{18}O$ towards lighter values of the order of 0.5-0.7‰ around 15Ka BP which they attributed mainly to the increased influx of fresh water related to the intensification of southwest monsoon in addition to the SST increase. The apparent adequacy of the reported SST change in accounting for the observed $\delta^{18}O$ changes implies that the contributions arising from shifts in the balance between evaporation and precipitation and water mass mixing should have been relatively minor at the sites of the cores analyzed in the present study.

5.3.2 Variations in benthic $\delta^{18}O$ records

The LGM to Holocene shift in $\delta^{18}O$ in core AAS-42/15 is ~1.25‰, which

is almost the same as the global ice volume effect (~1.2‰; Labeyrie et al., 1987; Fairbanks, 1989) but lower than the corresponding change in *G. ruber*, discussed above. As stated earlier, the $\delta^{18}O$ record in AAS-42/12A does not show any clear trend, although the range of measured values ($\delta^{18}O_{C.wuellerstorfi}$ 4.0–2.4‰) is comparable to the range observed by Schmeidl and Mackensen, (2006; $\delta^{18}O_{C.wuellerstorfi}$ 3.7–2.4‰; $\Delta\delta^{18}O$ ~1.1-1.3‰) and by Ahmad and Labeyrie (1994; $\delta^{18}O_{C.wuellerstorfi}$ 3.8–2.4‰). The observed benthic $\Delta\delta^{18}O$ of ~1.25‰ in core AAS - 42/15, which just matches the global ice volume effect, is lower than the value ($\Delta\delta^{18}O$ ~1.4‰) reported by Ahmad and Labeyrie (1994) but higher than the estimated ($\Delta\delta^{18}O$ ~0.9‰) by Thamban (1998). This supports the view that the bottom water temperatures did not change much during the last glacial-interglacial period (Savin and Yeh, 1981; Ahmad and Labeyrie, 1994). Furthermore, the salinity change also appears to have been minimal.

5.3.3 Controls on $\delta^{13}C$ variation in planktonic foraminifera - an overview

The stable carbon isotope composition of planktonic foraminifera, as mentioned in section 5.2.3, is complex and only a portion of the total $\delta^{13}C$ variations observed in planktonic foraminifers in deep sea sediments reflects local upwelling, productivity and nutrient variations (Prell and Curry, 1981; Ganssen and Sarnthein, 1983; Wefer and Berger, 1991). Though most foraminifera precipitate calcite in disequilibrium with the ambient dissolved CO_2, the degree of disequilibrium varies from species to species (Wefer and

Berger, 1991). It is now well established that in addition to the $\delta^{13}C$ of

dissolved ΣCO_2, other "vital effects" related to metabolic processes such as

respiration and symbiont photosynthesis affect the $\delta^{13}C$ of foraminifera shells

(Erez and Honjo, 1981). For example, Spero and Williams (1988) found that

environmental parameters like light (photosynthesis) and temperature

mutually controlled the signals for $\delta^{13}C$ and $\delta^{18}O$ values, respectively, while

SSTs did not significantly affect the $\delta^{13}C$ record of planktonic foraminifera.

Nonetheless, past changes in the tropical surface waters can be attributed to

variations in $\delta^{13}C$ composition of atmospheric CO_2 caused by variations in

terrestrial vegetation cover, and oceanic nutrient availability and primary

productivity (Thamban, 1998). The past $\delta^{13}C$ fluctuations in the tropical

surface waters have been mainly attributed to: 1) Variations on the $\delta^{13}C$

composition of the atmospheric CO2 caused by variation in forest biomass;

and 2) Variations in nutrient availability and primary productivity.

1) Variation in $\delta^{13}C$ of atmospheric CO_2

Any changes in the isotopic composition of the atmospheric CO_2, are

rapidly transmitted to surface waters through air-sea gas exchange and hence

to the shallow dwelling planktonic foraminifera (Shackleton, 1977; Prell and

Curry, 1981). G. ruber that generally occurs at water depths of 0-25 m

(Deuser, 1987) was chosen for this study, as has been done by numerous

previous workers. This species is more likely to reflect changes in the

atmospheric CO_2 compared with other species that reside deeper in the water

column (e.g. *Limacina inflata*, a pteropod species which lives at depths >50 m; Fabry and Deuser, 1992). *G. ruber* is also known to exhibit seasonal variations with higher isotopic values occurring during summer when the chlorophyll biomass and carbon fluxes are at their peaks (Fischer et al., 1996). The range of $\delta^{13}C_{G.ruber}$ values (~0-1.5‰; Figure 5.6a,b) observed in both cores are in good agreement with those observed by Thamban (1998) in the eastern Arabian Sea, and even by Fischer et al., (1999) in the South Atlantic. Kroopnick (1985) found the $\delta^{13}C$ of ΣCO_2 ($\delta^{13}C_{\Sigma CO2}$) in the Arabian Sea surface waters to be around 1.6‰.

The $\delta^{13}C$ records in the two cores are complex and not entirely consistent with each other. The long term mean for $\delta^{13}C$ in AAS-42/15 is ~0.5‰, and a long term secular trend is not observed over the period of accumulation of this core. The $\delta^{13}C$ values in AAS-42/12A also appear to fluctuate around this mean up to OIS 5, but in younger sediments the values are definitely higher. The following discussion will therefore be restricted to AAS-42/15 that has better resolution and age control. On a glacial-interglacial time scale, there occurred a net transfer of lighter carbon from the land to the ocean that lowered the mean oceanic $\delta^{13}C$ by up to ~0.5‰ (Curry et al., 1988; Duplessy et al., 1988). One would therefore expect lower $\delta^{13}C$ during the glacial stages. The values during OIS 2, early OIS 4, and OIS 6 are indeed lighter. Terrestrial vegetation also responds to precipitation and temperature variations at low latitudes (Street-Perrot et al., 1997). As the maxima in $\delta^{13}C$ are observed during the early Holocene, early OIS 3 and late OIS 5

(interglacial stages), these might arise from enhanced precipitation favouring C_3 vegetation (trees preferentially use ^{12}C) and an increase in $\delta^{13}C$ of the surface seawater. Prell and Curry (1981) concluded that the single most important factor responsible for the observed similarities in amplitude and timing of the past $\delta^{13}C$ events is the variation in $\delta^{13}C$ composition of atmospheric CO_2 caused by changes in terrestrial biomass.

2) Variations in the upwelling intensity and productivity

Another factor leading to glacial-interglacial variations in the $\delta^{13}C$ could be upwelling of subsurface waters. This process leads to inputs of isotopically lighter carbon to the surface layer, thereby lowering the $\delta^{13}C$ (Prell and Curry, 1981). However if the decrease in $\delta^{13}C$ is due to enhanced upwelling of cold deep waters, $\delta^{18}O$ would also be expected to record more positive (heavier) values at the same time. However, during the cold isotopic stages, when the $\delta^{13}C$ values are generally the lowest, heavier $\delta^{18}O$ values are largely due to the ice volume effect and some local cooling assuming no additional salinity change as discussed above, and it is well-established that upwelling was suppressed during these periods (Prell, 1984a). On the other hand, periods of more intense upwelling in the Arabian Sea were those of high precipitation that probably lowered the salinity of surface waters on a regional scale and also favoured greater fixation of ^{12}C on land. Moreover, upwelling promotes the growth of phytoplankton which strongly discriminates against the heavier isotopes. Isotopic analysis of *G. ruber* collected by sediment traps in the

Arabian Sea revealed that, unlike $\delta^{18}O$, the $\delta^{13}C$ values vary considerably in space and time. This led Curry et al. (1992) to conclude that the relation between $\delta^{13}C$ and upwelling intensity is complex in the region. Nevertheless, it would appear that changes in upwelling probably contributed little to the planktonic $\delta^{13}C$ variations observed in the present study.

5.3.4 The $\delta^{13}C$ record of epifaunal benthic species reflecting bottom water oxygenation

Over the past few decades, carbon isotope records of benthic foraminifera have been increasingly utilized to reconstruct past changes in deep water circulation and organic carbon remineralization as the $^{13}C/^{12}C$ ratio has been found to provide a wealth of information on carbon cycling in the oceans (e.g., Zahn et al., 1986; Curry et al., 1988; Duplessy et al., 1988; Mackensen et al., 1994, 2001). Since the marine organic matter and CO_2 released during its oxidation in the water column are significantly depleted in ^{13}C, the $\delta^{13}C_{\Sigma CO2}$ values in subsurface waters are lower, relative to the surface waters; also, $\delta^{13}C$ exhibits a distribution pattern mirroring that of phosphate - decreasing with oxygen consumption and downstream of the deep water flow such that subsurface waters of the North Indian and North Pacific oceans have the lowest $\delta^{13}C$ values (Kroopnick, 1985). Numerous studies have been carried out on $\delta^{13}C$ variations in benthics (especially *C. wuellerstorfi* and *U. peregrina*). The results have shown that the two species precipitate calcite with variable disequilibrium with the ambient dissolved CO_2 (e.g. Zahn et al.,

1986; Grossman, 1987; McCorkle et al., 1990). Of these the $\delta^{13}C$ of *C. wuellerstorfi* is close to that of CO_2 in bottom waters and so its application has been more widespread. Like $\delta^{13}C$, the Cd/Ca ratio in seawater also reflects the ambient nutrient (phosphate) levels (Boyle, 1986). However, the interpretation of the foraminiferal $\delta^{13}C$ and Cd/Ca data is not always straightforward in terms of the organic carbon mineralization and oxygenation of subsurface waters (Boyle, 1992, 1994). The limitation of benthic $\delta^{13}C$ as a paleo-chemical proxy stems from a lack of complete understanding of complex ecological, biogeochemical and physical interactions that together determine the isotopic composition of the chosen species (Schmiedl and Mackensen, 2006). Glacial-interglacial shifts of 0.32 to 0.46‰ $\delta^{13}C$ have been attributed to global changes in the carbon cycling on land and in the ocean (Curry et al., 1988; Duplessy et al., 1988). The departures from equilibrium for the $\delta^{13}C$ in the benthic foraminifera are attributed mainly to "vital effects" and microhabitat effects.

One observed "vital effect" based on measurements involving several species is the depletion of heavy isotopes in $CaCO_3$ due to *disequilibrium* with the dissolved CO_2 (Wefer and Berger, 1991). This disequilibrium occurs due to the incorporation of isotopically-light metabolic CO_2 into the carbonate tests and the magnitude of vital effect is proportional to the amount of metabolic CO_2 in the organisms, the size of the CO_2 pool and its calcification rate (Erez, 1978; Grossman, 1987; McConnaughey et al., 1997). Almost all biogenic carbonates are influenced by vital effect, with the degree of disequilibrium varying widely and also being specific for different species (Grossman, 1987).

In addition, the $\delta^{13}C$ composition of the test carbonate is closely related with the accumulation rates of organic carbon and varies with the microenvironment of different species, reflecting $\delta^{13}C$ variations of ΣCO_2 in the overlying/pore waters (Zahn et al., 1986; Grossman, 1987; McCorkle et al., 1990). Since the epifaunal C. wuellerstorfi remains in direct contact with the bottom waters, it incorporates the isotopic signatures of bottom water $\delta^{13}C$, while the infaunal species (e.g. Uvigerina peregrina) reflect $\delta^{13}C$ of the pore water i.e. substantially lower $\delta^{13}C$ values (Grossman, 1984a; McCorkle et al., 1990, 1997; Rathburn et al., 1996; Mackensen and Licari, 2004; Schmiedl et al., 2004; Fontanier et al., 2006). The $\delta^{13}C$ of CO_2 in pore waters of near-surface sediments varies as per the extent of organic matter remineralization (McCorkle and Emerson, 1988; McCorkle et al., 1985, 1990; Sayles and Curry, 1988; Stott et al., 2000; Holsten et al., 2004]. Under oxic conditions, the pore water $\delta^{13}C$ will vary depending on the amount of organic carbon fluxes reaching the seafloor and with higher carbon rain rates, the porewater $\delta^{13}C$ will be lower (Schmiedl and Mackensen, 2006). Thus, $\delta^{13}C$ of benthic foraminifera can provide information on bottom water oxygenation levels (Vidal et al., 2004; Schmiedl and A. Mackensen, 2006).

Benthic $\delta^{13}C$ measurements for both the cores in the present study were made on the C. wuellerstorfi that reliably incorporate the bottom water signatures, and whose $\delta^{13}C$ and also of some other species belonging to the same genus has been found to be very close to the bottom waters $\delta^{13}C$ (Curry et al., 1988). Figure 5.7a,b shows the observed downcore variations of $\delta^{13}C$.

The $\delta^{13}C$ record exhibits large changes most of which seem to relate very well with the $\delta^{18}O$ records (planktonic as well as benthic for AAS-42/15 and only planktonic for AAS-42/12A). In general, high values occur during the interglacial stages while low values are typical of glacial times. This would imply that bottom waters at the coring site were well oxygenated during the glacial periods and were relatively oxygen depleted during the interglacials. The core-top $\delta^{13}C$ values of 0.272 and 0.016‰ versus PDB in the AAS-42/15 and AAS-42/12A respectively, are lower than the values reported by Naqvi et al. (1996) and Thamban (1998), but quite comparable with the data of Schmiedl and Mackensen (2006). Moreover, these values are close to those expected in modern sediments from the water column measurements of Kroopnick (1985).

Of the two profiles presented, that from AAS-42/15 is more reliable because its resolution is better and also because, as mentioned earlier, the benthic $\delta^{18}O$ data for AAS-42/12A are not reasonable. Although the $\delta^{13}C$ record for this core shows general similarities with that of AAS-42/15, most of the inferences below are drawn from the latter record. The lowest $\delta^{13}C$ values (~ -0.6‰) in this core correspond to OIS 6. This suggests a poorly oxygenated state of bottom waters. Although a low $\delta^{13}C$ could also be caused by the microhabitat effect (Schmiedl and Mackensen, 2006), it would be hard to explain why such an effect would be manifested only during this period. Similarly, the high $\delta^{13}C$ values, most pronounced (~ 0.3‰) during the late OIS 5, could be caused by lower surface productivity that would lead to

enrichment of $\delta^{13}C$ in organic particles undergoing sedimentation (e.g. Zahn et al., 1986; Zahn and Pedersen, 1991); however, it is much more likely that these arise from a higher bottom water oxygen content. The total amplitude of benthic $\delta^{13}C$ oscillations in AAS-42/15 is remarkably large (~0.9‰) and it seems most likely that it reflects large changes in the bottom water oxygen content at the coring sites.

The $\delta^{13}C$ records in both cores seem to bear fairly good peak-to-peak visual correspondence with the corresponding C_{org} records (Figure 5.8) with few exceptions (most notably during the late OIS 5) even though the relative amplitudes of the peaks differ. For example, in AAS-42/15 the large increase in C_{org} during the OIS 3 is accompanied by relatively small increases in $\delta^{13}C$. Similarly, in core AAS-42/12A, the magnitude of $\delta^{13}C$ change is higher during the interglacial stages 3, 5 and 7, relative to the Holocene (Figure 5.8c) in spite of the much higher C_{org} content during the Holocene (Figure 5.8d) content. Nonetheless, when all the data points are carefully looked at, and compared with the C_{org} profile (Figure 5.8c,d), they show general overall resemblance. While this similarity is as expected because higher productivity (of which C_{org} is a proxy) should lead to greater remineralization of organic matter at depth, the lesser quantitative correlation is not surprising either because the benthic $\delta^{13}C$ is also determined by other physical factors and the vital effects as referred above. In particular, if the productivity increases (decreases) are associated by a more (less) vigorous ventilation at depths, these would obscure the relation between $\delta^{13}C$ and C_{org}.

5.3.5 Paleo-productivity inferences from C_{org} and its fluxes

As mentioned earlier in chapter 4, the origin of organic carbon enrichment in marine sediments has been a subject of widespread interest for the past several decades. The quality and quantity of organic matter in marine sediments are determined by the supply of organic materials from marine and terrestrial sources and their preservation in the sediments (Summerhayes, 1981; Tissot et al., 1980). Studies on carbon isotopic composition of the sedimentary organic matter suggested that the influence of terrestrial sources is limited to areas within a few tens of kilometers of the coastline so that marine organic matter is the dominant component in most of the sediments (Sackett, 1964; Fontugne and Duplessey, 1986). Primary production of organic matter in the ocean is carried out by a wide variety of unicellular planktonic organisms whose activities are governed by nutrient supply and solar radiation. Only a fraction of the organic matter produced in the euphotic zone is exported to the deep, aphotic layers. A part of this material is oxidized during settling, another part is used as food by benthic organisms, a yet another portion undergoes further degradation in the sediments, and the remainder is buried. Some commonly used proxies for paleo-productivity of surface waters are C_{org} (Muller and Suess, 1979; Pedersen 1983; Sarnthein et al., 1988; Ganeshram and Pedersen, 1998), biogenic barite (Schmitz, 1987; Dymond et al., 1992) and opal (Lyle et al., 1992; Gardner et al., 1997) in sediments. In addition, various biomarkers have been developed as proxies of bulk production as well as by specific groups of autotrophs (Prahl et al., 1989; Jasper and Gagosian, 1993; Ohkouchi et al., 1997; Schubert et al., 1998;

Werne et al., 2000). However each proxy has its own problems and limitations. In the case of C_{org}, preservation versus production is still a debated issue. It is also equally important to know as to what fraction of organic matter is of terrestrial origin, when C_{org} is used as a paleoproductivity proxy.

Productivity in the eastern Arabian Sea is known to have fluctuated in the recent geological past in response to changes in the monsoons. The eastern Arabian Sea has been divided into two zones by Satya Prakash and Ramesh (2007) based on physical forcing, responsible for the primary production. While Zone 1 (extending from 20 to 25°N and 62 to 75°E) falls under the influence of cold NEM, during which period convective mixing supports high productivity, Zone 2 (extending from 20 to 10°N and 62 to 75°E) is mainly influenced by the SWM upwelling-induced high production. Both core locations (Figure. 5.1) fall within Zone 2 according to Satya Prakash and Ramesh (2007), but being away from the influence of the WICC the coring sites are known to experience convection driven nutrient enrichment in winter (S.W.A. Naqvi, personal communication). By contrast, the water upwelling along the Indian coast does not reach that far offshore, and that advecting offshore from the upwelling centres of the western Arabian Sea generally loses most of its nutrients by the time, if ever, it reaches the coring sites. Nevertheless, the SWM enhances the productivity of the Arabian Sea as a whole (Naqvi et al., 2003), and so it is reasonable to assume that changes in both NEM and SWM would be recorded in the two cores examined here. Figure 5.9 and 5.10 presents the profiles of organic carbon, nitrogen, C/N
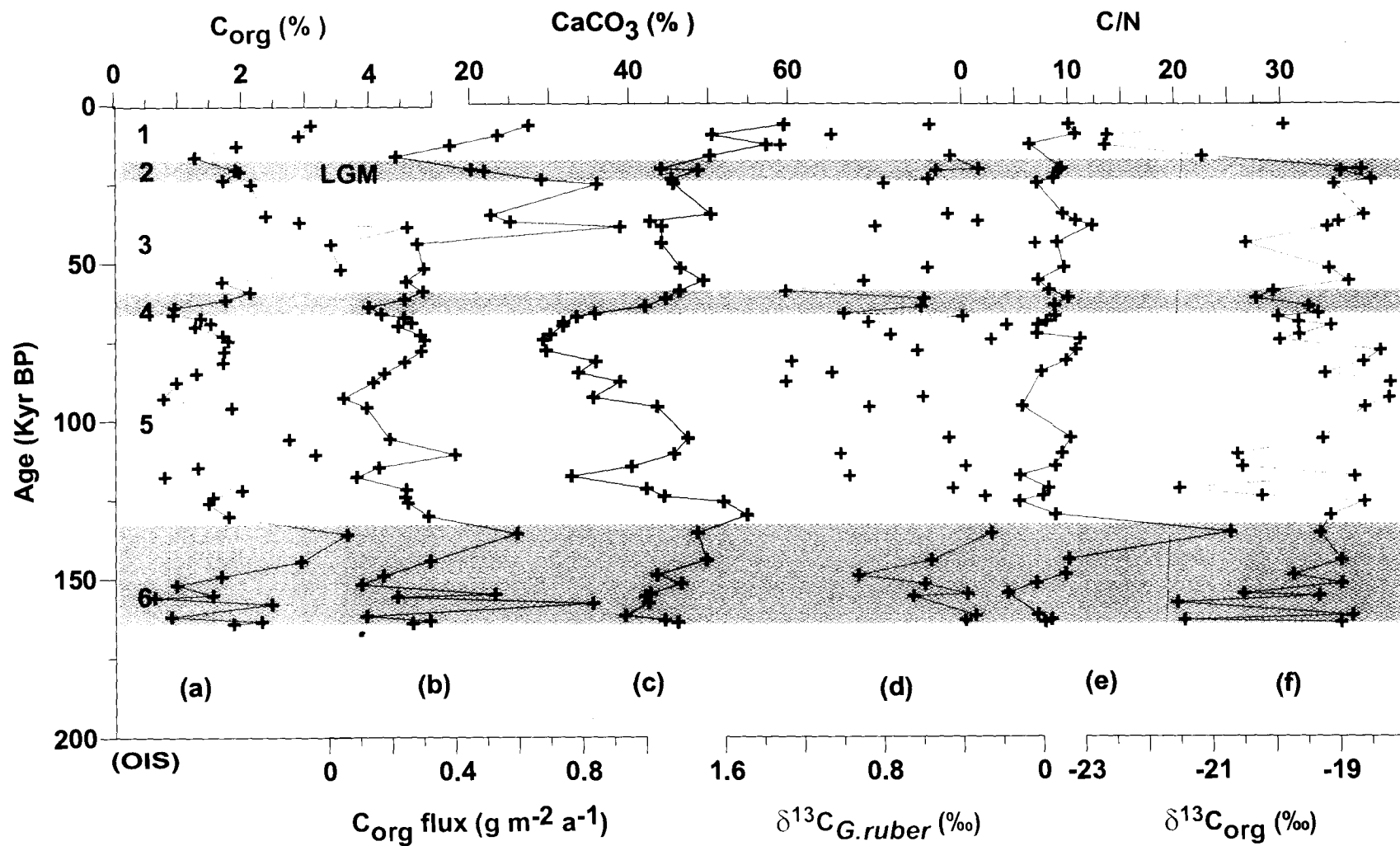
Figure 5.12: Downcore variation of (a)C_{org} (b)C_{org} flux (c)$CaCO_3$ (d)$\delta^{13}C_{G.ruber}$ (e)C/N and (f)$\delta^{13}C_{org}$ in core AAS-42/15. Oxygen Isotope Stages (OIS) are indicated in numbers (1-6). Shaded areas represent glacial periods.

ratio and calcium carbonate in cores AAS-42/15 and AAS-42/12A, respectively. The behaviours of various proxies in the two cores are discussed separately.

Core AAS-42/15

The C_{org} profile suggests higher productivity during the warmer stages as compared to glacial stages except for OIS 6 during which two major peaks with high C_{org} content are recorded. The highest C_{org} values occur during the warmer OIS 3 (Figure 5.12a). Other records of productivity indicators (total chlorine and N content) in the western Arabian Sea also show several events of enhancements of productivity during OIS 3 (of these only two peaks are recorded in the AAS-42/15 C_{org} record, presumably due to poor resolution). The C_{org} flux profile (Figure 5.12b) also exhibits a similar trend as that of C_{org}. The $CaCO_3$ and $\delta^{13}C$ of G. ruber profiles (Figure 5.12c,d) also exhibit more or less similar trends as C_{org}, albeit with different amplitudes (e.g. the $CaCO_3$ minimum for OIS 4 is much more pronounced than for the LGM). The paleoproductivity pattern provided by all the proxies in this core seems to be at variance with some earlier reports of high productivity during the glacial and low during interglacial periods in the vicinity of the coring sites. To list some of them, Fontugne and Duplessy (1986) found high productivity during glacial periods, while Thamban et al. (2001) showed productivity to be low during early Holocene. In both cases the reduced productivity was attributed to the dynamics of the circulation system and the hydrological cycle along the west coast of India. Furthermore, using $CaCO_3$ content of sediments as a

productivity indicator, Sarkar et al. (1993) showed that productivity was at its maximum during the LGM.

Paleoproductivity reconstructions based on alkenones and coccoliths (Rostek et al., 1997); *Florisphaera profunda* in the total coccolithophore flora (%Fp), C_{org}, and $CaCO_3$ contents (Prabhu and Shankar, 2005) also showed that primary productivity increased during glacial times and decreased at the beginning of interglacial periods. The enhanced productivity during glacial periods has been attributed to the strong NEM, which would bring nutrient-rich deep water to the euphotic zone by weakening water column stratification, while the reduced productivity was probably a result of the intensification of the SWM during the two terminations. Prabhu and Shankar (2005) also commented on the high C_{org} content observed during the interglacial periods as not being just an artifact of better preservation of organic matter due to high sedimentation rate.

The observed high (low) C_{org} contents during interglacials (glacials) indicating higher (lower) productivity in this study, however, is in agreement with the results of Reichart et al. (1997) for a core from the Murray Ridge in the northern Arabian Sea. This C_{org} distribution pattern also supports the conclusion of Pattan et al. (2003) based on analysis of a core from the southeastern Arabian Sea that productivity was lower during glacial periods and higher during major interglacials. The high C_{org} content observed during the Holocene in particular is consistent with previous reports of elevated productivity in the northeastern and northwestern Arabian Sea (Fontugne and Duplessy, 1986; Von Rad et al., 1995; Schulz et al., 1998; Schulte et al.,

1999; Sirocko et al., 2000), and the southern continental margin of India (Paropkari et al., 1991; Thamban et al., 1997). The observed high C_{org} contents during OIS 3 (4.5%; ~40Ky) and 5 (3.25%; ~110Ky) should also be due to high productivity and not greater preservation because a corresponding hike was observed in the $\delta^{13}C$ of G. ruber (Figure 5.12d) and C_{org} flux (Figure 5.12b) profiles as well. In spite of high sedimentation rate ~25 Ky BP, the C_{org} content is not exceptionally high, while the maximal C_{org} is observed when the sedimentation rate was ~3.7cm/Ky at ~38 Ky BP. The variation in C_{org} accumulation rate from 0.1 to 1.0 $g/m^2/ky$ in this core (Figure 5.12b) agrees well with that over the Oman margin (0.5 to 2.5 $g/m^2/ky$; Zahn and Pedersen, 1991) and is slightly higher compared to that over the southeastern Arabian Sea (0.05 to 0.50 $g/m^2/ky$; Pattan et al. 2003). It is much lower than the corresponding rate in the northeastern Arabian Sea (2 to 20 $g/m^2/ky$; Von Rad et al., 1995). Thus, it can be inferred from the above observations that the productivity at the core site is moderate and comparable with that in the western Arabian Sea.

The C/N ratio and $\delta^{13}C_{org}$ in the marine sediments were used to trace the source of organic carbon and to rule out the possibility that high accumulation of C_{org} could be due to inputs of organic matter of terrestrial origin. The C/N ratio of phytoplankton and zooplankton is ~6, freshly deposited organic matter has a C/N of ~10 while terrigenously derived organic matter has C/N exceeding 20 (Hedges and Parker, 1976; Emerson and Hedges, 1988; Meyers, 1994, 1997). The C/N ratio in this study core varied from 7 to 10 (Figure 5.12e), except for one single high value of 26 during the

late OIS 6 (~130Ky BP), suggesting the organic carbon to be mainly of marine origin.

The $\delta^{13}C_{org}$ values in AAS-42/15 mostly range between -20.5 and -18.5‰. Assuming the $\delta^{13}C_{org}$ values of -26‰ for the terrigenous and -20‰ for the marine organic matter (e.g. Fontugne and Duplessy, 1986), the fraction of terrigenous organic matter would be negligible. However there are three data points having values ~-21.5‰ around ~164 Ky BP, which falls in the glacial stage 6, and one value in the early interglacial stage 5 (~122 Ky). An even more depleted $\delta^{13}C_{org}$ value of -22.9‰ was found during the early Holocene indicating strong influence of SWM that could have led to relatively elevated inputs from land thereby lowering the $\delta^{13}C_{org}$ value. However, the $\delta^{13}C_{org}$ never reached the typical terrigenous value of -26.0‰. Thus, both the C/N ratio and $\delta^{13}C_{org}$ provide compelling evidence for a predominantly marine origin of organic matter in core AAS-42/15.

The observed high C_{org} content during stage 6 has to be accounted for. The cold glacial stage 6 has 3 warm interstadial stages (6.1, 6.3 and 6.5; Bassinot et al., 1994) and a hike in the C_{org} content was observed during these warm interstadial stages. These warm interstadials are again under the influence of comparatively stronger SWM. Thus, the observed C_{org} distribution trends in AAS-42/15 suggest that even though this site is located in the northeastern Arabian Sea, the overall productivity is still controlled predominantly by processes related to the SWM, as is the case in the western Arabian Sea (Prell, 1984b; Murray and Prell, 1991), in the Murray Ridge

region (Reichart et al., 1997) and in the southeastern Arabian Sea (Pattan et al., 2003).

Core AAS-42/12A

As in core AAS-42/15, the C_{org} profile in AAS-42/12A also shows generally high values during the interglacial stages 1, 3, 5 and 7 and low values during the glacial stages (Figure 5.13a). However while C_{org} content decreased during cold OIS 2 and 8, some increased during OIS 4, 6 and early 8 also occurred (Figure 5.13a). For the entire core, the range of C_{org} values is 0.7-3% except for the high value of ~5% during the Holocene. This range of C_{org} is in agreement with that (0.37-2.64%) reported by Prabhu and Shankar (2005).

Like AAS-42/15, this core is also located well above the lysocline (which in the Arabian Sea begins at ~3800 m; Peterson and Prell, 1985). Thus, the sedimentary $CaCO_3$ content should also provide a measure of the overhead productivity (Sirocko et al., 1993; Naidu and Malmgren, 1996; Agnihotri et al., 2003b). The C_{org} and $CaCO_3$ records in AAS-42/12A are, in fact, quite similar. Both records show particularly high values during the Holocene indicating very high productivity that is further supported by the $\delta^{13}C_{G.ruber}$ data (Figure 5.13c,d). The high C_{org} content is also accompanied by a high C_{org} accumulation rate (Figure 5.13b). These results are consistent with previous reports of high productivity during the Holocene, driven by an intense SWM (Prell, 1984b; Sirocko et al., 1993; Naidu and Malmgren, 1996; Overpeck et al., 1996).

The high C_{org} content during OIS 5.5 is also accompanied by corresponding increase in $CaCO_3$ and C_{org} accumulation rate, but a decrease in $\delta^{13}C_{G.ruber}$. The low $\delta^{13}C_{G.ruber}$ suggest that foraminiferal productivity was not favoured but the environment must have been overall productive, especially by cocolithophores, since the corresponding C_{org} flux and $CaCO_3$ contents are high. A sharp hike in C_{org} was also observed at ~ 225Ky BP (OIS 7.4; Bassinot et al., 1994) which was also reflected by a high C_{org} flux due to a high sedimentation rate (6.0 cm/Ky) at this time. The cold interstadial 7.4 should have had low C_{org} content compared with 7.3 and 7.5 because of the weakened SWM and consequently lower productivity as reflected by the $CaCO_3$ and $\delta^{13}C_{G.ruber}$ profiles. Overall, the C_{org} record for AAS-42/12A, as in the other core analyzed here, shows high productivity during the interglacial periods. The observed variations within OIS 5 are in agreement with those reported by Prabhu et al. (2004) who found correlations with pollen record to be high during warmer intervals (5.1, 5.3 and 5.5) and low during colder intervals (5.2 and 5.4).

The increase in C_{org} during the OIS 4 in AAS-42/12A is hard to explain as this was not found to occur in AAS-42/15. If real, then it would reflect regional variations of overall productivity or differences in the quality of production. The $CaCO_3$ and C_{org} flux profiles also exhibit peaks at this interval, indicating that coccolithophores could be important contributors to the productivity; whereas the $\delta^{13}C_{G.ruber}$ profile shows lighter values (Figure 5.13) implying low foraminiferal productivity. For the glacial stage 6 there should have been two peaks in the C_{org} profile corresponding to the warm
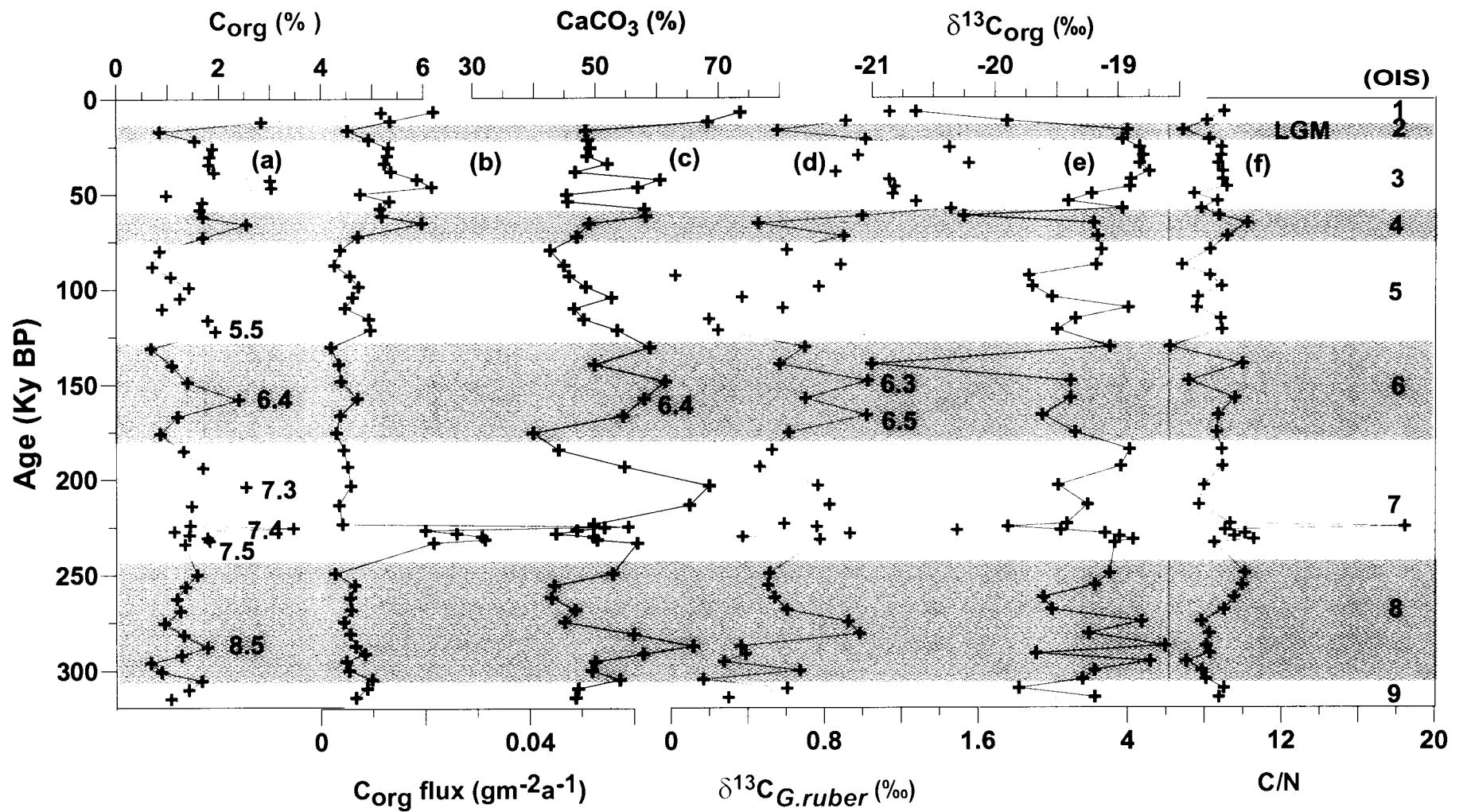
Figure 5.13: Downcore variations of (a)C_{org} (b)C_{org} flux (c)$CaCO_3$ (d)$\delta^{13}C_{G.ruber}$ (e) $\delta^{13}C_{org}$ and (f)C/N in core AAS-42/12A. Oxygen Isotope Stages (OIS) are indicated in numbers (1-9). Shaded areas represent glacial periods.

interstadials of 6.3 and 6.5 (Figure 5.13) as observed in the $\delta^{13}C_{G.ruber}$ profile. Instead, a hike in C_{org} is observed during the cold interstadial 6.4, which is also reflected by the $CaCO_3$ profile. The reasons for these differences are not obvious, but the signals should not be over-interpreted because of poorer resolution and age control in this core compared to AAS-42/15. For the glacial stage 8, the observed lower values in C_{org} are as expected, except for a slight increase in the beginning, which seems to represent more intense SWM during the warm interstadial OIS 8.5. The C_{org} peak is again accompanied by a $CaCO_3$ peak and a minimum in $\delta^{13}C_{G.ruber}$, which may again be due to the possible mechanism mentioned above.

The C/N values in AAS-42/12A fluctuate within a narrow range from 8-10, with a single high value of 18.3 at ~225 Ky BP (Figure 5.13f), that is coincident with maxima in C_{org} and its accumulation rate. This also happens to be the period when the sedimentation rates were high (~6.0 cm/Ky). However a decrease in $\delta^{13}C_{org}$ is not seen at this level, which means that C_{org} is of purely marine origin. The $\delta^{13}C_{org}$ varied within a narrow range between -19.75 and -18.75‰, with a few values reaching -20.75‰ (Figure 5.13e). The range of $\delta^{13}C_{org}$ observed in this core is very close to the isotopic composition of marine organic matter mentioned earlier.

The trends of variability observed in AAS-42/12A are generally consistent with those seen in AAS-42/15 as discussed in the preceding section supporting the view that the productivity in the eastern Arabian Sea is dominantly associated with the SWM, being higher during warm periods and lower during cold ones.

5.3.6 Glacial-interglacial variability in denitrification

Fixed nitrogen (N) is supplied to the ocean by rivers, N_2-fixation by cyanobacteria and atmospheric deposition, with N_2-fixation being the largest source term (Capone et al., 1997; Codispoti et al., 2001). The major sinks are denitrification in oxygen-deficient waters and in sediments, and the burial of organic nitrogen in sediments (Codispoti and Christensen, 1985; Codispoti et al., 2001). In the absence or near absence of oxygen, NO_3^- is used as an electron acceptor for the bacterially mediated degradation of organic matter (Goering, 1968; Cline and Richards, 1972). Water-column denitrification, which accounts for nearly a quarter of the total oceanic N-loss, occurs primarily in three areas: the ETNP, ETSP and Arabian Sea (Codispoti and Christensen, 1985; Codispoti et al., 2001). Each of these regions are characterized by an intense oxygen minimum zone and upwelling induced high primary production which supplies copious quantities of settling organic detritus that sustains high rates of denitrification in subsurface waters (Deuser, 1975; Codispoti et al., 2001). As a consequence of denitrification, these zones are sensitive to climate induced changes in upwelling intensity and hydrography, which are known to vary on the glacial-interglacial time scale (e.g. Ganeshram et al., 1995; 2000; Altabet et al., 1995, 2002).

Large deficiencies in the inorganic combined nitrogen occur within the intermediate waters of the northern Arabian Sea (Sen Gupta et al., 1976a; Deuser et al., 1978; Naqvi et al., 1982; Naqvi, 1987). It is estimated that denitrification in the Arabian Sea accounts for a third of the global oceanic water column denitrification (10-30 $TgNy^{-1}$; Naqvi, 1987; Mantoura et al.,1993;

Bange et al., 2005).

Changes in ocean chemistry due to those in biological productivity and circulation have been identified as the key factors modulating atmospheric pCO_2 over glacial-interglacial timescales (Berger et al., 1989; Broecker and Henderson, 1998). An increase in biological productivity caused by a higher oceanic NO_3^- inventory has been proposed to be a possible mechanism that could explain the drawdown of atmospheric CO_2 levels during glacial times (McElroy, 1983; Altabet and Curry, 1989; Ganeshram et al., 1995, 2000; Altabet et al., 1995, 2002; Falkowski, 1997; Broecker and Henderson, 1998). Berger and Keir (1984) showed that a glacial increase in NO_3^- inventory by 30% due to reduced oceanic denitrification could produce the pCO_2 decrease during glacial maxima.

5.3.6.1 Water column denitrification and nitrogen isotopes

The isotopic composition of NO_3^- supplied to surface waters through upwelling and vertical mixing and the isotopic fractionation of NO_3^- during uptake by phytoplankton determines the ratios of $^{15}N/^{14}N$ in organic matter produced in the euphotic zone (Altabet and Francois, 1994). The isotopic composition of NO_3^- in oxygenated waters is ~4-6‰ (Sigman et al., 1999). As discussed in Chapter 3, in denitrifying waters NO_3^- is highly enriched in ^{15}N with the $\delta^{15}N$ reaching up to 18‰ (Cline and Kaplan, 1975; Brandes et al., 1998). This is because isotopic fractionation associated with denitrification strongly discriminates against $^{15}NO_3^-$ with a fractionation factor of 20-30‰ (Cline and Kaplan, 1975; Brandes et al., 1998; Altabet et al., 1999a). The

isotopically heavy NO_3^- that is supplied to surface waters in these areas is utilized by the biota resulting in unusual $\delta^{15}N$ enrichments (8-10‰) in particulate organic material and the underlying modern sediments (Schafer and Ittekkot, 1993; Altabet et al., 1995, 2002; Suthhof et al., 2001). Therefore, the $\delta^{15}N$ of organic matter being deposited in the sediments overlain by the OMZ can serve as proxy for the past changes in water-column denitrification (Schafer and Ittekkot, 1993; Altabet et al., 1995, 2002; Ganeshram et al., 1995, 2000).

In this section variability of denitrification in the past is investigated using sedimentary $\delta^{15}N$ in the two open-ocean cores covering the last 160 and 320 kilo years. Downcore variations of $\delta^{15}N$ are shown in figure 5.14a for core AAS-42/15 and in figure 5.15a for AAS-42/12A. Again, the record from the former core is more detailed and will form the mainstay of the following discussion.

There are two striking features of the $\delta^{15}N$ records. First, they show remarkable similarities with the C_{org} records in both cores, and second the sedimentary $\delta^{15}N$ exhibits well-developed maxima and minima during the warm and cold periods, respectively. The $\delta^{15}N$ varied from 5.5 to 8.9‰ in core AAS-42/15 and from 6.5 to 9.5‰ in core AAS-42/12A. These ranges compares favourably with those in the literature [e.g. 7.7– 9‰ by Altabet et al. (1999a) and 5.9-9.6‰ by Agnihotri et al. (2003a)] for cores from the Arabian Sea. As observed in both the cores and also in conformity with the previous results, the highest $\delta^{15}N$ values (~8-9.5‰) are confined to the interglacial

stages with glacial values being ~2‰ lighter.

5.3.6.2 Factors influencing temporal variation of the $\delta^{15}N$ signal

As has been pointed out previously, changes in $\delta^{15}N$ of sedimentary organic matter can occur due to a number of processes in addition to denitrification. Therefore, for $\delta^{15}N$ to be used as a proxy of denitrification, the other possible explanations should be examined as follows.

5.3.6.2.1 Terrestrial organic matter inputs

Mixing of isotopically lighter terrestrial organic matter (~$\delta^{15}N$ = 2 to 4‰ (Sweeney and Kaplan, 1980; Kao and Liu, 2000) with marine organic matter can lower $\delta^{15}N$ in marine sediments (Peters et al., 1978). In order to evaluate this possibility, the relationships of $\delta^{15}N$ with C/N and $\delta^{13}C$ were examined (Figures 5.16a and 5.17a). Since these parameters are well established indicators of the terrestrial supply, one would expect them to co-vary with $\delta^{15}N$ if the terrestrial inputs were to be an important contributor to the observed $\delta^{15}N$ variability. Such is not the case as the correlations between $\delta^{15}N$ and C/N and between $\delta^{15}N$ and $\delta^{13}C$ are quite insignificant. This is consistent with the earlier conclusion that the source of organic matter in both cores remained predominantly marine throughout the periods of their deposition.

5.3.6.2.2 Alterations of organic matter in the water column and sediment diagenesis

The process of remineralization of organic matter during its sedimen-
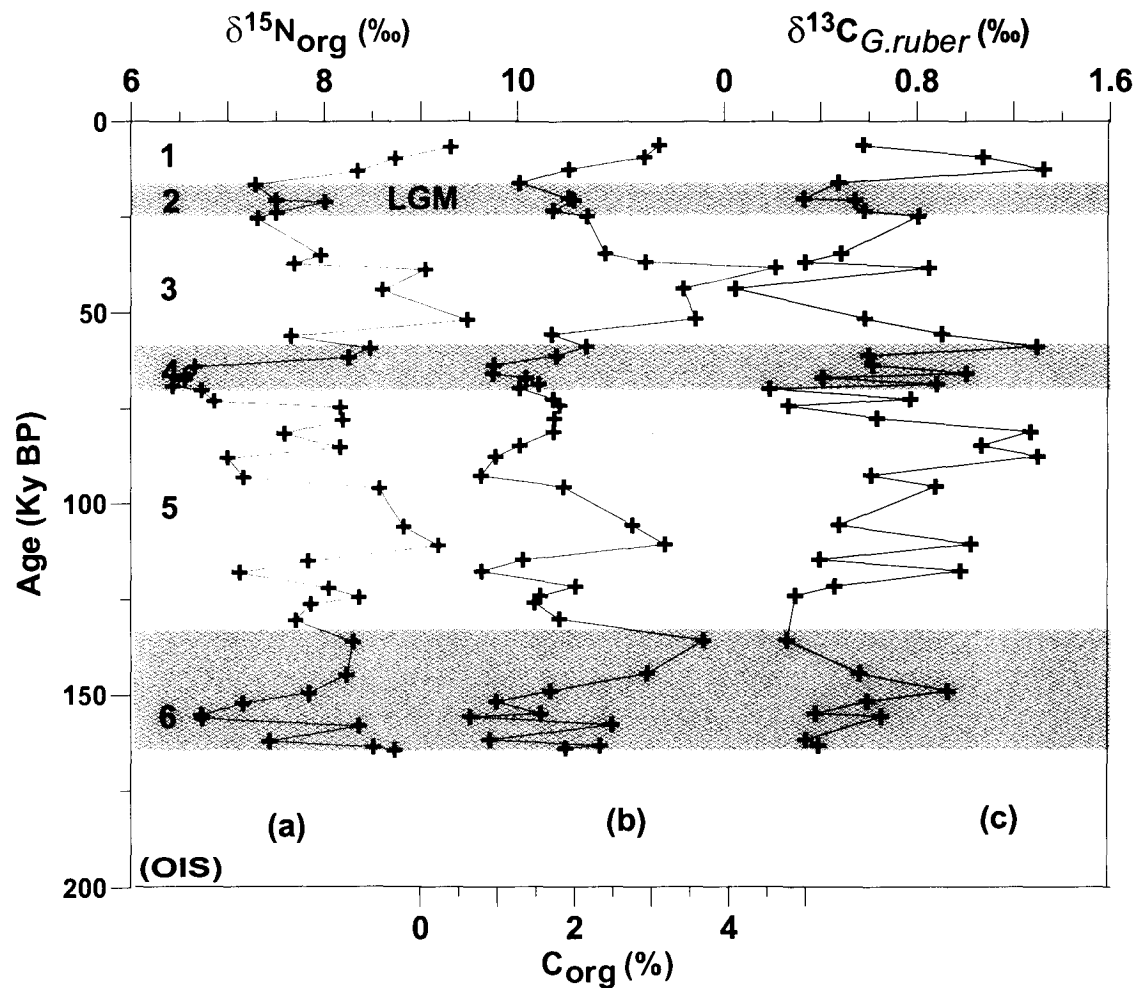
Figure 5.14: Downcore variations of (a)$\delta^{15}N$ (b)C_{org} (c)$\delta^{13}C_{G.ruber}$ for core AAS-42/15 . Low productivity with corresponding decrease in denitrification is seen during the glacial periods. Proxies indicate the influence of weakened summer monsoon during the glacial periods at the core site. Oxygen Isotope Stages (OIS) are in indicated in numbers (1-6). Shaded areas represent glacial periods.

Figure 5.15: Downcore variations of (a)δ^{15}N (b)C_{org} (c)$\delta^{13}C_{G.ruber}$ for AAS-42/12A .

High and low variations in denitrification (δ^{15}N) clearly indicate the corresponding levels of phytoplankton (C_{org}) and planktonic foraminifers ($\delta^{13}C_{G.ruber}$) productivity. All the proxy variations are influenced by summer monsoon intensity during various stages of glacial-interglacial periods. Oxygen Isotope Stages (OIS) are indicated in numbers (1-9). Shaded areas represent glacial periods.

tation through the water column and in sediments can affect the variations of sedimentary $\delta^{15}N$ signal. A uniform ~4‰ shift to heavier $\delta^{15}N$ values between settling material and near-surface sediments has been reported for the Southern Ocean and the equatorial Pacific (Altabet and Francois, 1994). In the northern Indian Ocean, Gaye-Haake et al. (2005) also found that $\delta^{15}N$ of material collected by the deepest sediment traps are consistently higher by 2-3‰ than the corresponding values in the surface sediments except for the two shallowest, northernmost trap locations in the Arabian Sea and the Bay of Bengal. This has been attributed to early diagenesis in sediments that removes isotopically lighter nitrogen; this interpretation is supported by a significant correlation between $\delta^{15}N$ and Degradation Index based on amino acid contents (Gaye-Haake et al., 2005).

The two cores analyzed in the present study have moderate sedimentation rates. Possible diagenetic effects on the $\delta^{15}N$ signal in these cores were examined through relationships among $\delta^{15}N$ and C_{org}, N and C/N ratios (Figures 5.16b,c,d and 5.17b,c,d). Positive correlations are observed between $\delta^{15}N$ and C_{org}, and also between $\delta^{15}N$ and N content. The correlation of $\delta^{15}N$ with C/N is negligible in both cores. This indicates that the effect of early diagenesis is probably not very large in these cores. Moreover, even if this effect were to be significant, it would be reasonable to assume that it is time invariable, such that changes observed within an individual record would still provide insights into trends of denitrification variability (Altabet et al., 1999a).

Figure 5.16: Correlation plots of (a)$\delta^{13}C_{org}$ (b)C_{org} (c)N_{org} (d)C/N with $\delta^{15}N$ for core AAS-42/15. The scatter in C_{org} and N_{org} vs $\delta^{15}N$ plots with a positive correlation rule out diagenetic effects on $\delta^{15}N$ depth profile. Poor correlations in $\delta^{15}N$ vs $\delta^{13}C_{org}$ and C/N show that downcore $\delta^{15}N$ signals are free from dilution effect due to terrestrial organic matter inputs.
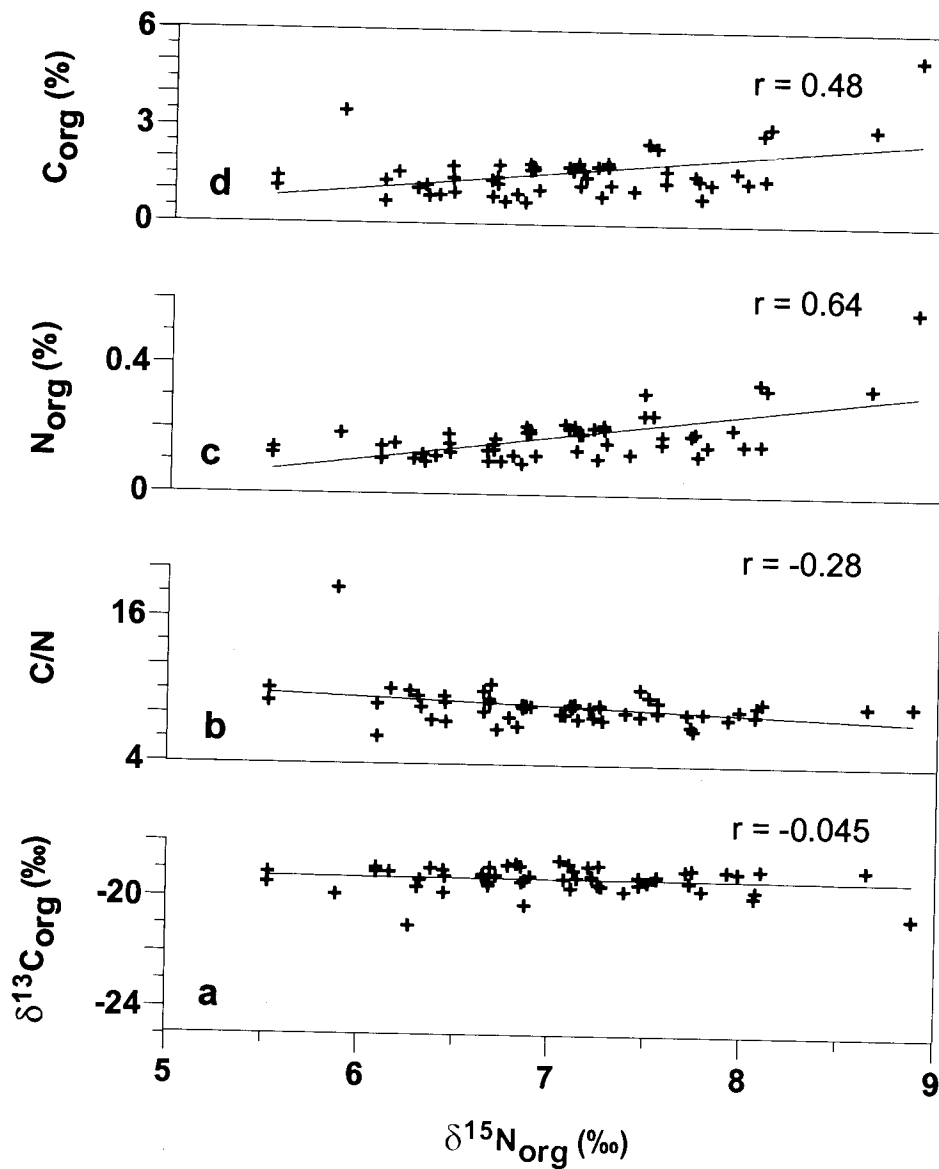
Figure 5.17: Correlation plots of (a)$\delta^{13}C_{org}$ (b)C_{org} (c)N_{org} (d)C/N with $\delta^{15}N$ for core AAS-42/12A. The scatter in C_{org} and N_{org} vs $\delta^{15}N$ plots with a positive correlation, rule out diagenetic effects on $\delta^{15}N$ depth profile. Poor correlations in $\delta^{15}N$ vs $\delta^{13}C_{org}$ and C/N show that downcore $\delta^{15}N$ signals are free from dilution effect due to terrestrial organic matter inputs.

5.3.6.2.3 Incomplete nitrate utilization

The next possible factor that would affect the sedimentary $\delta^{15}N$ variation is the partial utilization of NO_3^-, i.e. preferential uptake of $^{14}NO_3^-$ by the phytoplankton (Montoya, 1994; Waser et al., 1998). The water that upwells in the western Arabian Sea is advected over 1000 km from the coast before its NO_3^- is fully consumed (Naqvi et al., 2006b) and a substantial enrichment of ^{15}N is expected to occur in this water due to fractionation during phytoplankton uptake. Consistent with this expectation, Altabet et al. (1999a) recorded surface $\delta^{15}N$-NO_3^- values as high as ~10‰ at an offshore station arising from this effect, while Schäfer and Ittekkot (1995) observed a related seasonal minimum in $\delta^{15}N$ of sinking material at their western Arabian Sea trap site. Thus, even though on the basin scale the upwelled NO_3^- is fully consumed annually, one may expect gradients in sedimentary $\delta^{15}N$ along the trajectory flow of the upwelled water similar to those observed in the equatorial Pacific (Altabet and François, 1994). Given that the bulk of the vertical flux occurs during the SWM season, this potentially important effect needs to be investigated in detail. However, Altabet et al. (1999a) argued that despite the large horizontal gradients in $\delta^{15}N$ of NO_3^- within the OMZ, the homogenous distribution of heavy $\delta^{15}N$ values just below the euphotic zone facilitates uniform preservation of the denitrification signal all over the Arabian Sea. In contrast with the western Arabian Sea, water upwelling in the eastern Arabian Sea quickly loses its dissolved NO_3^- (Naqvi et al., 2006b), and so the enrichment of ^{15}N in sediments due to this effect is expected to be of even lesser importance here.

5.3.6.2.4 Nitrogen fixation

Nitrogen fixation by cyanobacteria is also expected to contribute to the variation of the $\delta^{15}N$ in sediments. The diazotrophs use atmospheric N_2 without much isotopic fractionation, producing organic matter with $\delta^{15}N$ of -1 to +1‰ (Wada and Hattori, 1991). In regions and during times of high N_2 fixation one may expect a dilution of the $\delta^{15}N$ signal due to this process. Thus, if N_2 fixation was enhanced during the glacial periods (Falkowski, 1997), this signal could be interpreted as one of reduced denitrification. Recent results have, however, shown that N_2 fixation and denitrification are tightly coupled (e.g. Deutsch et al., 2007). This is due to the fact that denitrification creates a pool of excess phosphate that in turn promotes N_2 fixation. Accordingly, regions such as the Arabian Sea that experience intense denitrification are also areas of high N_2 fixation (Devassy et al., 1978; Capone et al., 1997). Naqvi (2007) pointed out that sedimentary $\delta^{15}N$ actually reflects regional balance between denitrification and N_2 fixation, but how this balance has changed with time is not known. However, Haug et al. (1998) found that in the relatively nutrient depleted waters of the Cariaco Basin, N_2 fixation during the last 580 Ky occurred only during periods of enhanced subsurface denitrification. One may assume that the same applies to the Arabian Sea as well. That is, it is unlikely that high rates of N_2 fixation could have been supported in the region without intense denitrification, and despite the significant N_2 fixation in the region the role of denitrification in controlling the N isotopic composition remained dominant throughout.

5.3.6.3 Variabilty in water column denitrification

The high $\delta^{15}N$ values (8-9.5‰) obtained for the Holocene in the two cores (AAS-42/15 and AAS-42/12A) are similar to the values observed by several other researchers in recent sediments underlying zones of intense water column denitrification (e.g. Libes and Deuser, 1988; Schafer and Ittekkot, 1993; Pride et al., 1999; Altabet et al., 1995, 1999a, 2002; Ganeshram et al., 1995, 2000; Sutthof et al., 2001). Similarly, the low $\delta^{15}N$ values during the LGM have also been recorded by earlier workers in the Arabian Sea (Altabet et al., 1995, 1999a, 2002; Ganeshram et al., 2000; Sutthof et al., 2001; Agnihotri et al., 2003a) as well as in the denitrification sites of the Pacific (Ganeshram et al., 1995, 2000). This general trend of higher $\delta^{15}N$ values during the warmer periods and lower values during the colder periods are also seen in longer records (e.g. in the 1 Ma record of Altabet et al., 1999a). Moreover, as stated earlier, high-resolution $\delta^{15}N$ records show changes even within individual OIS (particularly the D/O cycles and Heinrich Events that occurred during the OIS 3; Sutthoff et al., 2001; Altabet et al., 2002).

The significance of the records presented in the present study is that they were generated from seamounts (where transport of terrestrial supply of organic matter is expected to be minimal) that are located directly beneath the zone of the most intense denitrification today (which makes the record sensitive to minor changes in denitrification intensity) in a region where the surface waters do not get significantly enriched with NO_3^- advecting from the western Arabian Sea such that the signal observed is purely of denitrification

origin. A noteworthy result obtained in the present study is that while the $\delta^{15}N$ values during the LGM are substantially lower than during the Holocene, they are considerably higher than those found during most other cold stages (e.g. by ~1‰ compared to OIS 4 and 6 in AAS-42/15; Figure 5.14). This clearly shows that denitrification in the Arabian Sea was suppressed but did not cease to occur during the LGM. The $\delta^{15}N$ data are supported by those on C_{org} for these periods (the two parameters show good correspondence with each other throughout the depositional periods of the cores). Apparently, OIS 4 and OIS 6 were the periods when Arabian Sea denitrification was at its minimum, possibly not occurring at all. It would also appear that denitrification during the LGM was slightly more intense or at least of comparable intensity than during two of the warm substages of OIS 5. On the other hand, the present-day intensity of denitrification appears to have been matched by parts of the warmer interglacial stages of OIS 3 and 5. Of these, the OIS 3 is of particular interest because of a high climatic variability during this period (manifested as D/O Cycles in Greenland ice cores and Heinrich Events in sediments of the North Atlantic). Previous studies by Sutthoff et al. (2001) and by Altabet et al. (2002) have shown that these events of warming and cooling in the North Atlantic region have been recorded as remarkably coeval changes in sedimentary $\delta^{15}N$ in the Arabian Sea. Apparently, the warming in the North Atlantic region affected the global climate including an intensification of the SWM that in turn could have led to more severe oxygen depletion at mid-depths in the Arabian Sea OMZ (Altabet et al., 2002). Some of the highest $\delta^{15}N$ and C_{org} values occurred in AAS-42/15 during OIS 3, but because of a

lower sampling resolution all such excursions are not seen in the records generated in the present study. These excursions have, since been confirmed by a very high resolution $\delta^{15}N$ record from the Murray Ridge (S.W.A. Naqvi, unpublished data).

5.3.6.4 Relative changes in productivity and circulation with respect to denitrification variability

The subsurface OMZ and associated denitrification is sustained by a complex but hitherto poorly understood the balance between oxygen supply through deep-water renewal and oxygen consumption rates determined by the productivity-related downward flux of organic matter from the surface layer. As stated earlier, high biological productivity in the Arabian Sea is largely due to widespread upwelling driven by the SWM winds, and a number of studies have focused on the variability of this process on a geological time scale. The various proxies used for this purpose include organic carbon and opal accumulation rates, Ba/Al ratios and foraminiferal assemblages (Clemens and Prell, 1990; Shimmield, 1992; Schulz et al., 1998). It is now well established that the productivity changes were largely associated with the 23-Ky precessional cycle which controls the strength of the SWM with a few Ky time lag. For instance, the last major maximum in biological productivity occurred ~9 Ky BP (Prell, 1984b), somewhat later than the maximum in northern hemisphere summer insolation ~11 Ky BP (this pecession-driven maximum enhances the seasonality i.e. warmer summers and cooler winters. Note that while warmer summers would lead to intensification of the SWM

upwelling, cooler winters should drive more connective mixing such that there will be greater reflux of nutrients from the subsurface to surface waters. The increased biological production would in turn raise the oxygen demand. Thus, the observed correspondence between $\delta^{15}N$ and C_{org} is not surprising. It provides a mechanistic relationship between the strengths of SWM and denitrification. What is not clear though is how the renewal processes respond to the natural climate change. There is some evidence that suggests that the cross-equatorial exchange of intermediate waters occurs mostly during the SWM (Swallow, 1984). But monsoonal forcing may not be the only driver of water and dissolved substances (oxygen and nutrients of relevance here). Changes in subsurface circulation will also occur in response to changes in the global thermohaline circulation, but very little information is available on this important aspect (Schulte et al., 1999). A novel approach has been followed in this study by generating the $\delta^{13}C$ record in C. wuellerstorfi ($\delta^{13}C_{C.wuell}$) and $\delta^{15}N$ in bulk sediments in the same core in order to address this issue. Of these, as stated earlier, the former is at least a semi-quantitative proxy of ambient oxygen levels (at the core depths of 2520 and 2270 m) while the latter reflects the oxygen deficiency within the OMZ (i.e. at depths of a few hundred metres).

A comparison of the $\delta^{13}C_{C.wuell}$ record and sedimentary $\delta^{15}N$ record for AAS-42/15 reveals excellent correspondence between the two over most of this core in that high values of one are associated with high values of the other and vice versa (Figure 5.14a,c). The high $\delta^{13}C_{C.wuell}$ value at the core top is consistent with high oxygen concentration in bottom waters at this site as

discussed in Chapter 3, while a high $\delta^{15}N$ value conforms to intense denitrification at this site today. During the LGM (OIS 2 and even more so during OIS 4), on the other hand, when the sedimentary $\delta^{15}N$ reached minimum values, so did the $\delta^{13}C_{C.wuell}$ as well. This is contrary to expectation because the Arabian Sea has an estuarine type of circulation where the deep waters entering the basin upwell slowly and flow southward at shallower depths. What these data seem to demonstrate is a sea-saw trend, one in which the most intense oxygen deficiency in the mesopelagic is associated with well-oxygenated conditions in deeper water (~2.2-2.5 km) and vice versa.

Based on isotopic measurements on *Cibicidoedes species*, Kallel et al. (1988) reported a hydrographic discontinuity between the intermediate and deep waters during the LGM in the Indian Ocean with the intermediate water being better ventilated and deep waters more slowly renewed and therefore quite oxygen depleted. The very high $\delta^{13}C_{C.wuell}$ values (>1‰) for deep waters observed by these authors have since not been reproduced, although enrichment of $\delta^{13}C_{C.wuell}$ substantially above the global glacial-interglacial shift has been observed by other workers as well (Naqvi et al., 1994; Boyle et al., 1995). Boyle (1997) postulated that the upper glacial North Atlantic intermediate/deep water (GNAI/DW) ventilated the western basins of the Indian Ocean instead of the Circumpolar Deep water that receives a large input from the North Atlantic deep water today. The results of the present study suggest that such a circulation pattern where the intermediate waters were better ventilated while the deep and bottom flows slowed down were typical of all glacial stages with the present type of circulation being restored

during interglacial times. This would result in vertical rearrangement of chemical structure with the intermediate waters of the glacial ocean being more oxygenated (i.e. the OMZ would have weakened) and the deep waters being less oxygenated than they are today. It may be emphasized that although the oxygen concentrations probably decreased considerably in deep waters (as indicated by the $\delta^{13}C_{C.wuell}$ data; Naqvi et al., 1994), complete oxygen depletion such as that reported by Sarkar et al. (1993) is most unlikely to have occurred. In any case, the results of this study suggest large changes in bottom water oxygen concentration [as inferred from the large (>0.75‰) shift in $\delta^{13}C_{C.wuell}$ from OIS 6 to OIS 5.1]. These changes in the vertical distribution of oxygen and of nutrients and other products of remineralization have potentially important implications for the glacial-interglacial changes in atmospheric carbon dioxide (Boyle, 1988).

Thus, it is proposed that the inferred relaxation of denitrification during glacial times was not merely because of a decrease in productivity, but also because of changes in the mid-depth circulation. However, it may be noted that the two factors are not exclusive. For example, changes in circulation (e.g. a more vigorous ventilation of subsurface waters) would also weaken the vertical gradients of nutrients in near surface waters thus lowering their reflux to the euphotic zone. This, in turn, would lead to a decrease in productivity, the signal for which will be preserved as low C_{org} in the sediments.

5.3.7 Geochemistry of major and redox elements on Glacial – Interglacial timescale in sediments

The interpretation of trace metal distribution in the sedimentary record

is usually constrained by their bahaviour in oxic (>10 μM dissolved oxygen) and anoxic (>1 μM hydrogen sulfide) environments. The promising tracers of chemical and biological processes include Ba (Schmitz, 1987; Dymond et al., 1992; Gingele and Dahmke, 1994, Prakash Babu et al., 2002), Cd, Cu, Mo, V, Re and U (reviewed in Calvert and Pedersen, 1993). Studies have been also performed on the geochemistry of redox-sensitive trace metals in suboxic (<10 μM dissolved oxygen and <1 μM hydrogen sulfide) depositional environments by Morford and Emerson (1999), Nameroff (1996), Nameroff et al. (2002, 2004), Sirocko et al. (2000), Agnihotri (2002) and Agnihotri et al. (2003a,b, 2007). These studies have covered all the three major open ocean OMZs viz. ETNP, ETSP, and the Arabian Sea. However, most of the studies carried out in the Arabian Sea so far have been on surface sediments, many were confined to the Holocene and some extended to cover the LGM. Thus, there exists very little information on the variability of trace/redox-sensitive metals on glacial-interglacial timescale.

5.3.7.1 Downcore variations in major elements

Downcore variations of Ti, Al, Fe and Mg in both cores mirror those of $CaCO_3$ and C_{org} (Figure 3.18 for core AAS-42/15 and Figure 3.19 for core AAS-42/12A). Data is presented in table 5.9 for core AAS-42/15 and table 5.10 for core AAS-42/12A. The average concentrations for these elements are Ti=0.22%, Al=3.85%, Fe=2.4% and Mg=1.63% for core AAS-42/15 and Ti=0.2%, Al=3.5%, Fe=2.25% and Mg=1.6% for core AAS-42/12A. The observed distribution of these elements, known to be of detrital origin, may be

due to their concentration in the clay fraction (Calvert and Pedersen, 1993) which shows a negative trend with $CaCO_3$ (a productivity proxy) as also observed by Thamban et al. (2001) in a core from the southeastern Arabian Sea. Agnihotri et al. (2003a) similarly found a negative trend of Al, Ti, Fe and Mg with $CaCO_3$, C_{org} and P/Al all productivity proxies and attributed the same to their concentration in the clay fraction of the sediments. However, his cores also came from the southeastern Arabian Sea and covered largely the Holocene period. In a more comprehensive study covering the entire Arabian Sea, Sirocko et al. (2000) also found negative relations between the detrital elements and C_{org} and $CaCO_3$. Results of the present study show less accumulation of these elements when the SWM was stronger and productivity was higher and vice versa.

The profile of Sr/Al shows a similar trend as that of $CaCO_3$ during all glacial-interglacial stages, suggesting a close association of the two (with r=0.86, for AAS-41/15, Figure 3.18f,g; and r=0.89, for AAS-42/12A, Figure 3.19f,g). Marchig (1972, 1974); Stackelberg (1972) and Mattiat et al. (1973) observed that the areas of extreme Sr enrichment were not confined to a specific water depth, but clusters of aragonitic needles occurred in the coarse fraction of the sediments collected from the western continental shelf of India. Lightfoot et al. (1990) reported that the basalts of the Deccan are rich in Sr. Due to intense chemical weathering in the region; the runoff gets enriched with Sr which may be removed along with aragonite after entering the ocean. The Sr/Al ratio ranges from 100 to 455 with an average of 208 for AAS-42/15, and from 160 to 600 with an average of 260 for core AAS-42/12A. The

Figure 5.18: Variations of major elements (Ti, Al, Fe, Mg and Sr) in comparision with C_{org} and $CaCO_3$ (indicator of overhead productivity) during various glacial-interglacial stages in core AAS-42/15. Profiles of Ti, Al, Fe, Mg are presented with their total concentration while Sr is normalized to Al. Glacial stages are indicated by shading. Oxygen Isotope stages (OIS, 1-6) are indicated.
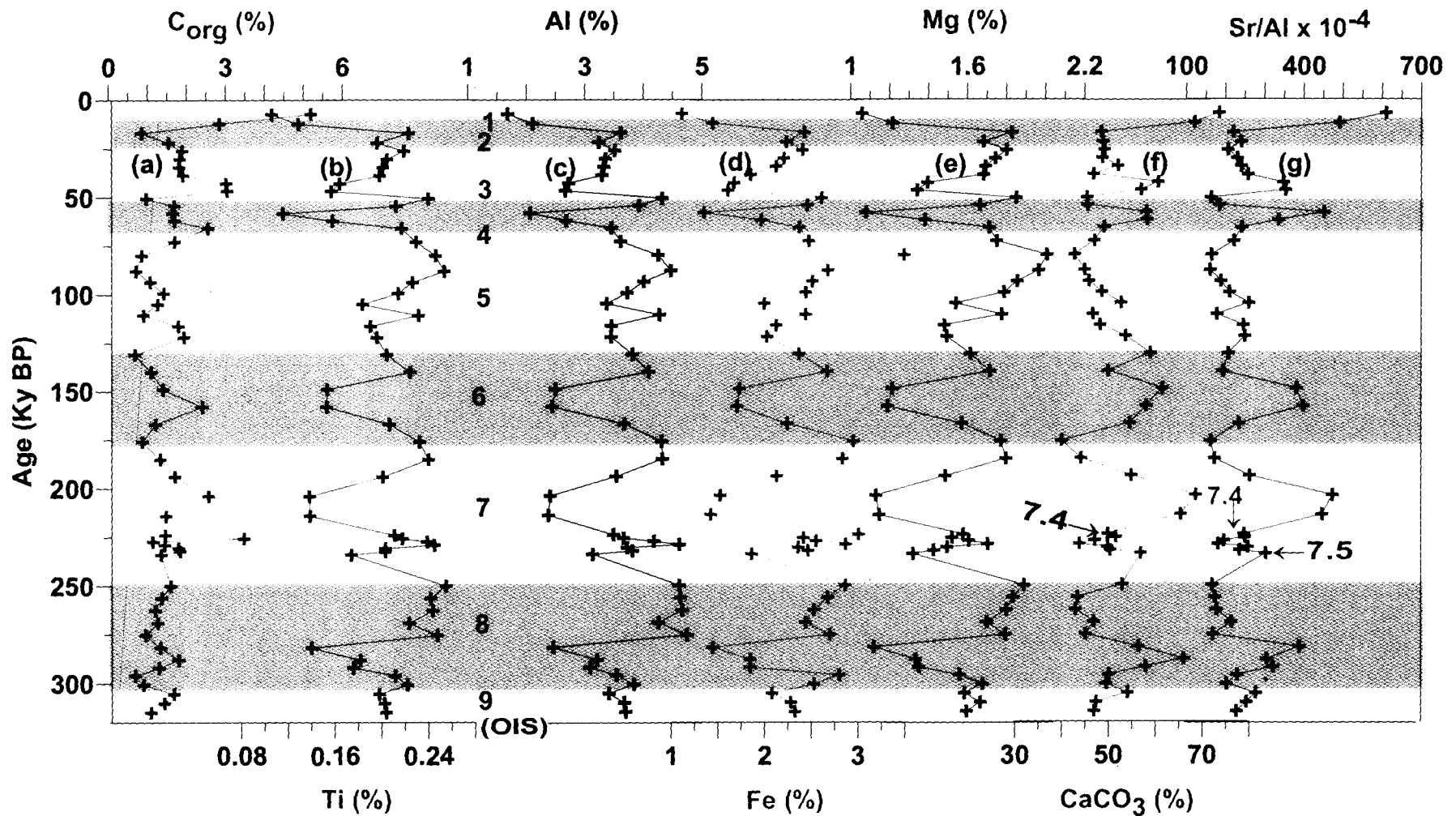
Figure 5.19 : Variations of major elements (Ti, Al, Fe, Mg and Sr) in comparision with C_{org} and $CaCO_3$ (indicator of overhead productivity) during various glacial-interglacial stages in core AAS-42/12A. Profiles of Ti, Al, Fe, Mg are presented with their total concentration while Sr is normalized to Al. Glacial stages are indicated by shading. Oxygen Isotope stages (OIS, 1-9) are indicated.

observed average values in both cores are very high compared to the average shale value (38 x 10^{-4}). In both the cores, the ratios during the Holocene are higher than those during other stages. Agnihotri et al. (2003a) observed a similar relation between Sr/Al and $CaCO_3$, with the average Sr concentration being 75% in excess over the average shale abundance. The high ratio of Sr/Al observed during the interglacial periods can be attributed to intense SWM promoting chemical weathering and transportation of Sr from the Deccan source.

The Sr/Al profile shows sharp decrease from the Holocene to the LGM in both the cores (Figure 5.18g and 5.19g), which was also observed by Sirocko et al. (2000) in a core from the western Arabian Sea. However, he ascribed the observed decrease to the lysocline effect as the core came from a water depth of 3200m (74KL), above the lysocline depth of ~2900m (Kallel et al., 1988; Kolla et al., 1976a). Due to shallower water depths, such effect can be ruled out for the cores examined in the present study and the decrease in Sr/Al ratio observed during the LGM or other stages such as 7.4 in core AAS-42/12A (Figure 5.19g) can be attributed to the weakening of the SWM.

5.3.7.2 Downcore variations in trace elements

Metals such as Fe, Mn, Cd, Mo, V and Re, which are commonly referred to as redox-sensitive metals, have been used for investigating changes in the oxidation state of the overlying water column and sediments during sediment deposition (Van Geen et al., 1996; Crusius et al., 1996;

Zheng et al., 2000b; Pailler et al., 2002; Nameroff et al., 2002, 2004). A number of processes affect the deposition of metals in the underlying sediments; some of them are discussed below.

5.3.7.2.1   Processes involved in accumulation of metals in sediments

1. *Depositional environment:* It includes redox states of water column and metals (solubility or precipitation in oxic or suboxic/anoxic environments). The principal factor controlling the redox state of the sediment is the balance between the flux of organic matter to the seafloor and the flux of oxidants to the sediments from the overlying seawater (Emerson et al., 1985). Thus, variations in sedimentary redox state are linked to the changes in pelagic export production and the vigour of water circulation.

2. *Adsorbtion onto other particulate matter and the flux of biological material:* Some fraction of the metal present above the background concentration is due to the delivery of metals through settling biological material to the sediment (e.g., Zheng et al., 2000b; Nameroff et al., 2002). However, most of the enrichment results from the changing redox conditions that occur as organic matter is degraded by the thermodynamically predictable sequence of oxidants (O_2, NO_3^-, Mn (IV), Fe(III) and SO_4^{2-}) (Froelich et al., 1979). Consequently, under optimal conditions, one should be able to use enrichments and depletions of individual trace metals to identify the redox conditions that prevailed in both the bottom water and in the sediment during sediment deposition.

3. *Diagenesis*: This includes processes that frequently, and sometimes extensively, modifies the original extent of metal enrichment in the upper layer of sediment (Calvert and Pedersen, 1993; Crusius et al., 1996; Gobeil et al., 1997, 2001). Authigenic inputs (fraction of metal added in sediment after deposition) of metals can also occur during diagenesis. In fact some of the minerals like Evaporite (common evaporite minerals are halite, gypsum and anhydrite, which can form as seawater evaporates, and the rocks limestone and dolostone) are authigenically (insitu) formed. The small amount of metals that are preserved in the geological record may reflect the redox conditions of this diagenetic modification in the sediments rather than those of the overlying water.

The effect of early diagenesis on redox-sensitive metal concentration buried into the geological record has not been well documented. However, Nameroff et al. (2002) investigated this aspect by analyzing redox-sensitive metals from the sediments of northwestern Mexican Margin together with the analysis of sinking particles and water column parameters. She observed signatures of diagenesis occurring in the sediments, but the concentrations of Cu, Ba, Cd, Mo, Re, U and V in the water column were unaffected by the low-O_2 conditions in the OMZ.

There exists very little information about the phases that control metal enrichment and the kinetics of their formation, and the understanding of the transport of metals by sinking particles. The post depositional diagenetic reactions that alter the distribution of metals in sediments is far from satisfactory, left alone, completely. Despite these limitations, the

concentrations of Mn, Fe, Cd, U, Mo, V and Re in marine sediments are promising tracers of the redox state of the sediment and overlying waters.

5.3.7.2.2 Evaluation of trace elements as ideal redox tracers

Sedimentary records of trace metals such as Fe, Mn, Cu, Mo, Cd, Re, U and V provide important clues to how the redox state of depositional environments has changed over time. It is equally important to know the chemistry of the redox- sensitive trace elements and their behaviour in the water column including their modes of transport from one phase to the other. Table 5.11 lists the characteristics of different redox-sensitive trace elements of interest here.

5.3.7.3 Glacial – interglacial variability of redox-sensitive trace metals

Downcore profiles of redox-sensitive trace metals (normalized to Al) are presented in figure 5.20 (for core AAS-42/15) and figure 5.21 (for core AAS-42/12A). Profiles of the denitrification proxy ($\delta^{15}N$) and the bottom water oxygen indicator ($\delta^{13}C_{C.wuell}$) are also presented for comparison. Both the cores show variations in response to the bottom water variability instead of the intermediate OMZ characteristics. Tables 5.12 (AAS-42/15) and 5.12 (AAS-42/12A) provides the trace metal concentration data while element/Al ratio data is presented in table 5.14 (AAS-42/15) and table 5.15 (AAS-42/12A)

Core AAS-42/15

All redox-sensitive elements show higher concentrations during the

Figure 5.20: Down core variations of redox sensitive elements (Fe, Mn, V, Co, Mo) in comparision with $\delta^{13}C$ of benthics (indicator of bottom water oxygen) and $\delta^{15}N$ (denitrification proxy) during various glacial-interglacial stages in core AAS-42/15. Glacial stages are indicated with shaded portions. Oxygen Isotope stages (OIS, 1-6) are indicated.
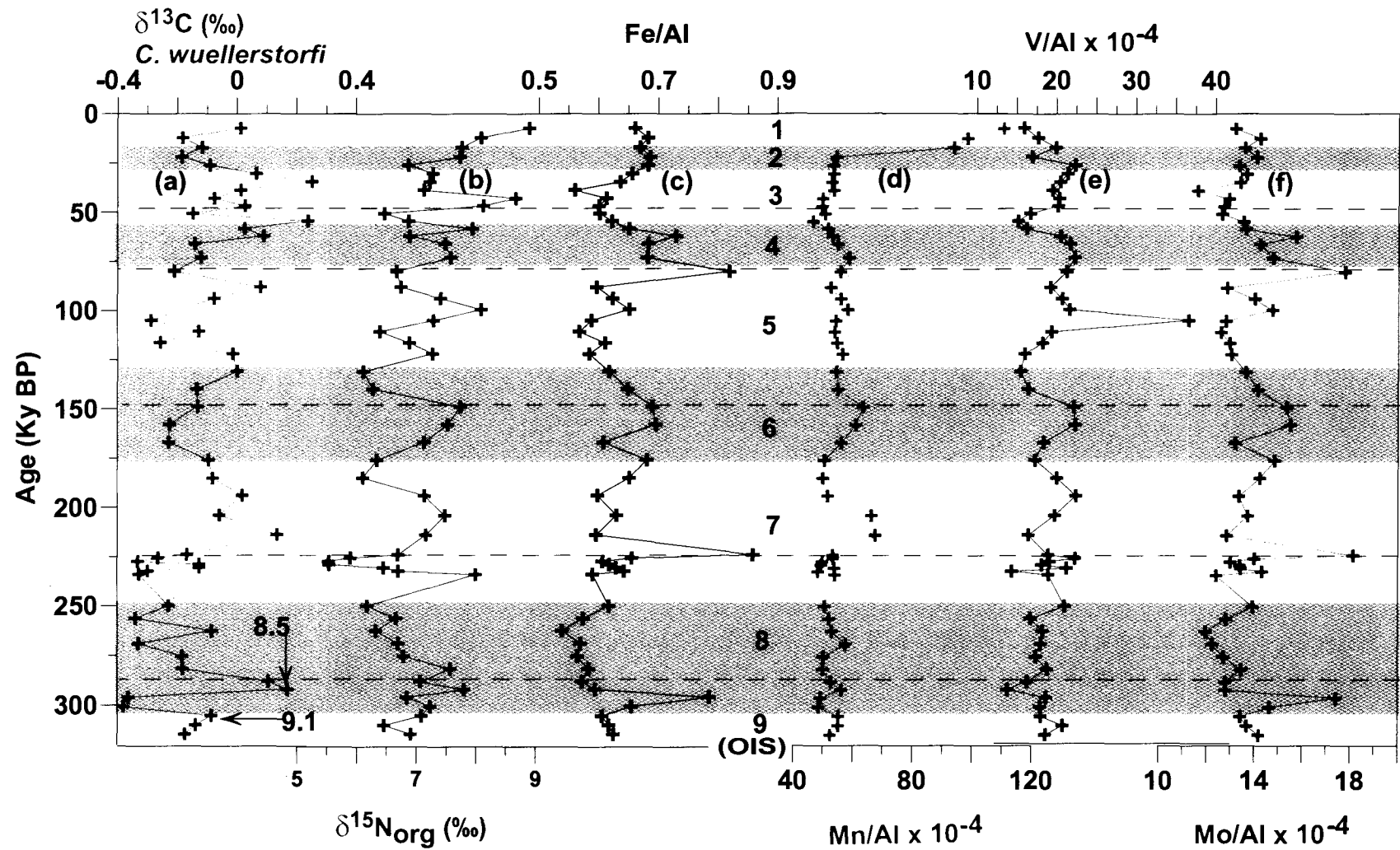
Figure 5.21: Down core variations of redox sensitive elements (Fe, Mn, V, Mo) in comparision with $\delta^{13}C$ of benthics (indicator of bottom water oxygen) and $\delta^{15}N$ (denitrification proxy) during various glacial-interglacial stages in core AAS-42/12A. Glacial stages are indicated with shaded portions. Oxygen Isotope stages (OIS, 1-9) are indicated.

Holocene (Figure 5.20). Fe and Mn should have been depleted in the Holocene sediments, showing a trend opposite to that of the $\delta^{15}N$ profile, had they been exposed to the OMZ. This is because Fe and Mn precipitates under oxic condition and get solubilised in reducing environments (Calvert and Pedersen, 1993). Instead, both the profiles (Fe/Al and Mn/Al) follow the same trend as $\delta^{15}N$ and $\delta^{13}C_{C.wuell}$. This general behavior persists throughout the cores, which suggests that the characteristics of bottom water that affects the sedimentary Fe and Mn distribution have contrasted those at intermediate depths.

The average Mn/Al ratio in the core is ~74 x 10^{-4}, which is less than the average shale value (~106 x 10^{-4}; Turekian and Wedepohl, 1961; please refer to table 4.xx for the average shale values in chapter 4). The lower Mn/Al ratio suggests a net Mn loss from the sediments particularly during glacial periods (as indicated by lower values during such periods) when the bottom water oxygen concentrations appear to have decreased (Figure 5.22d). Agnihotri et al. (2003a), Sirocko et al. (2000), Nameroff et al. (2004), Higginson et al. (2004) also reported lower values of Mn and higher values of Mo, V, Co in cores that were exposed to reducing environment during sediment deposition.

The Fe/Al ratio varied within a range of 0.55 to 0.75 with an average value of 0.63, which is slightly higher than the average shale value of ~0.55 (Wedepohl, 1971, 1991). The relatively higher Fe concentrations are probably due to the large amounts of Fe supply from the Fe-rich basalts of the Deccan Traps. Sirocko et al. (2000) recorded lower contents of Fe in sediments of the western Arabian Sea off Yemen compared to the eastern Arabian Sea off
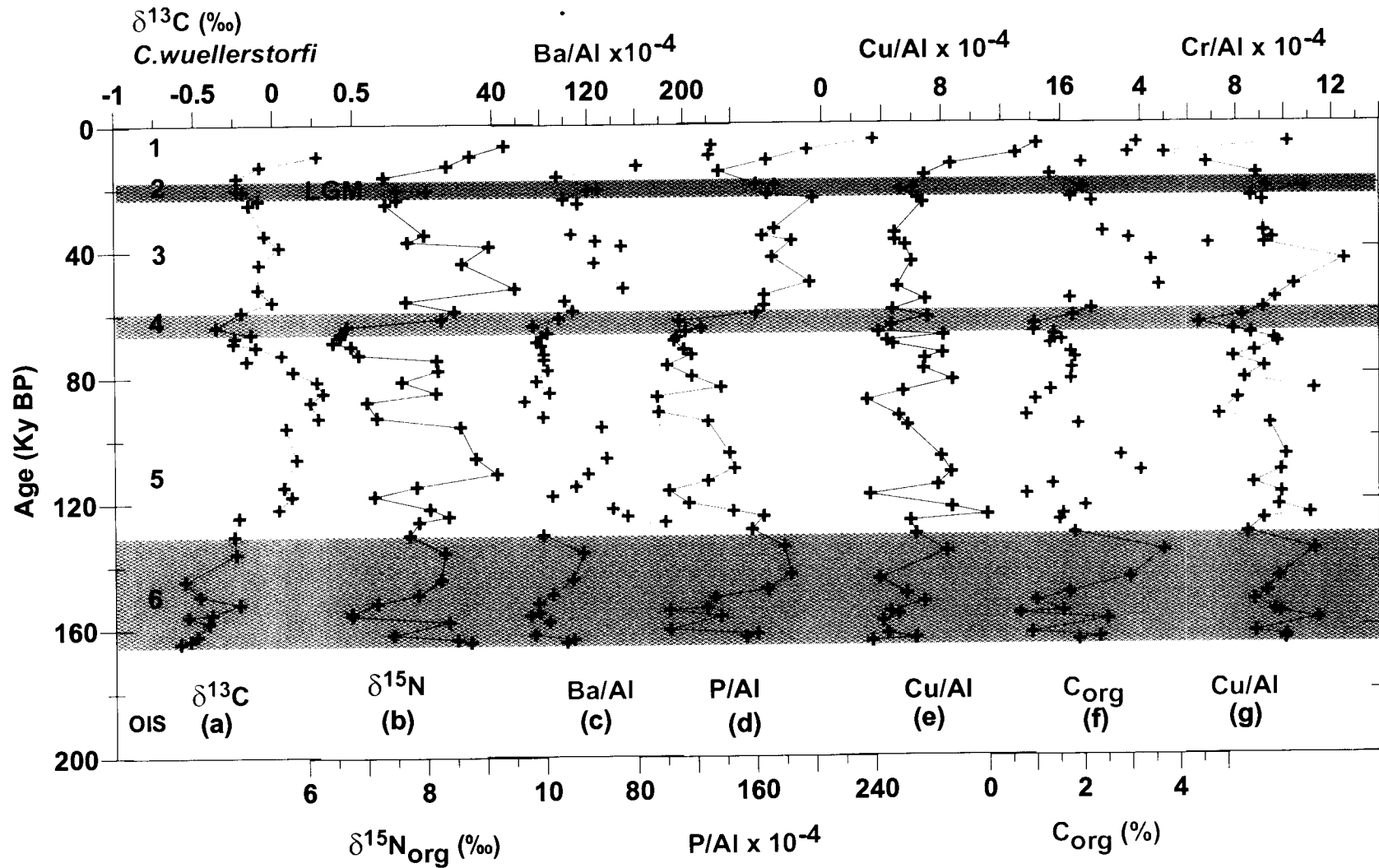
Figure 5.22: Temporal variability of productivity proxies and micro-nutrient type elements in comparison with $\delta^{13}C$ of benthics, $\delta^{15}N$ and C_{org} during various glacial-interglacial stages in core AAS-42/15. Glacial stages are indicated by shading. Oxygen Isotope stages (OIS, 1-6) are indicated.

India. He suggested the dust from Persian Gulf area is the predominant source of Fe in the western Arabian Sea and the Fe-rich basalts of the Deccan Traps in the eastern Arabian Sea.

V, Co and Mo are known to precipitate out from seawater under reducing conditions (Piper and Isaacs, 1996), and accordingly get enriched in the sediments. As observed in the profiles of these elements (Figure 5.20e,f,g), the values for V/Al, Co/Al and Mo/Al remain within narrow ranges of 10-28 x 10^{-4}, 0-5 x 10^{-4} and 12.5-16 x 10^{-4}, respectively. These elements are generally found to be enriched during the interglacial periods (especially V during OIS 3) compared to the glacial stages except during the LGM when higher values occur for all the three elements. The observed average value of ~19 x 10^{-4} for V/Al is slightly higher than its average shale value of 16 x 10^{-4} while the average value of ~13 x 10^{-4} for Mo/Al is much higher than the corresponding shale value of 0.15 x 10^{-4}. The average value of 1 x 10^{-4} for Co/Al ratio is, by contrast, half of the average shale value of 2.1 x 10^{-4}. Co concentration can be controlled by scavenging, uptake by organisms in the euphotic zone or adsorption onto Mn-hydroxides. In suboxic waters Co can be removed from the solid Mn and Co-phases and also after deposition the labile Co^{3+} can be transformed into Co^{2+} in reducing environments and become mobile like Mn (German and Elderfield, 1990). The low average value suggest that it is not enriched in sediments but with whatever amount is present follows the trend of productivity which is more during the interglacial and lower during the glacial periods. The enormously high value of Mo/Al could be due to its adsorption onto the Mn-oxyhdroxides (Shimmield and Price, 1986). The

solid phase of Mn-oxyhdroxide leads to the sorption enrichment of V too (Shaw et al., 1990; Nameroff et al., 2004) in oxic sediments, which could be the reason for its enrichment throughout the core. Reduced V and Mo are found to be adsorbed strongly onto particle surfaces without forming any sulphides (Wehrli and Stumm, 1989). Thus, the enrichment of V, Co and Mo observed during the interglacial compared to the glacial periods could be due to their adsorption on the particle surfaces resulting from higher productivity.

Core AAS-42/12A

The behaviours of redox-sensitive elements in this core are clearer, although somewhat different from those in core AAS-42/15. The Fe/Al profile exhibits enrichment during the glacial periods, with lower concentrations occurring during the interglacial times which mirror the $\delta^{15}N$ and $\delta^{13}C$ profiles. Profiles of Mn/Al, V/Al, Mo/Al showed similar trends as Fe/Al (Figure 5.21). The range of values observed for Fe/Al, Mn/Al, V/Al and Mo/Al are 0.54-0.79, 46-110 x 10^{-4}, 14-37 x 10^{-4} and 11–18 x 10^{-4}, respectively.

The average value of ~0.64 for Fe/Al is higher than the average shale value (~0.55) probably because of Fe inputs from basalts of the Deccan traps. However what is more important is its variability over the glacial-interglacial timescales. In the case of Mn/Al, except for the very high values in the Holocene sediments, the overall average value of ~56 x 10^{-4} is half of the average shale value (~106 x 10^{-4}), indicating mobilization of Mn from the sedimentary column, a process commonly observed in reducing sediments (Somayajulu et al., 1994; Agnihotri et al., 2003a, 2007).

The average values for V/Al ($\sim$19 x 10^{-4}), is slightly higher than its average shale value ($\sim$16 x 10^{-4}), while the average value for Mo/Al ($\sim$14 x 10^{-4}) is much higher than the corresponding average for the shale ($\sim$0.15 x 10^{-4}). Sirocko et al. (2000) found maximal values of Mo in sediments from the Indian continental margin, where C_{org} concentrations are very high (Marchig, 1972, 1974). He also reported high Mo values on the Carlsberg ridge in the glacial sediments, though the reason for its accumulation could not be ascertained. However, in view of the results of Shankar et al. (1987) from the Carlsberg ridge, the variation of Mo during the Holocene was suggested to be controlled by C_{org} while the enrichment during LGM was attributed to slower deep water ventilation (Sarkar et al., 1993) in addition to the linear response to the coherent C_{org} increase. The exorbitantly high values in Mo/Al could again be due to its adsorption onto the oxyhydroxides of Fe and Mn (Bertine and Turekian, 1973; Manheim, 1974; Kato et al., 1995; Cruisius et al., 1996) thus following their pattern of enrichment in sediments. The higher values in glacial sediments could be the effect of C_{org} and slower ventilation of bottom waters, even though, as stated earlier, these waters were not reducing/anoxic as inferred by Sarkar et al. (1993).

In oxygenated waters, the stable form of V(V) is vanadate, which gets adsorbed onto both Mn and Fe-oxyhydroxides (Wehrli and Stumm, 1989, Calvert and Piper, 1984). The higher contents of V/Al during the glacial periods again indicate more oxygenated bottom waters and the values on the higher side during the interglacial if at all, may be due to reduced vanadyl ion, $V(IV)O^{2+}$ which binds even more strongly to the chelating surface groups than

the larger anionic vanadate. However V reduction occurs below the level of either Mn or Fe oxyhydroxide reduction (Shaw et al., 1990; Kato et al., 1995; Hastings et al., 1996). The average value of V/Al being slightly more than the average shale value indicates its enrichment due to adsorption on Fe and Mn-oxyhydroxides in oxygenated waters thus indicating the bottom waters to be oxygenated. However, this is not consistent with the other evidence (especially $\delta^{13}C_{C.wuel}$) discussed above.

Cr, another trace metal, also occurs in sea water in at least two oxidation states and precipitates in its lower oxidation state, the predominant oxidized state being Cr(VI), chromate ion and, to a lesser extent, as the cationic Cr(III) aquahydroxy species $Cr(OH)_2^+$ $(H_2O)_4$ (Elderfield, 1970; Cranston and Murray, 1978; Cranston, 1983; Murray et al., 1983). Enrichments of Cr in sediments can be due to high proportions of detrital chromite, high Cr contents in clay-minerals or trapping of Cr in strongly reducing sediments. Cr concentrations in both cores average to ~35μg/g (Table 5.12 and 5.13) which is not even half of the average shale value (90μg/g). However, the Al-normalized Cr values fall within a range of 7-13 x 10^{-4} with average value of 9 x 10^{-4} for core AAS-42/15 (Figure 5.22g), while for core AAS-42/12A the range is 7-16 x 10^{-4} with an average of 10.8 x 10^{-4} (Figure 5.23g). The average normalized shale value of 11 x 10^{-4} for Cr/Al, is slightly higher compared to the value in core AAS-42/15 and almost same as the value in core AS-42/12A, suggesting the origin of Cr to be clastic in both the cores. Sirocko et al. (2000) recorded very high Cr contents which they attributed to inputs from the ophiolite-rich strata of Iran, Pakistan and Oman
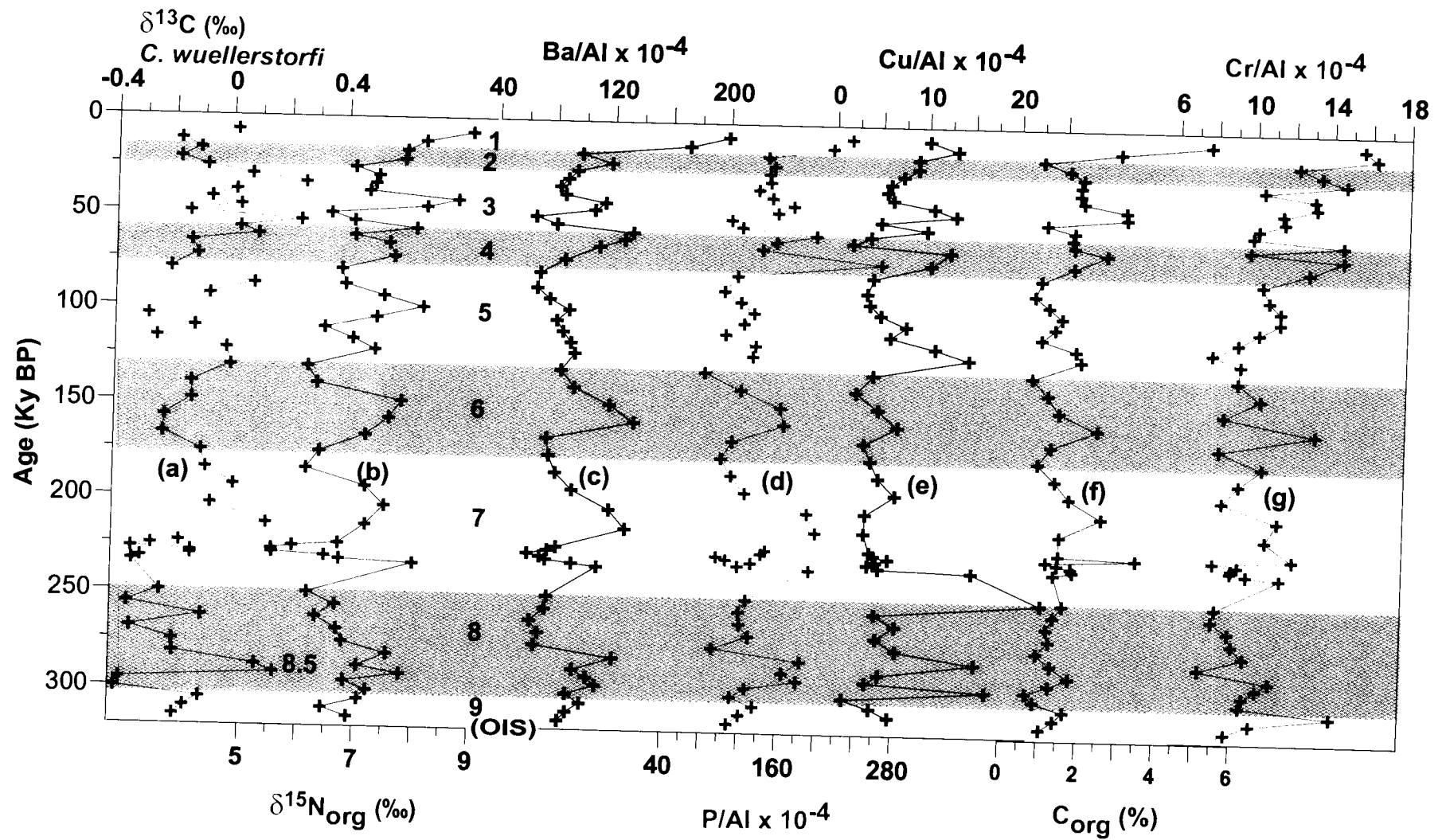
Figure 5.23: Temporal variability of productivity proxies and micronutrient type elements, in comparison with $\delta^{13}C$ of benthics, $\delta^{15}N$ and C_{org} during various glacial-interglacial stages in core AAS-42/12A. Glacial stages are indicated by shaded portions. Oxygen Isotope stages (OIS, 1-9) are indicated.

transported by the northwesterly winds blowing from the Persian Gulf region. The Cr data (both concentration and Al-normalized ratio) indicate the absence of reducing environments in bottom waters during sediment deposition. Thus, Cr distribution in both cores seems to be controlled by the aeolian transport from land and does not point to the prevalence of reducing conditions in the overlying water column.

Notwithstanding some inconsistencies in the redox-sensitive metal data among the two cores and even within the same core, one general conclusion that can be drawn from the above discussion is that the bottom waters at the study sites were perhaps never reducing over the investigated time period, even though substantial changes in bottom water oxygen concentration (i.e. decreases during the glacial periods) did occur in response to changes in circulation and associated shifts in the vertical hydrographic structure. It is likely that the decreased oxygen concentrations favoured the development of reducing conditions in the sediments, though.

5.3.7.4 Barium as a productivity proxy

Barium (Ba) has been employed as a productivity proxy ever since Goldberg and Arrhenius (1958) showed its enrichment in equatorial Pacific sediments. This was later supported by Dymond et al. (1992) who observed a linear relationship between Ba and C_{org}. This approach has been followed by several researchers (Bishop, 1988; Shimmield and Mowbray, 1991; Dymond et al., 1992; Francois et al., 1995, Prakash Babu et al., 2002). Schmitz (1987) even employed the Ba proxy for tracing the northward drift of the Indian plate

during the Cenozoic period; higher Ba concentrations were interpreted corresponding to the time when this plate was located below the equatorial high productivity belt. For more recent times, Shimmield and Mowbray (1991) found greater Ba abundance off Oman during interglacial periods due to enhanced productivity.

Ba/Al ratio ranges from 66 to 224 x 10^{-4} (Figure 5.22c), with an average value of 110 x 10^{-4} in core AAS-42/15, and from 64 to 198 x 10^{-4} (Figure 5.23c) with an average of 97 x 10^{-4} in core AAS-42/12A. In both cores the average values are higher than the average shale value (75 x 10^{-4}). The highest Ba contents are found in sediments rich in biogenic opal, since diatom frustules can contain up to 30,000 ppm Ba (Collier and Edmond, 1994). Ba present in the water column can be removed by either adsorption or formation of barite ($BaSO_4$) in reducing micro-environments of sinking organic particles (Bishop et al., 1977). The glacial-interglacial distribution pattern of Ba/Al follows a trend similar to that of C_{org}, with higher concentrations occurring during the interglacial and lower values during the glacial periods. This is consistent with the removal of Ba from seawater by adsorption on sinking organic particles whose flux would increase during interglacial periods of high productivity as seen in figure 5.22c,f (AAS-42/15) and figure 5.23c,f (AAS-42/12A). Lower values of the Ba/Al ratio during the glacial periods would conversely be due to decreased productivity.

The high Ba/Al values observed in both the cores also suggest that the bottom water conditions remained oxygenated during the depositional periods of the sediments. This is because the ratio has been known to fall in reducing

environments (McManus et al., 1998). This observation is at variance with the results of Agnihotri et al. (2007) who found significant depletion of Ba/Al (by a factor of 4), relative to its average shale abundance in the eastern Arabian Sea. However, as discussed in Chapter 4, the data from the shallower cores do demonstrate reductive losses of Ba. Finally, as the Ba/Al ratio in both cores follows the same pattern as C_{org} it lends further support to inferences about productivity changes based on the C_{org} abundance, and in turn the variability of the SWM strength.

5.3.7.5 Glacial-interglacial variability of nutrient-type elements

Profiles of sedimentary concentrations of the elements having nutrient type behavior, viz. P, Cr and Cu, are given in figure 5.22d,e (AAs-42/15) and figure 5.23d,e (AAS-42/12A). Phosphorus (P) is a major micronutrient and also has detrital supply from the igneous and sedimentary rocks with typical concentrations of < 0.1%, but values exceeding 0.15% may occur in deep sea clays (Sirocko et al., 2000). Sirocko et al. (2000) measured P content in the Arabian Sea sediments varying between 0.07% and 0.15%. The P concentrations observed in the present study are < 0.07% for both the cores (Table 5.12 and 5.13) indicating low detrital supply. In order to look for changes in the non-detrital component of P, its concentration was normalized with Al. The ranges of the P/Al ratio observed are 92-240 x 10^{-4} with an average of 145 x 10^{-4} for core AAS-42/15, and 92-260 x 10^{-4} with an average of 138 x 10^{-4} for core AAS-42/12A. In both cases the average values are higher than the average shale value (88 x 10^{-4}), thereby suggesting the

dominant presence of non-detrital P. Moreover, a visual covariance is seen among P/Al and C_{org} (Figure 5.22d,f and 5.23d,f) profiles in both the cores at all times.

Among the trace metals, Cu exhibits a unique characteristic in that it behaves partly like a micronutrient but is also scavenged from solution in the deep water (Calvert and Pedersen, 1993). Ni and Zn show variations similar to nutrients. The nutrient type behavior of Cu was earlier demonstrated by Bruland (1980) and Broecker and Peng (1982), who found the concentration of Cu in ocean waters to increase with depth. This is also supported by the chemical composition of plankton (Collier and Edmond, 1984). The mineral concentration of Cu averages between 5 and 100 $\mu g/g$, with basalts having the highest values and feldspars-rich rocks the lowest (Turekian and Wedepohl, 1961). In the present study, observed ranges of Cu concentration (Table 5.12 and 5.13) in both cores are rather narrow with an average value of ~25 $\mu g/g$. Going by the concentrations alone, it would appear that Cu deposited in the sediments, was mostly detrital. However, when the Cu concentrations are normalized with Al, the ratios in both cores again remain within narrow ranges with values varying from 3 to 14 x 10^{-4} and averaging 6.5 x 10^{-4} for core AAS-42/15 (Figure 5.22e), and from 2 to 23 x 10^{-4} with an average of 7.3 x 10^{-4} for the core AAS-42/12A (Figure 5.23e). The averages are marginally higher than the shale average of 6 x 10^{-4} (Turekian and Wedepohl, 1961) indicating the presence of non-detrital Cu which can be attributed to its nutrient type behavior. Saager et al. (1992), Sirocko et al. (2000), Agnihotri et al. (2007) have also reported the nutrient type behavior of

Cu in the Arabian Sea.

5.3.8 Synthesis on Paleo-Productivity based on various proxies

Organic Carbon (C_{org})

C_{org} is a paleo-productivity proxy often used (e.g. Ganeshram and Pedersen, 1998; Agnihotri et al., 2001a). The downcore records of C_{org}, N_{org}, and $CaCO_3$ in core CR-2 (Figure 4.4a,b,c), showed prominent minima during ~1650-1750 AD, a period that coincides the Little Ice Age (LIA, from 1500 to 1750 AD). All the three variables covaried suggesting close relations between organic and inorganic (calcareous) productivity in the region during the deposition period. A distinct increase in concentrations was also observed in C_{org}, and N_{org} in the last 4-5 decades indicating increased productivity.

C_{org} and N_{org} records in SaSu-1 (Figure 4.7a,b) and SaSu-3B (Figure 4.8a,b) also revealed increased productivity during the last 4-5 decades after ~60 y BP (~1940 AD). The concentration of C_{org} was as high as 5.3% in the recent years in SaSu-3B (core very close to coast) indicating enhanced productivity probably due to increased anthropogenic activities. The $CaCO_3$ profile covaried with C_{org} for SaSu-1 core (Figure 4.7c), except in the last two decades where $CaCO_3$ decreased rapidly suggesting decreased inorganic productivity. $CaCO_3$ varied between 4 and 8% in SaSu-3B (Figure 4.8c) with a prominent decreasing trend upward.

Variations in C_{org} profile for the deep gravity cores (AAS-42/15 and AAS-42/12A) suggest higher productivity during the warmer-interglacial stages as compared to cold glacial stages in general, with prominent

variations in core AAS-42/15. The highest C_{org} values for core AAS-42/15 occurred during the warmer OIS 3. N_{org} and $CaCO_3$ profiles also exhibited trends similar to that of C_{org}, albeit with different amplitudes (e.g. the $CaCO_3$ minimum for OIS 4 was much more pronounced than for the LGM, Figure 5.9a,b,e). In core AAS-42/12A, C_{org}, N_{org} and $CaCO_3$ profiles also covaried with the highest values during the Holocene (Figure 5.10a,b,e). As both the cores are located in the regions that come under the influence of South West Monsoon (Satya Prakash and Ramesh, 2007), higher productivity during the interglacials was attributed to stronger SWM. The weakening of SWM during the glacial periods resulted in lower productivity as reflected by the C_{org}, N_{org} and $CaCO_3$ proxies.

Barium (Ba)

Ba normalized to Al (Ba/Al) is a reliable paleo-productivity proxy in the oxic sediments when the terrestrial contribution is smaller. The downcore profile of Ba/Al (Figure 4.6d) in CR-2 did not agree with the C_{org} record. It was depleted by a factor of 4 relative to its average shale abundance of 75. In SaSu-1 and SaSu-3B also Ba/Al showed significant depletion (factor of 4.5) relative to its average shale value (Figure 4.24a,b). In all the three coastal cores, depleted Ba/Al values suggested the occurrence of strong reducing conditions in the cores thereby proving it to be a redox sensitive proxy rather than a productivity proxy under reducing conditions.

Ba/Al ratio ranged from 66 to 224 x 10^{-4} (Figure 5.22c), with an average value of 110 x 10^{-4} in core AAS-42/15, and from 64 to 198 x 10^{-4} (Figure 5.23c) with an average of 97 x 10^{-4} in core AAS-42/12A. In both the cores

average values were higher than the average shale value (75×10^{-4}). The highest Ba contents are found in sediments rich in biogenic opal, since diatom frustules can contain up to 30,000 ppm Ba (Collier and Edmond, 1994). Ba present in the water column can be removed by either adsorption or formation of barite ($BaSO_4$) in reducing micro-environments of sinking organic particles (Bishop et al., 1977). The glacial-interglacial distribution pattern of Ba/Al followed the trend of C_{org}, with higher concentrations occurring during the interglacial and lower during the glacial periods. This is consistent with the removal of Ba from seawater by adsorption on sinking organic particles whose flux would increase during interglacial periods of high productivity as seen in Figure 5.22c,f (AAS-42/15) and Figure 5.23c,f (AAS-42/12A). Lower values of the Ba/Al ratio during the glacial periods would obviously be due to decreased productivity. The high Ba/Al values observed in both the cores also suggested that the bottom water conditions remained oxygenated during the depositional periods of the sediments.

Phosphorus (P)

Phosphorus (P) which is a macro nutrient in the water column is also expected to reflect productivity changes occurring in the water column. In order to investigate variations in the non-detrital component of P, it was normalized with Aluminum (Al). A covariance was observed between P/Al and C_{org} (Figure 4.5d and 4.18d) in core CR-2 and SaSu-1, ensuring that non-detrital P/Al ratio could be used in deciphering productivity variations of the past. While no substantial similarity was observed between the P/Al and C_{org} records in SaSu-3B core (Figure 4.19d). However the P/Al ratios in all the

three cores were found to be considerably higher (factor of 2-3) relative to its average shale value of 88×10^{-4}.

A covariance was also seen between P/Al and C_{org} profiles (Figure 5.22d,f and 5.23d,f) in both the deep cores at all times. Also the average values of P/Al ratio (145×10^{-4} for core AAS-42/15 and 138×10^{-4} for core AAS-42/12A) in both cores were higher than the average shale value suggesting the dominant presence of non-detrital P. From the above observation, P/Al was found to serve as a productivity proxy in the gravity cores.

Copper (Cu) and Nickel (Ni)

In addition to C_{org}, N_{org}, $CaCO_3$, Ba and P non-detrital components of Copper and Nickel (in terms of Cu/Al and Ni/Al) can also be used as productivity proxies, as these elements act as micronutrient which are removed from surface waters during plankton growth, but released during decomposition in the sub-surface waters (Calvert and Pedersen, 1993). The Cu/Al and Ni/Al profiles did not exhibit any excess over its average shale value in all the three shallow cores viz CR-2 (Figure 4.6e,f), SaSu-1 (figure 4.25a,c) and SaSu-3B (Figure 4.25b,d). Nonetheless, the Cu/Al record in CR-2 and Ni/Al record in SaSu-3B does show a general trend of increase in the last few decades - the period of high productivity.

Variations in Cu/Al ratio in both the deep cores again remained within narrow ranges, with values averaging about 6.5×10^{-4} for core AAS-42/15 (Figure 5.22e) and 7.3×10^{-4} for core AAS-42/12A (Figure 5.23e). The averages are marginally higher than the shale average of 6×10^{-4}, indicating

the presence of non-detrital Cu which, can be attributed to its nutrient type behavior. As Ni could not be measured, use of Ni/Al could not be ascertained in these cores.

5.4   Conclusions

A number of proxies analyzed in two deep gravity cores raised from the northeastern Arabian Sea, in the region that experiences some of the most intense denitrification in the oceanic water column today at intermediate depths, exhibit significant downcore variations on the glacial-interglacial timescale. The major conclusions of the chapter are as follows:

1. The magnitudes of glacial to interglacial (LGM to Holocene) shift in $\delta^{18}O_{G.ruber}$ for the two cores substantially exceed the global ice volume effect (1.2‰) by 0.35‰ in AAS-42/15 and by 0.23‰ in AAS-42/12A. These shifts are smaller than those reported previously from the region and could be explained by a glacial decrease in SSTs by ~2°C without invoking any change in salinity.

2. The observed amplitude of ~1.25‰ in $\delta^{18}O_{C.wuell}$ for core AAS-42/15 is almost the same as the global ice volume effect and supports the view that bottom water (depth ~2.5 km) temperature and salinity during the LGM were probably similar to their present-day values.

3. The $\delta^{13}C_{C.wuell}$ record exhibits high and low values during the interglacial and glacial stages respectively, in both the cores, suggesting that bottom waters were well oxygenated during the interglacial period and comparatively less oxygenated during the glacial maxima.

4. Variations observed in all biogenic proxies in both the cores indicate that biological productivity had been higher during interglacial periods than the glacial periods. This is arguably due to vigorous upwelling associated with intense SWM during interglacials, with the intensity having decreased during glacial times. The $\delta^{13}C_{org}$ and C/N ratios demonstrate that the sedimentary organic matter at the study sites remained predominantly of marine origin throughout the depositional history of the core.

5. In conformity with earlier reports, marked changes in water-column denitrification intensity appear to have occurred in the geological past with the process being generally more intense during the interglacial periods (especially the Holocene and OIS 3) and less intense during the glacial maxima. At the LGM, the process was greatly subdued but not completely shut off, and it was even less intense (probably absent) during OIS 4. However, the most important result obtained in the present study is that the sedimentary $\delta^{13}N$ and $\delta^{13}C_{C.wuell}$ seem to have co-varied in AAS-42/15 such that there was a sea-saw variability in oxygen concentrations in deep water (depth ~2.5 km) and the mesopelagic (the depths of the present-day OMZ). That is, when the mesopelagic oxygen levels were lower, supporting denitrification (during interglacial periods such as today), deep-water oxygen was higher and vice versa. This shift in the vertical hydrographic structure probably resulted due to intrusion of ventilating water from the south at shallower depths during the LGM (in response to changes in the deep water formation in the North Atlantic). This has been previously proposed to occur in the Arabian Sea during the LGM, but the present study shows that this was a

common feature of all glacial stages.

6. Good correspondence between the Ba/Al and C_{org} records on one hand and $\delta^{15}N$ on the other suggest that changes in productivity along with those in circulation contributed to the observed changes in the denitrification intensity. It is pointed out that the changes in productivity and ventilation are related, often working in the same direction.

7. Records of redox-sensitive metals exhibit changes that mostly relate to the $\delta^{13}C_{C.wuell}$ record rather than the $\delta^{15}N$ record, which is not surprising given that the denitrifying zone lies much above the seafloor at the coring sites. The trace metal distributions generally suggest that bottom waters at the study sites had never been reducing over the investigated time period, even though substantial changes in bottom water oxygen concentration did occur in response to changes in circulation and associated shifts in the vertical hydrographic structure. However, it is likely that the decreased oxygen concentrations favoured the development of reducing conditions in the sediments.

Table 5.3

Oxygen isotope ($\delta^{18}O$) data using planktonic foraminifer (*Globigerinoide ruber*) for cores AAS-42/15 and AAS-42/12A.

AAS-42/15		AAS-42/12A	
Core Depth (cm)	$\delta^{18}O$ (‰)	Core Depth (cm)	$\delta^{18}O$ (‰)
0	-1.33	0	-1.33
10	-1.73	10	-1.64
20	-1.61	20	-0.28
30	-0.88	30	-0.26
48	-0.17	40	-0.46
50	-0.25	50	-0.21
70	-0.29	60	-0.80
80	-0.73	70	-0.73
116	-0.78	80	-0.93
124	-0.65	90	-0.70
130	-0.77	100	-0.77
138	-0.64	110	-0.48
150	-1.23	120	-0.51
160	-0.76	130	-0.64
168	-0.64	140	-0.22
174	-0.62	150	-1.02
180	-0.52	160	-1.37
188	-0.62	170	-0.86
192	-0.89	180	-1.44
198	-0.86	190	-1.24
202	-0.83	200	-1.54
212	-0.70	210	-1.79
218	-1.01	220	-1.85
230	-1.18	230	-3.16
240	-0.97	240	-0.80
250	-1.04	250	-1.06
258	-0.94	260	-0.73
264	-1.12	270	-0.77
270	-1.31	280	-1.02
280	-1.01	290	-0.29
290	-1.02	300	-1.42
298	-1.31	310	-1.96
304	-1.40	320	-0.85
312	-1.58	330	-0.94
320	-0.82	340	-0.43
326	-1.36	350	-0.66
340	-0.52	360	-0.69
352	0.10	370	-0.82
370	-0.19	380	-1.28
378	-0.46	390	-1.54
386	-0.67	400	-2.06
392	-0.43	410	-0.17
396	-0.47	420	-0.70
424	-0.10	430	-0.47
428	-0.62	440	-0.48
436	-0.53	450	-0.53
440	-0.69	460	-0.83
		470	-2.79
		480	-1.45
		490	-0.37
		500	-0.50
		510	-0.51
		520	-1.61
		530	-0.91

Table 5.4

Oxygen isotope data ($\delta^{18}O$) using benthic foraminifer (*Cibicidoides wuellerstorfi*) for cores AAS-42/15 and AAS-42/12A.

AAS-42/15		AAS-42/12A	
Core Depth (cm)	$\delta^{18}O$ (‰)	Core Depth (cm)	$\delta^{18}O$ (‰)
0		0	3.97
10	2.36	10	3.63
20	3.04	20	3.71
30	3.61	30	3.80
48	3.60	40	2.88
50	3.65	50	3.38
70	3.56	60	3.55
80	4.06	70	3.65
116	3.27	80	3.32
124	3.36	90	3.33
130	3.59	100	3.31
138	3.23	110	3.05
150	2.89	120	2.86
160	3.43	130	3.14
168	3.40	140	3.39
174		150	3.72
180	3.54	160	3.65
188	3.78	170	3.47
192	3.67	180	3.16
198	3.79	190	3.19
202	2.92	200	3.60
212	3.19	210	3.43
218	3.68	220	3.49
230	3.02	230	3.48
240	3.32	240	3.30
250	2.72	250	3.22
258	3.30	260	3.69
264	2.94	270	3.39
270	3.04	280	3.48
280	3.22	290	3.50
290		300	3.21
298	2.88	310	3.64
304	2.59	320	3.08
312	3.23	330	2.90
320	2.68	340	3.43
326		350	3.72
340	3.55	360	3.71
352	3.47	370	3.45
370	4.03	380	3.53
378	3.90	390	4.14
386	3.61	400	3.71
392	3.65	410	3.44
396	3.85	420	3.86
424	3.74	430	3.33
428	3.69	440	3.78
436	3.13	450	3.33
440	3.62	460	3.44
		470	3.06
		480	2.93
		490	3.97
		500	3.31
		510	3.32
		520	3.17
		530	2.97

Table 5.5

Carbon isotope ($\delta^{13}C$) data using planktonic foraminifer (*Globigerinoide ruber*) for cores AAS-42/15 and AAS-42/12A.

AAS-42/15		AAS-42/12A	
Core Depth (cm)	$\delta^{13}C$ (‰)	Core Depth (cm)	$\delta^{13}C$ (‰)
0	0.58	0	1.14
10	1.08	10	0.91
20	1.33	20	0.56
30	0.48	30	1.02
48	0.33	40	1.45
50	0.55	50	0.97
70	0.59	60	1.55
80	0.81	70	0.86
116	0.49	80	1.14
124	0.34	90	1.17
130	0.85	100	1.16
138	0.05	110	1.28
150	0.59	120	1.46
160	0.91	130	1.00
168	1.30	140	0.46
174	0.60	150	0.90
180	0.62	160	0.60
188	1.01	170	0.89
192	0.41	180	0.02
198	0.88	190	0.77
202	0.19	200	0.37
212	0.78	210	0.58
218	0.27	220	0.20
230	0.64	230	0.25
240	1.27	240	0.70
250	1.07	250	0.57
258	1.31	260	1.03
264	0.61	270	0.70
270	0.88	280	1.02
280	0.48	290	0.62
290	1.03	300	0.53
298	0.40	310	0.46
304	0.98	320	0.77
312	0.46	330	0.83
320	0.30	340	0.59
326		350	0.76
340	0.214	360	1.49
352	0.27	370	0.93
370	0.57	380	0.38
378	0.93	390	0.78
386	0.60	400	
392	0.39	410	0.52
396	0.66	420	0.51
424		430	0.54
428	0.34	440	0.61
436	0.39	450	0.93
440		460	0.99
		470	0.37
		480	0.39
		490	0.28
		500	0.68
		510	0.17
		520	0.61
		530	0.30

Table 5.6

Carbon isotope (δ^{13}C) data using benthic foramnifer (*Cibicidoides wuellerstorfi*) for cores AAS-42/15 and AAS-42/12A.

AAS-42/15			AAS-42/12A		
Core Depth (cm)	^{13}C	(‰)	Core Depth (cm)	^{13}C	(‰)
0			0	0.02	
10	0.27		10	-0.18	
20	-0.08		20	-0.11	
30	-0.23		30	-0.18	
48	-0.23		40	-0.09	
50	-0.19		50	0.07	
70	-0.09		60	0.25	
80	-0.15		70	0.01	
116	-0.05		80	-0.08	
124			90	0.03	
130	0.04		100	-0.15	
138	-0.09		110	0.24	
150	-0.09		120	0.03	
160	-0.01		130	0.09	
168	-0.20		140	-0.14	
174			150	-0.12	
180	-0.36		160	-0.21	
188	-0.14		170	0.08	
192	-0.24		180	-0.08	
198	-0.25		190		
202	-0.11		200	-0.29	
212	0.05		210	-0.13	
218	-0.17		220	-0.26	
230	0.12		230	-0.01	
240	0.28		240	0.00	
250	0.31		250	-0.13	
258	0.23		260	-0.13	
264	0.28		270	-0.22	
270	0.08		280	-0.23	
280	0.14		290	-0.09	
290			300	-0.08	
298	0.06		310	0.02	
304	0.11		320	-0.06	
312	0.03		330	0.14	
320	-0.22		340	-0.17	
326			350	-0.26	
340	-0.25		360	-0.33	
352	-0.24		370	-0.12	
370	-0.56		380	-0.12	
378	-0.47		390	-0.30	
386	-0.22		400	-0.33	
392	-0.39		410	-0.23	
396	-0.54		420	-0.34	
424	-0.41		430	-0.08	
428	-0.49		440	-0.33	
436	-0.53		450	-0.18	
440	-0.59		460	-0.18	
			470	0.11	
			480	0.17	
			490	-0.36	
			500	-0.38	
			510	-0.08	
			520	-0.14	
			530	-0.17	

Table 5.7

Organic carbon, nitrogen, C/N weight ratios and $CaCO_3$ for cores AAS-42/15 and AAS-42/12A.

AAS-42/15					AAS-42/12A				
Core Depth (cm)	C_{org} (%)	N_{org} (%)	C/N	CaCO3 (%)	Core depth (cm)	C_{org} (%)	N_{org} (%)	C/N	CaCO3 (%)
0	3.09	0.30	10.15	59.55	0	5.19	0.58	9.01	73.61
10	2.90	0.27	10.74	50.55	10	2.84	0.35	8.11	68.36
20	1.92	0.30	6.45	57.36	20	0.85	0.12	6.88	48.46
30	1.28			50.28	30	1.54	0.19	8.23	48.79
48	1.92	0.20	9.45	44.15	40	1.89	0.21	8.89	49.21
50	1.99	0.21	9.25	48.78	50	1.83	0.21	8.87	48.70
70	1.72	0.20	8.71	45.45	60	1.81	0.21	8.70	52.05
80	2.16	0.30	7.13	45.65	70	1.92	0.21	8.95	46.80
116	2.39	0.25	9.60	50.39	80	3.02	0.34	8.95	60.58
124	2.92	0.27	10.79	42.73	90	3.04	0.33	9.16	56.96
130	4.60	0.37	12.37	44.24	100	0.97	0.13	7.46	45.42
138	3.40	0.38	9.07	44.17	110	1.69	0.19	8.68	45.60
150	3.57	0.37	9.72	46.57	120	1.65	0.21	7.84	58.06
160	1.70	0.23	7.30	49.45	130	1.70	0.19	8.77	58.27
168	2.15	0.26	8.32	46.47	140	2.55	0.25	10.24	49.08
174	1.76	0.17	10.14	44.74	150	1.70	0.19	9.18	47.05
180	0.96	0.11	8.87	42.12	160	0.86	0.10	8.31	42.73
188	0.94			35.83	170	0.71	0.10	6.84	44.94
192	1.37	0.15	8.89	33.54	180	1.07	0.13	8.29	45.84
198	1.53	0.19	8.09	31.87	190	1.42	0.16	8.90	48.56
202	1.28	0.18	7.28	31.84	200	1.25	0.16	7.66	52.70
212	1.72	0.24	7.18	30.23	210	0.90	0.12	7.62	46.64
218	1.81	0.16	11.27	29.33	220	1.80	0.20	8.86	48.20
230	1.74	0.16	10.85	29.69	230	1.94	0.22	8.91	53.62
240	1.72	0.17	9.95	35.98	240	0.68	0.11	6.22	58.89
250	1.29	0.17	7.61	33.74	250	1.10	0.11	10.00	49.90
258	0.98			39.01	260	1.40	0.19	7.20	61.47
264	0.79			35.62	270	2.40	0.25	9.62	58.00
270	1.86	0.32	5.80	43.62	280	1.21	0.14	8.73	54.51
280	2.75	0.27	10.35	47.51	290	0.87	0.10	8.67	39.98
290	3.17	0.33	9.59	45.77	300	1.32	0.15	8.92	44.13
298	1.33	0.15	8.95	40.43	310	1.70	0.19	8.95	54.83
304	0.79	0.14	5.61	32.85	320	2.55	0.32	8.00	68.64
312	2.01	0.24	8.31	42.30	330	1.47	0.19	7.73	65.42
320	1.56	0.20	7.81	44.55	340	1.46	0.16	9.36	49.85
326	1.48	0.27	5.56	51.99	350	3.47	0.19	18.46	51.61
340	1.80	0.20	8.96	54.97	360	1.13	0.12	9.09	47.11
352	3.67	0.14	25.42	48.74	370	1.44	0.14	10.13	43.73
370	2.95	0.29	10.23	49.85	380	1.79	0.19	9.57	49.79
378	1.69	0.17	9.94	43.60	390	1.83	0.17	10.58	50.38
386	0.99	0.14	7.17	46.66	400	1.35	0.16	8.53	56.89
392	1.56	0.35	4.46	42.79	410	1.59	0.16	10.14	52.92
396	0.65			42.18	420	1.36	0.14	10.00	43.43
424	2.48	0.02		42.57	430	1.19	0.12	9.58	42.97
428	0.90	0.12	7.34	39.67	440	1.26	0.14	9.05	46.83
436	2.33	0.27	8.61	44.62	450	0.95	0.12	7.88	45.10
440	1.88	0.24	8.01	46.26	460	1.33	0.16	8.29	56.36
					470	1.79	0.22	8.13	66.00
					480	1.28	0.15	8.31	57.89
					490	0.68	0.10	7.08	50.09
					500	0.89	0.11	7.89	49.54
					510	1.68	0.21	8.11	54.11
					520	1.42	0.16	9.04	47.35
					530	1.07	0.12	8.77	46.91

Table 5.8

Sedimentary carbon ($\delta^{13}C_{org}$) and nitrogen ($\delta^{15}N_{org}$) isotopes in cores AAS-42/15 and AAS-42/12A.

AAS-42/15			AAS-42/12A		
Core Depth (cm)	$\delta^{13}C_{org}$ (‰)	$\delta^{15}N_{org}$ (‰)	Core Depth (cm)	$\delta^{13}C_{org}$ (‰)	$\delta^{15}N_{org}$ (‰)
0	-19.93	9.31	0	-20.64	8.88
10	-22.68	8.74	10	-19.90	8.07
20	-22.72	8.35	20	-18.92	7.75
30	-21.20	7.29	30	-18.96	7.72
48	-18.69	7.50	40	-18.82	6.86
50	-19.01	8.01	50	-18.79	7.26
70	-18.54	7.51	60	-18.82	7.21
80	-19.13	7.32	70	-18.74	7.11
116	-18.65	7.97	80	-18.89	8.65
124	-19.05	7.69	90	-18.90	8.11
130	-19.22	9.05	100	-19.21	6.46
138	-20.51	8.61	110	-19.40	6.86
150	-19.20	9.49	120	-18.96	7.93
160	-18.89	7.66	130	-20.25	6.88
168	-20.08	8.48	140	-19.19	7.47
174	-20.34	8.26	150	-19.16	7.57
180	-19.52	6.67	160	-19.13	6.66
188	-19.36	6.56	170	-19.17	6.72
192	-20.00	6.56	180	-19.72	7.40
198	-19.67	6.43	190	-19.69	8.08
202	-19.16	6.73	200	-19.53	7.28
212	-19.66	6.86	210	-18.91	6.38
218	-19.98	8.18	220	-19.34	6.87
230	-18.38	8.20	230	-19.49	7.26
240	-18.66	7.59	240	-19.06	6.10
250	-19.26	8.17	250	-21.00	6.27
258	-18.24	7.00	260	-19.38	7.74
264	-18.25	7.17	270	-19.38	7.52
270	-18.63	8.57	280	-19.61	7.12
280	-19.29	8.83	290	-19.34	6.33
290	-20.63	9.19	300	-18.90	6.10
298	-20.55	7.83	310	-18.97	7.13
304	-18.79	7.12	320	-19.48	7.48
312	-21.54	8.06	330	-19.24	7.15
320	-20.24	8.37	340	-19.41	6.68
326	-18.64	7.87	350	-19.89	5.89
340	-19.17	7.71	360	-19.46	5.53
352	-19.33	8.30	370	-19.10	5.53
370	-18.99	8.24	380	-18.98	6.45
378	-19.75	7.85	390	-18.87	6.69
386	-18.99	7.17	400	-19.02	7.99
392	-20.52	6.73	410	-19.06	6.17
396	-19.34	6.74	420	-19.18	6.65
424	-21.56	8.36	430	-19.60	6.31
428	-18.82	7.44	440	-19.53	6.69
436	-21.45	8.51	450	-18.80	6.79
440	-19.00	8.73	460	-19.23	7.56
			470	-18.61	7.06
			480	-19.66	7.80
			490	-18.73	6.83
			500	-19.18	7.23
			510	-19.28	7.08
			520	-19.80	6.45
			530	-19.18	6.90

Table 5.9

Major element (Al, Fe, Mg, Ti) concentration for core AAS-42/15.

Core Depth (cm)	Al (%)	Fe (%)	Mg (%)	Ti (%)
0	2.19	1.64	1.21	0.15
10	1.67	1.20	1.31	0.11
20	2.42	1.74	1.32	0.15
30	3.00	2.13	1.55	0.20
48	3.03	1.88	1.52	0.20
50	3.06	2.08	1.59	0.20
70	3.53	2.48	1.67	0.23
80	3.41	2.26	1.58	0.22
116	3.45	2.22	1.73	0.22
124	3.85	2.56	1.72	0.24
130	3.48	2.40	1.73	0.23
138	3.67	2.54	1.64	0.24
150	2.95	2.12	1.63	0.20
160	3.27	2.10	1.54	0.20
168	3.19	2.13	1.63	0.19
174	3.36	2.02	1.66	0.20
180	3.99	2.42	1.72	0.23
188	4.04	2.71	1.84	0.24
192	4.33	2.67	1.72	0.26
198	4.84	2.84	1.85	0.26
202	5.22	3.08	1.81	0.28
212	5.04	3.14	1.95	0.27
218	4.77	3.08	1.91	0.26
230	5.16	3.10	1.80	0.26
240	4.75	3.13	1.73	0.27
250	4.33	2.64	1.79	0.24
258	5.12	2.99	1.78	0.28
264	5.11	2.94	1.71	0.27
270	4.05	2.70	1.52	0.22
280	3.59	2.10	1.40	0.19
290	3.85	2.21	1.58	0.21
298	4.22	2.42	1.64	0.22
304	5.21	3.09	1.71	0.28
312	4.24	2.50	1.56	0.23
320	3.96	2.35	1.59	0.21
326	3.55	2.07	1.38	0.19
340	3.07	2.06	1.37	0.18
352	3.36	2.02	1.50	0.18
370	3.53	2.23	1.46	0.21
378	3.37	2.03	1.55	0.20
386	4.08	2.34	1.63	0.24
392	4.03	2.27	1.72	0.24
396	4.39	2.41	1.74	0.25
424	4.30	2.51	1.72	0.24
428	4.66	2.71	1.57	0.25
436	3.74	2.25	1.60	0.21
440	3.73	2.33	1.60	0.21

Table 5.10

Major element (Al, Fe, Mg, Ti) concentration for core AAS-42/12A.

Core Depth (cm)	Al (%)	Fe (%)	Mg (%)	Ti (%)
0	1.68	1.12	1.06	0.11
10	2.12	1.45	1.22	0.13
20	3.62	2.42	1.83	0.22
30	3.25	2.23	1.68	0.20
40	3.52	2.40	1.80	0.22
50	3.36	2.20	1.74	0.20
60	3.33	2.12	1.69	0.20
70	3.30	1.85	1.68	0.20
80	2.73	1.67	1.40	0.16
90	2.67	1.61	1.34	0.16
100	4.32	2.61	1.85	0.24
110	3.93	2.45	1.66	0.21
120	2.07	1.35	1.08	0.12
130	2.69	1.96	1.38	0.16
140	3.46	2.37	1.71	0.22
150	3.62	2.47	1.75	0.23
160	4.26	3.49	2.01	0.25
170	4.48	2.68	1.96	0.25
180	4.02	2.51	1.85	0.23
190	3.73	2.44	1.79	0.21
200	3.38	1.99	1.54	0.18
210	4.28	2.44	1.77	0.23
220	3.46	2.12	1.48	0.19
230	3.46	2.02	1.49	0.20
240	3.82	2.37	1.61	0.20
250	4.10	2.67	1.71	0.22
260	2.50	1.73	1.21	0.15
270	2.45	1.71	1.19	0.15
280	3.68	2.24	1.57	0.21
290	4.32	2.94	1.77	0.23
300	4.33	2.83	1.80	0.24
310	3.54	2.13	1.49	0.20
320	2.41	1.52	1.13	0.14
330	2.38	1.42	1.15	0.14
340	3.49	3.00	1.58	0.21
350	3.67	2.41	1.52	0.22
360	4.19	2.55	1.61	0.24
370	4.62	2.86	1.70	0.24
380	3.73	2.36	1.49	0.20
390	3.82	2.46	1.43	0.20
400	3.14	1.86	1.32	0.17
410	4.62	2.86	1.89	0.25
420	4.64	2.68	1.83	0.24
430	4.67	2.53	1.80	0.24
440	4.26	2.44	1.70	0.22
450	4.75	2.70	1.79	0.25
460	2.46	1.44	1.12	0.14
470	3.21	1.85	1.34	0.18
480	3.10	1.85	1.35	0.18
490	3.55	2.80	1.56	0.21
500	3.84	2.53	1.68	0.22
510	3.42	2.08	1.58	0.20
520	3.68	2.28	1.67	0.20
530	3.70	2.32	1.59	0.20

Table 5.11.

Geochemistry of trace elements used to characterize the redox state of sedimentary depositional environments. Data sources: (1) Boyle et al. (1976), (2) Bruland (1978); Knauer and Martin (1981), (3) McCorkle and Klinkhammer (1991), (4) Boyle et al. (1977), (5)Sawlan and Murray (1983); Heggie et al. (1987), (6)Landing and Bruland (1980), (7) Martin and Knauer (1984), (8)Froelich et al. (1979), (9) Landing and Bruland (1987), (10) Collier (1985), (11) Shaw et al. (1990), (12) Emerson and Huested (1991), (13)Collier (1984), (14)Brumsack and Gieskes (1983)

Element	Oxic Oxidation state	Speciation in oxic seawater	Processes controlling distribution in oxic seawater	Reduced Oxidation state	Speciation in reduced environment	Processes controlling accumulation in sediments
Fe	Fe (III)	$Fe(OH)_{3(s)}$	Nutrient cycling, non-conservative (9)	Fe (II)	Fe^{2+} (aq)	Precipitates as hydroxides. Delivery by detrital material (9). FeOOH reduction (8)
Mn	Mn(IV)	$Mn(OH)_{4(s)}$	non-conservative (6)	Mn(II)	Mn^{2+} (aq)	Precipitates as hydroxides. Delivery by detrital material (7). MnO_2 reduction (8)
Cd	Cd (II)	$CdCl^+$ (aq)	Nutrient cycling, non-conservative (1)	Cd(II)	$CdS_{(s)}$	Precipitation in presence of free sulfide. Released during diagenesis of organic matter (2). Complexes strongly with bisulfide (3).
Cu	Cu (II)	$CuCl^+$ (aq)	Nutrient cycling, non-conservative (4)	Cu(II), Cu(I)	$CuS_{(s)}$, Cu_2S	Precipitates as disseminated sulfides and released during diagenesis of organic matter (5).
Mo	Mo(VI)	MoO_4^{2-} (aq)	Conservative (10)	Mo(V), Mo(IV)	MoO^{2+}(aq), $MoS_{2(s)}$	Diffusion across sediment-water interface to precipitate at depth (11,12), MnO_2 reduction (11), direct Mo-Sulfide precipitation (19)
V	V(V)	HVO_4^{2-}(aq) $H2VO_4$-(aq)	some nutrient cycling, nearly conservative (13)	V(IV), V(III)	VO^{2+}(aq), $VO(OH)_3^-$(aq) $V(OH)_3$(aq)	MnO_2 and FeOOH reduction (11), diffusion (11,12), Accumulation in anoxic sediments. Reduced V(IV) strongly scavenged (14).

Table 5.12

Elemetal (Ba, Sr, Co, Cr, Cu, Mn, Mo, V, P) concentration for core AAS-42/15.

Core Depth (cm)	Ba (ug/g)	Sr (ug/g)	Co (ug/g)	Cr (ug/g)	Cu (ug/g)	Mn (ug/g)	Mo (ug/g)	V (ug/g)	P (ug/g)
0	492	877	11	22	32	-	34	44	523
10	372	763	3	8	22	269	24	44	324
20	391	861		16	21	367	36	43	405
30	283	840		26	21	269	45	42	404
48	390	720	1	28	18	247	39	87	486
50	367	716	6	33	16	243	50	70	528
70	351	720	5	30	23	268	50	81	591
80	381	831		31	23	241	46	53	675
116	365	752	6	32	17	257	46	74	595
124	488	766	4	37	19	251	54	69	633
130	516	769	1	32	19	235	49	40	639
138	459	790	5	46	22	241	52	41	627
150	443	814	4	31	15	224	44	81	578
160	331	861		32	23	249	45	44	541
168	343	819	3	29	15	249	46	50	528
174	321	814	3	28	24	256	42	43	537
180	297	813		26	19	275	51	77	432
188	348	618	0	32	15	262	59	79	497
192	351	715	3	37	35	285	56	90	487
198	372	585		46	21	289	62	87	515
202	423	580	3	51	25	310	66	101	547
212	418	568	5	44	41	287	66	109	561
218	396	562		37	33	266	64	95	555
230	447	591	1	47	35	291	67	95	517
240	365	641	3	40	42	283	67	90	554
250	381	704	0	49	24	316	58	82	590
258	341	556	3	41	15	285	64	84	476
264	418	589	4	37	26	287	65	88	481
270	532	796	5	38	23	271	56	90	516
280	487	841	6	36	29	255	46	76	509
290	462	841	5	38	33	277	48	78	559
298	464	702	5	37	33	268	55	73	538
304	468	592	5	52	17	296	68	90	527
312	597	774	5	42	37	278	57	67	486
320	607	782	6	44	44	267	53	99	572
326	658	849	3	33	21	257	48	71	586
340	252	996	3	26	19	220	48	60	481
352	389	858	1	38	28	235	46	71	601
370	379	887	10	35	13	284	52	76	646
378	304	760	6	31	19	285	46	71	564
386	318	749	3	36	28	317	53	86	538
392	318	745	4	39	18	298	51	77	510
396	314	705		43	22	304	57	74	445
424	375	711	4	49	17	310	57	88	586
428	348	629	6	41	21	270	64	82	474
436	403	813	5	38	23	312	50	94	601
440	380	814	10	37	13	311	53	72	570

Table 5.13

Elemental (Ba, Sr, Cr, Cu, Mn, Mo, V, P) concentration for core AAS-42/12A.

Core Depth (cm)	Ba (ug/g)	Sr (ug/g)	Cr (ug/g)	Cu (ug/g)	Mn (ug/g)	Mo (ug/g)	V (ug/g)	P (ug/g)
0	334	1027	26	17	186	22	27	380
10	363	1040	34	28	208	30	38	437
20	352	797	44	32	339	49	72	505
30	383	779	43	29	176	46	55	475
40	330	726	52	26	187	47	79	496
50	294	773	35	20	179	46	72	478
60	274	800	43	19	175	44	68	434
70	284	850	43	21	176	38	64	477
80	311	947	31	29	135	35	56	454
90	285	943	31	35	132	34	54	403
100	286	706	44	21	218	55	73	442
110	317	727	39	39	183	53	60	446
120	277	933	30	8	107	28	34	396
130	344	899	26	5	143	42	55	403
140	383	836	51	43	190	49	76	470
150	315	802	46	38	212	53	81	938
160	297	702	44	18	237	76	91	470
170	303	720	48	16	233	57	87	433
180	309	757	46	16	224	56	84	459
190	337	784	42	19	217	55	81	477
200	277	876	35	27	183	43	124	399
210	370	763	40	27	230	54	84	424
220	318	849	27	38	189	45	64	452
230	328	862	32	51	195	45	56	442
240	327	794	35	17	207	52	60	299
250	389	791	43	11	225	58	68	477
260	299	953	21	13	158	38	56	395
270	335	975	33	18	149	38	55	396
280	281	863	31	13	206	48	68	398
290	338	699	46	19	217	64	75	420
300	360	746	41	23	215	62	88	468
310	337	928	30	25	183	47	80	432
320	291	1142	28	10	160	33	48	451
330	315	1063	26	9	160	31	40	467
340	296	863	43	16	186	63	67	508
350	289	916	30	18	196	51	83	517
360	271	821	40	27	208	54	81	395
370	340	837	42	24	228	62	85	481
380	290	962	34	16	201	50	80	488
390	366	903	38	21	184	55	56	446
400	356	951	37	49	170	39	60	600
410	366	768	38	107	233	64	98	583
420	361	806	38	24	241	60	78	554
430	316	830	42	35	247	56	86	562
440	312	920	39	23	245	52	78	554
450	337	799	47	36	239	60	84	439
460	309	958	19	40	123	33	47	454
470	315	979	36	19	169	41	53	533
480	334	995	33	13	174	40	43	560
490	405	818	35	62	175	62	67	454
500	361	780	37	7	187	56	70	433
510	355	948	49	17	189	46	62	467
520	347	933	38	26	203	50	77	450
530	329	845	33		194	53	70	406

Table 5.14

Element/Al ratio of Ba, Sr, Co, Cr, Cu, Mn, Mo, V and P for core AAS-42/15

Core Depth (cm)	Ba/Al x10^{-4}	Sr/Al x10^{-4}	Co/Al x10^{-4}	Cr/Al x10^{-4}	Cu/Al x10^{-4}	Mn/Al x10^{-4}	Mo/Al x10^{-4}	V/Al x10^{-4}	P/Al x10^{-4}
0	224	399	5	10	14		15	20	238
10	222	455	2	5	13	161	14	26	194
20	161	355	0	7	9	151	15	18	167
30	94	280	0	9	7	90	15	14	135
48	128	237	0	9	6	81	13	29	160
50	120	234	2	11	5	79	16	23	173
70	100	204	2	9	6	76	14	23	168
80	112	244	0	9	7	71	13	16	198
116	106	218	2	9	5	75	13	21	172
124	127	199	1	10	5	65	14	18	164
130	148	221	0	9	6	68	14	12	184
138	125	215	1	13	6	66	14	11	171
150	150	276	1	10	5	76	15	28	196
160	101	263	0	10	7	76	14	13	165
168	108	257	1	9	5	78	15	16	165
174	96	242	1	8	7	76	12	13	160
180	74	203	0	6	5	69	13	19	108
188	86	153	0	8	4	65	15	19	123
192	81	165	1	9	8	66	13	21	112
198	77	121	0	10	4	60	13	18	107
202	81	111	1	10	5	59	13	19	105
212	83	113	1	9	8	57	13	22	111
218	83	118	0	8	7	56	13	20	116
230	87	114	0	9	7	56	13	18	100
240	77	135	1	8	9	60	14	19	117
250	88	163	0	11	5	73	13	19	136
258	67	108	1	8	3	56	12	16	93
264	82	115	1	7	5	56	13	17	94
270	131	196	1	9	6	67	14	22	127
280	136	234	2	10	8	71	13	21	142
290	120	218	1	10	9	72	12	20	145
298	110	166	1	9	8	64	13	17	128
304	90	114	1	10	3	57	13	17	101
312	141	183	1	10	9	66	13	16	115
320	153	197	1	11	11	67	13	25	144
326	185	239	1	9	6	72	13	20	165
340	82	325	1	8	6	72	16	20	157
352	116	255	0	11	8	70	14	21	179
370	107	251	3	10	4	81	15	21	183
378	90	225	2	9	6	85	14	21	167
386	78	184	1	9	7	78	13	21	132
392	79	185	1	10	5	74	13	19	127
396	72	161		10	5	69	13	17	101
424	87	165	1	11	4	72	13	20	136
428	75	135	1	9	4	58	14	18	102
436	108	217	1	10	6	83	13	25	161
440	102	218	3	10	3	83	14	19	153

Table 5.15

Element/Al ratio of Ba, Sr, Cr, Cu, Mn, Mo, V and P for core AAS-42/12A.

Core Depth (cm)	Ba/Al x10^{-4}	Sr/Al x10^{-4}	Cr/Al x10^{-4}	Cu/Al x10^{-4}	Mn/Al x10^{-4}	Mo/Al x10^{-4}	V/Al x10^{-4}	P/Al x10^{-4}
0	198	610	16	10	110	13	16	225
10	172	491	16	13	98	14	18	206
20	97	220	12	9	94	14	20	140
30	118	240	13	9	54	14	17	146
40	94	206	15	7	53	13	22	141
50	88	230	10	6	53	14	21	142
60	82	240	13	6	53	13	21	130
70	86	258	13	6	53	12	20	144
80	114	347	11	11	50	13	20	167
90	107	353	12	13	49	13	20	151
100	66	163	10	5	51	13	17	102
110	81	185	10	10	46	14	15	113
120	134	451	15	4	52	14	16	191
130	128	335	10	2	53	16	21	150
140	111	242	15	13	55	14	22	136
150	87	222	13	10	59	15	22	259
160	70	165	10	4	56	18	21	110
170	68	161	11	4	52	13	19	97
180	77	188	11	4	56	14	21	114
190	90	210	11	5	58	15	22	128
200	82	259	10	8	54	13	37	118
210	86	178	9	6	54	13	20	99
220	92	245	8	11	55	13	18	131
230	95	250	9	15	56	13	16	128
240	86	208	9	4	54	14	16	78
250	95	193	10	3	55	14	17	117
260	120	381	9	5	63	15	22	158
270	137	398	13	7	61	15	23	162
280	76	235	8	4	56	13	19	108
290	78	162	11	4	50	15	17	97
300	83	172	9	5	50	14	20	108
310	95	262	9	7	52	13	23	122
320	121	474	11	4	66	14	20	187
330	132	447	11	4	67	13	17	196
340	85	247	12	4	53	18	19	145
350	79	250	8	5	53	14	23	141
360	65	196	9	6	50	13	19	94
370	74	181	9	5	49	13	18	104
380	78	258	9	4	54	13	21	131
390	96	236	10	6	48	14	15	117
400	113	303	12	16	54	12	19	191
410	79	166	8	23	50	14	21	126
420	78	174	8	5	52	13	17	119
430	68	178	9	7	53	12	18	120
440	73	216	9	5	58	12	18	130
450	71	168	10	8	50	13	18	92
460	126	389	8	16	50	13	19	184
470	98	305	11	6	53	13	16	166
480	108	321	11	4	56	13	14	181
490	114	230	10	17	49	17	19	128
500	94	203	10	2	49	15	18	113
510	104	277	14	5	55	13	18	137
520	94	254	10	7	55	14	21	122
530	89	228	9		52	14	19	110

CHAPTER 6

Chapter 6

CONCLUSIONS AND RECOMMENDATIONS

6.1 Conclusions

This chapter summarizes the results and findings of the present work, mainly on the changes in the oxygen minimum zone of the coastal waters and the deep Arabian Sea. Sedimentological and paleoceanographical studies were carried out on three coastal shallow and two open ocean deep cores. Studies based on multiple geological proxies are integrated and paleo-climatic conditions on centennial and millennial timescales during the glacial-interglacial periods have been suggested. The following points summarize the salient features and findings of this study:

1. Various proxies (C_{org}, N_{org}, $CaCO_3$, C/N, SiO_2, $\delta^{13}C_{org}$, $\delta^{15}N_{org}$, Al, Fe, Mg, Sr, Mn, V, Co, Mo, Ba, Cu, Cr and Ni) analyzed in the three shallow cores raised from the inner- and mid-shelf areas that are seasonally overlain by suboxic/anoxic waters, at present, exhibit significant downcore variations.

2. A consistent trend in enhanced productivity over the past few decades is found in the shallow cores records. In most probability this increase is a consequence of human activities (fertilizer inputs from land).

3. Higher values of C_{org} in all the shallow cores (especially in SaSu-3B) at depths, indicative of the last few decades reveals the preservation of organic carbon due to unavailability of sufficient oxygen to oxidize huge

amount of organic matter sinking due to high productivity.

4. Terrestrial input tracers ($\delta^{13}C_{org}$, C/N), clearly indicated the organic matter to be of marine origin; though nitrogenous based fertilizers discharge is expected to increase C/N ratio but the actual increase does not seem to be significant.

5. Despite the increased surface productivity, which is expected to result in higher rate of near-bottom denitrification (the evidence for which is available from the water column measurements), the sediments do not exhibit an enhanced $\delta^{15}N$ signal. Nevertheless, $\delta^{15}N$ might still serve as a proxy of denitrification in deeper sediments (CR-2), particularly during the Little Ice Age.

6. Redox sensitive trace metals in the shallow cores revealed no clear trends in their variability, except indicating a general persistence of reducing conditions throughout the depositional period.

7. Down core oxygen isotope records of planktic foraminifers *Globigerinoide ruber*, in the two deep ocean cores, revealed the difference in amplitudes of $\delta^{18}O$ values (~1.55 & ~1.43‰) between the LGM and Holocene to be a result of the global continental ice volume effect and an increase in the sea surface temperature by ~2°C during the Holocene.

8. The benthic amplitude value of $\delta^{18}O_{C.wuellerstorfi}$ of ~1.25‰, represents the 'ice volume effect' (~1.2‰), thus supporting the assumption that bottom water temperatures are nearly unchanged during the last glacial-interglacial period.

9. The maximum in $\delta^{13}C$ value of planktics observed during the early Holocene, early OIS 3 and late OIS 5 (interglacial stages), is due to the enhanced monsoonal precipitation resulting in an increase in C_3 vegetation (trees preferentially use ^{12}C) and $\delta^{13}C$ of the atmospheric CO_2. This increases the surface seawater $\delta^{13}C$ giving rise to high $\delta^{13}C$ in planktics.

10. The observed lower values of $\delta^{13}C$ during glacial periods indicated that they were due to the climatic variations and are devoid from effects of any denitrification or upwelled waters, which was inferred from the co-variability between $\delta^{18}O$ and $\delta^{13}C$ of planktics.

11. The benthic $\delta^{13}C$ record exhibits high and low values during the interglacial and glacial stages, respectively, for both the cores suggesting the bottom waters to be well oxygenated. The highly depleted value of $\delta^{13}C$ observed during the glacial stage 6 (AAS-42/15) is attributed to the combined effect of microhabitat and remineralization.

12. The coherent glacial-interglacial down core variations of C_{org} with respective low and high contents indicate higher productivity during the interglacial periods due to intense upwelling triggered by strong southwest monsoons and low productivity during glacial periods to that of reduced upwelling because of weakened monsoons.

13. The C_{org} flux profile, $CaCO_3$ and $\delta^{13}C$ of *G. ruber* profiles also exhibit a similar trend as that of C_{org}, indicating higher productivity during the interglacial than the glacial periods.

14. The down core variations in carbon isotope ratios of organic matter $(\delta^{13}C_{org})$, and the C/N weight ratio, in both deep cores indicate that the C_{org} is dominantly of marine in nature. However, the observed $\delta^{13}C_{org}$ variations may correspond to varying supply of organic matter from terrestrial and marine sources.

15. A relaxation/cessation of denitrification during the glacial periods and its intensification during interglacial times, as suggested by earlier works, is confirmed by results of this study. The sediments are also confirmed to be relatively less affected by diagenetic changes, with high intensity of denitrification during interglacial period and strong OMZ driven by increased productivity.

16. The downcore variations in Ti, Al, Fe and Mg of both cores, mirrored the surface productivity proxies, namely $CaCO_3$ and C_{org}. The observed distributions of detrital elements (Ti, Al, Fe, Mg), is due to their concentration in the clay fraction, and showed negative relations with $CaCO_3$ (a productivity/monsoonal proxy).

17. A comparison of the detrital/lithogenic elements with the productivity proxies, reveal that the negative trends were observed in all the glacial-interglacial stages. Therefore, the low abundance of detrital/lithogenic elements is due to dilution by biogenic materials during high productivity and vice versa.

18. The down core variation of Sr/Al was similar to $CaCO_3$ during all the glacial-interglacial stages suggesting their close association [r=0.86 (AAS-41/15) and r=0.89 (AAS-42/12A)]. Since most of the Sr is expected

to have been derived from the aragonitic phase (which is the main mineral), its association with carbonate fraction could be proportional and linear.

19. Enrichment and depletion of redox sensitive metals in sediments reflects the changes in the intensity of the OMZ. Decreased Mn and Fe concentrations observed during the glacial periods when the productivity was less and higher values during the interglacial even when the productivity was high, irrespective of the reducing conditions in the intermediate waters suggest that, Fe and Mn are influenced by bottom waters at the time of deposition and indicate the bottom water conditions, rather than indicating the signatures of suboxic intermediate waters. Close observations at the profiles indicate the behavior to be present throughout the core during all the glacial – interglacial periods.

20. While, the enrichment of V, Co and Mo observed during the interglacial compared to the glacial periods, appears to be due to their association with particles resulting from higher productivity. The average value of V/Al being slightly more than the average shale value could also indicate its enrichment due to adsorption on Fe and Mn – oxy-hydroxides in oxygenated waters, again indicating the bottom water environment to be oxygenated.

21. The overall depleted values of Cr in the sediments with respect to its shale value (both concentration and Al-normalized ratio) indicate non existence of reducing environments in bottom waters during deposition. Also Cr does not indicate any signatures of intermediate reducing waters

(as indicated by denitrification proxy variation), as inferred from its depleted values and supports the inferences drawn from other redox sensitive elements that they are indicative of the deposition environment with bottom waters being more oxygenated and do not provide any information about the intermediate reducing waters or the OMZ intensity.

22. Trace metal results from both the open ocean cores confirm the tight coupling among ocean circulation, marine productivity and global change and indicate the bottom waters to be oxygenated during the time of sediment deposition.

23. The glacial-interglacial distribution pattern of Ba/Al follows a similar trend as that of C_{org} with higher contents during the interglacial and lower contents during the glacial periods, suggesting the removal of Ba from seawater by adsorption on organic materials and sinking organic particles, whose flux increases during high productivity of interglacial sediments.

24. Higher average values of Ba/Al ratio, in both the cores also indicate that the bottom water conditions were oxygenated during the deposition of sediments because had the waters been reducing, it would have reflected with a decreased value of Ba/Al ratio as is observed by McManus et al. (1998); Agnihotri et al. (2007).

25. Thus the Ba/Al ratio in both cores follow the same pattern as C_{org} confirming that it can be employed as productivity proxy and also gives inferences about the bottom water conditions, whether oxic or reducing.

26. Covariance of P/Al and C_{org} in both cores, with the average value of P/Al being higher than the average shale value, suggests the dominant presence of non-detrital, biogenic P, during all the glacial-interglacial stages.

27. The average values of Cu/Al also being slightly higher than the average shale value indicates the presence of non-detrital Cu which can be attributed to its nutrient type behaviour, because of which it is removed from the surface waters during plankton growth.

28. Since the OMZ does not reach the seafloor at the study sites, the records generated enable evaluation of changes in the intermediate as well as bottom waters through comparison of different proxies of conditions in the two domains. For example, while the sedimentary $\delta^{15}N$ record can be taken to represent denitrification, those of benthic $\delta^{13}C$ and trace metals are expected to reflect conditions prevailing in near-bottom waters. The most important and unexpected result obtained in the present study is that the environmental changes in the intermediate and bottom waters very often occurred in opposite directions, probably caused by reorganization of the subsurface circulation, over the past climatic cycle.

6.2   Recommendations for further research

The detailed multi-core and multi-proxy study from the coastal shallow and deep ocean sediments of the eastern Arabian Sea described in this work has provided valuable information on the processes influencing the

distribution of various chemical and isotopic proxies in these sediments. The study has thus brought into focus the increasing intensity of suboxia over the coastal regions for the last few decades and the existing decoupling of the intermediate waters from the bottom waters in the deep waters. This study also raises several intriguing questions, which need to be addressed for the better understanding of the complex behavior of the monsoons and its spatial and temporal variability. These include -

- Whether the monsoonal variability on decadal scales can be inferred from coastal sediments? For which a number of coastal cores will have to be investigated, to provide insights into the processes through proxies that respond on seasonal time-scales.

- Investigations on terrestrial inputs of organic matter due to anthropogenic activities needs to be looked in more detail by adopting more specific proxies in this regard.

- Inferences from various proxies (from deep cores) regarding the dominating behavior of the southwest summer monsoon in the northeastern Arabian Sea at least at the coring site, needs to be reinforced with more detailed studies on sediment cores focusing on the provenance of the sediments.

- More sediment cores from areas impinged with OMZ waters and deep waters, for comparison, need to be studied for the coherency among millennial scale variations in the OMZ intensity, denitrification and other paleo-climatic processes.

- Sediment cores along the periphery of the oxygen minimum zone (as demarcated by Naqvi, 1991, based on the nitrite contour) needs to be investigated, with all possible chemical and geological proxies to infer the existence and extent of paleo oxygen deficient zone in the Arabian Sea.

REFERENCES

REFERENCES

Adelson, J.M., G.R. Helz, and C.V. Miller. (2001). Reconstructing the rise of recent coastal anoxia; molybdenum in Chesapeake Bay sediments, Geochim Cosmochim. Acta, 65 (2), 237-252.

Agnihotri R., S. Kurian, M. Fernandes, K. Reshma, W. D' Souza and S.W.A. Naqvi, (2007). Variability of subsurface denitrification and surface productivity in the coastal eastern Arabian Sea over the past seven centuries. Holocene (under review).

Agnihotri, R., M.A. Altabet, and T.D. Herbert (2006). Influence of marine denitrification on atmospheric N_2O variability during the Holocene. Geophys. Res. Lett. 33, L13704.

Agnihotri R., S.K. Bhattacharya, M.M. Sarin, and B.L.K. Somayajulu (2003a). Changes in surface productivity, sub-surface denitrification and SW monsoon during the Holocene: a multi proxy record from the eastern Arabian Sea. Holocene, 13, 701-713.

Agnihotri R., M.M. Sarin, B.L.K. Somayajulu, A.J.T Jull, G.S. Burr, and A. Sarkar (2003b). Late- Quaternary Paleo-productivity and Organic carbon deposition record from the Eastern Arabian Sea, Paleogeology Paleoclimatology Paleoecology, 197, 43-60.

Agnihotri R. and K. Dutta, (2003). Centennial scale changes in the Indian, east equatorial and Chinese Monsoons during the last millennium: Manifestations of Solar activity changes. Current Science, 85, 459-463.

Agnihotri R., K. Dutta, R. Bhushan, and B.L.K. Somayajulu. (2002) Evidence for solar forcing on the Indian monsoon during the last millennium. Earth and Planetary Science Letters, 198, 3-4, 521-527.

Agnihotri R., (2002) date of publishing Thesis. "Chemical and Isotopic studies of sediments from the Arabian Sea and Bay of Bengal".

Ahmad, S. M. and L. Labeyrie (1994). Glacial to Holocene $\delta^{13}C$ variations in intermediate depth water masses of North Indian Ocean. Geo-Marine Letters, 14, 36-40.

Altabet, M. A., (2007). Constraints on oceanic N balance/imbalance from sedimentary ^{15}N records. Biogeosciences, 4 (1), 75-86.

Altabet, M. A. (2006). Constraints on oceanic N balance/imbalance from sedimentary 15N records. Biogeosciences Discussions, 3, 1121–1155.

Altabet, M.A., M.J. Higginson and D.W. Murray (2002). The effect of millennium scale changes in Arabian Sea denitrification on atmospheric CO_2. Nature, 415,159-162.

Altabet, M.A., D.W. Murray and W.L. Prell (1999a). Climatically linked oscillations in Arabian Sea denitrification over the past 1 m.y.: Implications for the marine N cycle. Paleoceanography, 14, 732-743.

Altabet, M.A., C. Pilskaln, R. Thunell, C. Pride, D. Sigman, F. Chavez and R. Francois (1999b). The nitrogen isotope biogeochemistry of sinking particles from the margin of the eastern North Pacific. Deep-Sea Research, 46, 655-679.

Altabet, M.A., R. Francois, D.W. Murray and W.L. Prell (1995). Climate-related variations in denitrification in the Arabian Sea from sediment $^{15}N/^{14}N$ ratios, Nature, 373, 506-509.

Altabet, M.A., and R. Francois, (1994). The Use of Nitrogen Isotopic Ratio for Reconstruction of Past Changes in Surface Ocean Nutrient Utilization In: Carbon Cycling in the Glacial Ocean, NATO ASI Series, edited by R. Zahn, M. A. Kaminski, L. Labeyrie, and T. F. Pederson, 281-306.

Altabet, M.A. and W.B. Curry (1989). Testing models of past ocean chemistry using foraminiferal $^{15}N/^{14}N$. Global Biogeochemical Cycles, 3, 107-119.

Altabet, M. A., (1988). Variations in nitrogen isotopic composition between sinking and suspended particles: Implications for nitrogen cycling and particle transformation in the open ocean. Deep-Sea Research, 35, 535-554.

Altabet, M. A. and J. J. McCarthy, (1985). Temporal and spatial variations in the natural abundance of ^{15}N in PON from a warm-core ring. Deep-Sea Research, 32, 755-772.

Altenbach, A. V. and M. Sarnthein, (1989). Productivity record in benthic foraminifera. In: Productivity of the Ocean: Present and Past, Berger, W. H., Smetacek, V. S. and Wefer, G. (Eds.), Dahlem Konferenzen, John Wiley & Sons, 255-269.

Anderson, D. M., and W. L. Prell, (1993). A 300 k.y. record of upwelling off Oman during the late Quaternary: evidence of the Asian Southwest Monsoon. Paleoceanography, 8, 193-208.

Anderson, D. M., W. L. Prell and N. J. Barrat, (1989a). Estimates of sea surface temperature in the coral sea at the last glacial maximum. Paleoceanography, 193-208.

Anderson, R.N., Alt, J.C., and Malpas, J., (1989b). Geochemical well logs and the determination of integrated chemical fluxes in Hole 504B, eastern equatorial Pacific. In Becker, K., Sakai, H., et al., Proc. ODP, Sci. Results, 111: College Station, TX (Ocean Drilling Program), 119–132.

Andrews, J. E., G. Samways, P.F. Dennis, B.A. Maher, (2000). Origin, abundance and storage of organic carbon and sulphur in the Holocene Humber Estuary: emphasizing human impact on storage changes. In: Shennan, I., Andrews, J.E. (Eds.), Holocene Land-Ocean Interaction and Environmental Change around the North Sea. Geological Society London, Special Publications, vol. 166, 145-170.

Andrews, J.E., Greenaway, A.M., Dennis, P.F., (1998). Combined carbon isotope and C/N ratios as indicators of source and fate of organic matter in a poorly flushed, tropical estuary: Hunts Bay, Kingston Harbour, Jamaica. Estuarine, Coastal and Shelf Science, 46, 743–756.

Banakar V.K., T. Oba, A.R. Chodankar, T. Kuramoto, M. Yamamoto, M. Mingawa, (2005). Monsoon related changes in sea surface productivity and water column denitrification in the Eastern Arabian Sea during the last glacial cycle. Marine Geology, 219, 99-108.

Bange H. W., S. W. A. Naqvi and L.A. Codispoti. (2005).The nitrogen cycle in the Arabian Sea. Progress in Oceanography, vol. 65 (2-4), 45-158.

Bange, H.W, M.O. Andreae, S. Lal, C.S. Law, S.W.A. Naqvi, P.K. Patra, T. Rixen and R.C. Upstill-Goddard (2001). Nitrous oxide emissions from Arabian Sea: A Synthesis, Atmospheric Chemistry and Physics,1, 61-71.

Bange, H.W., S. Rapsomanikis and M.O. Andreae (1996). Nitrous oxide emissions from the Arabian Sea. Journal of Geophysical Research Letters, 23, 3175-3178.

Banse, K. (1987). Seasonality of phytoplankton chlorophyll in the central northern Arabian Sea. Deep Sea Research, 38:531-533.

Banse, K., and C.R. McClain (1986). Winter blooms of phytoplankton in the Arabian Sea as observed by the Coastal Zone Color Scanner, Marine Ecological Progress Series, 34, 201-211.

Banse, K. (1984). Overview of the hydrography and associated biological phenomena in the Arabian Sea, off Pakistan. In: Marine geology and oceanography of Arabian Sea and coastal Pakistan, edited by: Haq, B. U. and Milliman, J. D., Van Nostrand Reinhold Co., New York, 271–303.

Banse, K. (1968). Hydrography of the Arabian Sea Shelf of India and Pakistan and effects on demersal fishes. Deep-Sea Research, 15, 45-79.

Banse, K. (1959). On upwelling and bottom trawling off the southwest coast of India. Journal of Marine Biological Assessment, India, 1, 33-49.

Barber, R.T., J. Marra, R.R. Bidigare, L.A. Codispoti, D. Halpern, Z. Johnson, M. Latasa, R. Goericke and S.L. Smith (2001). Primary productivity and its

regulation in the Arabian Sea during 1995. Deep-Sea Research. II, 48, 1127-1172.

Bard, E., G., Raisbeck, F. Yiou, and J. Jouzel, (2000). Solar irradiance during the last 1200 years based on cosmogenic nuclides. Tellus 52B: 985-992.

Barford, C.C., J.P. Montoya, M.A. Altabet, and R. Mitchell, (1999). Steady-state nitrogen isotope effects of N_2 and N_2O production in Paracoccus denitrificans. Applied and Environmental Microbiology, 65 (3), 989–994.

Bassinot, F. C., L. D. Labeyrie, E. Vincent, X. Quidelleur, N. J. Shackleton, and Y. Lancelot (1994). The astronomical theory of climate and the age of the Brunhes-Matuyama magnetic reversal. Earth and Planetary Science Letters, 126, 91-108.

Bauer, J.E., and E.R.M., Druffel, (1998). Ocean margins as a significant source of organic matter to the deep open ocean. Nature 392, 482–485.

Benschneider, K., and R. J Robinson, (1952). A new spectrophotometric determination of nitrite in seawater. Journal of Marine Research, 11, 87-96.

Berger, W.H., V.S., Smetacek, G., Wefer, (1989). Ocean productivity and paleoproductivity —an overview. In: Berger, W.H., Smetacek, V.S., Wefer, G. (Eds.), Productivity of the Ocean: Present and Past. Dahlem Konferenzen. Wiley, Chichester, pp. 1–34.

Berger, W. H. and R. S. Keir (1984). Glacial-Holocene changes in atmospheric CO_2 and the deep-sea record. In: J. E. Hansen and T. Takahashi (eds) Climate Processes and Climate Sensitivity, Geophysical Monograph, 29, American Geophysical Union, Washington, 337–351.

Berger, W. H., L. Diester-Haas, and J. S. Killingley, (1978). Upwelling off Northwest Africa: the Holocene decrease as seen in carbon isotopes and sedimentological indicators. Oceanologica Acta, 1, 1-7.

Bertine, K. K. and K. K. Turekian. (1973). Molybdenum in Marine Deposits. Geochim Cosmochim Acta, 37, 1415-1434.

Bhushan, R. K., K. Dutta, and B.L.K. Somayajulu, (2001). Concentrations and burial fluxes of organic and inorganic carbon on the eastern margins of the Arabian Sea. Marine Geololy, 178, 95-113.

Bishop, J.K.B. (1988). The barite-opal-organic carbon association in oceanic particulate matter. Nature 332, 341-343.

Bishop, J.K.P., J.M., Edmond, D.R., Ketten, M.P., Bacon, and W.B. Silker, (1977). The chemistry, biology and vertical flux of particulate matter from the upper 400 m of the equatorial Atlantic Ocean. Deep-Sea Research, 24, 511-548.

Bonnefille, R., F., Chalié, J. Guiot, and A. Vincens, (1992). Quantitative estimates of full glacial temperatures of equatorial Africa from palynological data. Climate Dynamics, 6, 251-257.

Bonnefille, R., J.C. Roeland, and J. Guiot, (1990). Temperature and rainfall estimates for the past 40,000 years in Equatorial Africa. Nature, 346, 347-349.

Bordovskiy, O.K. (1965). Accumulation of organic matter in bottom sediments. Marine Geology, 3, 33-82.

Boyle, E. A. (1997). Characteristics of the deep-ocean carbon system during the past 150,000 years: CO_2 distributions, deep water flow patterns, and abrupt climate change, Proc. Natl. Acad. Sci. U.S.A., 94, 8300–8307.

Boyle, E.A., L. Labeyrie, and J.C. Duplessy, (1995). Calcitic foraminiferal data confirmed by cadmium in aragonitic Hoeglundina: application to the last glacial maximum in the northern Indian Ocean. Paleoceanography, 10 (1995), 881–900.

Boyle, E.A. (1994). A comparison of carbon isotopes and cadmium in the modern and glacial maximum ocean: can we account for the discrepancies?.In: Carbon Cycling in the Glacial Ocean: Constraints on the Ocean's Role in Global Change (eds. R. Zahn, T.F. Pedersen, M.A. Kaminski, and L. Labeyrie), NATO ASI Series, Vol. 17, Springer-Verlag, Berlin, pp. 167-194.

Boyle, E.A. (1992). Cadmium and $\delta^{13}C$ paleochemical ocean distributions during the stage 2 glacial maximum, Annual Review of Earth and Planetary Sciences, 20, 245-287.

Boyle, E.A., (1988). Vertical oceanic nutrient fractionation and glacial/interglacial CO_2 cycles. Nature, 331, 55-56.

Boyle, E.A., (1986). Paired carbon isotope and cadmium data from benthic foraminifera: implications for changes in oceanic phosphorus, oceanic circulation, and atmospheric carbon dioxide. Geochim Cosmochim Acta, 50, 265-276.

Bralower, T. J., and H. R., Thierstein, (1987). Organic carbon and metal accumulation in Holocene and mid-Cretaceous marine sediments: palaeoceanographic implications.In: Fleet, A., and Brooks, J., eds., Marine Petroleum Source Rocks, Special Publication of the Geological Society of London, vol. 24, pp. 377-398.

Brandes, J. A., and A. H. Devol, (2002). A global marine fixed nitrogen isotopic budget: Implications for Holocene nitrogen cycling. Global Biogeochemical Cycles, 16 (4), 1-67.14, doi: 10.1029/20001GB001856.

Brandes, J. A., A.H. Devol, D.A. Jayakumar, T. Yoshinari and S.W.A. Naqvi (1998). Isotopic composition of nitrate in the central Arabian Sea and eastern tropical North Pacific: a tracer for mixing and nitrogen cycles. Limnology and Oceanography, 43, 1680-1689.

Bratton, J. F., S. M., Colman, E. R., Thieler, R. R., Seal, (2003). Birth of the modern Chesapeake Bay estuary 7,400 to 8,200 years ago and implications for global sea-level rise. Geophysical Marine Letters, 22,188–197.

Broecker, W. S. and G. Henderson, (1998). The sequence of events surrounding termination II and their implications for the cause of glacial-interglacial CO_2 changes. Paleoceanography, 13, 352-364.

Broecker, W.S. (1986). Oxygen isotope constraints on surface ocean temperatures. Quaternary Research, 26,121-134.

Broecker, W. S. and T. H. Peng. (1982). Tracers in the Sea, 690 pp. Eldigio Press, Palisades, NewYork.

Bruland, K. W. (1980). Oceanographic distributions of cadmium, zinc, nickel and copper in the NorthPacific. Earth and Planetary Science Letters, 47, 176-I 98.

Butler J. H., J. W. Elkins, T. H. Thompson and K. B. Egan (1989). Tropospheric and dissolved N_2O of the west Pacific and east Indian Oceans during the El Niño Southern Oscillation event of 1987, Journal of Geophysical Research, 94 (D12), 14865–14877.

Calvert, S. E., T. F. Pedersen, P. D. Naidu, and U. von Stackelberg, (1995). On the organic carbon maximum on the continental slope of the eastern Arabian Sea. Journal of Marine Research, 53, 269-296.

Calvert, S. E. and T. F. Pedersen, (1993). Geochemistry of recent oxic and anoxic marine sediments: Implications for the geological record. Marine Geology, 113, 67-88.

Calvert, S. E. and T. F. Pedersen, (1992). Organic carbon accumulation and preservation in marine sediments: How important is anoxia? In: Whelan, J. K. & Farrington, J. W. (eds) Productivity, Accumulation and Preservation of Organic Matter in Recent and Ancient Sediments. Columbia University Press, New York, 231–263.

Calvert, S. E. (1990). Geochemistry and origin of the Holocene sapropel in the Black Sea. In: Facets of modern biogeochemistry, V. Ittekkot, Editor, Springer-Verlag, Berlin, pp. 327–353.

Calvert, S. E., and D. Z. Piper, (1984). Geochemistry of ferromanganese nodules from DOMES Site A, Northern Equatorial Pacific: Multiple diagenetic metal sources in the deep sea. Geochim Cosmochim Acta, 48, 1913–1928.

Calvert, S. E., and N.B. Price, (1971). Upwelling and nutrient regeneration in the Benguela Current, October, 1968. Deep Sea Research, 18, 505-523.

Capone, D.G., J.P. Zehr and H.W. Paerl, (1997). Trichodesmium, a globally significant marine cyanobacterium. Science 276, pp. 1221–1229.

Carpenter, J. H. (1965). The Chesapeake Bay Institute technique for the Winkler dissolved oxygen method. Limnology and Oceanography, 10, 140-143.

Carruthers, J. N., S. S. Gogate, J.R. Naidu, T. Laevastu, (1959). Shoreward upslope of the layer of minimum oxygen off Bombay: Its influence on Marine biology, especially fisheries. Nature, 183, 1084-1087.

Chmura, G. L., A. Santos, V., Pospelova, Z., Spasojevic, R. Lam, JK.S. Latimer (2004). Resonse of three paleo-primary production proxy measures to development of an urban estuary. Science of the Total Environment, 320, 225-243.

Clemens, S., and W.L. Prell, (2003). A 350,000 year summer-monsoon multi-proxy stack from the Owen Ridge, Northern Arabian Sea. Marine Geology, 201, 35-51.

Clemens, S., W.L. Prell, D. Murray, G. B. Shimmield, and G., Weedon, (1991). Forcing mechanisms of the Indian Ocean monsoon. Nature, 353, 720-725.

Clemens, S. and W. L. Prell, (1990). Late Pleistocene variability of Arabian Sea summer monsoon winds and continental aridity; eolian records from the lithogenic component of deep-sea sediments. Paleoceanography, 5(2), 109-145.

Cline, J.D. and I.R. Kaplan (1975). Isotopic fractionation of dissolved nitrate during denitrification in the Eastern Tropical North Pacific Ocean. Marine Chemistry, 3, 271--299

Cline, J. D. and F.A. Richards (1972). Oxygen deficient conditions and nitrate reduction in the eastern tropical North Pacific Ocean. Limnology Oceanography, 17, 885-900.

Codispoti L. A. (2007). An oceanic fixed nitrogen sink exceeding 400 Tg Na^{-1} vs the concept of homeostasis in the fixed-nitrogen inventory. Biogeosciences Discussions, 4, 233-253.

Codispoti, L.A, J.A. Brandes, J.P. Christensen, A.H. Devol, S.W.A. Naqvi, H.W. Paerl and T. Yoshinari (2001). The oceanic fixed nitrogen and nitrous oxide budgets: Moving targets as we enter the anthropocene. Scientia Marina, 85-105.

Codispoti, L. A. (1989) Phosphorus vs. nitrogen limitation of new and export production. In: Productivity of the ocean: Present and past, edited by W. H. Berger, V. Smetacek and G. Wefer, Wiley, p. 377-394.

Codispoti, L.A., R.T. Barber and G.E. Friederich. (1989). Do nitrogen transformations in the Poleward Undercurrent off Peru and Chile have a globally significant influence? pp. 281-310. In: J. Neshyba, C. Mooers and R. Barber, (eds.) Poleward Flows on Eastern Boundaries, Springer-Verlag, New York.

Codispoti, L.A. and J.P. Christensen (1985). Nitrification, denitrification and nitrous oxide cycling in the eastern tropical South Pacific Ocean. Marine Chemistry, 16, 277-300.

Codispoti, L.A. and T.T. Packard (1980). Denitrification rates in the eastern tropical South Pacific. Journal of Marine Research, 38, 453 - 477.

Codispoti, L.A. and F.A. Richards (1976). An analysis of the horizontal regime of denitrification in the eastern tropical North Pacific. Limnology Oceanography, 21, 379 - 388.

Cohen, Y. and L. Gordon (1978). Nitrous oxide in the oxygen minimum of the eastern tropical North Pacific: evidence for its consumption during denitrification and possible mechanisms for its production. Deep-Sea Research, 25, 509-524.

Collier, R. and J. M. Edmond, (1984). The trace element geochemistry of marine biogenic particulate matter. Progress in Oceanography, 13, 113–199.

Colodner D., J. Edmond and E. Boyle (1995). Rhenium in the Black Sea: comparison with molybdenum and uranium, Earth and Planetary Science Letters, 131, 1–15.

Colodner D, J. Lin, K .Von Damm, L. Buttermore, R. Kozlowski, J.L. Charlou, J.P. Donval, C. Wilson, The Lucky Strike Team (1993). Chemistry of Lucky Strike hydrothermal fluids: initial results. EOS 74:99 (Abstract).

Cornwell, J. C., D. J. Conley, M. Owens, and J. C. Stevenson. (1996). A sediment chronology of the eutrophication of Chesapeake Bay. Estuaries, 19, 488-499.

Cowie, G. L., J. I. Hedges. , F. G. Prahl, and G. J. De Lange (1995). Elemental and major biochemical changes across an oxidation front in a

relict turbidite: an oxygen effect. Geochimica et Cosmochimica Acta, 59, 33–46.

Craig, H., (1957). Isotopic standards for carbon and oxygen and correction factors for mass-spectro-metric analysis of carbon dioxide. Geochimica et Cosmochimica Acta, 12, 133-149.

Craig, H., (1953). Carbon-13 in plants and the relationships between carbon-13 and carbon-14 variations in nature. Geology, 62, 115-149.

Cranston R.E., (1983). Chromium in cascadal Basin, northeast Pacific Ocean. Marine Chemistry, 13, 109–125.

Cranston R. E. and J. W. Murray (1978). The determination of chromium species in natural waters. Analytica Chimica Acta, 99, 275-282.

Crusius J., T.F. Pedersen, S.E. Calvert, G.L. Cowie and T. Oba. (1999). A 36 kyr geochemical record from the Sea of Japan of organic matter flux variations and changes in intermediate water oxygen concentrations. Paleoceanography, 14, 248–259.

Crusius J., S. E. Calvert, T. F.Pedersen, and D. Sage (1996). Rhenium and molybdenum enrichments in sediments as indicators of oxic, suboxic and anoxic conditions of deposition. Earth and Planetary Science Letters, 145, 65-78.

Curry W.B., D.R. Ostermann, M.V.S. Guptha and V. Ittekkot, (1992). Foraminiferal production and monsoonal upwelling in the Arabian Sea, evidence from sediment traps. In: C.P. Summerhays, W.L. Prell, K.C. Emeis et al. Upwelling Systems. Evolution since the Early Miocene. Geological Society Special Publication, vol. 64, pp. 93–106.

Curry W.B., J.C. Duplessy, L.D. Labeyrie and N.J. Shackleton, (1988). Changes in the distribution of $\delta^{13}C$ of deep water ΣCO_2 between the last glaciation and the Holocene. Paleoceanography, 3, 317–341.

Dalsgard T, D.E. Canfield, J. Pederesen, B. Thamdrup, J. Acuna-Gonzalez, (2003). N_2 production by the anammox reaction in the anoxic water column of the Golfo Dulce, Costa Rica. Nature, 422, 606-608.

Dawson, A.G. (1992). Ice Age Earth – Late Quaternary geology and climate. Physical Environment Series, Routledge, London New York, 293 pp.

De Wilde, H.P.J., W. Helder (1997). Nitrous oxide in the Somali Basin: the role of upwelling. Deep-Sea Research II, 44(6-7), 1319-1340.

Dean W.E., D.Z. Piper and L.C. Peterson (1999). Molybdenum accumulation in Cariaco basin sediment over the last 24 k.y.: a record of water-column anoxia and climate. Geology, 27, 507–510.

Dean, W.E., J.V. Gardner and D.Z. Piper (1997). Inorganic geochemical indicators of glacial-interglacial changes in productivity and anoxia on the California continental margin. Geochimica et Cosmochimica Acta, 61, 4507– 4518.

Demaison, G.J. and G.T.Moore, (1980). Anoxic environments and oil source bed genesis. American Assocciation on Petrology Geological Bulletin., 64, 1179-1209.

Delwiche, C.C., and P.L. Steyn, (1970). Nitrogen isotope fractionation in soils and microbial reactions. Envrionmental Science and Technology, 4, 929-935.

Deuser, W.G., (1987). Seasonal variations in isotopic composition and deep-water fluxes of the test of perenially abundant planktonic foraminifera of the Sargasso Sea: results from sediment trap collections and their paleoceanographic significance. Journal of Foram Research, 19, 268-293.

Deuser, W.G., E.H. Ross and Z.J. Mlodzinska, (1978). Evidence for and rate of denitrification in the Arabian Sea. Deep-Sea Research. 25, 47-146.

Deuser W.G., (1975). Reducing environments. In: J.P. Riley and G. Skirrow, Editors, Chemical Oceanography vol. 3, Academic Press, New York, pp. 1–38.

Deutsch, C., J., Sarmiento, D.M Sigman, N. Gruber and J. Dunne. (2007). Spatial coupling of nitrogen inputs and losses in the ocean. Nature, 445, 163-167.

Deutsch C., D.M. Sigman, R.C. Thunell, A.N. Meckler and G.H. Hau, (2004). Isotopic constraints on glacial/interglacial changes in the oceanic nitrogen budget. Global Biogeochemical Cycles, 18 (4), doi:10.1029/2003GB002189.

Devassy, V.P., P.M.A. Bhattathiri, and S.Z. Qasim, (1978). Trichodesmium Phenomenon. Indian Journal of Marine Sciences, 7, 168-186.

Devol A. H., A.G. Uhlenhopp, S.W.A. Naqvi, J.A. Brandes, D.A. Jayakumar, H. Naik, S. Gaurin, L.A. Codispoti, and T. Yoshinari, (2006). Denitrification rates and excess nitrogen gas concentrations in the Arabian Sea oxygen deficient zone. Deep-Sea Research, I, 53, 1533–1547.

Diaz, R.J. and R. Rosenberg (1995). Marine benthic hypoxia: A review of its ecological effects and the behaviour responses of benthic macrofauna. Oceanography and Marine Biology: Annual Review, 33, 245-303.

Dickens G R and R M Owen (1994). Late Miocene - Early Pliocene manganese redirection in the Central Indian Ocean: Expansion of the

intermediate water oxygen minimum zone. Palaeoceanography, 9, 169-181.

Dow, (1978). Radiolarian distribution and the Late Pleistocene history of the southeastern Indian Ocean. Marine Micropaleontology, 3, 203-227.

Dugdale , R. C. , A. G. Wischmeyer, R. T. Barber, F. P. Wilkerson, , F. Chai, M. S. Jiang and T. H. Peng (2002). Meridional asymmetry of source nutrients to the equatorial Pacific upwelling ecosystem and its potential impact on ocean–atmosphere CO_2 flux; a data and modeling approach. Deep Sea Research, II, 49 (13-14), 2513-2531.

Duplessy J. C., N. J. Shackleton, R. G. Fairbanks, L. Labeyrie, D. W. Oppo, and N. Kallel (1988). Deepwater source variations during the last climatic cycle and their impact on the global deep-water circulation. Paleoceanography, 3, 343–360.

Duplessy, J. C., (1982). Glacial to interglacial contrast in the northern Indian Ocean. Nature, 295, 494-498.

Duplessy, J. C., P. L. Blanc and A. W. H. Bé, (1981). Oxygen-18 enrichment of planktonic foraminifera due to gametogenic calcification below the euphotic zone. Science, 213, 1247-1250.

Dymond, J., E. Suess, and M. Lyle, (1992). Barium in deep-sea sediment: A geochemical proxy for paleoproductivity. Paleoceanography, 7, 163-181.

Eadie, B. J., B. A. McKee, M.B. Lansing, J.A. Robbins, S. Metz, and J.H. Trefry (1994). Records of nutrient-enhanced coastal productivity in sediments from the Louisiana continental shelf. Estuaries, 17, 754-765.

Eckelman, W. R., W.S. Broecker, D. W. Whitlock, and J. R. Allsup, (1962). Implications of carbon isotopic composition of total organic carbon of some recent sediments and ancient oils. American Association of Petroleum Geologists Bulletin, 46, 699-704.

Elderfield, H. (1970). Chromium speciation in sea-water. Earth and Planetary Science Letters, 9, 10-16.

Elkins, J. W., S. C. Wofsy, M. B. Mcelroy, C. E.Kolb, and W. A Kaplan (1978). Aquatic sources and sinks for nitrous oxide. Nature, 275, 602-606.

Emeis K. C., D.M. Anderson, H. Doose, D. Kroon and D. Schulz-Bull, (1995). Sea-surface temperatures and history of monsoon upwelling in the northwest Arabian Sea during the last 500,000 years. Quaternary Research, 43, 355–361.

Emerson, S.R. and S.S. Huested, (1991). Ocean anoxia and the concentrations of molybdenum and vanadium in seawater. Marine Chemistry, 34, 177-196.

Emerson and Hedges, (1988). S. Emerson and J.I. Hedges, Processes controlling the organic carbon content of open ocean sediments. Paleoceanography, 3, 621–634.

Emerson, S., K. Fischer, C. Reimers, and D. Heggie, (1985). Organic carbon dynamics and preservation in deep-sea sediments. Deep-Sea Research, 32, 1-21.

Emiliani, C., (1955). Pleistocene temperatures. Journal of Geology, 63(6), 538-578.

Emrich, K., D. H. Ehhalt, and J. C. Vogel, (1970). Carbon isotope fractionation during the precipitation of calcium carbonate. Earth and Planetary Science Letters, 8, 363-371.

Epstein, S., R. Buchsbaum, H. A. Lowenstam, and H. C. Urey, (1953). Revised carbonate, water isotopic temperature scale. Geological Society of America Bulletin, 64, 1315-1326.

Erez, J. and S. Honjo, (1981). Comparison of isotopic composition of planktic foraminifera in plankton tows, sediment traps and sediments. Palaeogeography, Palaeoclimatology, Palaeoecology, 33, 129-156.
Erez, J., (1978). Vital effect on stable-isotope composition seen in foraminifera and coral skeletons. Nature, 273, 199.

Fabry V.J. and W.G. Deuser, (1992). Seasonal changes in the isotopic compositions and sinking fluxes of euthecosomatous pteropod shells in the Sargasso Sea. Paleoceanography, 7, 195-213.

Fairbanks, R. G., (1989). A 17,000 year glacio-eustatic sea level record: Influence of glacial melting rates on the Younger Dryas event and deep-ocean circulation. Nature, 342, 637-642.

Falkowski, P.G. (1997). Evolution of the nitrogen cycle and its influence on the biological sequestration of CO_2 in the ocean. Nature, 387, 272-275.

Farías, L., A. Paulmier, M. Gallegos, (2007). Nitrous oxide and N-nutrient cycling in the oxygen minimum zone off northern Chile. Deep-Sea Research I, 54, 164-180.

Fischer, H., M. Kalberer, B. Donner and G. Wefer, (1999). Stable isotopes of pteropod shells as recorders of sub-surface water conditions: Comparision to the records of G. ruber and to measured values. In: Use of proxies in paleoceanography – Examples from the south Atlantic, editors Gerhard Fischer and Gerold Wefer, Spriger-Verlag, Berlin Heidelberg, 191-206.

Fischer,G., S. Neuer, and G. Wefer, (1996). Short-term sedimentation pulses recorded with a fluorescence sensor and sediment traps at 900-m depth in the Canary basin. Limnology and Oceanography, 41(6), 1354-1359.

Flagg, C.N. and H. S. Kim, (1998). Upper ocean currents in the northern Arabian Sea from ADCP measurements during the 1994–1996 JGOFS program. Deep Sea Research II, 45, 1917–1959.

Fluckiger J., E. Monnin, B. Stauffer, J. Schwander, and T. F. Stocker (2002). High resolution Holocene N_2O ice core record and its relationship with CH_4 and CO_2. Global Biogeochemical Cycles, 16(1), 1010, doi:10.1029/2001GB001417

Fofonoff, N.P., Millard Jr., R.C., (1983). Algorithms for computation of fundamental properties of seawater. Technical Report 44, UNESCO, Technical Papers in Marine Science

Fonselius, S.H., (1962). Hydrography of the Baltic deep basins. Fishery Board of Sweden, Ser. Hydmgr. Rep. 13, 1-41.

Fontanier C., A. Mackensen, F. Jorissen, P. Anschutz, L. Licari and C. David, (2006). Stable Oxygen and Carbon Isotopes of Live Benthic Foraminifera from the Bay of Biscay: Microhabitat Impact and Seasonal Variability. Marine Micropaleontology, 58, 159-183.

Fontugne, M.R. and J.C. Duplessy, (1986). Variations of the monsoon regime during the upper Quaternary: evidence from carbon isotopic record of organic matter in north Indian Ocean sediment cores. Palaeogeography Paleoclimatology Palaeoecology, 56, 69-88.

Francois R., (1997). Contributions of Southern Ocean surface-water stratification to low atmospheric CO_2 concentrations during the last glacial period. Nature, 389, 929–935.

François, R., S. Honjo, S.J. Manganini and G.E. Ravizza, (1995). Biogenic barium fluxes to the deep sea: implications for paleoproductivity reconstruction. Global Biogeochemical Cycles, 9 (2), 289–303.

Froelich, N., G. P. Klinkhammer, M. L. Bender, N. A. Luedtke, G. R. Heath, D. Cullen, P. Dauphin, D. Hammond, B. Hartman and V. Maynard (1979). Early oxidation of organic matter in pelagic sediments of the eastern equatorial Atlantic: suboxic diagenesis. Geochimica et Cosmochimica Acta, 43, (7), 1075-1090.

Fry, B., and E. B. Sherr, (1989). $\delta^{13}C$ measurements as indicators of carbon flow in marine and freshwater ecosystems. In: Rundel, P.W., Ehleringer, J.R., Nagy, K.A. (Eds.), Stable Isotopes in Ecological Research. Springer-Verlag, New York, pp. 196-229.

Ganeshram, R.S., T. F. Pedersen, S. E. Calvert, and G. W. McNeill, (2000). Glacial-interglacial variability in denitrification in the world's oceans: Causes and consequences. Paleocenagraphy, 15, 361-376.

Ganeshram, R.S., and T.F. Pedersen, (1998). Glacial-interglacial variability in upwelling and bioproductivity off NW Mexico: Implications for Quaternary paleoclimate. Paleoceanography, 13, 634-645.

Ganeshram, R.S., T.F. Pedersen, S.E. Calvert and J. W. Murray (1995). Large changes in oceanic nutrient inventories from glacial to interglacial periods. Nature, 376, 755-758.

Ganssen, G. and M. Sarnthein, (1983). Stable-isotope composition of foraminifers: the surface and bottom water record of coastal upwelling. In: Coastal upwelling, its sediment record, Suess, E. and Thiede, J. (Eds.). Plenum, New York, 10A: 99-121.

Gardner, W.S., J.F. Cavaletto, J.B. Jr. Cotner, and J.R. Johnson, (1997). Effects of natural light on nitrogen cycling rates in the Mississippi River plume. Limnology and Oceanography 42 (2), 273– 281.

Gardner, W. S. and D. W. Menzel, (1974). Phenolic aldehydes as indicators of terrestrially derived organic matter in the sea. Geochimica et Cosmochimica Acta, 38, 813-822.

Garrison, D.L., M.M. Gowing, and M.P. Hughes, (1998). Nano- and microplankton in the northern Arabian Sea during the Southwest Monsoon, August-September, 1995: a US JGOFS study. Deep-Sea Research II 45, 2269-2300.

Gaye-Haake, B., N. Lahajnar, K-Ch. Emeis, D. Unger, T. Rixen, A. Suthhof, V. Ramaswamy, H. Schulz, A.L. Paropkari, M.V.S. Guptha, and V. Ittekkot (2005). Stable nitrogen isotopic ratios of sinking particles and sediments from the northern Indian Ocean. Marine Chemistry, 96, 243-255.

German, C.R. and H. Elderfield, (1990). Application of the Ce anomaly as a paleoredox indicator: the ground rules, Paleoceanography 5, pp. 823–833.

Gilson, H.C. (1937). The nitrogen cycle. In: Scientific reports. John Murray expeditions. 1933-1934. 2, 21-81.

Gingele, F., and A. Dahmke, (1994). Discrete barite particles and barium as tracers of paleoproductivity in SouthAtlantic sediments. Paleoceanography 9, 151–168.

Gobeil C., B. Sundby, R. W. Macdonald, and J. N. Smith, (2001). Recent change in organic carbon flux to Arctic Ocean deep basins: Evidence from

acid volatile sulfide, manganese and rhenium discord in sediments. Geophysical Research Letters, 28, 1743–1746.

Gobeil, C., R. MacDonald, and B. Sundby, (1997). Diagenetic separation of cadmium and manganese in suboxic continental margin sediments. Geochimica et Cosmochimica Acta, 61, (21), 4647-4654.

Goericke, R., R.J. Olson, and A. Shalapyonok, (2000). A novel niche for Prochlorococcus sp. in low-light suboxic environments in the Arabian Sea and the Eastern Tropical North Pacific. Deep-Sea Research, I 47, 1183–1205.

Goering, J.J. (1968). Denitrification in the oxygen minimum layer of the eastern tropical Pacific Ocean. Deep-Sea Research, 15, 157 - 164.

Goes, J.I., P. G. Thoppil, H. Gomes, and J.T. Fasullo, (2005). Warming of the Eurasian Landmass is Making the Arabian Sea More Productive. Science, 308, 545-547.

Gogate, S. S., (1960). Some aspects of hydrobiology of Bombay waters. M.Sc. thesis, Univ. Bombay. 111 pp.

Goldberg, E.D., G. Arrhenius, (1958). Chemistry of Pacific pelagic sediments. Geochimica et Cosmochimica Acta, 13, 153–212.

Goreau, T.J., W.A. Kaplan, S.C. Wofsy, M.B. McElroy, F.W. Valois, and S.W. Watson (1980). Production of NO_2^- and N_2O by nitrifying bacteria at reduced concentrations of oxygen. Appl. Environ. Microbiol., 40, 526-532.

Grasshoff K., M. Ehrhardt and K. Kremling (1983). Methods of seawater analysis, Verlag Chemie GmbH, Weinheim.

Grasshoff, K. (1969). Zur Chemie des Roten Meeres und des inneren Golf von Aden nach Beobachtungen von F S 'meteor' wahrender Indischen Ozean Expedition 1964/65. Meteor Foprschungsergeb, Reihe A, A6, 76pp.

Grossman, E.L., (1987). Stable isotopes in modern benthic foraminifera: A study of vital effect. Journal of Foraminiferal Research, 17, 48-61.

Grossman, E. L. (1984a), Carbon isotopic fractionation in live benthic foraminifera—Comparison with inorganic precipitate studies, Geochimica et Cosmochimica Acta, 48, 505–1512.

Gruber N. and J. L. Sarmiento (1997). Global patterns of marine nitrogen fixation and denitrification. Global Bigeochemical Cycles, 11, 235-266.

Gupta, A., D. Anderson, and J. Overpeck (2003). Abrupt changes in the Asian southwest monsoon during the Holocene and their links to the North Atlantic Ocean. Nature, 421, 354–357.

Hastings D. W., S. R. Emerson, and B. K. Nelson, (1996). Determination of picogram quantities of vanadium in calcite and seawater byisotope dilution inductively coupled plasma mass spectrometry with electrothermal vaporization. Anal. Chem. 68, 371–377.

Hastings D. W. (1994). Vanadium in the Ocean: A Marine Mass Balance and Paleoseawater Record. Ph.D. thesis, University of Washington.

Haug, G.H., T.F. Pedersen, D.M. Sigman, S.E. Calvert, B Nielsen, L.C. Peterson, (1998). Glacial/interglacial variations in production and nitrogen fixation in the Cariaco Basin during the last 580 kyr, Paleoceanography, 13, 427-432.

Hedges, J.I. and P.L. Parker, (1976). Land-derived organic matter in surface sediments from the Gulf of Mexico. Geochimica et Cosmochimica Acta, 40, 1019-1029.

Helly, J.J.and Levin, L.A. (2004). Global distribution of naturally occurring marine hypoxia on continental margins. Deep-Sea Research, I, 51, 1159–1168

Hida, T.S. and W.T. Pereira (1966). Results of bottom trawling in Indian seas by R.V. Anton Bruun. Proc Indo-Pacific Fish Coun , 11, 156-71.

Higginson, M.J., M.A. Altabet, D.W. Murray, R.W. Murray, and T.D. Herbert, (2004). Geochemical evidence for abrupt changes in relative strength of the Arabian monsoons during a stadial/interstadial climate transition. Geochimica et Cosmochimica Acta, 68, (19), 3807-3826.

Hoefs, J., (1987). Stable Isotope Geochemistry, Third Edition, Springer-Verlag, Berlin, 241 p.

Holsten, L. Stott and W. Berelson, (2004). Reconstructing benthic carbon oxidation rates using $\delta^{13}C$ of benthic foraminifers. Marine Micropaleontology, 53, 117–132.

Howarth, R.W., A. Sharpley and D. Walker. (2002). Sources of nutrient pollution to coastal waters in the United States: implications for achieving coastal water quality goals. Estuaries 25(4b), 656-676.

Howell, E.A., S.C. Doney, R.A. Fine and D.B. Oslon (1997). Geochemical estimates of denitrification in the Arabian Sea and Bay of Bengal. Journal of Geophysical Research Letters, 24, 2549-2552.

Howell, P. and D. Simpson. (1994). Abundance of marine resources in relation to dissolved oxygen in Long Island Sound. Estuaries, 17, 394-402.

Hutchins A. and K.W. Bruland, (1998). Iron-limited diatom growth and Si:N uptake ratios in a coastal upwelling regime. Nature, 393, 561–564.

Imbrie Z., J.D. Hays, D.G. Martinson, A. MacIntyre, A. Mix, A.C. Morley, N.G. Pisias, W.L. Prell and N.J. Shackleton, (1984). The orbital theory of Pleistocene climate: support from a revised chronology of the marine $\delta^{18}O$ record. In: A. Berger, J.Z. Imbrie, J.D. Hays, G. Kukla and B. Saltzman, Editors, Milankovitch and Climate Part I, Reidel, Dordrecht, pp. 269–305.

Ivanochko S. T. and T.F. Pedersen, (2004). Determining the influences of Late Quaternary ventilation and productivity on Santa Barbara Basin sedimentary oxygenation: a multi-proxy approach. Quaternary Science Reviews, 23, 467–480.

Intergovernmental Panel on Climate Change (IPCC), 2007. Climate Change 2006: The Scientific Basis. Contribution of Working Group I to the Fourth Assessment Report of the Intergovernmental Panel on Climate Change. S. Solomon, D. Qin, M. Manning, Z. Chen, M. Marquis, K. B. Averyt, M. Tignor, and H. L. Miller, eds., Cambridge University Press.

Jasper, J.P., Gagosian, R.B., (1993). The relationship between sedimentary organic carbon isotopic composition and organic biomarker compound concentration. Geochimica Cosmochimica Acta 57, 167–186.

Kallel, N., L.D. Labeyrie, A. Juillet-Leclerc, and J.-C. Duplessy, (1988). A deep hydrological front between intermediate and deep-water masses in the glacial Indian Ocean. Nature, 333, 651–655.

Kamykowski D.Z. and S.J. Zentara (1990). Hypoxia in the world ocean as recorded in the historical data set. Deep-Sea Research, 37, 1861–1874.

Kao S.J. and K.K. Liu, (2000). Stable carbon and nitrogen isotope systematic in a human-disturbed watershed (Langyang-Hsi) in Taiwan and the estimation of biogenic particulate organic carbon and nitrogen fluxes. Global Biogeochemical Cycles, 14, 189–198.

Kato N., F. Zapata and H. Axmann (1995). Evaluation of the agronomic effectiveness of natural and partially acidulated phosphate rocks in several soils using P-32 isotopic dilution techniques. Fert. Res. 41, 235-242.

Kerherve, P., M. Minagawa, S. Heussner, and A. Monaco, (2001). Stable isotopes ($^{13}C/^{12}C$ and $^{15}N/^{14}N$) in settling organic matter of the northwestern Mediterranean Sea: biogeochemical implications, Oceanologica Acta, 24, Supplement 1, 77–85.

Kim, H. S., C. N. Flagg, & S. D. Howden, (2001). Northern Arabian Sea variability from TOPEX/Poseidon altimetry data: an extension of the US JGOFS/ONR shipboard ADCP study. Deep-Sea Research, II, 48, 1069–1096.

Klinkhammer G. P. and M. R. Palmer, (1991). Uranium in the oceans: Where it goes and why. Geochimica et Cosmochimica Acta, 55, 1799–1806.

Klump, J., D. Hebbeln, and G. Wefer, (2000). The impact of sediment provenance on barium-based productivity estimates. Marine Geology, 169, 259–271.

Knap, A.H., K.S. Binkley, and W.G. Deuser, (1986). Synthetic organic chemicals in the deep Sargasso Sea. Nature, 319, 572-574.

Kolla, V., J. A. Kostecki, F. Robinson, P. Biscaye, and P. K. Ray, (1981a). Distribution and origin of clay minerals and quartz in surface sediments of the Arabian Sea. Journal of Sedimentary Petrology, 51, 563-569.

Kolla, V., P.K. Ray, J.A. Kostecki, (1981b). Surficial sediments of the Arabian Sea. Marine Geology, 41, 183–204.

Kolla, V., A.W.H. Ba, and P.E. Biscaye, (1976a). Calcium carbonate distribution in the surface sediments of the Indian Ocean. Journal of Geophysical Research, 81 (15), 2605–2616.

Kolla, V., L. Henderson, and P. E. Biscaye, (1976b). Clay mineralogy and sedimentation in the western Indian Ocean. Deep Sea Research, 23, 946-961.

Koroleff F., (1983). Determination of Phosphorus. In: K. Grasshoff. M. Ehrhardt and K. Kremling (eds.), Methods of sea water analysis. Verlag Chemise, 126p.

Koroleff F. (1970). Direct determination of ammonia in natural waters as indophenol blue. ICES Interlaboratory Report, 3, 19-22.

Kroopnick, P., (1985). The distribution of ^{13}C of $\sum$CO2 in the world oceans. Deep-Sea Research, 32 (1), 57–84.

Kroopnick, P. (1974). The dissolved O_2–CO_2–^{13}C system in the eastern equatorial Pacific. Deep-Sea Research, 21, 211–227.

Kumar, S. P. and T. G. Prasad, (1996). Winter cooling in the northern Arabian Sea. Current Science (JGOFS-India Special Section), 71, 834-841.

Kuypers, MM, G. Lavik, D. Woebken, M. Schmid, B.M. Fuchs, R. Amann, B.B. Jorgensen, and M.S.M. Jetten (2005). Massive nitrogen loss from the Benguela upwelling system through anaerobic ammonium oxidation. Proceedings of the National Academy of Sciences, 102, 6478-6483.

Kuypers M. M. M., A. O. Sliekers, G. Lavik, M. Schmid, B. B. Jørgensen, J. G. Kuenen, J. S. Sinninghe Damsté, M. Strous and M. S. M. Jetten (2003).

Anaerobic ammonium oxidation by anammox bacteria in the Black Sea. Nature, 422, 608-611.

Labeyrie, L.D., J.-C. Duplessy and P.L. Blanc, (1987), Variations in mode of formation and temperature of oceanic deep waters over the past 125,000 years. Nature, 327, 477–482.

Lewis B.L. and G.W. Luther, (2000). Processes controlling the distribution and cycling of manganese in the oxygen minimum zone of the Arabian Sea. Deep-Sea Research, II, 47, 1541–1561.

Libes, S.M., and W.G. Deuser, (1988). The isotope geochemistry of particulate nitrogen in the Peru upwelling area and the Gulf of Maine. Deep-Sea Research 35, 517-533.

Lightfoot P.C., C.J. Hawkesworth, C.W. Devey, N.W. Rogers and P.W.C. Van Calsteren, (1990). Source and differentiation of Deccan Trap lavas: implications of geochemical and mineral chemical variations, J. Petrol. 31, 1165–1200.

Liu, K. K. and I. R. Kaplan, (1989). The eastern tropical Pacific as a source of 15N-enriched nitrate in seawater off southern California. Limnology and Oceanography, 34, 820–830.

Luther III, G. W., B. Sundlby, B. L. Brendel, and N. Silverberg, (1997). Interactions of Manganese with the nitrogen cycle: alternative pathways to dinitrogen. Geochimica et Cosmochimica Acta, 61, 4043-4052.

Lyle, M., R. Zahn, F. Prahl, J. Dymond, R. Collier, N. Pisias and E. Suess, (1992). Paleoproductivity and Carbon burial across the California current: The Multitracers transect, 42°N, Paleoceanography, 7, 251–272.

Mackensen, A., and L. Licari (2004). Carbon isotopes of live benthic foraminifera from the South Atlantic: Sensitivity to bottom water carbonate saturation state and organic matter rain rates. In, The South Atlantic in the Late Quaternary: Reconstruction of Material Budget and Current Systems, edited by G. Wefer, S. Mulitza, and V. Rathmeyer, pp. 623– 644, Springer, New York.

Mackensen, A., M. Rudolph, and G. Kuhn (2001), Late Pleistocene deep-water changes and paleoproductivity in the subantarctic eastern Atlantic. Global Planetary Change, 30, 197–229.

Mackensen, A., H. Grobe, H.-W. Hubberten, and G. Kuhn (1994). Benthic foraminiferal assemblages and the δ^{13}C-signal in the Atlantic sector of the Southern Ocean: Glacial-to-interglacial contrasts. In, Carbon Cycling in the Glacial Ocean: Constraints on the Ocean's Role in Global Change, NATO ASI Ser., Ser. I, edited by R. Zahn et al., pp. 105 – 144, Springer, New York.

Madhupratap, M., S. Kumar, P.M.A. Bhattathiri, M. Dileep Kumar, S.Raghukumar, K. K. C Nair and N. Ramaiah, (1996). Mechanism of the biological response to winter cooling in the northeastern Arabian Sea. Nature, 384, 549–552.

Madhupratap, M. S.R.S. Nair, P. Haridas, and G. Padmavati, (1990). Response of zooplankton to physical changes in the environment: coastal upwelling along the central west coast of India. Journal of Coastal Research, 6, 413-426.

Makshymowska D., P. Richard, H. Piekarek-Jankowska and P. Riera (2000). Chemical and isotopic composition of the organic matter sources in the Gulf of Gdansk (Southern Baltic Sea), Estuarine, Coastal and Shelf Science, 51, 585–598.

Malakoff, D., (1998). Death by suffocation in the Gulf of Mexico. Science, 281, 190-192.

Manheim F.T., (1974). Red Sea geochemistry. In: R.B. Whitmarsh, O.E. Weser and D.A. Ross, Editors, Initial Reports of Deep Sea Drilling Project vol. 23, US Goverment Printing Office, Washington D.C. pp. 975–998.

Mantoura R.F.C., C.S. Law, N.J.P. Owens, P.H. Burkill, E.M.S. Woodward, R.J.M. Howland and C.A. Llewellyn (1993). Nitrogen biogeochemical cycling in the north western Indian Ocean. Deep-Sea Research, II, 40, 651-671.

Mantyla A. W. and J. L. Reid, (1995). On the origins of deep and bottom waters of the Indian Ocean. Journal of Geophysical Research, 100, 2417–2439.

Marchig, V. (1974). Zur Geochemie rezenter Sedimente des Indischen Ozeans II. Arabisches Meer, afrikanischer Kontinentalrand und Vergleich mit dem indisch-pakistanischen Kontinentalrand, Meteor Forschungsergebnisse, Deutsche Forschungsgemeinschaft, Reihe C Geologie und Geophysik, Gebrüder Bornträger, Berlin, Stuttgart, C18, 1-34.

Marchig, V. (1972). Zur Geochemie rezenter Sedimente des Indischen Ozeans. "Meteor" Forsch.-Ergebnisse, Reihe C, 11, 1–104.

Mariotti, A., J. C. Germon, P. Hubert, P. Kaiser, R. Letolle, A. Tardieux, and P. Tardieux, (1981). Experimental determinations of nitrogen kinetic isotope fractionation: Some principles; illustration for the denitrification and nitrification processes. Plant Soil, 62, 413-430.

Matson, E.A., and M.M., Brisnon, (1990). Stable isotopes and the C:N ratio in estuaries of the Pamlico and Neuse Rivers, North Carolina. Limnology and Oceanography, 35,1290-1300.

Mattiat, B., J. Peters, and F. J. Eckhardt, (1973). Ergebnisse petrographischer Untersuchungen an Sedimenten des indisch-pakistanischen Kontinentalrandes (Arabische See). "Meteor" Forsch.-Ergebnisse, Reihe C, 14, 1–50.

McAuliff C. (1971). GC determination of solutes by multiple phase equilibration. Chem. Tech., 1, 46-50.

McCarthy, J. J. and E. J. Carpenter (1983). Nitrogen cycling in near-surface waters of the open ocean. In: Carpenter, E. J., Capone, D. C. (ed.) Nitrogen in the marine environment. Academic Press, New York, p. 487-572.

McConnaughey, T., J. Burdett, J. F. Whelan, and C. K. Paull (1997). Carbon isotopes in biological carbonates: Respiration and photosynthesis. Geochimica et Cosmochimica Acta, 61, 611 – 622.

McCorkle, D. C., B. H. Corliss, and C. A. Farnham (1997). Vertical distributions and stable isotopic compositions of live (stained) benthic foraminifera from the North Carolina and California continental margins. Deep Sea Research, I, 44, 983–1024.

McCorkle, D. C., L. D. Keigwin, B. H. Corliss, and S. R. Emerson (1990). The influence of microhabitats on the carbon isotopic composition of deep-sea benthic foraminifera. Paleoceanography, 5, 161– 185.

McCorkle, D. C., and S. R. Emerson (1988). The relationship between pore water carbon isotopic composition and bottom water oxygen concentration. Geochimica et Cosmochimica Acta, 52, 1169– 1178.

McCorkle, D. C., S. R. Emerson, and P. D. Quay (1985). Stable carbon isotopes in marine porewaters. Earth and Planetary Science Letters, 74, 13– 26.

McCreary J.P., P.K. Kundu and R.L. Molinari, (1993). A numerical investigation of dynamics, thermodynamics and mixed-layer processes in the Indian Ocean. Progress in Oceanography, 31, 181–244.

McElroy M.B. (1983). Marine biological controls of atmospheric CO_2 and climate. Nature, 302, 328-329.

McKay, J.L., T.F. Pederson, and A. Mucci, (2007). Sedimentary redox conditions in continental margin sediments (N.E. Pacific) — Influence on the accumulation of redox-sensitive trace metals. Chemical Geology, 238, (3-4), 180-196.

McKay, J.L., T.F. Pedersen, and J. Southon, (2005). Intensification of the oxygen minimum zone in the Northeast Pacific during the last deglaciation: ventilation and/or export production? Paleoceanography, 20, doi:10.1029/2003PA000979.

McManus J., W. M Berelson., G. P Klinkhammer., K. S Johnson., K. H. Coale, R. F Anderson, N. Kumar, D. J., Burdige, D. E Hammond, H. J., Brumsack D. C., McCorkle and A. Rushdi (1998). Geochemistry of barium in marine sediments: Implications for its use as a paleoproxy. Geochimica et Cosmochimica Acta, 62, 3453-3473.

McNichol A. P. and L. I. Aluwihare (2007). The Power of Radiocarbon in Biogeochemical Studies of the Marine Carbon Cycle: Insights from Studies of Dissolved and Particulate Organic Carbon (DOC and POC). Chemical Reviews, 107(2) 443 - 466; (Review) DOI: 10.1021/cr050374g

Meyers, P.A. (1997). Organic geochemical proxies of paleoceanographic, paleolimnologic, and paleoclimate processes. Organic Geochemistry, 27, 213–250.

Meyers P.A. (1994). Preservation of elemental and isotopic source identification of sedimentary organic matter, Chemical Geology, 114, 289–302.

Moffett, J. W. (1990). Microbially mediated cerium oxidation in sea water. Nature, 345, 421-423.

Montoya, J.P. and M. Voss (2006). Nitrogen cycling in anoxic waters: Isotope signatures of nitrogen transformations in the Arabian Sea oxygen minimum zone. In Past and Present Water Column Anoxia, edited by Neretin, L., NATO Science Series, Springer, Dordrecht, pp. 259-281.

Montoya, P. (1994). Nitrogen isotope fractionation in the modern ocean implication for sedimentary record. In: Zahn, R. (Editor), Carbon Cycling in the Glacial Ocean Constraints on the Ocean's Role in Global Change, Berlin Heidelberg, pp. 259-279.

Morford J. and S. Emerson (1999). The geochemistry of redox sensitive trace metals in sediments. Geochimica et Cosmochimica Acta, 63, (11/12), 1735–1750.

Morrison, J.M., L.A. Codispoti, S. L. Smith, K. Wishner, C Flagg., W. D. Gardner, S. Gaurin, S.W.A. Naqvi , V. Manghnani, L. Prosperie, and J. S. Gundersen (1999). The oxygen minimum zone in the Arabian Sea during 1995. Deep-Sea Research, II, 46 , 1903-1931.

Morrison J. M., L. A. Codispoti, S. Gaurin, B. Jones, V. Manghnani and Z. Zheng (1998). Seasonal variation of hydrographic and nutrient fields

during the US JGOFS Arabian Sea process study. Deep-Sea Research, II, 45, 2053-2101.

Morrison, J.M., (1997). Inter-monsoonal changes in the T–S properties of the near-surface waters of the northern Arabian Sea. Geophysical Research Letters, 24, 2553–2556.

Müller A. and M. Voss, (1999). The palaeoenvironments of coastal lagoons in the southern Baltic Sea: II. $\delta^{13}C$ and $\delta^{15}N$ ratios of organic matter–sources and sediments. Palaeogeography, Palaeoclimatology, Palaeoecology, 145, 17–32.

Muller, P.J. and E. Suess, (1979). Productivity, sedimentation rate, and sedimentary organic matter in the oceans-I. Organic carbon preservation. Deep-Sea Research, 26A, 1347 to 1362.

Murray, D.W. and W. L. Prell, (1992). Late Pleistocene climate oscillations and monsoon upwelling recorded in sediments from the Owen Ridge, northwestern Arabian Sea. In: Summerhayes, C.P., Prell, W.L., Emeis, K.C. (Eds.), Upwelling Systems: Evolutions Since the Easrly Miocene. Geol. Soc. London Spec. Publ. 64, 301-321.

Murray D.W. and W.L. Prell, (1991). Pliocene to Pleistocene variations in calcium carbonate organic carbon, and opal on the Owen Ridge, northern Arabian Sea. In: W.J. Prell and N. Niitsuma et al., Editors, Proceedings of the Ocean Drilling Program. Scientific Results vol. 117, pp. 343–363 College Station, Texas.

Murray J. W., B. Spell, and B. Paul, (1983). The contrasting geochemistry of manganese and chromium in the eastern tropical Pacific Ocean. In Trace Metals in Sea Water (eds. C. S. Wong, E. Boyle, K. W. Bruland, J. D. Burton, and E. D. Goldberg), pp. 643–669. Plenum, New York.

Murthy, P.S.N., C.V.G. Reddy and V.V.R. Varadachari (1969). Distribution of organic matter in the marine sediments off the west coast of India. Proceedings of National Institute of Science India, 35B, 377-384.

Murty, P.S.N., Ch. M. Rao, A. L. Paropkari, and R. S. Topgi, (1978). Distribution pattern of aluminium, titanium, manganese, copper and nickel in sediments of the northern half of the western continental shelf of India. Indian Journal of Marine Science, 7, 67-71.

Naidu P. D., (2004). Isotopic evidences of past upwelling intensity in the Arabian Sea. Global and Planetary Change, 40, 285-293.

Naidu P.D., and N.Niitsuma, (2003). Carbon and oxygen time series records of planktonic and benthic foraminifera from the Arabian Sea: implications on upwelling processes. Palaeogeography, Palaeoclimatology, Palaeoecology, 202, 85-95.

Naidu, P.D., (1998). Driving forces of Indian summer monsoon on Milankovitch and sub-Milankovitch time scales: a review. Journal of Gological Society of India, 63, 257-272.

Naidu P.D., and B.A. Malmgren (1996). A high-resolution record of late Quaternary upwelling along the Oman Margin, Arabian Sea based on planktonic foraminifera. Paleoceanography, 11, 129–140.

Naidu P.D., and B.A. Malmgren (1995). A 2,200 years periodicity in the Asian monsoon system. Gephysical Research Letters, 22, 2361-2364.

Naidu P.D. C. PrakashBabu, Ch.M. Rao, (1992). The upwelling record in the sediments of the westen continental margin of India. Deep-Sea Research, 39, 715-723.

Naik H. and S.W.A. Naqvi, (2002). Sedimentary nitrogen cycling over the western continental shelf of India. EOS-Trans Amer Geophys Union 2002; 83(4) OSM Suppl.:Abs. OS 121-05.

Nameroff, T.J., S.E. Calvert and J.W. Murray (2004). Glacial–interglacial variability in the eastern tropical North Pacific oxygen minimum zone recorded by redox-sensitive trace metals. Paleoceanography, 19, A1010.

Nameroff, T.J., L. S. Balistrieri and J. W. Murray (2002). Suboxic trace metal geochemistry in the eastern tropical North Pacific. Geochimica et Cosmochimica Acta, 66(7), 1139–1158,

Nameroff T. J. (1996). Suboxic Trace Metal Geochemistry and Paleo-Record in Continental Margin Sediments of the Eastern Tropical North Pacific. Ph.D. thesis, University of Washington.

Naqvi S.W.A., G. W. Moffet, M. Gauns, P.V. Narvekar, A. Pratihary, H.Naik, M.S. Shailaja, D.A Jayakumar, T.J. Goepfert, A. Al-Azri, S.I. Ahmed, (2007). Trace-metal deficiency and suboxia limit productivity of upwelled water in the Arabian sea. Submitted to Oceanology and Limnology.

Naqvi S.W.A., H.Naik, W.D' Souza, P.V. Narvekar, A.L. Paropkari, H.W. Bange, (2007) Carbon and nitrogen fluxes in the North Indian Ocean. In Carbon and Nutrient Fluxes in Continental Margins: A Global Synthesis, edited by Liu, K.K., Atkinson, L., Quinones, R. and Talaue-McManus, L., Springer, in press.

Naqvi, S.W.A, H.Naik, D.A Jayakumar, M.S. Shailaja, and P.V. Narvekar (2006a). Seasonal oxygen deficiency over the western continental shelf of India. In: Past and Present Water Column Anoxia, edited by Neretin, I., NATO Science Series, IV. Earth and Environmental Sciences – Vol. 64, Springer, pp. 195-224.

Naqvi S.W. A. , H. Naik, A. Pratihary, W.D'Souza, P. V. Narvekar, D. A. Jayakumar , A. H. Devol, T. Yoshinari, and T. Saino (2006b). Coastal versus open-ocean denitrification in the Arabian Sea. Biogeosciences, 3, 621–633.

Naqvi S.W.A., H. W. Bange, S. W. Gibb, C. Goyet, A.D. Hatton and C. Robert Upstill-Goddard (2005). Biogeochemical ocean-atmosphere transfers in the Arabian Sea. Progress in Oceanography, 65, (2-4), 116-144.

Naqvi, S.W.A., H. Naik, and P.V. Narvekar (2003). The Arabian Sea. In: Black, K., Shimmield, G. B. Blackwell, (Eds.), Biogeochemistry of Marine Systems, Oxford, UK, 157–207.

Naqvi, S.W.A., V.V.S.S. Sarma, D.A. Jayakumar, (2002). Carbon cycling in the northern Arabian Sea during the northeast monsoon: Significance of salps. Marine Ecological Progression Series, 226, 35-44.

Naqvi S.W.A., (2001). Chemical Oceanography. In: The Indian Ocean: A perspective. Editors: SenGupta, R., Desa E., Oxford & IBH; New Delhi (India): 1, 159-236.

Naqvi S.W.A., and D. A. Jayakumar (2000). Ocean biogeochemistry and atmospheric composition: significance of the Arabian Sea. Current Science, 78, 289-299.

Naqvi S.W.A., D. A. Jayakumar, P. V. Narvekar, H. Naik, V. Sarma, W. D'Souza, S. Joseph and M. D. George (2000). Increased marine production of N_2O due to intensifying anoxia on the Indian Continental Shelf. Nature, 408, 346-349.

Naqvi, S.W.A., T. Yoshinari, J.A. Brandes, A.H. Devol, D.A. Jayakumar, P.V. Narvekar, M.A. Altabet and L.A. Codispoti (1998). Nitrogen isotopic studies in the suboxic Arabian Sea. Proc. Indian Acad. Sci. (Earth Planet Sci.), 107, 367-378.

Naqvi, S. W. A., M. S. Shailaja, M. Dileep Kumar and R. Sen Gupta (1996). Respiration rates in subsurface waters of the northern Indian Ocean: evidence for low decomposition rates of organic matter within the water column in the Bay of Bengal. Deep Sea Research Part II: Topical Studies in Oceanography, 43, (1), 73-81.

Naqvi, S.W.A., (1994). Denitrification processes in the Arabian Sea. In: Lal, D. (Ed.), Biogeochemistry of the Arabian Sea: Present information and gaps. (Proceedings of Indian Acadamy of Sciences (Earth & Planet Sci.)), Indian Academy of Sciences, Bangalore, India, 103(2), 279-300.

Naqvi, S.W.A., C. D. Charles, R. G. Fairbanks, (1994). Carbon and oxygen isotopic records of benthic foraminifera from the Northeast Indian Ocean:

implications on glacial-interglacial atmospheric CO_2 changes. Earth and Planetary Science Letters, 121, 99-110.

Naqvi S.W.A., M.D. Kumar, P.V. Narvekar, S.N De Sousa, M.D. George, C. DeSilva, (1993). An intermediate nepheloid layer associated with high microbial metabolic rates and denitrification in the northwest Indian Ocean. Journal of Geophysical Research, 98 (9), 16469-16479.

Naqvi S.W.A. (1991). Geographical extent of denitrification in the Arabian Sea in relation to some physical processes. Oceanologica Acta, 14, 281-290.

Naqvi S.W.A. and R.J. Noronha (1991). Nitrous oxide in the Arabian Sea. Deep-Sea Research, 38, 871-890.

Naqvi S.W.A., R.J. Noronha, K. Somasundar and R. Sen Gupta (1990). Seasonal changes in the denitrification regime of the Arabian Sea. Deep-Sea Research, 37, 693-711.

Naqvi S.W.A. (1987). Some aspects of the oxygen-deficient conditions and denitrification in the Arabian Sea. Journal of Marine Research, 45, 1049-1072.

Naqvi, S.W.A., and T.W. Kureishy, (1986). Deep and bottom water characteristics in the Owen Fracture Zone, Western Arabian Sea. Indian Journal of Marine Science, 15, 48-49.

Naqvi S.W.A. and R. Sen Gupta, (1985). 'NO', a useful tool for the estimation of nitrate deficits in the Arabian Sea. Deep Sea Research, 32, 665-674.

Naqvi S.W.A., R.J. Norhona and C.V.G. Reddy (1982). Denitrification in the Arabian Sea. Deep-Sea Research, 29, 459-469.

Narayana A. C., K. Pandarinath, N. Shinu, B.S. Sukhija and K. Nagabhushanam, (2005). Sedimentation patterns and clay mineral records on southwestern continental margin of India: clues to Paleomonsoon and Paleoenvironmental changes. Asia Oceania Geosciences Society, 2nd Annual Meeting, P. 09:15 OA22/4A-01-4/306.

Narayana A. C. and A. D. Singh, (1997). Upwelling record in a sediment core from the innershelf off Mangalore, west coast of India. Indian Journal of Marine Sciences, 26, 88-90.

Nevison, C., J.H. Butler, and J.W. Elkinns (2003). Global distribution of N_2O and the N_2O- AOU yield in the subsurface ocean. Global Biogeochemical Cycles, 17, 1119, doi:10.1029/2003GB002068.

Newman, J. W., P. L. Parker, and E. W. Behrens, (1973). Organic carbon isotope ratios in Quaternary cores from the Gulf of Mexico. Geochim et Cosmochimca Acta, 37, 225-238.

Nicholls J.C., A.C. Davies, and M. Trimmer, (2007) High-resolution profiles and ^{15}N isotope tracers reveal a dominant source of nitrous oxide and multiple pathways of nitrogen gas formation in the Arabian Sea. *Limnology and Oceanography* 52 (1), 156-168.

Nissenbaum, A. (1974). Deuterium content of humic acids from marine and non-marine environments. Marine Chemistry, 2, 59-63.

Ohkouchi, N., K. Kawamura, E. Wada, and A. Taira (1997). High abundances of hopanols and hopanoic acids in Cretaceous black shale. Ancient Biomol., 1, 183-192.

Olson, D. B., G. L. Hitchcock, R. A. Fine, Warren, B. A. (1993). Maintenance of the low-oxygen layer in the central Arabian Sea. Deep-Sea Research, 40, 673–685.

Overpeck, J. T., D. M. Anderson, S.Trombore and W. L. Prell, (1996). The Southwest Monsoon over the last 18,000 years. Climate Dynamics, 12, 213-225.

Owen R. B. and R. Lee, (2004). Human impacts on organic matter sedimentation in a proximal shelf setting, Hong Kong. Continental Shelf Research, 24, 583-602.

Pailler D., E. Bard, F. Rostek, Y. Zheng, R. Mortlock, A. van Green (2002). Burial of redox-sensitive metals and organic matter in the equatorial Indian Ocean linked to precession. Geochimica et Cosmochimica Acta, 66, (5), 849–865.

Pandarinath K. and A. C. Narayana, (1998). Elemental distribution in innershelf sediments off Coondapur, West coast of India. Journal of Geophysical Society of India, 51, 493-508.

Parker, P. L., E. W. Behrens, J. A. Calder, and D. J. Shultz, (1972). Stable carbon isotope ratio variations in the organic carbon form from Gulf of Mexico sediments. Contribution of Marine Science, University of Texas, 16, 139-147.

Paropkari A. L., C. Prakash Babu and A. Mascarenhas (1993a). New evidence for enhanced preservation of organic carbon in contact with oxygen minimum zone on the western continental slope of India. Marine Geology, 111, 7-13.

Paropkari A. L., A. Mascarenhas and C.Prakash Babu (1993b). Comment on "Lack of enhanced preservation of organic matter in sediments under the oxygen minimum on the Oman Margin" by T. F. Pedersen, G. B. Shimmield, and N. B. Price Geochimica et Cosmochimica Acta, 57, (10), 2399-2401.

Paropkari A.L., C. Prakash Babu and A. Mascarenhas (1992). A critical evaluation of depositional parameters controlling the variability of organic carbon in Arabian Sea sediment. Marine Geology, 107, 213-226

Paropkari, A. L., S. D. Iyer, O. S Chauhan and C. P Babu (1991). Depositional environments inferred from variations of calcium carbonate, organic carbon and sulfide sulfur: A core from southwestern Arabian Sea. Geo-Marine Letters, 11, 96-102

Paropkari, A. L., Ch. M. Rao and P. S. N. Murty (1987). Environmental controls on the distribution of organic matter in recent sediments of the western continental margin of India. In: Petroleum Geochemistry and Exploration in the Afro-Asian Region. Kumar, R. K., Dwivedi, P., Banerji, V. and Guptha, V. (Eds.). Rotterdam, A. A. Balkema, 347-361.

Paropkari, A. L., CH. M. Rao and S. N. Murty, (1978). Geochemical studies on the shelf sediments off Bombay. Indian Journal of Marine Sciences, 7, 8-11.

Parrish, J.T., (1982). Upwelling and petroleum source beds, with reference to Paleozoic. Am. Assoc. Pet. Geol., 6, 750-774.

Patra P.K., S. Lal, S. Venkataramani, S.N. de Sousa, V.V.S.S. Sarma, and S. Sardessai (1999). Seasonal and spatial variability in N_2O distribution in the Arabian Sea. Deep-Sea Research, I, 46, 529-543.

Pattan J.N., T. Masuzawa, P.D. Naidu, and M. Yamamoto, (2003). Productivity fluctuations in the southeastern Arabian Sea during the last 140 ka. Palaeogeography, Palaeoclimatology, Palaeoecology, 193, 575-590.

Pedersen, T.F., G.B. Shimmield, and N.B.Price, (1993). Reply to the comment on "Lack of enhanced preservation of organic matter in sediments under the oxygen minimum in the Oman Margin. Geochimica et Cosmochemica Acta, 57, 2403-2405.

Pedersen, T. F., G. B. Shimmield and N. B.Price (1992). Lack of enhanced preservation of organic matter in sediments under the oxygen minimum in the Oman margin. Geochimica et Cosmochimica Acta, 56, 545-551.

Pedersen, T.F., B. Neilsen and M. Pickering (1991). The timing of Late Quaternary productivity pulses in the Panama Basin and implications for atmospheric CO_2. Paleoceanography, 6, 657-677.

Pedersen, T.F., and S. E. Calvert, (1990). Anoxia vs. productivity: what controls the formation if organic carbon rich sediments and sedimentary rocks? Am. Assoc. Pet. Geol., 74, 454-466.

Pedersen, T.F. (1983). Increased productivity in the eastern equatorial Pacific during the last glacial maximum (19000 to 14000 yr B.P.). Geology, 11, 16-19.

Peters, K.E., R.E. Sweeney and I.R. Kaplan, (1978). Correlation of carbon and nitrogen stable isotope ratios in sedimentary organic matter. Limnology and Oceanography, 23, 598-604.

Peterson, B.J., R.W. Howarth and R.H. Garrett, (1985). Multiple stable isotopes used to trace the flow of organic matter in estuarine food webs. Science, 227, 1361-1363.

Petit J. R., J. Jouzel, D. Raynaud, N. I. Barkov, J. M. Barnola, I. Basile, M. Bender, J. Chappellaz, M. Davis, G. Delaygue, M. Delmotte, V. M. Kotlyakov, M. Legrand, V. Y. Lipenkov, C. Lorius, L. Pepin, C. Ritz, E. Saltzman, M. Stievenard (1999) Climate and atmospheric history of the past 420,000 years from the Vostok ice core, Antarctica. Nature, 399, 429-436.

Piper, D.Z.. and C.M. Isaacs (1996). Instability of bottom-water redox conditions during accumulation of Quaternary sediment in the Japan Sea. Paleoceanography, 11, 171-190.

Pocklington, R. (1976). Terrigeneous organic matter in surface sediments from the Gulf of St. Lawrence. Journal of the Fisheries Research Board of Canada, 33, 93-97.

Prabhu C.N. and R. Shankar (2005). Palaeoproductivity of the eastern Arabian Sea during the past 200 ka: A multi-proxy investigation. Deep-Sea Research, II, 52, 1994–2002.

Prabhu C.N., R. Shankar, K. Anupama, M Taieb, R. Bonnefille, L. Vidal, and S. Prasad (2004). A 200-ka pollen and oxygen-isotopic record from two sediment cores from the eastern Arabian Sea. Palaeogeography, Palaeoclimatology, Palaeoecology, 214, 309– 321.

Prahl, F.G., G.J. De Lange, M. Lyle, and M.A. Sparrow, (1989). Post-depositional stability of long-chain alkenones under contrasting redox conditions. Nature, 341, 434-437.

Prakash Babu, C., J Brumscak, B. Schnetger, and M.E Boettcher (2002). Barium as a productivity proxy in continental margin sediments: A study from the eastern Arabian Sea. Marine Geology, 184, 189-206.

Prell, W.L. and E. Van Campo, (1986). Coherent response of Arabian Sea upwelling and pollen transport to late Quaternary monsoonal winds. Nature, 323, 526-528.

Prell, W. L. (1984a). Variation of monsoonal upwelling: A response to changing solar radiation. In: Climate Processes and Climate Sensitivity. Hansen, J. E. and Takahashi, T. (Eds.). Geophysical Monograph Series, AGU, Washington D.C., 29, 48-57.

Prell, W. L., (1984b). Monsoonal climate of the Arabian Sea during the Late Quaternary: A response to changing solar radiation. In: Milankovitch and climate-Part I, Berger, A., Imbrie, J., Hays, J., Kukla, G. and Saltzman, B. (Eds.). D. Reidal Publishing Company, Dordrecht, The Netherlands, pp. 349-366.

Prell, W. L. and W.B. Curry (1981). Faunal and isotopic indices of monsoonal upwelling: Western Arabian Sea. Oceanologica Acta, 4(1), 91-98.

Prell, W. L., W. H. Hutson, D. F. Williams, A. W. H. Bé, K. Geitzenauer, B. Molfino (1980). Surface circulation of the Indian Ocean during the last glacial maximum, approximately 18,000 yr B.P. Quaternary Research, 14, 309-336.

Pride, C., R. Thunell, D. Sigman, L. Keigwin, M. Altabet, and E. Tappa, (1999). Nitrogen isotopic variations in the Gulf of California since the last deglaciation: Response to global climate change. Paleoceanography, 14, 397-409.

Rabalais, N., and S. Nixon, (2002). Nutrient over-enrichment in coastal waters: Global patterns of cause and effect. Estuaries, 25, 639-900.

Ramaiah, N., J.T. Paul, V., Fernandes, T., Raveendran, O., Raveendran, D., Sunder, C., Ravichandran, D.M., Shenoy, M., Gauns, S., Kurian, V.J., Gerson, D.T., Shoji, N.V., Madhu, S., Sreekumar, P.A., Lokabharathi, S.R., Shetye, (2005). The September 2004 stench off southern Malabar coast- A consequences of holococolithophore bloom. Current Science, 551-554.

Ramesh R. and M. Tiwari, (2007). Comment on "Monsoon related changes in sea surface productivity and water column denitrification in the Eastern Arabian Sea during the last glacial cycle" by V.K. Banakar, T. Oba, A.R. Chodankar, T. Kuramoto, M. Yamamoto and M. Minagawa. Current Science, 238, 115-116.

Rao P.S., A Mascarenhas, A. L Paropkari, Ch. M. Rao (1994). Organic carbon-sulfur relationships in sediment cores from the western and eastern continental margins of India. Marine Geology, 117, 227-236.

Rao, V.P., and B.G. Wagle (1997). Geomorphology and surficial geology of the western continental shelf and slope of India: A review. Current Science, 73, 330-350.

Rao, B. R. and Rao, K. S., (1989). Continental slope off Bombay and Ratnagiri: its morphology and sedimentation. Recent Geoscientific Studies in the Arabian Sea off India. Geol. Surv. India. Spec. Publ., 24, 3-20.

Rathburn, A. E., B. H. Corliss, K. D. Tappa, and K. C. Lohmann (1996). Comparisons of the ecology and stable isotopic compositions of living (stained) benthic foraminifera from the Sulu and South China seas. Deep Sea Research, I, 43, 1617–1646.

Rau, G. H., M. A. Arthur and W.E. Dean, (1987). $^{15}N/^{14}N$ variations in cretaceous Atlantic sedimentary sequences: Implication for past changes in marine nitrogen biogeochemistry. Earth and Planetary Science Letters, 82, 269-279.

Redfield ,A.C., B.H. Ketchum and F.A. Richards (1963). The influence of organisms on the composition of seawater. In:M.N. Hill, ed., The Sea, Vol. 2, Interscience, New York, 26-77.

Reichart G.J., S.J. Schenau, G.J. de Lange, and W.J. Zachariasse, (2002). Synchroneity of oxygen minimum zone intensity on the Oman and Pakistan Margins at sub-Milankovitch time scales. Marine Geology, 185, 403-415.

Reichart G.J., L. J. Lourens and J. W. Zachariasse (1998). Temporal variability in the northern Arabian Sea Oxygen minimum zone OMZ during the last 225,000 years. Paleoceanography, 13, 6, 607-621.

Reichart G.J., M. den Dulk, H. J. Visser, C. H. van der Weijden, and W. J. Zachariasse. (1997). A 225 Kyr record of dust supply paleoproductivity and the oxygen minimum zone from the Murray Ridge Northern Arabian Sea. Paleogeography, Paleoclimatology, Paleoecology, 134, 149-169.

Reichart, G. H., (1997). Late Quaternary variability of the Arabian Sea monsoon and oxygen minimum zone. PhD Thesis, University of Utrecht, The Netherlands, p. 173.

Repetta D.J., D.J. Simpson, B.B. Jorgensen and H.W. Jannasch (1989). Evidence for anoxygenic photosynthesis from the distribution of bacteriochlorophylls in the Black Sea. Nature, 342, 69-72.

Richards F.A. (1965). Anoxic basins and fjords. In: J.P. Riley and G. Skirrow (eds.), Chemical Oceanography, Vol. 1, Academic Press, 611-645.

Rixen et al., 2000a Rixen, T., Haake, B., Ittekkot, V., 2000a. Sedimentation in the western Arabian Sea the role of coastal and open-ocean upwelling. Deep-Sea Research II 47 (9–11), 2155– 2178.

Rixen, T., Ittekkot, V., Haake-Gaye, B., Scha¨fer, P., 2000b. The influence of the SW monsoon on the deep-sea organic carbon cycle in the Holocene. Deep-Sea Research II 47, 2629–2651.

Rosenthal Y., P. Lam, E. A. Boyle and J. Thompson (1995a). Authigenic cadmium enrichments in suboxic sediments: Precipitation and post-depositional mobility. Earth and Planetary Science Letters, 132, 99-111.

Rosenthal Y., E.A. Boyle, L. Labeyrie and D. Oppo (1995b). Glacial enrichments of authigenic Cd and U in subantarctic sediments: A climatic control on the elements oceanic budget . Paleoceanography, 10, (3), 395-413.

Rostek F., E. Bard, L. Beaufort, C. Sonzogni, and G. Ganssen, (1997). Sea surface temperature and productivity records for the past 240 kyr in the Arabian Sea. Deep-Sea Research, II, 44 (6-7), 1461–1480.

Rostek, F., G. Ruhland, F. C. Bassinot, P. J. Mtiller, L. D. Labeyrie, Y. Lancelot, and E. Bard, (1993). Reconstructing sea surface temperature and salinity using $\delta^{18}O$ and alkenone records. Nature, 364,319-321.

Saager, P.M., H.J.W. DeBaar, and R.J. Howland (1992). Cd, Zn, Ni and Cu in the Indian Ocean. Deep-Sea Research, 39, 9–35.

Saager P.M., H.J.W. De Baar, and P.H. Burkill (1989). Manganese and iron in Indian Ocean waters. Geochimica et Cosmochemica Acta, 53, 2259-2267.

Sackett, W. M. (1964). The depositional history and isotopic organic carbon composition of marine sediments. Marine Geology, 2, 173-185.

Saino and Hottori (1987). Geographical variation of water column distribution of suspended particulate organic nitrogen and its ^{15}N natural abundance in the Pacific and its marginal seas. Deep Sea Research, 34, 807-827.

Saino and Hattori (1980). [15]N natural abundance in oceanic suspended particulate matter. Nature, 283, 752-754.

Sarin, M. M., R. Bhushan, and K. Dutta, (1997). Determination of organic carbon and nitrogen in marine sediments using elemental analyzer. Abstract presented at the Conference on Recent Advances in Elemental Analysis held at Homi Bhabha Centre for Science Education (TIFR), Mumbai, India.

Sarin, M.M., R. Bhushan, R. Rengarajan, and D.N. Yadav, (1992). Simultaneous determination of [238]U series nuclides in waters of Arabian Sea and Bay of Bengal. Indian Journal of Marine Sciences, 21, 12-127.

Sarkar, A., R. Ramesh, B.L.K. Somayajulu, R. Agnihotri, A.J.T. Jull, and G.S. Burr, (2000). High resolution Holocene monsoon record from the eastern Arabian Sea. Earth and Planetary Science Letters, 177, 209-218.

Sarkar, A., S.K Bhattacharya, and M.M. Sarin (1993). Geochemical evidence for anoxic deep water in the Arabian Sea during the last glaciation. Geochimica et Cosmochimica Acta, 57, 1009–1016.

Sarkar, A., R. Ramesh, S. K. Bhattacharya and G. S. Rajagopalan (1990). Oxygen isotope evidence for a stronger winter monsoon current during the last glaciation, Nature, 343, 548–551.

Sarnthein, M., K. Winn, J. C. Duplessy, and M. Fontugne (1988). Global variations of surface ocean productivity in low and mid latitudes: influence on CO_2 reservoirs of the deep ocean and atmosphere during the last 21,000 years. Paleoceanography, 3(3), 361-399.

Satya Prakash and R. Ramesh (2007). Is the Arabian Sea getting more productive? Current Science, 92, (5), 667-671.

Savin, S. M. and H. W. Yeh (1981). Stable isotopes in ocean sediments. In: Emiliani, C. (Ed.). The Sea, Vol. 7, Wiley-Inter Science, pp. 1521-1554.

Sayles, F. L., and W. B. Curry (1988), $\delta^{13}C$, TCO_2, and the metabolism of organic carbon in deep sea sediments. Geochimica Cosmochimica Acta, 52, 2963– 2978.

Schäfer, P. and V. Ittekkot, (1995). Isotope biogeochemistry of nitrogen in the northern Indian Ocean. Mitt. Geol.-Palaont. Inst. Univ. Hamburg, 78, 67-93.

Schäfer, P. and V. Ittekkot, (1993). Seasonal variability of $\delta^{15}N$ in settling particles in the Arabian Sea and its paleogeochemical significance, Naturwissenschaften, 80, 511-513.

Schelske, C. and D. A. Hodell, (1995). Using carbon isotopes of bulk sedimentary organic matter to reconstruct the history of nutrient loading and eutrophication in Lake Erie. Limnology Oceanography, 40, 918-929.

Schenau S.J., H.F. Passier, G.J. Reichart and G.J. de Lange, (2002). Sedimentary pyrite formation in the Arabian Sea. Marine Geology, 185, 393-402.

Schmaljohann R, M. Drews, S. Walter, P. Linke, U von Rad, and J.F. Imhoff (2001). Oxygen-minimum zone sediments in the northeastern Arabian Sea off Pakistan: a habitat for the bacterium Thioploca. Mar Ecol Prog Ser, 211, 27–42.

Schmiedl, G. and A. Mackensen (2006). Multispecies stable isotopes of benthic foraminifers reveal past changes of organic matter decomposition and deepwater oxygenation in the Arabian Sea. Paleoceanography, 21, PA4213.

Schmiedl,G., M. Pfeilsticker, C. Hemleben and A Mackensen (2004). Environmental and biological effects on the stable isotope composition of recent deep-sea benthic foraminifera from the western Mediterranean Sea, Mar. Micropaleontology, 51, 129–152.

Schmitz, B., (1987). The TiO_2/AlO_2 ratio in Cenezoic Bengal abyssal fan sediments and its use as a pleostream energy indicator. Marine Geology. 76, 195-206.

Schott F. A., and J. P. McCreary Jr., (2001). The monsoon circulation of the Indian Ocean. Progress in Oceanography, 51, 1–123.

Schott, F., and J. Fischer, (2000). Winter monsoon circulation of the northern Arabian Sea and Somali Current. Journal of Geophysical Research, 105, 6359–6376.

Schubert, C.J., J. Villanueva, S.E. Calvert, G.L. Cowie, U. von Rad, H. Schulz, U. Berner, and H. Erlenkeuser, (1998). Stable phytoplankton community structure in the Arabian Sea over the past 200,000 years. Nature, 394, 563–566.

Schulte S., F. Rostek, E. Bard, J. Rullko"tter, and O. Marchal (1999). Variations of oxygen-minimum and primary productivity recorded in sediments of the Arabian Sea. Earth and Planetary Science Letters, 173, 205–221.

Schulz, H., U. von Rad, and H. Erlenkeuser, (1998). Correlation between Arabian Sea and Greenland climate oscillations of the past 110,000 years. Nature, 393, 54-57.

Seitzinger S.P. (1990). In: Revsbech NP, Sorensen J. eds., Denitrification in aquatic sediments denitrification in soil and sediments. FEMS Symposium, plenum press, New York, 301-322pp.

Sen Gupta R. and S.W.A. Naqvi, (1984). Chemical oceanography of the Indian Ocean, north of the equator. Deep Sea Research, 31, 671-706.

Sen Gupta R., M.D. Rajagopal and S.Z. Qasim (1976a). Relationship between dissolved oxygen and nutrients in the north-western Indian ocean. Indian Journal of Marine Sciences, 5, 201-211.

Shackleton, N. J., (1987). Oxygen isotopes, ice volume and sea level. Quaternary Science Reviews, 6, 183-190.

Shackleton, N. J. and E. Vincent (1978). Oxygen and carbon isotope studies in recent foraminifera from the southwest Indian Ocean. Marine Micropaleontology, 3, 1-13.

Shackleton, N. J., (1977). Carbon-13 in Uvigerina: Tropical rainforest history and the equatorial Pacific carbonate dissolution cycles. In: The fate of fossil fuel CO_2 in the Ocean, Anderson, N.R. and Malhoff, A. (Eds.). Plenum, New York, pp. 401-428.

Shankar, R., K.V. Subbarao, and V. Kolla (1987). Geochemistry of surface sediments from the Arabian Sea. Marine Geology, 76, 253–279.

Sharma, O., D.V. Borole, and M.D Zingde (1994). ^{210}Pb based trace element fluxes in the near shore and estuarine sediments off Bombay, India. Marine Chemistry, 47, 227-241.

Shaw, T.J., J.M. Gieskes, and R.A. Jahnke (1990). Early diagenesis in differing depositional environments: the response of transition metals in pore water. Geochimica et Cosmochimica Acta, 54, 1233–1246.

Shetye S.R. and A. D. Gouveia (1998). Coastal circulation in the north Indian Ocean (14, S-W). In: The Sea. 11, 523-556.

Shetye, S.R., A.D. Gouveia, S.S.C. Shenoi, (1994). Circulation and water masses of the Arabian Sea, In: Lal, D. (Ed.), Proceedings of the Indian Academy of Sciences, Lotus Printers, New Delhi, India, pp. 9-25.

Shetye S.R., A. Gouveia, S.S.C. Shenoi, G.S. Michael, D. Sundar, A.M. Almeida, and K. Santanam (1991a). The coastal current off western India during northeast monsoon. Deep-Sea Research, 38, 1517-1529.

Shetye S.R., A.D Gouveia, S.S.C Shenoi, G.S Michael, D. Sundar, A.M. Almeida, M. Santanam (1990). Hydrography and circulation off the west coast of India during the southwest mosoon. Journal of Marine Research, 48, 359-378.

Shimmield, G.B. (1992). Can sediment geochemistry record changes in coastal upwelling paleoproductivity? Evidence from northwest Africa and the Arabian sea. In: Summerhayes, C., Prell, W., Emeis, K. (Eds.), Upwelling Systems Since the Early Miocene. Geol. Soc. Spec. Publ. 64, 29-46.

Shimmield, G.B., and S.R. Mowbray, (1991). The inorganic geochemical record of the northwest Arabian sea: A history of productivity variation over the last 400 ka from sites 722 and 724. In: Prell, W.L., Niitsuma et al., Proc. Ocean Drilling Programme, Scientific Results, 117, College Station, TX, pp. 409-429.

Shimmield, G.B. and N. Price (1986). The behaviour of molybdenum and manganese during early sediment diagenesis-Offshore Baja California, Mexico. Marine Chemistry 19, 261–280.

Sigman, D. M., M. A. Altabet, D. C. McCorkle, R. Francois, and G. Fischer, (1999). The $\delta^{15}N$ of nitrate in the Southern Ocean: Consumption of nitrate in surface waters. Global Biogeochemical Cycles, 13, 1149-1166.

Sigman, D. M., M. A. Altabet, R. Michener, D. C. McCorkle, B. Fry, and R. M. Holmes, (1997). Natural abundance-level measurement of the nitrogen isotopic composition of oceanic nitrate: An adaptation of the ammonia diffusion method. Marine Chemistry, 57, 227-242.

Singh A.D., D. Kroon and R. S. Ganeshram, (2006). Millenial scale Variations in Productivity and OMZ Intensity in the Eastern Arabian Sea. Journal of Geological Society of India, 68, 369-377.

Sirocko F., D. G. Schonberg, and C. Devey (2000). Processes controlling trace element geochemistry of Arabian Sea sediments during the last 25,000 years. Global and Planetary Change, 26, 217–303.

Sirocko F., D.G. Schonberg, A. McIntyre, and B. Molfino, (1996). Teleconnections between the subtropical monsoons and high latitude climates during the last glaciation. Science, 272, 526-529.

Sirocko, F., M. Sarnthein, H. Erlenkeuser, H. Lange, M. Arnold and J. C. Duplessy (1993). Century scale events in monsoon climate over the past 24,000 years. Nature, 364, 322-324.

Smith, S., K. Banse, J. Cockran, L. Codispoti, H. Ducklow, M. Luther, D. Olson, W. Peterson, W. Prell, N. Surgi, J. Swallow, and K. Wishner, (1991). US JGOFS: Arabian Sea Process Study. US JGOFS Planning Report No. 13, Woods Hole Oceanographic Institution, Woods Hole, 164pp.

Smith, B.N. and S. Epstein. (1971). Two categories of $^{13}C/^{12}C$ ratios for higher plants. Plant Physiology, 47, 380-384.

Somayajulu, B. L. K., D. N. Yadav, and M. M. Sarin, (1994). Recent sedimentary records from the Arabian Sea. Proc. Indian Acad. Sci. 103, 315-327.

Sonzogni, C., E. Bard, and F. Rostek, (1998). Tropical sea-surface temperature during the last glacial period: a view based on alkenones in Indian Ocean sediments. Quaternary Science Reviews, 17, 1185–1201.

Spero, H. J. and D. F Williams (1988). Extracting environmental information from planktonic foraminiferal $\delta^{13}C$ data. Nature, 335, 717-719.

Stackelberg, V.U. (1972). Faziesverteilung in Sedimenten des Indisch-Pakistanischen Kontinentalram. Metero Forschungsergebnisse Reihe C, 9, pp. 1-73.

Stein, R. (1991) Accumulation of organic carbon in marine sediments. Results from the Deep Sea Drilling Project/Ocean Drilling Program. Lecture Notes in Earth Sciences, vol. 34. Berlin: Springer-Verlag. 217pp.

Stott, L. D., W. Berelson, R. Douglas, and D. Gorsline (2000). Increased dissolved oxygen in Pacific intermediate waters due to lower rates of carbon oxidation in sediments. Nature, 407, 367– 370.

Street-Perrot, F. A., Y. Huang, R. A. Perrott, G. Eglinton, P. Barker, L. B. Khelifa, D. Harkness and D. O. Olago, (1997). Impact of lower atmospheric carbon dioxide on tropical mountain ecosystems. Science, 278, 1422-1426.

Strous, M., J.A. Fuerst, E.H.M. Kramer, S. Logemann, G. Muyzer, K.T. van de Pas-Schoonen, R. Webb, J.G. Kuenen and M.S.M. Jetten, (1999). Missing lithotroph identified as new planetomycete. Nature, 400, 446-449.

Summerhayes, C. P., (1987). Organic rich Cretaceous sediments from the North Atlantic. In: J. Brooks and A.J. Fleet (Editors), Marine Petroleum Source Rocks. Geol. Soc. Spec. Publ., 26, 301-316.

Summerhayes, C. P., (1981). Organic facies of middle Cretaceous Black shales in deep north Atlantic. American Association of Petroleum Geologists Bulletin, 65, 2364-2380.

Sundby, B., P. Martinez, and C. Gobeil, (2004). Comparative geochemistry of cadmium, rhenium, uranium, and molybdenum in continental margin sediments. Geochimica et Cosmochimica Acta, 68, 2485–2493.

Suthhof, A., V. Ittekkot, and B.G. Haake (2001). Millennial scale oscillation of denitrification intensity in the Arabian Sea during the late Quaternary and its potential influence on atmospheric N2O and global climate. Global Biogeochemical Cycles, 15, 637-649.

Swallow, J.C., (1984). Some aspects of the physical oceanography of the Indian Ocean. Deep Sea Research, 30, 639-650.

Sweeney, J.R. and I.R Kaplan. (1980). Natural abundance of ^{15}N as a source indicator for near shore marine sedimentary and dissolved nitrogen. Marine Chemistry, 9, 81-94

Talbot, M.R., (2001). Nitrogen isotopes in palaeolimnology. In: Last, W.M., Smol, J.P. (Eds.), Tracking environmental change using lake sediments. Vol. 2, Physical and Geochemical methods. Kluwer Academic Publishers, Dordrecht, The Netherlands, pp. 401–439.

Tanaka, T. and T. Saino, (2002). Modified method for the analysis of nitrogen isotopic composition of oceanic nitrate at low concentration. Journal of Oceanography, 58, 539–546.

Thamban, M., V.P. Rao, R.R. Schneider, and P.M. Grootes (2001). Glacial to Holocene fluctuation in hydrography and productivity along the southwestern continental margin of India. Palaeogeography, Palaeoclimatology, Palaeoecology, 165, 113–127.

Thamban M. (1998). Sedimentological investigations on sediments from the Western Continental margin of India: Inferences on the palaeocenography during late quaternary. Thesis submitted to Goa University.

Thamban, M., V. P Rao and S. V. Raju (1997). Controls on organic carbon distribution in the sediment cores from the eastern Arabian Sea. Geo-Marine Letters, 17 (3), 20-27.

Thamdrup, B., T. Dalsgaard, M. M. Jensen, Ulloa, O., Farias, L., and Escribano, R. (2006). Anaerobic ammonium oxidation in the oxygen-deficient waters off northern Chile. Limnology and Oceanography, 51, 2145–2156.

Thornton, S.F., and J. McManus, (1994). Application of organic carbon and nitrogen stable isotope and C/N ratios as sources indicators of organic matter provenance in estuarine systems: evidence from the Tay Estuary, Scotland. Estuarine, Coastal and Shelf Science, 38, 219–233.

Thunell, R. C., and A. B. Kepple, (2004). Glacial-holocene $\delta^{15}N$ record from the Gulf of Tehuantepec, Mexico: Implications for denitrification in the eastern Equatorial Pacific and changes in atmospheric N_2O, Global Biogeochemical Cycles, 18, 1011, doi:10.1029/2002GB002028.

Tissot, B. P., G. Demaison, P. Masson, J. R. Delteil, and A., Combaz, (1980). Palaeoenvironment and petroleum potential of middle Cretaceous black shales in Atlantic basins. American Association of Petroleum Geologists Bulletin, 64, 2051-2063.

Tiwari M., R. Ramesh, B. L. K.Somayajulu, A. J. T. Jull and G. S. Burr, (2005a). Solar control of southwest monsoon in centennial timescales. Current Science, 89, No. 9, 1583-1588.

Tiwari M., R. Ramesh, M. G. Yadava, B. L. K.Somayajulu, A. J. T. Jull and G. S. Burr, (2006). Is there a persistent control of monsoon winds by precipitation during the late Holocene? Geochemistry Geophysics Geosystems, Vol. 7, no. 3, Q03001, doi:10.1029/2005GC001095.

Tomczak, M. and J. S. Godfrey (2003) Regional Oceanography: an Introduction. 2nd improved edition, 390p. Daya Publishing House, Delhi.

Tomczak , M., and J. S. Godfrey, (1994). Regional Oceanography: An Introduction, 422 pp., Pergamon, Terry town, New York.

Toole, J. M., and B. Warren, (1993). A hydrographic section across the subtropical South Indian Ocean. Deep-Sea Research, I, 40, 1973–2019.

Totland M., I. Jarvis and K. E Jarvis (1992). An assessment of dissolution techniques of the analysis of geological sample by plasma spectrometry. Chemical Geology, 95, 35-62.

Tribovillard, N.P., J.P. Caulet, C.V. Grazzini, N. Moureau, and P. Tremblay, (1996). Lack of organic matter accumulation on the upwelling-influenced Somalia margin in a glacial-interglacial transition. Marine Geology, 133, 157-182.

Turekian, K.K., and K.H. Wedepohl, (1961). Distribution of the elements in some major units of the Earth's crust. Geological Society of American Bulletin, 72, 175-192.

Turner, R. E. and N. N. Rabalais (1994). Coastal eutrophication near the Mississippi river delta. Nature, 368, 619-621.

Turner, R. E. and N. N. Rabalais (2003). Linking Landscape and water quality in the Mississippi River basin for 200 years, Bioscience 53 (6), 563–572.

Tyson, R.V. (1995) Sedimentary organic matter. Organic facies and palynofacies. London: Chapman & Hall. 615pp.

Vaccaro, R. F. 1965. Inorganic nitrogen in sea water, p. 365-408. In. J. P. Riley and G. Skirrow [eds.], Chemical oceanography, v. 2. Academic Press, New York.

Van Campo, E., (1986). Monsoon fluctuations in two 20,000 yr B.P. oxygen-isotope/ pollen records off southwest India. Quaternary Research, 26, 376-388

Van der Weijden, C.H., G.J. Reichart, and H.J. Visser, (1999). Enhanced preservation of organic matter in sediments deposited within the oxygen minimum zone in the northeastern Arabian Sea. Deep Sea Research. 46, 807-830.

Van Geen, A., R.G. Fairbanks, P. Dartnell, M. McGann, J. V. Gardner, and M. Kashgarian, (1996). Ventilation changes in the northeast Pacific during the last deglaciation. Paleoceanography, 11, 519-528.

Van Geen A., D. C. McCorkle and G. P. Klinkhammer (1995). Sensitivity of the phosphate-cadmium-carbon isotope relation in the ocean to cadmium removal by suboxic sediments. Paleoceanography, 10, 159–169.

Vidal, L., S. Sepulcre, K. Tachikawa, and E. Bard (2004). Multi-benthic species stable isotope to reconstruct changes in pore waters 13C/12C gradients and bottom water oxygen concentrations in the Arabian Sea over the last 450 kyr, paper presented at 8th International Conference on Paleoceanography, Environ. et Pale'oenviron. Oceaniques, UMR Cent. Natl. de la Rech. Sci., Biarritz, France.

Von Rad, U., H. Schulz, and SONNE 90 Scientific Party (1995). Sampling the oxygen minimum zone off Pakistan: glacial-interglacial variations of anoxia and productivity (preliminary results, SONNE 90 Cruise). Marine Geology, 125, 7-19.

Voss, M., J. W. Dippner, and J. P. Montoya, (2001). Nitrogen isotope patterns in the oxygen-deficient waters of the eastern tropical North Pacific Ocean. Deep Sea Research, II, 48, 1905–1921.

Wada E. and A. Hattori eds. (1991). Nitrogen in the Sea: Forms, Abundances and Rate Process. 208 p. CRC Press, Florida, U.S.A.

Wada E. and A. Hattori, (1971). Nitrite metabolism in the euphotic layer of the central North Pacific Ocean. Limnology Oceanography, 16, 766-772.

Warnken, K. W., L. L. Gary., Griffin and P. H. Santschi. (2001) Sediment-water exchange of Mn, Fe, Ni and Zn in Galveston bay, Texas, Marine Chemistry, 73, 215-231.

Warren, B.A., (1994). Context of the suboxic layer in the Arabian Sea. Proceedings of the Indian Academy of Sciences. Earth and Planetary Sciences, 103, 203-216.

Waser, N. A. D., P. J. Harrison, B. Neilsen, and S. E. Calvert, (1998). Nitrogen isotopic fractionation during the uptake and assimilation of nitrate, nitrite, ammonium and urea by a marine diatom. Oceanol. Limnol., 43, 215-224.

Wedepohl, K.H., (1991). The composition of the upper earth's crust and the natural cycles of selected metals. Metals in natural raw minerals. Natural resources. In: Merian, E. (Ed.). Metals and Their Compounds in the Environment. VCH, Weinheim, pp. 3-17.

Wedepohl, K.H., (1971). Environmental influences on the chemical composition of shales and clays. In: Ahrens, L.H. (Ed.), Physics and chemistry of the Earth. Pergamon, Oxford, pp. 305-333.

Wefer, G., and W. H. Berger, (1991). Isotope paleontology: growth and composition of extant calcareous species. Marine Geology, 100, 207-248.

Wehrli B. and W. Stumm (1989). Vanadyl in natural waters: Adsorption and hydrolysis promote oxygenation. Geochimica et Cosmochimica Acta, 53, 69-77.

Weiss, R. F., (1978). Nitrous Oxide in surface water and marine atmosphere of the North Atlantic and Indian Oceans. Transactions of the American Geophysical Union, 59, 1101.

Werne, J.P., D.J. Hollander, T.W. Lyons, and L.C. Peterson (2000). Climate-induced variations in productivity and planktonic ecosystem structure from the Younger Dryas to Holocene in the Cariaco Basin, Venezuela. Paleoceanography, 15, 19–29.

Wiggert, J. D., R. G. Murtugudde, and J. R. Christian, (2006). Annual ecosystem variability in the tropical Indian Ocean: Results of a coupled bio-physical ocean general circulation model, Deep-Sea Research, II, 53, 644–676.

Wiggert J.D., R. G. Murtugudde, and C.R. McClain (2002).Processes controlling interannual variations in wintertime (northeast monsoon) primary productivity in the central Arabian Sea. Deep Sea Research II, 49, 2319-2343.

Wishner, K., M., Gowing, and C., Gelfman, (1998). Zooplankton biomass in the upper 1000 m in the Arabian Sea: overall seasonal; and geographic patterns, and relationship to oxygen gradients. Deep-Sea Research, II, 45, 2405-2432.

Wu, J., S. E. Calvert, and C. S. Wong, (1997). Nitrogen isotope variations in the subarctic northeast Pacific: relationships to nitrate utilization and trophic structure, Deep-Sea Research, I, 44, 287–314.

Wyrtki, K. (1973). Physical oceanography of the Indian Ocean. In: B. Zeitzschel, (ed.), The biology of the Indian Ocean, Springer-Verlag, Berlin, 18-36pp.

Wyrtki, K. (1971). Oceanographic Atlas of the International Indian Ocean Expedition, National Science Foundation, Washington D.C., 531p.

Wyrtki, K. (1962). The oxygen minima in relation to ocean circulation. Deep-Sea Research, 9, 11-23.

Yadav, D.N., M.M. Sarin and B.L.K. Somayajulu, (1992). Western Continental margins of India: Are they sink or source for trace elements in the Arabian Sea? In:Oceanography of the Indian Ocean (ed) B.N. Desai (New Delhi: Oxford and IBH) pp. 359-367.

Yarincik, K.M., R.W Murray, T.W. Lyons, L.C. Peterson and G.H. Haug (2000). Oxygenation history of bottom waters in the Cariaco Basin, Venezuela, over the past 578,000 years: results from redox sensitive metals (Mo, V, Mn, Fe). Paleoceanography, 15, 593–604.

Yoshinari, T., (1976). Nitrous oxide in the sea. Marine Chemistry, 4, 189–202.

You, Y. and M. Tomczak (1993). Thermocline circulation and ventilation in the Indian Ocean
derived from water mass analysis. Deep Sea Research, 40, 13-56.

Zahn, R. and T. F., Pedersen (1991). Late Pleistocene evolution of surface and mid-depth hydrography at the Oman margin: planktonic and benthic isotope records at Site 724. In: Proceedings of the Ocean Drilling Program, Prell, W. L., Niitsuma, N., et al. (Eds.). College station, Texas, 117, 291-308.

Zahn, R., K. Winn, M. Sarnthein (1986). Benthic foraminiferal d13C and accumulation rates of organic carbon: Uvigerina peregrine group and Cibicidoides wuellerstorfi. Paleoceanography, 1, 27– 42.

Zheng, Y., R. F. Anderson, A. van Geen, and J. Kuwabara (2000a). Authigenic molybdenum formation in marine sediments: A link to porewater sulfide in the Santa Barbara Basin. Geochimica et Cosmochimica Acta, 64, 4165–4178.

Zheng, Y., A. van Geen, R. F. Anderson, J. V. Gardner, and W. E. Dean, (2000b). Intensification of the northeast Pacific oxygen-minimum zone during the Bølling-Allerød warm period. Paleoceanography, 15, 528-536.

Zimmerman, A. R., and E. A. Canuel, (2000). A geochemical record of eutrophication and anoxia in Chesapeake Bay sediments: Anthropogenic influence on organic matter composition. Marine Chemistry, 69, 117-137.

Zobell, C.E. (1973). Microbial degradation of oil: Present status, problems and perspectives. In: Ahearn DG, Meyers SP (eds) The microbial degradation of oil pollutants. Georgia State University, Atlanta.